KADIR HAS UNIVERSITY

GRADUATE SCHOOL OF SCIENCE AND ENGINEERING

PROGRAM OF BIOINFORMATICS AND GENETICS

TARGETING CANCER EPIGENETIC MODIFIERS: THE DESIGN OF ISOFORM-SELECTIVE HISTONE DEACETYLASE INHIBITORS

ABDULLAHI IBRAHIM UBA

DOCTOR OF PHILOSOPHY THESIS

ISTANBUL, JUNE, 2018

Abdullahi Ibrahim Uba

Ph.D. Thesis

2018

TARGETING CANCER EPIGENETIC MODIFIERS: THE DESIGN OF ISOFORM-SELECTIVE HISTONE DEACETYLASE INHIBITORS

ABDULLAHI IBRAHIM UBA

PHD THESIS

Submitted to the Graduate School of Science and Engineering of Kadir Has University
in partial fulfillment of the requirements for the degree of PhD in the Program of
Bioinformatics and Genetics

ISTANBUL, JUNE, 2018

DECLARATION OF RESEARCH ETHICS / METHODS OF DISSEMINATION

I, ABDULLAHI IBRAHIM UBA, hereby declare that;

- this PhD Thesis is my own original work and that due references have been appropriately provided on all supporting literature and resources;
- this PhD Thesis contains no material that has been submitted or accepted for a degree or diploma in any other educational institution;
- I have followed "Kadir Has University Academic Ethics Principles" prepared in accordance with the "The Council of Higher Education's Ethical Conduct Principles"

In addition, I understand that any false claim in respect of this work will result in disciplinary action in accordance with University regulations.

Furthermore, both printed and electronic copies of my work will be kept in Kadir Has Information Center under the following condition as indicated below

☐ The full content of my thesis will be accessible from everywhere by all means.

ABDULLAHI IBRAHIM UBA
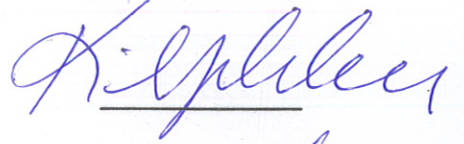
DATE AND SIGNATURE

KADIR HAS UNIVERSITY

GRADUATE SCHOOL OF SCIENCE AND ENGINEERING
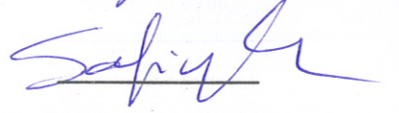
ACCEPTANCE AND APPROVAL

This work entitled **TARGETING CANCER EPIGENETIC MODIFIERS: THE DESIGN OF ISOFORM-SELECTIVE HISTONE DEACETYLASE INHIBITORS** prepared by **ABDULLAHI IBRAHIM UBA** has been judged to be successful at the defense exam held on **6th JUNE, 2018** and accepted by our jury as **Ph.D. THESIS.**
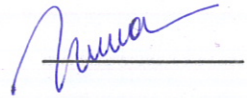
APPROVED BY:

(Prof. Dr. Kemal Yelekçi) (Advisor)   (Kadir Has University)
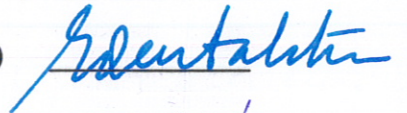
(Prof. Dr. Safiye S. Erdem)   (Marmara University)
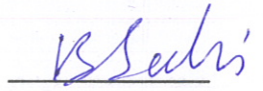
(Prof. Dr. Nurcan Ş. Tüzün)   (Istanbul Technical University)

(Assoc. Prof. Dr. E. Demet Akten Akdoğan) (Kadir Has University)

(Dr. Hatice Bahar Şahin)   (Kadir Has University)

I certify that the above signatures belong to the faculty members named above.

(Assoc. Prof. Dr., E. Demet Akten Akdoğan)

Dean of Graduate School of Science and Engineering

DATE OF APPROVAL: (06/June/2018)

TABLE OF CONTENTS

TARGETING CANCER EPIGENETIC MODIFIERS: THE DESIGN OF ISOFORM-SELECTIVE HISTONE DEACETYLASE INHIBITORS

ABSTRACT

Epigenetic alterations are believed to be the common hallmark of human cancers. Histone deacetylase (HDAC) inhibitors have proven to be effective in cancer cases where HDACs are up-regulated. However, lack of selectivity of many of the HDAC inhibitors in clinical use and those at various stages of preclinical and clinical trials causes toxicity to the normal cells. It is believed that the continuous identification of isoform-selective HDAC inhibitors can eliminate this adverse effect — a task that remains particularly challenging due to the high sequence and structural conservations around the active site of HDAC isoforms. The original contribution of this study was analyzing the similarity among class I HDACs (1, 2, 3 and 8) and class IIb HDACs (6 and 10) by sequence and structural alignments, catalytic channel extraction, and identification of catalytically essential amino acid residues. In addition, homology model of human HDAC10 was built using a recently-released X-ray crystal structure of *Danio rerio* (zebrafish) HDAC10 as a template. Using these data, isoform-selective HDAC inhibitors were designed by topology-based scaffold hopping, structure- and ligand-based virtual screening. The top inhibitors (in terms of both binding affinity and selectivity) were subjected to structure-based *in silico* absorption, distribution, metabolism, elimination and toxicity (ADMET) prediction, which showed their drug-likeness. Furthermore, their docking complexes were submitted to molecular dynamics (MD) simulations to examine the stability of ligand binding modes. These potential isoform-selective HDAC inhibitors showed stable binding mode over time of the simulation. They can therefore serve as drug candidates or viable lead compounds for further modeling-based and experimental optimization towards the design of safe, potent and selective HDAC inhibitors.

Keywords: Epigenetic alterations in cancer, Homology modeling of human HDAC10, Structure-based drug design, Structure-based ADMET prediction, Isoform-selective HDAC inhibitors.

KANSER EPİGENETİK MODİFİYE EDİCİLERİN HEDEFLENMESİ: İZOFORMA ÖZEL SEÇİMLİ HİSTON DEASETİLAZ İNHİBİTÖR DİZAYNI

ÖZET

Epigenetik değişiklikler insan kanserlerinin karakteristik bir özelliğidir. Histon deasetilaz (HDAC) inhibitörlerinin, HDAC seviyesinin yükseldiği kanser vakalarında etkili olduğu görülmüştür. Fakat, HDAC inhibitörlerinin izoformlar arasında seçici olmaması, klinik olarak kullanımda olan, klinik ve pre-klinik denemelerde normal hücreler üzerinde toksik etki göstermesine neden olmaktadır. HDAC izoformlarına özgü inhibitör keşfinin bu yan etkileri gidereceğine inanılmaktadır. Ama bu keşif, bilhassa HDAC izoformlarının yüksek sekans benzerliği ve aktif yüzeylerindeki yapısal korunmuşluk yüzünden bir hayli zordur. Bu çalışmanın orijinal katkısı, sınıf I HDAC'ların (HDAC 1, 2, 3 ve 8) ve sınıf IIb HDAC'ların (HDAC 6 ve 10) sekans ve yapısal benzerliklerini, katalitik kanalın çözümlenmesini, ve kataliz için elzem amino asitleri çalışmak oldu. Bunun yanı sıra, X-ray yapısı yeni yayınlanmış *Danio rerio* (zebra balığı) HDAC10 proteinini kullanarak insan HDAC10 homoloji modeli inşa edildi. Bu veriyi kullanarak, topoloji temelli iskelet sekmesi, yapı temelli ve ligand temelli sanal tarama yöntemleriyle, izoforma özgü HDAC inhibitörleri dizayn ettim. Bağlanma afinitesi ve seçicilik açısından en iyi inhibitör adayları, ilaç benzerlik özelliklerini gösteren ADMET (*in silico* soğurma, dağılma, metabolizma, atılma ve seçicilik) öngörü testine tabii tutuldu. Bunların kenetlenme (docking) kompleksleri, ligand bağlanmasının stabilitesini ölçmek üzere, moleküler dinamik simülasyonlarına sokuldu. Potansiyel HDAC izoformuna özgü inhibitör adayları, simülasyon boyunca stabil bağlanma gösterdi. Bu sebepten ilaç adayı veya kuvvetli öncü moleküller olabilirler; ilerde bu molekülleri modelleme yöntemleri veya deneysel optimizasyon yöntemleri ile geliştirerek daha güvenli, kuvvetli, ve seçici HDAC inhibitörleri de elde edilebilir.

Anahtar Sözcükler: Kanserde epigenetik değişiklikler, İnsan HDAC10 proteininin homoloji modellemesi, Yapı temelli ilaç dizaynı, Yapı temelli ADMET öngörüsü, İzoforma özgü HDAC inhibitörleri.

ACKNOWLEDGEMENTS

First and foremost, praise be to Almighty ALLAH (S.W.T) on whom ultimately we depend for sustenance and guidance. I thank ALLAH for the gift of life and all that he has made possible for me to accomplish with it. His continuous grace and mercy kept me upright, ever more during the tenure of my research.

My deepest gratitude to my parents, **Alhaji Ibrahim Uba Abdullahi** and **Late Hajiya Halima Sani Spikin**, for the proper upbringing, unconditional support, and tremendous love they have offered me throughout my life — without which, of course, I could not have attained this milestone. My mother, **Hajiya Halima (Hajiya Aula)**, was known as a selfless, peaceful and supportive woman, whose ultimate goals in this world were to spread peace and offer motherly mentorship to all. It was her act of consoling that kept me steady throughout my educational pursuit. She departed this world peacefully, near the completion of this program. I pray to ALLAH to reward her for and benefit her from what I have accomplished in life as she continues to rest in eternal peace. I thank **all my family members** for their strength and fortitude in bearing this loss and for their continuous support as we navigate our way through this painful period.

I am hugely indebted to my wife, **Hussaina Salihi Bichi** who has always been supportive of my dreams, and who demonstrates great deal of patience and understanding, and of course, to **my son, Ibrahim (Khalil)**, born during the tenure.

My sincere appreciation to my humble supervisor, **Professor Dr**. **Kemal Yelekçi** for introducing me to this field, giving me all the freedom to pursue my research, and providing enabling environment for me to thrive, such as networking opportunity with the **European Cooperation in Science and Technology (COST) Epigenetic Chemical Biology Action CM1406**. Indeed, **Prof Yelekçi** offered me tremendous academic support towards satisfactory and timely completion of this dissertation.

Finally, I appreciate the encouragement support I received and continue to receive from **good friends and academic colleagues of mine** from **Nigeria, Turkey, and abroad.** I thank everyone who contributed in any way to my entire educational pursuit.

To my beloved parents,

Alhaji Ibrahim Uba Abdullahi

Late Hajiya Halima (Aula) Sani Spikin

LIST OF TABLES

LIST OF FIGURES

LIST OF ABBREVIATIONS

ADMET: Absorption, Distribution, Metabolism, Elimination and Toxicity

ADP: Adenosine Diphosphate

ADT: AutoDockTool

AMBER: Assisted Model Building with Energy Refinement

AML: Acute Myeloid Leukemia

Anti-PDGFRα mAb: Growth factor receptor α monoclonal antibody

AR: Androgen Receptor

BCL6: B-Cell Lymphoma 6

BLAST: Basic Local Alignment Search Tool

BLASTp: protein BLAST

CATS: Chemically Advanced Template Search

Caco-2: Human epithelial colorectal adenocarcinoma

CD1: Catalytic Domain 1

CD2: Catalytic Domain 2

CHARMM: Chemistry at Harvard Macromolecular Mechanics

CGenFF: CHARMM general Force Field

c-Myc: Avian myelocytomatosis virus oncogene cellular homolog

CoREST: Corepressor to Silencing Transcription Factor (REST)

CRC: Colonic adenomas and carcinomas

CREB3: Cyclic AMP-responsive element-binding protein 3

CTCL: Cutaneous T-cell lymphoma

DAC: Deacetylase domain

DFT: Density Functional Theory

DMB: Dynein Motor Binding

DNA: DeoxyriboNucleic Acid

DNMT3B: DNA (cytosine-5-)-methyltransferase 3 beta

DUD-E: Directory of Useful Decoys, Enhanced

E2F: E2 Transcription factor

EMEA: European Agency for the Evaluation of Medicinal Products

ER-1 or ER-α: Estrogen receptor 1 or ER-alpha

FAD: US Food and Drug Administration

GA: Genetic Algorithm

GAFF: General AMBER force-field

GH: Goodness of Hit

GROMOS: GROningen MOlecular Simulation

H2A: Histone 2A

H2B: Histone 2B

H3: Histone 3

H3K4me3: Trimethylation on lysine 4 of histone 3

H3K9ac: Acetylation on lysine 9 of histone 3

H3K9me2: Dimethylation on lysine 9 of histone 3

H3K9me3: Trimethylation on lysine 9 of histone 3

H3K27me2: Dimethylation on lysine 27 of histone 3

H3K27me3: Trimethylation on lysine 27 of histone 3

H4: Histone 4

HATs: Histone Acetyltransferases

Hda1: Yeast histone deacetylases 1

HBA: Hydrogen Bond Acceptor

HBD: Hydrogen Bond Donor

HDAC: Histone Deacetylases

HCC: Hepatocellular Carcinoma

HDACs: Histone Deacetylase

HIF-1α: Hypoxia-inducible factor 1 alpha

HRPC: Hormone Refractory Prostate Cancer

HSF-1: Heat-Shock Factor 1

HSP90: Heat Shock Protein 90

HTC: High-Throughput Screening

Hypo1: Hypothesis 1

ILP: Inductive Logic Programming

IUPAC: International Union of Pure and Applied Chemistry

JNK: Jun amino-terminal kinase

LMMC: Local Move Monte Carlo

LRD: Leucine-rich domain

M001-17: Model 1-17

MC: Monte Carlo

MD: Molecular Dynamics

MDS: Myelodysplastic Syndromes

mRNA: messenger RNA

miR: microRNA

MPNST: Malignant Peripheral Nerve Sheath Tumors (MPNST)

MT: Microtubule

MyoD: Myogenic Determination Factor

MlogP: Moriguchi model of octanol-H_2O partition coefficient, log P

MMP: Matrix Metalloproteinase

NAD+: Nicotinamide Adenine Dinucleotide

NAMD: Nanoscale Molecular Dynamics

NCBI: National Center for Biotechnology Information

NCOR1: Nuclear receptor co-repressor 1

NES: Nuclear Export Signal

NF-κB: Nuclear factor κ B

NIH: National Institutes of Health

NLS: Nuclear Localization Signal

NMR: Nuclear Magnetic Resonance

NURD: Nucleosome Remodeling and Deacetylating (complex)

NY-ESO1: Suitable target for the immunotherapy of human malignancies

OECD: Organization for Economic Co-operation and Development

OPLS: Optimized Potential for Liquid Simulations

OPLS-AA: OPLS all-atom force-field

P53: Tumor suppressor protein that protects from DNA damage

PDAC: Pancreatic Ductal Adenocarnoma

PI/NI: Positively and negatively ionizable groups

PML-RARα: Promyelocytic Leukemia Retinoic Acid Receptor Alpha

PLZF-RARα: Promyelocytic Leukemia Zinc Finger Retinoic Acid Receptor Alpha

PTCL: Peripheral T-cell Lymphoma

QSAR: Quantitative Structure–Activity Relationship

RAMD: Random Acceleration Molecular Dynamics

Rb: Retinoblastoma protein

Rg: Radius of gyration

RMSD: Root-Mean-Squared Deviation

RMSF: Root-Mean-Squared Fluctuations

RNA: Ribonucleic Acid

RPD3: Reduced Potassium Dependency-3

Ruleof5: Computational filter for oral absorption identical to the Lipinski's "Rule of Five"

SAHA: Suberoylanilide Hydroxamic Acid

SE14: Serine-glutamate tetradecapeptide repeat

SFN: Sulforaphane

siRNA: Small interfering RNA

Sirt: Sirtuin proteins

Smad: Contraction of Sma and Mad (Mothers against decapentaplegic)

SMRT: Silencing mediator for retinoic acid receptor and thyroid-hormone receptor

SNIP1: Smad nuclear-interacting protein 1

Stat: Signal transducer and activator of transcription

S+logP: Simulation Plus Model of octanol-H_2O partition coefficient, log P

TDAC: Tubulin Deacetylase

TMRAs: Tissue microarrays

TPSA: Topological Polar Surface Area

TRAIL: Tumor necrosis factor-related apoptosis-inducing ligand

TSA: Trichostatin A

TNBC: Triple-Negative Breast Cancer

TIQ: Tetrahydroisoquinoline

Tubacin: Tubulin Acetylation Inducer

XVOL: Exclusion volumes

YY1: Yin Yang 1

ZnF-UBP: Zinc finger ubiquitin-binding protease.

1. INTRODUCTION

Cancer is a term used to describe the uncontrolled growth of abnormal cells that can spread to other parts of the body. Cancer is generally treated with chemotherapeutic agents that act via different mechanisms. These include microtubule (MT) inhibitors such as Vincristine, Vinblastine, and Colchicine – these drugs bind tubulin and inhibit MT polymerization thereby blocking mitosis. Another drug, Taxol stabilizes the MT and blocks cell division (Cooper and Hausman, 2007). Alkylating agents which directly bind and inhibit DNA replication include Cytoxan and Temodar. Antimetabolites such as 5-fluorouracil and 6-mercaptopurine damage cell during S-phase. Antitumor antibiotics such as Anthracyclines interfere with enzymes involved in DNA replication. Other chemotherapeutic agents include topoisomerase inhibitors (Teniposide, doxorubicin, Irinotecan and Topotecan), mitotic inhibitors (Docetaxel, Estramustine, Paclitaxel, and Vinblastine), PARP inhibitors (Olaparib and Iniparib) and corticosteroids. Recently, Bcl-2 inhibitor (Venetoclax) was at phase II clinical trial for the treatment of relapsed or refractory chronic lymphocytic leukaemia with 17p deletion (Stilgenbauer et al., 2016). In addition, other types of cancer-fighting strategies that are not considered as chemotherapy include "Targeted therapies" with agents such as Imatinib, Gefitinib, Sunitinib and Bortezomib. Differentiating agents such as Retinoids, Bexarotene, and Arsenic trioxide. Hormone therapy (anti-estrogens, aromatase inhibitors, anti-androgens). Immunotherapy which involves the use of monoclonal antibody therapy, non-specific immunotherapies and adjuvants, immunomodulating drugs. For example, Anti-PD-L1 mAb (Atezolizumab) is at phase II trial in patients with locally advanced and metastatic urothelial carcinoma who have progressed following treatment with platinum-based chemotherapy (Rosenberg et al., 2016). Anti-PDGFRα mAb (growth factor receptor α monoclonal antibody) (Olaratumab) in combination with doxorubicin for treatment of soft-tissue sarcoma at randomized phase II trial (Tap et al., 2016).

Despite the above-mentioned cancer-fighting agents many have died and continue to die of cancers every year, prompting further investigation of complementary and alternative therapeutic targets of cancer.

Much effort has been invested in identifying genetic mutations resulting in constitutive activation of oncogenes or functional inactivation of tumor suppressor genes in various types of cancers (Knudson, 1971; Wooster et al., 1995; Jackson and Loeb, 1998; Xing, 2005; Beerenwinkel et al., 2007; Kadota et al., 2009; Montagut et al., 2012; Alexandrov et al., 2013; Burrell et al., 2013; Tamborero et al., 2013). Mutations early in the genesis of common cancers have also been identified, and these are likely to be associated with tumor initiation (Mamane et al., 2006; Bauer et al., 2014). In contrast, few specific genetic mutations have been linked to tumor progression (Yokota, 2000; Derynck et al., 2001; Furuta et al., 2010a, 2010b; Ichikawa et al., 2011; Takeda et al., 2015). This led to the investigation of epigenetic changes in various cancer pathogenesis (Novak, 2004; Feinberg and Tycko, 2004; Feinberg et al., 2006; Esteller, 2008; Risch and Plass, 2008; Sharma et al., 2009; Rodríguez-Paredes et al., 2011). Epigenetics refers to somatically heritable changes to molecular processes that occur without a change in the DNA sequence — and these changes can be induced by various factors (Eccleston et al., 2007; Armstrong, 2013).

The human genome is packaged into chromatin inside the nucleus of the cell. Nucleosomes are structural units of chromatin containing approximately 146 base pairs of DNA wrapped around a histone octamer: two copies each of histones H2A, H2B, H3, and H4. The lysine and arginine residues of histone protein are subject to an array of post-translational modifications. The best characterized of these are acetylation, methylation, and phosphorylation (Egger et al., 2004; Zhang and Dent, 2005). For each modification, there are enzymes responsible for either adding the appropriate mark or removing it. Active genes tend to be enriched with particular modifications (e.g. H3K4me3 and H3K9ac), whereas inactive genes have a different specific combination of marks (e.g. H3K9me2 and H3K9me3; H3K27me2 and H3K27me3). Even though there are no absolute rules and many active and inactive genes have overlapping

patterns of histone modifications, it is believed that aberrant epigenetic regulation may contribute to the progression of cancer (Egger et al., 2004; Zhang and Dent, 2005).

The N-terminal of histones (the histone 'tails') is crucial in maintaining the chromatin stability by allowing acetylation and deacetylation of various lysine residues within these regions. The acetylation state of histones is reversibly regulated by two classes of enzymes, histone acetyltransferases (HATs) and histone deacetylases (HDACs) (Roth et al., 2001; Richmond and Davey, 2003; Khorasanizadeh, 2004; Kouzarides, 2007). HDACs are components of transcriptional co-repressor complexes and catalyze the deacetylation of acetyl-L-lysine side chains in histone proteins thereby altering chromatin structure and repressing gene transcription.
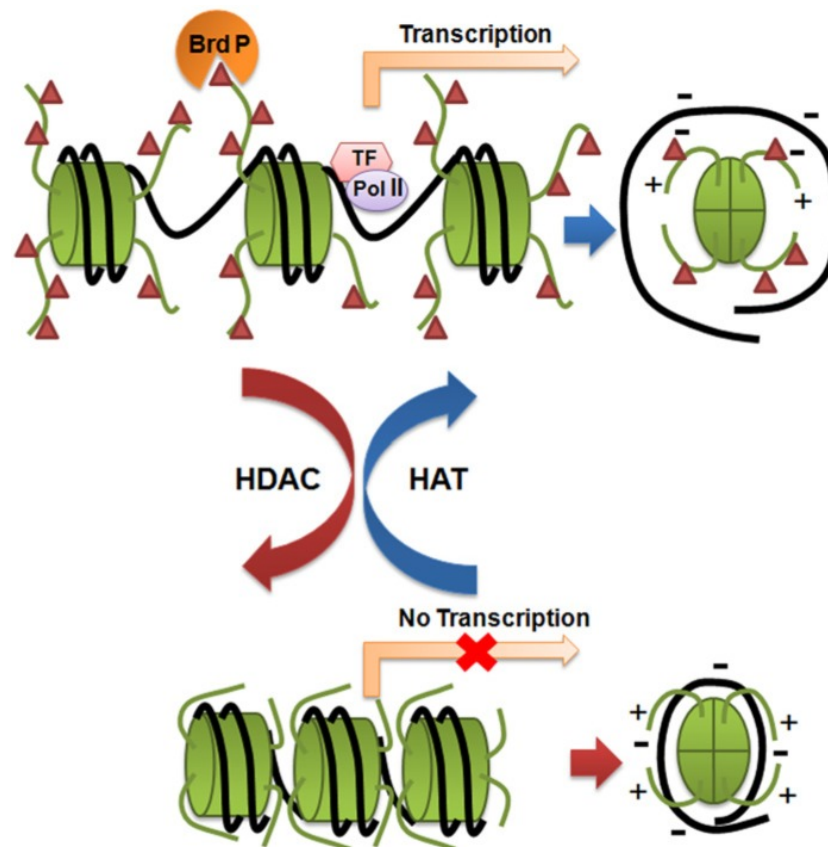
Figure 1. 1. Structure of nucleosome showing dynamics on reversible activities of HAT and HDAC for regulating gene expression through addition and removal of acetyl groups from the N-terminal region (histone tail) thereby respectively, allowing and repressing gene transcription.

This removal of acetyl group creates a positive charge that causes the negatively charged phosphate backbone of DNA to tightly coil and restrict chromatin structures (Figure 1.1). In addition, HDAC-promoted deacetylation of acetylated lysine is a key epigenetic marker read by bromodomains within transcription factor complexes that recruit RNA polymerases which further dampens the transcriptional activity of hypoacetylated chromatin. HDACs have been shown to act not only on histone proteins but also on non-histone substrates (Yang and Seto, 2008; Singh et al., 2010), and hence more generally designated as "lysine deacetylases". These non-histone proteins identified as HDAC substrates with diverse biological functions include α-tubulin, chaperons (HSP90), transcription factors (E2F, p53, c-Myc, NF-κB) , estrogen receptor 1 (ER 1), androgen receptor (AR), hypoxia-inducible factor 1 alpha (HIF-1α), signaling mediators (Stat3, Smad7), MyoD, β-catenin, retinoblastoma protein (pRb), DNA repair proteins (Ku70) and many more (Singh et al., 2010; Kim and Bae, 2011). Using high-resolution mass spectrometry 3,600 acetylation sites in 1,750 human proteins have been identified and these data suggested that lysine acetylation plays a major role in the regulation of nearly all nuclear functions and many cytoplasmic processes (Choudhary et al., 2009).

HDACs have already gained a lot of attention as epigenetic targets in various diseases including cystic fibrosis, muscular dystrophy, sickle cell anemia, HIV infection, and neurodegenerative and inflammatory disorders (Wiech et al., 2009; Wagner et al., 2010; Marks, 2010). HDACs are well-validated targets of anticancer drugs giving rise to a huge number of publications over the last 2 decades. They are implicated in the pathologies of various cancer types in which their genetic knockdown and pharmacological blockade have proven to be promising in reversing the malignant phenotypes.

To date, few HDAC inhibitors have been approved by the United State Food and Drug Administration (FDA) and these are Suberoylanilide hydroxamic acid (SAHA)-(Vorinostat), a pan-HDAC inhibitor for the treatment of cutaneous T-cell lymphoma in 2006; Romidepsin for the treatment of peripheral T-cell lymphoma (PTCL) in 2011;

Belinostat for the treatment of patients with relapsed or refractory PTCL in 2014 (Bolden et al., 2006) and recently (2015), Panobinostat for the treatment of multiple myeloma (Bailey et al., 2015).

Currently, many potential drugs are in clinical trials for use against various solid and non-solid cancers alone or in combination with other established cancer-fighting agents. Mocetinostat is an HDAC inhibitor with remarkable potency against HDAC1 compared with HDACs 2, 3 and 11, in the clinical trial for the treatment of leukemia or myelodysplastic syndromes (MDS) (Garcia-Manero et al., 2008). Entinostat and Tacedinaline are class I selective, in clinical trials for the treatment of advanced solid tumor (Pili et al., 2011; Prakash et al., 2001). MRLB-223 is in the preclinical trial as HDACs 1- and 2- selective inhibitor (Newbold et al., 2013). BG45 in combination with bortezomib is in the preclinical trial as a class I-selective inhibitor (McConkey et al, 2012). Rocilinostat (ACY-1215) is in phase II trial as an HDAC6-selective inhibitor (Cosenza et al., 2014). Tubacin, another HDAC6-selective inhibitor (Haggarty et al., 2003), is in various stages of trial for the treatment of cancers and neurodegenerative diseases. PCI-34051 is in the preclinical trial as an HDAC8-selective inhibitor (Balasubramanian, 2008).

HDAC inhibitors have the ability to influence a variety of cellular processes such as cell cycle arrest, immune modulation, angiogenesis, and apoptosis by targeting both histone and non-histone proteins (Bolden et al, 2006; Peng and Seto, 2011; Barneda-Zahonero and Parra, 2012). However, the exact mechanisms by which they work are unclear — epigenetic pathways are proposed (Richon et al., 2000; Vigushin and Coombes, 2004; Claude-Monneret, 2007).

HDAC inhibitors are generally classified into hydroxamic acids, benzamides, short chain fatty acids and cyclic peptides (Jung, 2001; Drummond et al., 2005; Bolden et al, 2006; Dokmanovic et al., 2007; Mottamal et al., 2015). Most of HDAC inhibitors obey a common "cap-linker-chelator" pharmacophore model. The chelator refers to the metal binding group that can engages zinc metal ion in the deep HDAC active site. The linker generally mimics lysine side chain and spans the narrow catalytic channel thereby

connecting the chelator to aromatic or macrocyclic cap group (Figure 1.2). The   cap
group capping group is a critical determinant of isoform selectivity.
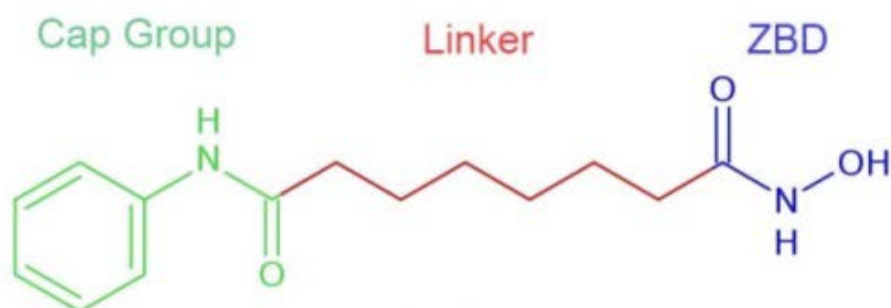
Figure 1. 2. Structure of Vorinostat (SAHA) showing the general pharmacophore features of HDAC inhibitors. The capping group, linker and zinc-binding domain are highlighted in green, red, and blue colors respectively.

To discover more potent and selective inhibitors, various rational drug design approaches have been applied. Computer-aided scaffold replacement method is used wherein a portion of a molecule could be replaced, or a group added to achieve a polar or steric interaction that may enhance the binding affinity or selectivity. In addition, a database of a large chemical library can be probed for potential inhibitors. For instance, both structure- and ligand-based virtual screening have been applied for identification of selective HDAC inhibitors (Wang et al., 2013; Huang et al., 2016). Structure- and ligand-based pharmacophore modeling (Chen et al., 2008), flexible docking, and three-dimensional QSAR (3D–QSAR) have been applied towards this goal (Nair et al., 2012). Micelli and Rastelli, (2015) suggested that the high plasticity of HDAC8 catalytic channel may provide the opportunity for achieving selectivity. Very recently, SAHA analogs modified at the C2 position displayed HDAC6/8 dual selectivity (Negmeldin et al., 2017). Previously, Wagner et al. (2013) speculated that HDAC6 selectivity could be achieved by careful choice of linker element only. Taha et al. (2017) evaluated C1-substituted tetrahydroisoquinoline (TIQ)-based HDAC8-selective inhibitors in neuroblastoma cell.

Here, because of abundant information regarding the sequences and structures of the HDACs, a combination of structure-based drug design techniques will be applied for the design of isoform-selective HDAC inhibitors.

Background

HDAC inhibitors have proven to be effective in cancer cases where HDACs are up-regulated. However, lack of selectivity of many of the HDAC inhibitors in clinical use and those at various phases of preclinical and clinical trials have contributed to the toxicities being reported. This is as a result of disruption of multiple signaling pathways by HDAC inhibitors (Peng and Seto, 2011; Barneda-Zahonero and Parra, 2012). It is believed that the continued identification of isoform-selective inhibitors can eliminate these undesirable adverse effects — the task that remains a major challenge to HDAC inhibitor design due to high structural similarity of the highly conserved active sites of HDACs. This poses difficulty in specific targeting of these individual isoforms. Class I HDACs 1-3 are components of repressive complexes crucial for tumorigenesis and share high structural homology. Aberrant recruitment of these complexes to the promoter of the tumor suppressor, p53 epigenetically represses transcriptional activity of the gene (Luo et al., 2000). Thus, anti-tumor effect of HDAC inhibitors is widely linked to class I HDACs inhibition (Dejligbjerg et al., 2008).

The original contribution of this study was designing potential isoform-selective inhibitors of each individual member of the human class I HDACs using a combined rational drug design. While undertaking this research work, the crystal structure of human HDAC6 catalytic domain 2 (CD2) was solved (PDB ID; 5EDU, release date 27-07-2016) (Hai and Christianson, 2016) — another druggable target in cancer. HDAC6 controls motility and metastatic potential of the cell through its influence on microtubule formation which allows progression and growth of malignancies by enabling them to survive even in the absence of adequate anchoring to the extracellular matrix (Witt et al., 2009). According to evolutionary origin, HDACs 6 and 10 are the

7

closest relative of each other. However, the experimental crystal structure of human HDAC10 has not been resolved to date. Therefore, here, a homology model of the enzyme was built using the recently-released X-ray crystal structure of *Danio rerio* (zebrafish) HDAC10 (PDB ID; 5TD7, release date 24-05-2017). Taken together, class I (HDACs 1, 2, 3 and 8) and class IIb (HDACs 6 and 10) are critical targets for anticancer drug design. Their individual pharmacological blockade may provide insight into their role in a given cancer pathogenesis. Moreover, additional isoform-selective HDAC inhibitors may help reduce the adverse effects associated with the current HDAC inhibitors in clinical use and trials.

Aim and Objectives

These studies are aimed at designing isoform-selective HDAC inhibitors as epigenetic-based anticancer agents that may serve as potential lead compounds for further optimization.

The following specific objectives are hereby pursued:

i. Comparative sequence and structural analyses of class I HDACs

ii. The design of isoform-selective HDAC inhibitors of individual members of class I HDACs by scaffold hopping approach.

iii. Identification of isoform-selective HDAC inhibitors of each individual member of the class I HDACs and a class IIb HDAC6 by structure-based virtual screening.

iv. The search for potential inhibitors of HDAC6 catalytic domain 2 via pharmacophore modeling

v. Homology modeling of human HDAC10 and the design of selective inhibitors by ligand-based virtual screening.

2. LITERATURE REVIEW

2.1 Histone Deacetylases

Histone deacetylases (HDACs) are enzymes that remove an acetyl group from the lysine sidechain in histone tail thereby regulating gene expression. There are eighteen genes encoding HDAC family members in human genome grouped into four classes based on their homology to yeast. Their size, cellular location, and enzymatic activity are given in Table 2.1 (Bernstein et al., 2000; Ruijter et al., 2003; Gregoretti et al., 2004). Classes I, II and IV are zinc-dependent whereas Class III are NAD^+ (nicotinamide adenine dinucleotide)-dependent enzymes. **Class I show strongest enzymatic activity among the HDAC classes and consist of HDACs 1, 2, 3 and 8 isoforms** (Zhang and Zhong, 2014). They share sequence homology with yeast reduced potassium dependency-3 (RPD3) and are localized in the nucleus of the cells (Bertos et al., 2001; Gregoretti et al., 2004; Brosch et al., 2008). Class II HDACs share sequence homology with the yeast histone deacetylase 1 (Hda1) and are further subdivided into Class IIa (HDACs 4, 5, 7 and 9) and Class IIb (HDAC6 and 10), and are primarily localized in the cytoplasm, but can be shuttled between the cytoplasm and nucleus depending on the phosphorylation status. The NAD^+-dependent Class III HDACs consist of seven mammalian sirtuin proteins (Sirt1–Sirt7) (Sir2 family), also shown to be critically important in carcinogenesis (Saunders and Verdin, 2007; Bosch-Presegue and Vaquero, 2011; McGuinness et al., 2011; Martinez-Pastor and Mostoslavsky, 2012; Roth and Chen, 2014; Chalkiadaki and Guarente, 2015). HDAC11 is the only known member of class IV HDAC with conserved residues in the catalytic core regions shared by both class I and II mammalian HDACs (Haberland et al., 2009).

Table 2. 1. Classification of HDACs by structure and cellular localization. Classes I and IIb HDACs studied here, are highlighted in bold.

HDAC	Size (a.a)	Location	Activity
Class I			
HDAC1	482	Nucleus	Deacetylase
HDAC2	488	Nucleus	Deacetylase
HDAC3	428	Nucleus	Deacetylase
HDAC8	377	Nucleus	Deacetylase
Class IIa			Deacetylase
HDAC4	1084	Nucleus/Cytoplasm	Deacetylase
HDAC5	1122	Nucleus/Cytoplasm	Deacetylase
HDAC7	952	Nucleus/Cytoplasm	Deacetylase
HDAC9	1011	Nucleus/Cytoplasm	Deacetylase
ClassIIb			
HDAC6	1215	Mainly cytoplasm	Deacetylase
HDAC10	669	Mainly cytoplasm	Deacetylase
Class III			
Sirt1	747	Nucleus/Cytoplasm	Deacetylase
Sirt2	389	Nucleus	Deacetylase
Sirt3	399	Mitochondria	Deacetylase
Sirt4	314	Mitochondria	ADP ribosyltransferase
Sirt5	310	Mitochondria	Demalonylase-desuccinylase
Sirt6	355	Nucleus	Weak deacetylase/ ADP-ribosyltransferase
Sirt7	400	Nucleus	Week deacetylase
Class IV			
HDAC11	347	Nucleus/Cytoplasm	Deacetylase

HDACs induce the formation of a compacted, transcriptionally repressed chromatin structure. HDACs 1-3 are components of multiprotein complexes in which they act as their catalytic subunit to repress gene expression. Class I HDACs are involved in cell proliferation and survival (Marks, 2010; Haberland et al., 2009). Human HDACs 1 and 2 are the product of recent evolutionary gene duplication, exhibit a high degree of homology (Gregoretti et al., 2004) and have undergone little functional divergence, although each of them has specific and distinct roles (Brunmeir et al., 2009).

HDACs 1–3 are assembled into at least five large multiprotein corepressor complexes are recruited to chromatin through interaction with repressive transcription factors (Watson et al., 2012). Significant enhancement of the enzymatic activity of HDACs 1–3 is observed when incorporated into their cognate corepressor complexes (Lechner et al., 2000; Guenther et al., 2001) These distinct corepressor complexes include NuRD (Xue et al., 1998), Sin3A (Hassig et al.,1997), CoREST (You et al., 2001) and MiDAC (Bantscheff et al., 2011) for HDACs 1 and 2 (Figure 2.1). HDAC3, however, is exclusively recruited to the SMRT/NCoR corepressor complex (Guenther et al., 2000). Very recently, Corin, a synthetic hybrid agent derived from a HDAC inhibitor (Entinostat) and an LSD1 inhibitor (tranylcypromine analog) targeting the CoREST complex, was designed to split into LSD1 and HDAC inhibitor components after LSD1 inactivation (Kalin et al., 2018). These authors sought to rationally incorporate multi-target pharmacology in this anticancer agent.

Structural and functional studies of class I HDACs in complex with their cognate corepressors have suggested that their activity is regulated by inositol 1,4,5,6-tetrakisphosphate (Ins(1,4,5,6)P4) present in the HDAC3:SMRT crystal structure (Figure 2.2) (Watson *et al*., 2016).
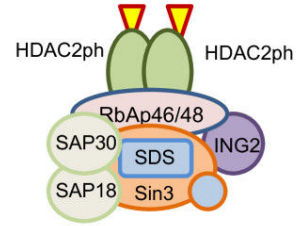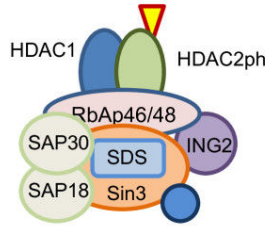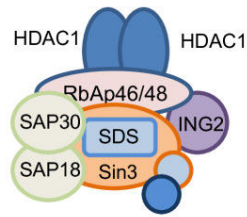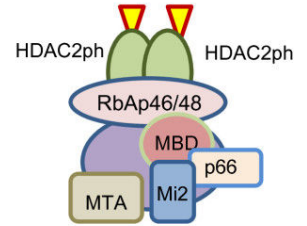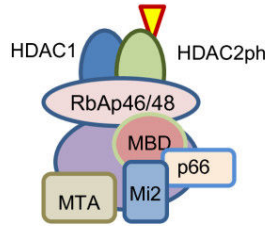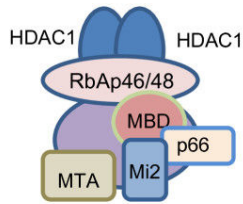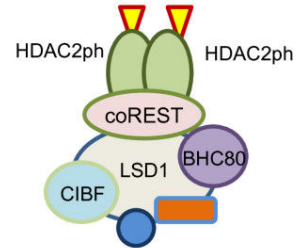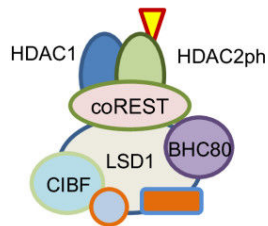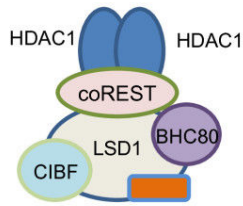
Figure 2. 1. Multiprotein complexes containing HDACs 1 and 2 homo- or heterodimers. HDAC2 requires to be in a phosphorylated form for multiprotein complex formation. Phosphorylation is shown in a red-outlined yellow triangle (Delcuve *et al*., 2012).
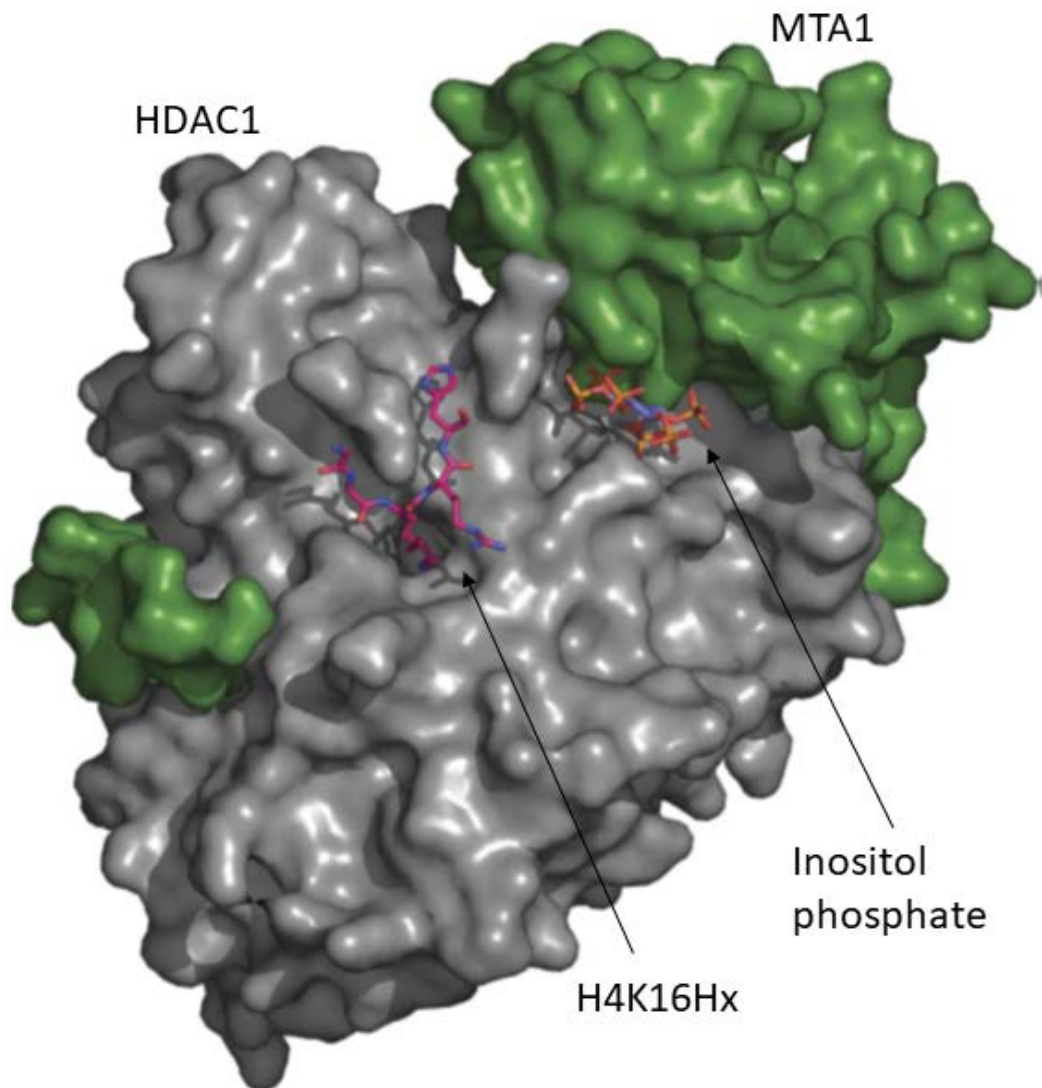
Figure 2. 2. Crystal structure of HDAC1:MTA1 with Inositol phosphate (InsP6) bound at the interface between the two proteins (Watson *et al*., 2016).

2.3 Mechanism of Histone Deacetylation

Structural analysis revealed that classes I, II and IV HDACs have similar active sites and are thought have a common catalytic mechanism. These metal-dependent HDACs catalyze the hydrolysis of acetyl-L-lysine side chains in histone and non-histone proteins to yield L-lysine and acetate. Removal of an acetyl group from substrate proceeds through a "charge-relay system" consisting of two adjacent histidine residues, two aspartic residues, and one tyrosine residue at the bottom of the pocket (Finnin et al.,

1999). The two active-site HIS-ASP "dyads" work as a general acid-base catalytic pair (Finnin et al., 1999; Somoza et al., 2004; Vannini et al., 2004, 2007; Dowling et al., 2008). The proposed mechanism is illustrated in Figure 2.3 below.
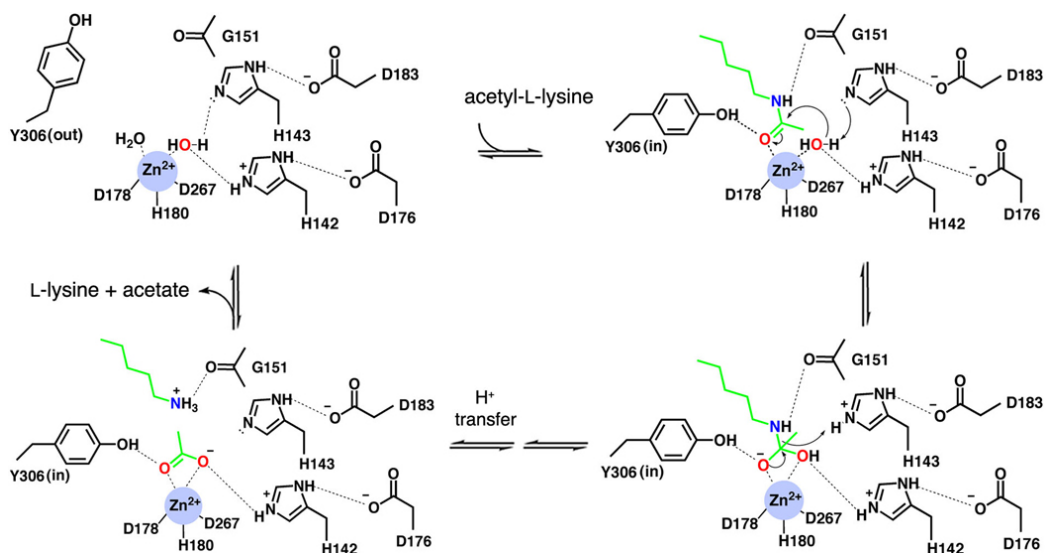
Figure 2. 3. Proposed mechanism of HDAC catalysis (Lombardi et al., 2011).

With reference to HDAC8, the active-site transition metal ion (Zn^{2+}) and H143 acting as a general base promote the nucleophilic attack of a metal-bound H_2O molecule on the zinc-coordinated carbonyl group of the acetyl-L-lysine substrate. Upon proton abstraction, the nucleophilic lone pair on the metal-bound H_2O molecule becomes available (e.g., the electron pair of the broken O-H bond could add to the π^* orbital of the substrate carbonyl group). The oxyanion of the tetrahedral intermediate and its flanking transition states are stabilized by zinc coordination as well as H-bond interactions with Y306, H143, and H142. H143 serves as a general acid catalyst to facilitate the collapse of the tetrahedral intermediate to form acetate and L-lysine after an intervening proton transfer. Lombardi et al. (2011) speculated that the side chain of Y306 might undergo a conformational transition from an "out" conformation to an "in" conformation to accommodate substrate and subsequent catalysis, based on the conformational mobility of the corresponding residue in related enzymes (Y976 in H976Y HDAC4 (Bottomley et al., 2008) and Y323 in APAH).

2.4 The Role of Class I HDACs in Cancer Pathogenesis

A study on post-translational modifications to histone H4 of normal tissues and cancer cell lines suggests that "global loss of monoacetylation at Lys16 and trimethylation at Lys20 of histone H4 is a common hallmark of human cancer cells" (Fraga et al., 2005). The aberrant expression of HDAC1 tend to be common in cancers and was associated with dedifferentiation, enhanced proliferation, and invasion (Witt et al., 2009). Overexpressed HDAC1 upregulated hypoxia-inducible factor-α and promoted angiogenesis in pancreatic carcinoma (Miyake et al., 2008). Knockdown of HDAC1 by siRNA in cancer cells could arrest cell cycle either at the G1 phase or at the G2/M transition, resulting in the loss of mitotic cells, cell growth inhibition, and increased apoptosis (Glaser et al., 2003; Senese et al., 2007). Halkidou et al. (2004) found HDAC1 to play roles in cell proliferation and the development of prostate cancer and thus proposed a mechanism for HDAC1 nuclear recruitment. Overexpression of HDAC1 might play a critical role in the development of hepatocellular carcinoma via systemic regulation of mitotic effectors (Xie et al., 2012). HDAC1 was indicated in impaired spermatogenesis and testicular cancer (Cacan et al., 2014). HDAC1 was shown to interact with ER- 1 *in vitro* and *in vivo*, and to suppress ER-1 transcription activity thereby playing a role in breast cancer progression (Kawai et al., 2003). Overexpression of HDAC1 independently predicts biochemical recurrence and is associated with rapid tumor cell proliferation and genomic instability in prostate cancer (Burdelski et al., 2015). High expression of Smad nuclear-interacting protein 1 (SNIP1) correlates with poor prognosis in non-small cell lung cancer. SNIP1 interferes with the recruitment of HDAC1 to Rb *in vitro* (Jeon et al., 2013). A study aimed at understanding the molecular mechanism of ER-1 gene silencing showed that p53 protein binds to the promoter of ER-1 through direct interaction with HDAC1 (Arabsolghar et al., 2013). A cancer-testis antigen, NY-ESO1 (suitable target for the immunotherapy of human malignancies), requires the sequential recruitment of the HDAC1-mSin3a-NCOR, Dnmt3b-HDAC1-Egr1 repressor complexes (Cartron et al., 2013). A significant reduction in the HDAC activity of Sin3A, NuRD, and CoREST corepressor complexes was caused by germline deletion of HDAC1 (Dovey et al., 2010). Pharmacological blockade and specific genetic elimination of HDACs 1 and 2

was found to reduce the expression of mutant p53 mRNA and protein levels (Stojanovic et al., 2017).

Although functional redundancy between HDACs 1 and 2 exists (Haberland et al., 2009), HDAC2 was shown to be independently implicated in various types of human cancers. The up-regulation of tumor-promoting genes, such as those of tyrosine kinases, mediators of cell cycle progression and angiogenic factors by HDAC2 mutant cells in human cancer has been reported (Ropero et al., 2008). Evaluation of HDAC2 expression and the acetylation of histones H4K12 and H3K18 in colonic adenomas and carcinomas (CRC) revealed that HDAC2 plays a significant role in CRC progression (Ashktorab et al., 2009). HDAC2 inhibition in the pancreatic cancer cell lines induced apoptosis by sensitization of the tumor necrosis factor-related apoptosis-inducing ligand (TRAIL) (Schüler et al., 2010). HDAC2 maintains HIF-1α stability, which in turn leads to the increase in cell invasion/migration ability in oral cancer progression (Chang et al., 2011). Aberrant expression of HDAC2 accelerated the proliferation of gastric cancer cells by deregulating expressions of G1/S cell cycle proteins and restored the activity of proapoptotic factors (Kim et al., 2013). HDAC2 was involved in repressing micro-RNA 183 (miR-183) tumor suppressive properties in neuroblastoma (Lodrini et al., 2013). Blockade of HDAC2 by Valproic acid significantly reduced adenoma formation in mice (Zhu et al., 2004). High expression of HDAC2 was also reported in hepatocellular carcinoma (HCC)(Kim et al., 2014; Noh et al., 2014). Class I HDACs are highly expressed in prostate cancer — specifically, HDACs 1 and 2 are significantly associated with tumor dedifferentiation (Weichert et al., 2008). HDAC2 was associated with decreased intestinal tumor rates in HDAC2-mutant mice (Zimmermann et al., 2007).

Several studies reported the overexpression of HDAC3 in diverse cancer types. High expression of HDAC3 and other class I HDACs in colon cancer is associated with deregulation of p21expression (Wilson et al., 2006; Spurling et al., 2008). Godman et al. (2008) propose that HDAC3 overexpression alters the epigenetic programming of colon cancer cells. Cell cycle arrest at G2/M transition phase was noted over the period of 6-72 hours in Sulforaphane (SFN)-treated colon cancer cells due to SFN-induced dissociation of HDAC3/SMRT complexes (Rajendran et al., 2011). The

immunhistochemical expression of class I HDACs analyzed on tissue microarrays (TMAs) from 238 patients with primary breast cancer showed that HDACs 1-3 are differentially expressed in breast cancer (Müller et al., 2013). In another study, HDAC3 specifically, repressed cyclic AMP-responsive element-binding protein 3 (CREB3)-mediated transcriptional activation and chemotactic signaling in human metastatic breast cancer cell (Kim et al., 2010). HDAC3 in corepressor complex is implicated in microRNA-29 (miR-29) repression by MYC in aggressive B-Cell Lymphomas (Zhang et al., 2012). The suppression of HDAC3 enhances apoptosis induced by paclitaxel in newly diagnosed human maxillary cancer cells *in vitro* and *in vivo*, suggesting the enzyme as a potential chemotherapeutic target for the treatment of these diseases (Narita et al., 2010).

HDAC8 is structurally unique compared to other class I isoforms and is not considered a viable target for efficient cancer treatment, probably because it is not a component of any corepressor complexes. Recently, with intensifying research in this field, the roles of HDAC8 in the pathogenesis of certain types of cancers have started to be uncovered. For instance, HDAC8 mRNA was upregulated in urothelial cancer tissues and urothelial cancer cell lines compared to benign controls (Lehmann et al., 2014). HDAC8 inhibition was speculated to be a potential chemotherapeutic target in malignant peripheral nerve sheath tumors (MPNST) — an aggressive sarcoma that is notoriously therapy resistant (Lopez et al., 2015). In another study, HDAC8 inhibition by SAHA and sodium butyrate reduced the binding of transcription factor Yin Yang 1 (YY1) to human p53 promoter in triple-negative breast cancer (TNBC) treatment (Wang et al., 2016). A study on Taiwanese breast cancers revealed that significant hypomethylation of the HDAC8 promoter is correlated with overexpression of HDAC8 and breast cancer progression (Hsieh et al., 2016). Specific inhibition of HDAC8 can suppress the growth of neuroblastoma cells via up regulation of microRNA-137 (miR-137) (Zhao et al., 2017) – a short non-coding RNA molecule that regulates the expression levels of other genes by various mechanisms.

Class I HDACs are recruited by chimeric oncoproteins such as PML-RARα, PLZF-RAα, and AML1-ETO (seen in leukemia), to mediate aberrant gene silencing

(Johnstone and Licht, 2003). Class I HDACs can also interact with non-chimeric oncogenes such as BCL6, whose repressive activity is controlled by dynamic acetylation (Bereshchenko et al., 2002). Data indicate that chromatin inactivation mediated by class I HDACs and DNA methylation is a critical component of ER-1 silencing in human breast cancer cells (Kawai et al., 2003). Studies cited above and many more reported class I HDACs to be directly or indirectly involved in the pathogenesis of various cancers via mainly, epigenetic mechanisms. Therefore, there are sufficient evidence for considering the individual isoforms of class I HDAC family as crucial targets for epigenetics-based anticancer drug design.

2.5 The Role of Class IIb HDACs in Cancer Pathogenesis

HDAC6 is the largest HDAC yet identified in humans with 1215 amino acids (Grozinger et al., 1999). HDAC6 is identified as the first HDAC to be actively maintained in the cytoplasm (Verdel et al., 2000) and it predominates in the cytoplasm due to the nuclear export signal (NES) and serine-glutamate tetradecapeptide repeat (SE14) motifs (de Ruijter et al., 2003; Boyault et al., 2007). HDAC6 is unique among HDACs harboring 2 homologous catalytic domains CD1 and CD2 (Verdel and Khochbin, 1999), and a conserved cysteine- and histidine-rich domain in its C-terminus part – also present in ubiquitin-specific proteases and hence named zinc finger ubiquitin-binding (ZnF-UBP) (Seigneurin-Berny et al., 2001) (Figure 2.4). HDAC6 ZnF-UBP domain organization allows its binding to monomeric ubiquitin (Kd = 60 nM), which is the highest known affinity for ubiquitin binding among all known ubiquitin-interacting proteins (Boyault et al., 2006). Both catalytic domains are fully functional and contribute independently to the overall activity of the HDAC6 isoform. Some studies suggested that both HDAC6 catalytic domains are required for full tubulin deacetylase (TDAC) activity (Zhang et al., 2006), however, in other studies, the TDAC activity is attributed to the second domain (Haggarty et al., 2003; Zou et al., 2006).
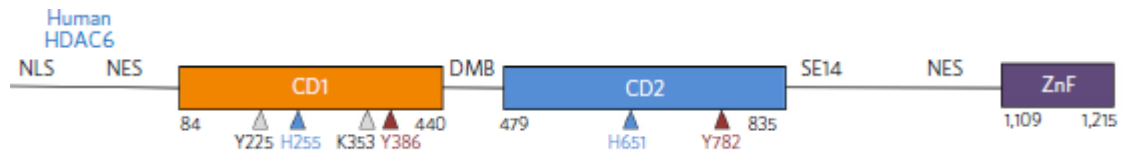
Figure 2. 4. Domain organization: NLS, nuclear localization signal; NES, nuclear export signal; DMB, dynein motor binding; SE14, serine-glutamate tetradecapeptide repeat; ZnF, zinc-finger ubiquitin-binding domain (Hai and Christianson, 2016).

HDAC6 deacetylates lysine 40 (K40) in α-tubulin subunit of the microtubule (Hubbert et al., 2002), thereby regulating microtubule dynamics — thus HDAC6 inhibition leads to hyperacetylation of α-tubulin and suppression of microtubule dynamics, whereas overexpression of HDAC6 reduces tubulin acetylation and increases cell motility (Parab et al., 2015). Thus, HDAC6 deacetylase functions at the "heart of a cellular regulatory mechanism capable of coordinating various cellular functions largely relying on the microtubule network" (Boyault et al., 2007). HDAC6 also regulates the chaperone activity of HSP90 (Kovacs et al., 2005), thereby mediating various cellular events in response to different stressful stimuli. The enzyme was shown to mediate the transport of misfolded protein in the proteasome system through its simultaneous interaction with ubiquitin and dynein motors (Kawaguchi et al., 2003). Subsequently, p97/VCP, upon binding to HDAC6, can extract HDAC6 bound to ubiquitinated proteins and therefore allows their further processing (Goldberg et al., 2002). It is also a critical component of stress granules involved in the stress response (Kwon et al., 2007).

The overexpression of HDAC6 in a variety of cancer cell lines and mouse tumor models has been reported. A study on 135 female patients with invasive breast cancer suggested that HDAC6 mRNA expression may have potential both as a marker of endocrine responsiveness and also as a prognostic indicator in breast cancer (Zhang et al., 2004). HDAC6 regulates cell motility and prognosis in estrogen receptor-positive breast cancer via estrogen signaling (Saji et al., 2005). HDAC6 was found to be highly expressed in low-grade and high-grade ovarian carcinomas compared with benign lesions and immortalized ovarian surface epithelium cell lines (Bazzaro et al., 2008).

Investigation in prostate epithelial cells and mouse embryonic fibroblast cells revealed that oncogenic Ras can lead to up-regulation of HDAC6 (Lee et al., 2008), suggesting that HDAC6 plays a major role in the survival of tumor cells. In another study, HDAC6 was shown to regulate AR hypersensitivity and nuclear localization, mainly via modulating HSP90 acetylation in castration-resistant prostate cancer (Ai et al., 2009).

HDAC6 expression was also upregulated in primary oral squamous cell lines and its level of expression correlated with primary tumor stage (Sakuma et al., 2006). In a different study, HDAC6 was consistently overexpressed in primary acute myeloid leukemia (AML) blasts and in some myeloblastic cell lines (Bradbury et al., 2005). The expression levels of HDAC6 in hepatocellular carcinoma (HCC) was explored by Ding et al. (2013) and in this study, both mRNA and protein levels of HDAC6 were up-regulated in HCC tissues and cell lines by inhibiting P53 transcriptional activity. Contrarily, HDAC6 was shown to have a tumor suppressor function, and the molecular mechanism of this function is by induction of JNK-mediated Beclin 1-dependent autophagic cell death in liver cancer and the loss or suppression of tumor suppressor function of HDAC6 is caused by induction of miR-221 through coordinated JNK/c-Jun- and NF-κB-signaling pathways during liver tumorigenesis (Bae et al., 2015).

HDAC6, like all other HDACs, is inhibited by TSA. However, HDAC6 is uniquely resistant to the potent HDAC inhibitors Trapoxin-B and Sodium butyrate and thus these drugs were used to show that HDAC6 is a deacetylase for tubulin in vivo, and in vitro (Matsuyama et al., 2002; Haggarty et al., 2003; Zou et al., 2006). HDAC6 was found not to interact with histones *in vivo*, whilst it was able to deacetylate histones *in vitro* (Grozinger et al., 1999). This finding prompted an investigation of HDAC inhibitor that mediates acetylation of non-histone proteins. One of these inhibitors, Tubacin (Tubulin acetylation inducer), possesses HDAC6 inhibition activity. Tubacin was isolated via a multidimensional chemical genetic screen and cell-based assay targeting acetylation of non-histone protein. Contrary to the mechanism through which other HDAC inhibitors act, Tubacin was shown to inhibit the deacetylation of tubulin in mammalian cells without affecting the level of histone acetylation, gene expression, or cell cycle progression (Haggarty et al., 2003).

HDAC10 has an active deacetylase domain (DAC) and a catalytically inactive leucine-rich domain (LRD) (Tong et al., 2002; Kao et al., 2002; Guardiola et al., 2002). Scientists have begun to elucidate the function of HDAC10 in recent years and determined that it plays a role in homologous recombination (Kotian et al., 2011). HDAC10 suppresses expression of matrix metalloproteinase (MMP) 2 and 9 genes, which are known to be critical for cancer cell invasion and metastasis. At the molecular level, HDAC10 binds to MMP2 and -9 promoter regions, reduces the histone acetylation level, and inhibits the binding of RNA polymerase II to these regions, promotes autophagy and survival in neuroblastoma cells (Oehme et al., 2013), suppresses cervical cancer metastasis (Song et al., 2013). HDAC10 is highly expressed in lung cancer cells and is required for tumor growth and survival (Yiwei et al., 2016). These findings are consistent with those mentioned in a recent report stating that HDAC10 regulates the cell cycle (Li et al., 2015).

2.6 HDAC Inhibitors for Cancer Therapy

HDAC inhibitors have proven to be effective in the treatment of the hematological and solid tumor. HDAC inhibitors induce hyperacetylation of transcription factors, resulting in a permissive or more open chromatin configuration, leading to potential reactivation of aberrantly suppressed (e.g., tumor suppressor) genes (Glance, 2002; Wilson et al., 2010). They have been reported to induce apoptosis and growth arrest in tumor cells by facilitating tumor cell differentiation and promoting the expression of the silenced of proapoptotic genes (Camphausen and Tofilon, 2007; Botrugno et al., 2009; Buchwald et al., 2009; Ellis and Pili, 2010; Thurn et al., 2011). However, The exact mechanisms by which the compounds may work are unclear, but epigenetic pathways are proposed (Vigushin and Coombes, 2004; Monneret, 2007; Mack, 2010). HDAC inhibitors can induce apoptosis by re-establishing expression of the key co-suppressor proteins such as $p21^{(Cip1/WAF1)}$, independent of p53 (Huang et al., 2005). The structural classes and selectivity of HDAC inhibitors are given in Table 2.2 below.

Table 2. 2. Sructural classes of HDAC inhibitors and their enzyme specificity. Approved drugs are highlighted in bold.

HDAC inhibitor	Class	Selectivity
Trichostatin A	Hydroxamic acid	I, II IV
Vorinostat (SAHA)	Hydroxamic acid	I, II IV
Abexinostat(PCI-24781)	Hydroxamic acid	I and II
Pracinostat (SB939)	Hydroxamic acid	I, II and IV
Resminostat	Hydroxamic acid	I and II
Givinostat (ITF-2357)	Hydroxamic acid	I and II
CUDC-101	Hydroxamic acid	I and II
Panobinostat	Hydroxamic acid	I, II and IV
Belinostat	Hydroxamic acid	I
Romidepsin	Cyclic Peptide	I
Apicidin	Cyclic Peptide	I
Entinostat	Benzamide	I
Mocetinostat	Benzamide	I and IV
Tacedinaline	Benzamide	I
Valparoic acid	Short chain fatty acid	I
Butyrate	Short chain fatty acid	I and II

Based on their chemical structures, HDAC inhibitors are classified into:

(1) Hydroxamic acids: e.g Vorinostat, TSA, Panobinostat (LAQ824), Belinostat (PXD101) (Meinke and Liberator, 2001; Kelly et al., 2003, 2005; Plumb et al., 2003; Remiszewski, 2003; Garcia-Manero, Yang, et al., 2008; Kato et al., 2007; Qian et al., 2006).

(2) Aliphatic (short-chain fatty) acids: e.g. Valproic acid, Butyric acid.

(3) Benzamides: e.g CI-994, Entinostat (MS-275), Mocetinostat (MGCD0103) (Prakash et al., 2001; Richards et al., 2006; Gojo et al., 2007; Garcia-Manero et al., 2008)) and

(4) Cyclic tetrapeptides: e.g. Romidepsin (FK228) (Byrd et al., 2005; Bolden et al., 2006).

Vorinostat is a pan HDAC inhibitor with IC50 of ~10 nM in cell-free assays (Schölz et al., 2015), and was the first HDAC inhibitor to be approved by FDA for the treatment of cutaneous T-cell lymphoma (CTCL) in 2006 (Mann et al., 2007). Romidepsin, a bicyclic peptide, is a potent inhibitor of HDAC1 and HDAC2 with IC50 of 36 nM and

47 nM in cell-free assays, respectively (Bantscheff et al., 2011), and was approved by FAD in 2009 for CTCL and other peripheral T-cell lymphoma (PTCL) in patients who have received at least 1 prior therapy (Ellis and Pili, 2010). Belinostat is an HDAC inhibitor with IC50 of 27 nM in a cell-free assay (Bantscheff et al., 2011), approved by FDA for use against PTCL in 2014 (Lee et al., 2015). Recently, Panobinostat (LBH589), a broad-spectrum HDAC inhibitor with IC50 of 5 nM in a cell-free assay (Schölz et al., 2015), gained approval for treatment of multiple myeloma in 2015 (Laubach et al., 2015).

Several HDAC inhibitors are in different phases of clinical investigation either alone or in combination with other cancer-fighting agents. Some preclinical studies suggest improved tumor cell destruction by combining HDAC inhibitors with radio-(chemo) therapy (Kelly et al., 2003; Vigushin and Coombes, 2004; Thurn et al., 2011). Phase III clinical trials of Valproic acid (as Magnesium valproate) for cervical cancer (Chavez-Blanco et al., 2005) and ovarian cancer was completed (Duenas-Gonzalez et al., 2014). Mocetinostat is a potent HDAC inhibitor with most potency for HDAC1 (IC50 = 0.15 μM) in a cell-free assay, show 2- to 10- fold selectivity against HDACs 2, 3, and 11 and is in clinical trials for treatment of various cancers including, Hodgkin lymphoma, acute myeloid leukemia and follicular lymphoma (Schölz et al., 2015). Abexinostat show activity against HDAC1 with Ki of 7 nM, modest potency against HDACs 2, 3, 6, and 10 and > 40-fold selectivity for HDAC8 (Schölz et al., 2015). The phase II clinical trials of Abexinostat for sarcoma (Sholler et al., 2013) and for lymphoma have started (Morschhauser et al., 2015). Entinostat is a potent inhibitor of HDACs 1 and 3 with respective IC50 of 0.51 μM and 1.7 μM in cell-free assays (Schölz et al., 2015), and has entered phase III clinical trial for Hodgkin lymphoma, breast cancer and lung cancer (Tan et al., 2010). The phase II clinical trial of SB939 for hormone refractory prostate cancer (HRPC) has started (Chu et al., 2015) after a successful phase I trial (Razak et al., 2011). Resminostat (4SC-201) selectively inhibits HDACs 1/3/6 with IC50 of 42.5 nM/50.1 nM/71.8 nM respectively, with modes potency for HDAC8 (IC50 of 877 nM), underwent clinical trials for hepatocellular carcinoma (R. et al., 2010), and was found to inhibit proliferation and induces apoptosis in multiple myeloma cells (Mandl-Weber et al., 2010). Givinostat (ITF2357) induces potent caspase-dependent apoptosis in human

lymphoblastic leukemia (Ying et al., 2016). Quisinostat (JNJ-26481585) is a second-generation HDAC inhibitor with highest potency for HDAC1 (IC50 of 0.11 nM) in a cell-free assay, and > 30-fold selectivity against HDACs 3, 5, 8, and 9; shows modest potency for HDACs 2, 4, 10, and 11; and lowest potency to HDACs 6 and 7 (Suzuki et al., 2016). A selective inhibitor of HDAC2, Kevetrin passed pharmacokinetic and pharmacodynamic studies in patients with advanced solid tumors (Shapiro et al., 2015)

The clinical trial for CUDC-101 for various cancers has started (Lai et al., 2010; Wang et al., 2013; Jin et al., 2014; Galloway et al., 2015). CUDC-101 was also found to inhibit class I/II HDACs with IC50 of 4.4 nM (Shimizu et al., 2014; Galloway et al., 2015). AR-42 has anticancer activity with IC50 of 30 nM, currently at phase 1 trials (Lin et al., 2010; Lucas et al., 2010; Zhang et al., 2011; Burns et al., 2013; Lee et al., 2013; Mims et al., 2013; Li et al., 2015; Tseng et al., 2015; Xu et al., 2015). CHR-2845 (Ossenkoppele et al., 2010; Zabkiewicz et al., 2016), CHR-3996 (Banerji et al., 2012) and 4SC-202 (Zhijun et al., 2016) show selectivity for advanced hematological cancers, whereas CG200745 show efficacy against solid tumors (Hwang et al., 2012; Oh et al., 2012). Ricolinostat (ACY-1215) show selectivity for HDAC6 with IC50 of 5 nM in a cell-free assay. It is > 10-fold more selective for HDAC6 than HDACs 1, 2, 3 with slight activity against HDAC8 (Dhanyamraju et al., 2015; Terranova-Barberio et al., 2016; Hasanov et al., 2017). Ricolinostat is currently under evaluation for multiple myeloma in combination with bortezomib and with lenalidomide (Yee et al., 2014). ME-344 is intended for solid refractory tumors (Bendell et al., 2015). Different HDAC inhibitors are continuing to be evaluated on other types of cancers. Most recently, TSA in combination with Gemcitabine showed enhanced apoptosis-inducing capability (compared to SAHA) against pancreatic ductal adenocarcinoma (PDAC) cells through depletion of HDACs 1, 7 and 8 (Cai et al., 2018). NDACI054 was very effective at very low concentrations (2.5 nM) in combination with significant radiosensitization of tumor cells grown under more physiological cell culture conditions (Hehlgans et al., 2013). In a recent study, SAHA induced radiosensitization in lung carcinoma cells A549, thereby killing the cancer cells in combination with γ-rays, proton, and carbon ion exposure (Gerelchuluun et al., 2018).

Both peptide-based macrocyclic (Olsen et al., 2012; Rajak et al., 2013) and non-peptide macrocyclic HDAC inhibitors have been shown to possess selective and potent anti-proliferative activity against human lungs, prostate and breast cancer cell lines (Oyelere et al., 2009; Mwakwari et al., 2010; Tapadar et al., 2015).

Desirable alteration in a gene, mRNA and protein expression, protein-protein interactions, the shift from euchromatin to heterochromatin, and signal transduction have been shown to be the fates of tumor cells following treatment with HDAC inhibitor. (Roskelley et al., 1994; Lee et al., 2007; Pampaloni et al. 2007; Eke et al., 2013). HDAC inhibitors can induce both mitochondria-mediated apoptosis and caspase-independent autophagic cell death (Shao et al., 2004).

2.7 Rational Drug Design Techniques

Advances in human genome sequencing have increased the number of new therapeutic targets for drug discovery. At the same time, high-throughput crystallography and nuclear magnetic resonance (NMR) methods have contributed to the acquisition of the atomic structures of proteins and protein-ligand complexes (Langer and Hoffmann, 2001; Bajorath, 2002; Kitchen et al., 2004). These allow biocomputation to continue to thrive as an indispensable component of structure-based drug discovery. The current approach to structure-based drug design methods allow for the design of ligands containing the necessary features for surface complementarity with target receptor or enzyme (Mandal et al., 2009; Press, 2013). Selective interaction of high-affinity ligands with target proteins interferes with specific cellular processes, leading ultimately, to the desired pharmacological effects (Urwyler, 2011). Molecular modeling procedures reduce the cost of discovering new drug — as only most promising compounds are synthesized (Wilson and Lill, 2011). These compounds are subject to evaluations of biological properties such as potency, affinity, and efficacy using diverse experimental platforms (Fang, 2012). Molecular modeling approaches such as molecular docking, molecular dynamics, homology modeling and virtual screening are applied alone or in combination towards structure-based drug design (Figure 2.5).
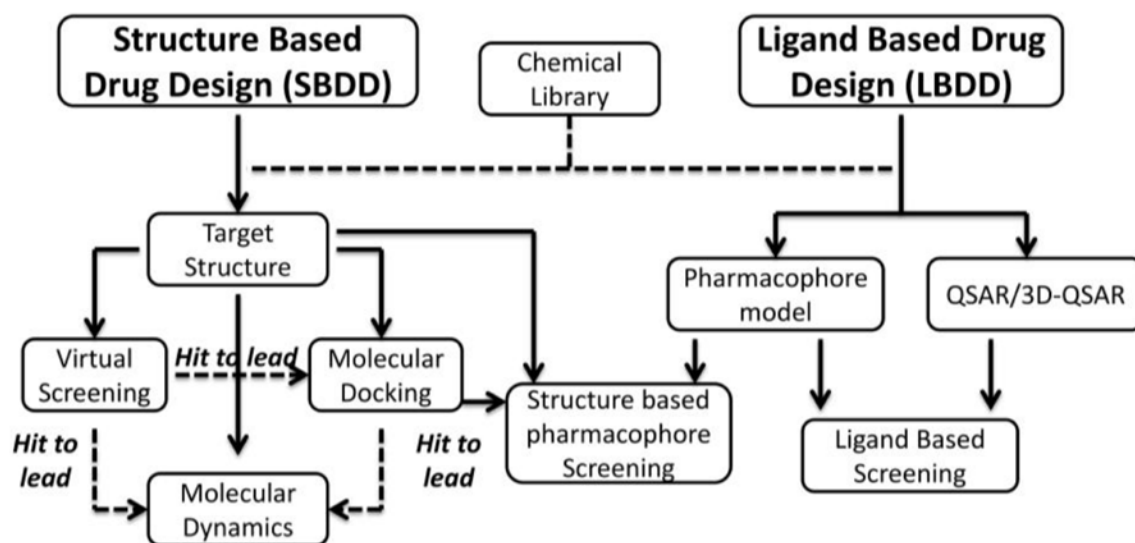
Figure 2. 5. Schematic representation of *in silico* rational drug design techniques
(Cozza, 2017).

2.7.1 Molecular docking

Since the development of the first algorithms in the early 1980s, molecular docking
became an essential tool in drug discovery (López-Vallejo et al., 2011). The main
objective of molecular docking is to predict the correct binding mode of a ligand in the
binding pocket of a target. This method is routinely used to gain insight into the
interaction between the enzyme and its inhibitors. Several docking studies have been
reported towards this goal in the literature (Mai et al., 2005; Selvam et al., 2005; Tewari
et al., 2010; Shultz et al., 2011; Brunsteiner and Petukhov, 2012; Yao et al., 2014; Abd
El-Karim et al., 2015; Zhang et al., 2015). The binding energy is predicted by
application of the various scoring function. The optimized docked conformer is one
with the lowest free energy of binding. The final estimated free energy of binding
(ΔGbind) is modeled in terms of dispersion and repulsion (ΔGvdw), electrostatic
(ΔGelec), H-bond (ΔGhbond), torsional free energy (ΔGtor), desolvation (ΔGdesolv),
final total internal energy (ΔGtotal) and unbound system's energy (ΔGunb) (Walters et
al., 1998). There are two basic steps in docking process: prediction of the ligand
conformation, its position and orientation within these sites (referred to as pose), and
assessment of the binding affinity.

The ligand-receptor binding mechanism was elucidated to be "the lock-and-key theory". In this theory, Fischer (Fischer, 1894) proposed that ligand fits into the receptor's binding pocket like lock and key. The earliest reported docking methods (Kuntz et al., 1982; Kollman, 1994) were based on this theory and both the ligand and receptor were treated as rigid bodies. Later, Koshland, (1963) put forward the "induced-fit" theory in which he states that the active site of the protein undergoes conformational changes to accommodate ligands as the ligands interact with the protein. According to this theory, both ligand and receptor should be treated as flexible during docking. This theory describes the binding events more accurately than the rigid treatment considering the dynamic behavior of the protein in the real biological environment. The most popular and longstanding docking practice is that in which ligand is allowed to be flexible around rigid receptor (Rarey et al., 1996; Morris et al., 1998; McGann et al., 2003; Perola et al. 2004; Moitessier et al., 2008). However, proteins are not static — they show dynamic behavior in the biological system. Thus, many efforts have been made to allow flexibility in the receptor (Jiang and Kim, 1991; Alonso et al. 2006; Sherman et al., 2006; Subramanian et al., 2006; Sander et al., 2008). However, for available docking methods, flexibility in the receptor, especially in its backbone, still presents a major challenge. Meng et al. (2011) proposed a Local Move Monte Carlo (LMMC) approach to solving flexible receptor docking problems.

Molecular docking programs perform a search algorithm in which the conformation of the ligand is evaluated recursively until the convergence to the minimum energy is reached. Finally, an affinity scoring function, ΔG [U total in kcal/mol], is employed to rank the candidate poses as the sum of the electrostatic and van der Waals energies. With the increase in computational power, a large number of docking programs which use different scoring functions have been developed including. The scoring function of Autodock (Morris and Huey, 2009), one of the most used docking program, is represented by the following equation:

$$\Delta G = \Delta G_{vdW} \sum_{ij} \left(\frac{A_{ij}}{r_{ij}^{12}} - \frac{B_{ij}}{r_{ij}^{6}} \right) + \Delta G_{h-bond} \sum_{ij} E(t) \left(\frac{C_{ij}}{r_{ij}^{12}} - \frac{D_{ij}}{r_{ij}^{10}} \right) +$$

$$\Delta G_{elec} \sum_{ij} \frac{q_i q_j}{\varepsilon r_{ij}^{2}} + \Delta G_{tor} N_{tor} + \Delta G_{sol} \sum_{ij} \left(S_i V_j + S_j V_i \right) e^{\frac{-r_{ij}^{2}}{2\sigma^2}} \qquad (2.1)$$

where ΔG stands for free energy of binding, r_{ij} is the magnitude of the distance between i and j atoms, q_i and q_j are the charge at points i and j respectively, in C and ε_0 is the permittivity of a vacuum, S - solvation term for atom V – atomic fragmental volume of atom σ – Gaussian distance constant; it is a sum of van der Walls, H-bonds, Electrostatics (Coulomb's Law), torsions and desolvation energies.

Other docking programs include Dock (Ewing et al., 2001), FlexX (Rarey et al., 1996), Glide (Halgren et al., 2004), GOLD (Jones et al., 1997), Surflex (Jain, 2003), ICM (Schapira et al. 2003), Cdocker, LigandFit (Venkatachalam et al., 2003), Drugster (Vlachakis et al., 2013), and eHiTS (Zsoldos et al., 2006, 2007; Ravitz et al., 2011), MCDock, FRED (McGann et al. 2003), MOE-Dock (Corbeil et al. 2012), LeDock (Zhao and Caflisch 2013), AutoDock Vina (Trott and Olson 2010), rDock (Ruiz-Carmona et al. 2014), UCSF Dock (Allen et al. 2015), and many others.

Docking programs utilize various methods of conformational search for exploration of the ligand conformational space. These are categorized as follows: (a) Systematic methods such as Matching algorithm (Brint and Willett, 1987; Fischer et al., 1993; Norel et al., 1994), which after considering all degrees of freedom, place ligands in the predicted binding site. Matching algorithms for ligand docking are available in FLOG (Miller et al., 1994), LibDock (Diller and Merz, 2001) and SANDOCK (Burkhard, Taylor and Walkinshaw, 1998) programs. Incremental construction (IC) (DesJarlais et al., 1986; Leach and Kuntz, 1992; Rarey et al., 1996) methods put the ligand into an active site in a fragmental and incremental fashion. The incremental construction method has been used in DOCK 4.0 (Ewing et al., 2001), FlexX (Rarey et al., 1996), Hammerhead (Welch et al., 1996), SLIDE (Schnecke and Kuhn, 2000) and eHiTS (Zsoldos et al., 2006). (b) Stochastic torsional conformational searches about rotatable

bonds, such as genetic Monte Carlo (MC) (Hart and Read, 1992; Goodsell et al., 1993) and genetic algorithm (GA) (Oshiro et al., 1995; Morris et al., 1998) to "evolve" new low energy conformers, (c) Molecular dynamics simulation methods and energy minimization for exploring the energy landscape of a molecule.

MC methods generate poses of the ligand through a bond rotation, rigid body translation or rotation. The resulting conformation is then tested with an energy-based selection criterion. If it meets the criterion, it will be retained and further modified to generate next conformation. These iterations proceed until the predefined quantity of conformations is collected. The main advantage of MC is that the change can be quite large allowing the ligand to cross the energy barriers on the potential energy surface, a point that isn't achieved easily by molecular dynamics-based simulation methods. Examples of applying the Monte Carlo methods include an earlier version of AutoDock (Goodsell and Olson, 1990), ICM (Abagyan et al., 1994), QXP (McMartin and Bohacek, 1997), and Affinity (Dassault Systèmes BIOVIA, 2017).

GA is based on Darwin's theory of evolution. In GA binary strings called genes, encode degrees of freedom of the ligand while chromosomes represent the pose of the ligand. Two kinds of genetic operators in GA are mutation and crossover. Through mutation, random changes are made to the genes; when crossover takes place, genes are exchanged between two chromosomes. Genetic operators affect the genes which result in a new ligand structure. These new ligand structures are assessed by the scoring function, and the ones that survived among them (i.e., exceeded a threshold) can be used for the next generation. GA have been used in AutoDock (Morris and Huey, 2009), GOLD (Verdonk et al., 2003), DIVALI (Clark, 1995) and DARWIN (Taylor and Burnett, 2000). Pagadala et al. (2017) in their article entitled "Software for molecular docking: a review" provided a comprehensive review of docking software and their accuracy in prediction the correct ligand binding mode.

2.7.2. Virtual screening

Drug discovery and development is a very complex, exhaustive and expensive process. Combinatorial chemistry and high-throughput screening (HTS) have accelerated the drug discovery process by enabling large libraries of compounds to be screened in a short time. However, due to the high cost and low hit rate of HTS, virtual screening is gaining prominence as a method to filter very large chemical space that can be created by combinatorial synthesis into a manageable library of likely favorable scaffolds to be tested by HTS. Virtual screening can be structure based or ligand-based. In structure-based virtual screening approach, the 3D structure of the target biological molecule is utilized to screen a large library of chemical compounds to identify structurally diverse compounds with similar bioactivity. The 3D structure can be X-ray crystal structure, Nuclear Magnetic Resonance (NMR) structure or derived via theoretical modeling (eg homology modeling). In contrast, the ligand-based virtual screening approach is based on the information from existing ligand as a template, resulting in the identification of scaffold that is less diverse in structures. Thus, structure-based virtual is believed to be more effective at detecting novel chemical scaffolds and is more commonly used in academic labs (Walters et al., 1998) – hence, one of the methods applied for identifying potential isoform-selective HDAC inhibitors in this study.

2.7.3 Pharmacophore modeling

The concept of pharmacophore was first introduced in 1909 by Ehrlich, (1909), who defined pharmacophore as 'a molecular framework that carries (phoros) the essential features responsible for a drug's (pharmacon) biological activity'. Following a century's improvement, the essential pharmacophore idea still stays unaltered, however, its purposeful significance and application go have been extended impressively. According to the International Union of Pure and Applied Chemistry (IUPAC), a pharmacophore model is 'an ensemble of steric and electronic features that is necessary to ensure the optimal supramolecular interactions with a specific biological target and to trigger (or block) its biological response' (Wermuth et al., 1998). These features that represent the chemical functionalities of active small molecules are H-bond donors (HBDs), H-bond

acceptors (HBAs), hydrophobes (H), positively and negatively ionizable groups (PI/NI), and metal coordinating groups (M). Additional size restrictions in the form of a shape or exclusion volumes (XVOL) – forbidden areas – can be added to represent the size and the shape of the binding pocket.

A pharmacophore model can be developed by superposing a set of active molecules and extracting common chemical features that are essential for their bioactivity — this approach is referred to as ligand-based pharmacophore model. Alternatively, when the interaction between target and ligands is probed to generate a pharmacophore model, it is referred to as structure- or receptor-based pharmacophore model. Thus, pharmacophore modeling and pharmacophore-based virtual screening are aimed at predicting activities by sorting compounds that match the model into actives, and those not fitting to the model into inactive. This outputs a list of compounds (hit list) that are proposed to be active. Therefore, the advantage of pharmacophore-based virtual screening is that compounds that are not likely to be active can be dumped at a very early stage of a project thereby saving a lot of resources in the further drug discovery process, especially in vitro experiments (Vuorinen and Schuster, 2015). The successful applications of pharmacophore modeling in virtual screening, de novo design, and lead optimization have been reviewed (Langer and Hoffman, 2006; Yang, 2010).

2.7.4 Molecular dynamics simulation

X-ray crystallography has been the main experimental technique used over decades to elucidate the molecular structures of macromolecules. However, it can only provide a static snapshot of a protein functional state and thus NMR was increasingly used for protein structure determination in the past decades due to the relative flexibility revealing an ensemble of conformations. Still, NMR spectroscopy is time-consuming for a large protein complex and this prompts the search for a complementary tool that allows the study of dynamic behavior of biological targets and ligand binding. MD simulation has become a new major technique in the design of novel bioactive molecules by examining the stability of biomolecular complexes and ligand binding mode in time (Aqvist et al., 2002; Khandelwal and Balaz, 2007).

MD is a computational method that utilizes structural data obtained experimentally to extrapolate the possible conformations of molecular systems. In classical MD simulations, the potential energy function commonly denoted as the "force-field" describes the interactions between atoms. It consists of bonded terms between covalently bound atoms (bonds, angles, torsions) and non-bond terms (van der Waals interactions and electrostatic interactions). Traditional biomolecular force fields such as AMBER (Cornell et al., 1995), OPLS (Jorgensen and Tirado-Rives, 1988), CHARMM (MacKerell et al., 1998) and GROMOS (Oostenbrink et al., 2004) have proven to be promising in modeling these interactions. On the other hand, due to diversity of small organic molecules, ligands have to be modeled most commonly, using general AMBER force-field (GAFF) (Wang et al., 2004), the CHARMM general force-field (CGenFF) (Vanommeslaeghe and MacKerell, 2012), the GROMOS automatic topology builder (Malde et al., 2011) and the OPLS all-atom force-field (OPLS-AA) (Jorgensen et al., 1996). Parameters for the bonded terms and the van der Waals interactions are typically taken from a generalized force-field, whereas that of partial atomic charges are derived from a Quantum Mechanical calculation.

Molecular dynamics simulation consists of the step-by-step numerical solution of the classical equations of motion, which for a simple atomic system may be written as:

$$m_i r_i = f_i \qquad f_i = -\frac{\partial}{\partial r_i} u \qquad (2.2)$$

where f_i is the force acting on the atoms and is usually derived from a potential energy U(rN), where rN = (r1; r2;………..rN).

The part representing the bonded terms of potential energy function is written as:

$$U_{non-bonded} = \sum_{bonds} \frac{k_l}{2}(l - l_0)^2 + \sum_{angles} \frac{k_\theta}{2}(\theta - \theta_0)^2 + \sum_{torsions} \frac{V_n}{2}(1$$
$$+ \cos(n\varphi - \gamma)) \qquad (2.3)$$

The bonds will typically involve the separation $r_{ij} = l - l_0$ between adjacent pairs of atoms in a molecular framework. The bend angles, θ_{ijk} are between successive bond

vectors such as r_i - r_j and r_j - r_k, and therefore involve three atom coordinates. The torsion angles, φ_{ijkl} are defined in terms of three connected bonds.

The part of the potential energy representing the non-bond terms are divided into 2 components: van der Waals forces; modeled using Lennard-Jones potential as below:

$$\sum_{i=1}^{N}\sum_{j=1+1}^{N}(4\varepsilon_{ij}[\left(\frac{\sigma_{ij}}{r_{ij}}\right)^{12} - \left(\frac{\sigma_{ij}}{r_{ij}}\right)^{6}] + \cdots \tag{2.4a}$$

where pair potential $v(r_i; r_j) = v(r_{ij})$, with two parameters: σ, the diameter, and ε, the well depth.

The second part of the non-bond terms are Coulomb potentials in the presence of charges and is given by:

$$\frac{q_i q_j}{4\pi\varepsilon_0 r_{ij}} \tag{2.4b}$$

where $q_i q_j$ are the charges and ε_0 is the permittivity of free space.

Thus, the potential energy function ($\mathcal{V}(r^N)$ is the sum of bonded and non-bond terms and is written as:

$$\mathcal{V}(r^N) = \sum_{bonds}\frac{k_l}{2}(l - l_0)^2 + \sum_{angles}\frac{k_\theta}{2}(\theta - \theta_0)^2 + \sum_{torsions}\frac{V_n}{2}(1 + \cos(n\varphi - \gamma))$$

$$+ \sum_{i=1}^{N}\sum_{j=1+1}^{N}(4\varepsilon_{ij}[\left(\frac{\sigma_{ij}}{r_{ij}}\right)^{12} - \left(\frac{\sigma_{ij}}{r_{ij}}\right)^{6}] + \frac{q_i q_j}{4\pi\varepsilon_0 r_{ij}}) \tag{2.5}$$

These parameters were determined experimentally, or modeled theoretically (Maitland et al., 1987).

MD trajectory of a macromolecule-ligand complex is analyzed to extract information such as distances and interactions between atoms or residues of interest. Root-mean-squared deviations (RMSD) from a reference configuration, the root-mean-squared fluctuations (RMSF) and most importantly, in context of drug design, the free energy of binding (ΔG^{bind}) which is the difference between the free energy of ligand free in

solution (G^{free}) and ligand bound to protein (G^{complex}) and is directly related to the binding constant, Ki as follows:

$$\Delta G^{bind} = G^{complex} - G^{free} = RT ln(Ki) \qquad (2.6)$$

The application of molecular dynamics in drug design has been reported (Alonso, et al., 2006; Durrant and McCammon, 2011; Zhao and Caflisch, 2014, 2015). With recent advances in the field due to an increase in computational power, the timescale of MD simulation could be extended to microsecond to enable relevant events to be observed (Maragakis et al., 2008). Considering this progress, Mortier et al. (2015) studied the impact of MD simulation on drug design by specifically characterizing ligand–macromolecule complexes.

Relevant to this dissertation, MD simulation studies have been successfully applied to examine the stabilities of HDAC-inhibitor complexes in search of selective HDAC inhibitors. To explore the release of the N-(2-aminophenyl)- benzamide from the active sites of HDACs 1 and 2, random acceleration MD (RAMD) simulations coupled with classical MD were conducted (Kalyaanamoorthy and Chen, 2012). MD simulation studies have been carried out to examine the stability of ligand binding modes over time and potential HDAC inhibitors were identified by approach (Thangapandian et al., 2012; Tambunan et al., 2013; Noor et al., 2015).

2.7.5 Scaffold hopping in medicinal chemistry

Scaffold hopping is an approach aimed at identifying core structures of compounds responsible for the biological activity of those compounds containing them. It refers to the search for compounds sharing the same activity but having different core structures (Schneider et al., 1999), by core structure replacement. Scaffold hopping plays an essential role in the design of structurally novel active molecules (Böhm et al., 2004; Schuffenhauer, 2012). Scaffold hopping was used in combination with other computational methods such as virtual screening and molecular dynamics simulation for identification of novel potential inhibitors of different biological targets.

Major motivations for scaffold hopping include finding alternative starting points for lead generation. This concept has been linked to computational methods and virtual screening even though meaningful scaffold replacements can also be accomplished based on medicinal chemistry knowledge and intuition. Despite the intrinsic advantage of pharmacophore and shape methods used to facilitate scaffold hopping, many different computational approaches have been successfully applied including simple 2D similarity searching property principle. This could be attributed to small molecule binding promiscuity of many pharmaceutical targets rather than special algorithmic features (Hu et al., 2016). To date, there are no generally accepted standards for the assessment of scaffold hopping potential, in the computational community. Nonetheless, new computational approaches and protocols continue to be reported specifically for scaffold hopping applications, to further advance the field.

Various approaches exist for scaffold hopping including fragment-based in which scaffolds are created by cutting bonds of existing compounds in a combinatorial fashion (Vainio et al., 2013); chemically advanced template search (CATS), which based on topological pharmacophore models (Schneider et al., 1999); inductive logic programming (ILP), which uses the observed spatial relationships between pharmacophore types in pre-tested active and inactive compounds and learns human-readable rules describing the diverse structures of active compounds (Tsunoyama et al., 2008); similarity searching using 2D fingerprints (Gardiner et al., 2011).

2.7.6 ADMET prediction in drug design

Absorption, Distribution, Metabolism, Elimination, and Toxicity (ADMET) properties are very important in current drug discovery and development. In addition to good efficacy, the success of drug candidate is also determined by good ADMET profile. Although *in vitro* ADMET screens are available, *in silico* prediction of ADMET properties proves to be valuable in current drug discovery. In silico methods estimates ADMET properties using statistical approaches (Biswas et al., 2006; Rayan et al., 2010), molecular descriptors (Li et al., 2007) and experimental data to model complex

biological processes (e.g. oral bioavailability, intestinal absorption, permeability and mutagenicity (van de Waterbeemd and Gifford, 2003; Norinder and Bergström, 2006; Dearden, 2007; Cheng et al., 2013). Structure-based ADMET profiling which makes use of the 3D structure of the ADMET protein was also studied and suggested to be the alternative method in the near future (Moroy et al., 2012). Various models have been successfully developed towards improvement of ADMET prediction goals and different opinions regarding their application suitability have been presented in several review articles (Ekins et al., 2000; Krejsa et al., 2003; Yamashita and Hashida, 2004; Hou and Wang, 2008; Cruciani et al., 2009; Egan, 2010; Madden, 2010; Tao et al., 2015; Hyun et al., 2016). The rules for drug-likeness or lead-likeness (Muegge, 2003) or metabolite-likeness (Dobson et al., 2009) relying on simple physicochemical properties are implemented in ADMET prediction tools (Lagorce et al., 2008, 2011; Cheng et al., 2012).

There are strong regulations and guidelines for the toxicity testing of pharmaceutical substances established by Organization for Economic Co-operation and Development (OECD), the European Agency for the Evaluation of Medicinal Products (EMEA) the U.S. Food and Drug Administration (FDA), the National Institutes of Health (NIH). In these guidelines, the use of alternative *in vitro* or *in silico* methods for toxicity assessment that do not involve animals are strongly recommended (Benz, 2007; Parasuraman, 2011). However, the high cost and time consumption of *in vitro* method prompted the development of *in silico* prediction models of oral acute toxicity (Lei et al., 2016). Therefore, *in silico* model of structure-based ADMET prediction will be employed in the present study.

3. MATERIALS AND METHODS

3.1 Protein Dataset and Setup

The following crystal structures of human histone deacetylases were retrieved from the Protein Data Bank (PDB) (http://www.rcsb.org) (Berman et al., 2000): (1) 4BKX; ("The structure of HDAC1 in complex with the dimeric ELM2-SANT domain of MTA1 from the NuRD complex", resolution: 3.00 Å) (Millard et al., 2013). (2) 4LXZ ("Structure of human HDAC2 in complex with SAHA", resolution: 1.85 Å) (Lauffer et al., 2013). (3) 4A69 ("Structure of HDAC3 bound to corepressor and inositol tetraphosphate", resolution: 2.06 Å) (Watson et al., 2012). (4) 3C5K ("Crystal structure of human HDAC6 zinc finger domain", resolution: 1.55 Å) (5) 5EDU ("Crystal structure of human histone deacetylase 6 catalytic domain 2 in complex with trichostatin A", resolution: 2.79 Å) (Miyake et al., 2016). (6) 3C0Y ("Crystal structure of human HDAC7 catalytic domain in complex with SAHA") (Schuetz et al., 2008). (7) 1T64 ("HDAC8 in complex with the inhibitor TSA", resolution: 1.9 Å) (Somoza et al., 2004).

The co-crystallized ligands were subsequently removed from each protein structure. Missing loops were estimated and hydrogen atoms were added based on the protonation state of the titratable residues at a pH of 7.4 using Biovia Discovery Studio (DS) 4.5 molecular modeling program (Dassault Systèmes BIOVIA, 2017). These native ligands were then docked back into their respective crystal structures, and their RMSD with respect to the reference ligand were found to be < 2.0 Å. In addition, a series of known HDAC inhibitors were docked into these proteins to assesss the quality of the 3D structures, and their binding affinity was found to be consistent with their Ki (or IC50) from the literature. The detailed description of the protocols was given under molecular docking subsections.

3.1.1 Protein structure analysis (Ramachandran plot)

Ramachandran analysis of Class I HDACs, HDACs 6 and 7 was carried out using Biovia DS 4.5 and the energetically allowed conformations were compared in Figure 3.1.
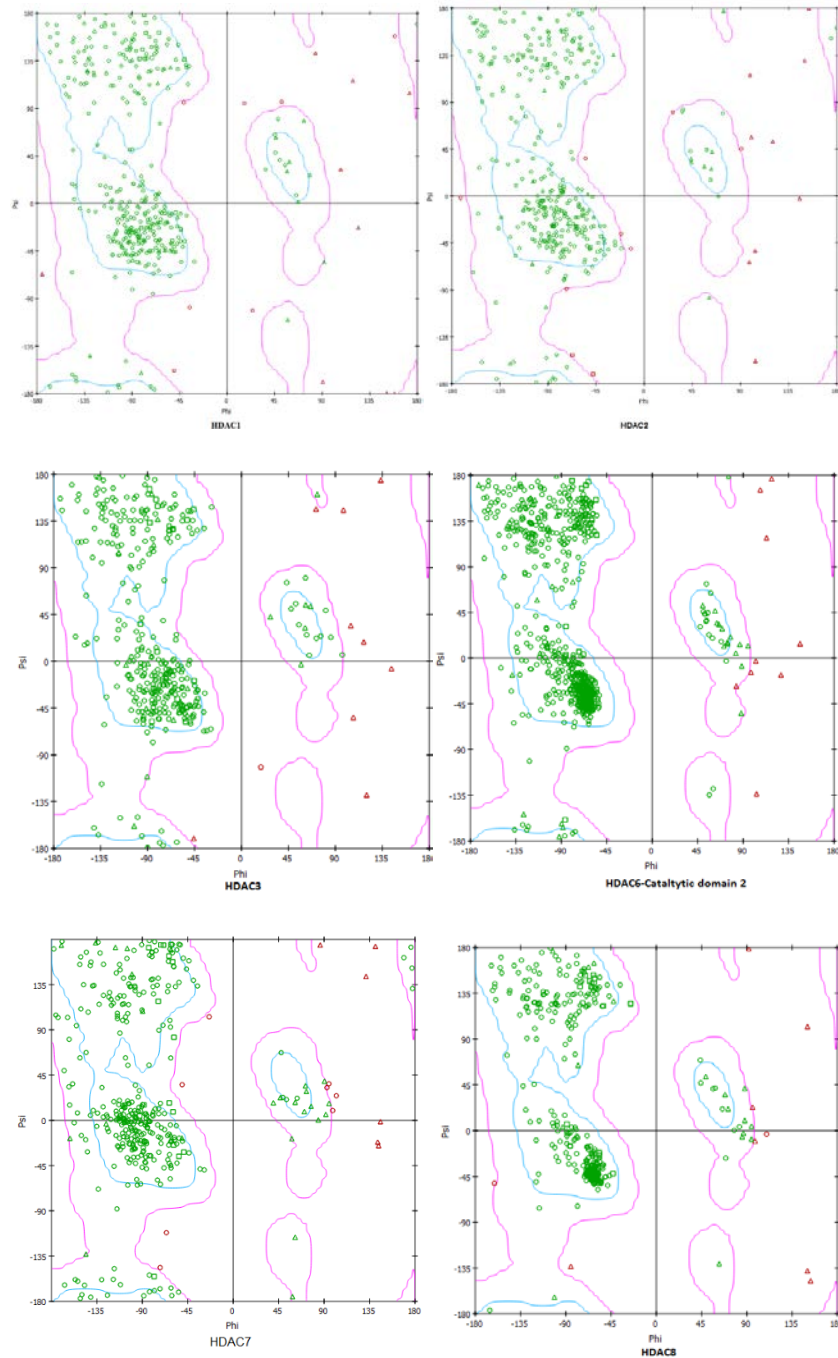
Figure 3. 1. Ramachandran plots of class I HDACs and HDAC6.

3.1.2 Sequence alignment and structural superimposition

The amino acid sequences of class I HDACs were aligned using Biovia discovery studio software (Figures 3.2) and their corresponding three dimensional (3D) structures superimposed (Figure 3.3). The conserved amino acid residues in HDACs'catalytic channels that are components of the "charge relay system of HDAC catalysis were also aligned (Table 3.1). Moreover, to gain insight into the evolutionary relationship among these isoforms, a phylogenetic tree was constructed from multiple sequence alignment using Basic Local Alignment Search Tool (BLAST) available on the National Center for Biotechnology Information (NCBI) database (Figure 3.4).

Table 3. 1. Superimposition of common residues among class I HDACs that are components of charge-relay system of HDAC catalysis.

HDAC1	HDAC2	HDAC3	HDAC8
HIS140	HIS145	HIS134	HIS142
HIS141	HIS146	HIS135	HIS143
HIS178	HIS183	HIS172	HIS180
ASP176	ASP181	ASP170	ASP178
PHE205	PHE210	PHE200	PHE208
ASP264	ASP266	ASP259	ASP267
TYR303	TYR308	TYR298	TYR306
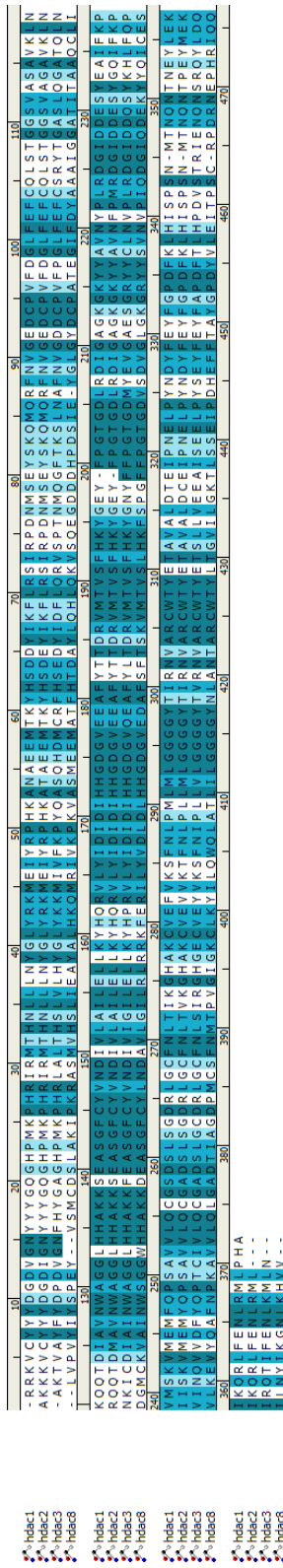
Figure 3. 2. Multiple sequence alignment of class I HDACs (1, 2, 3, and 8). Identity is indicated in dark blue, similarity in light blue and difference in white. The amino acids in the catalytic channels of these isoforms were similar even though the overall sequence identity is 33.1% and sequence similarity is 57.8%.
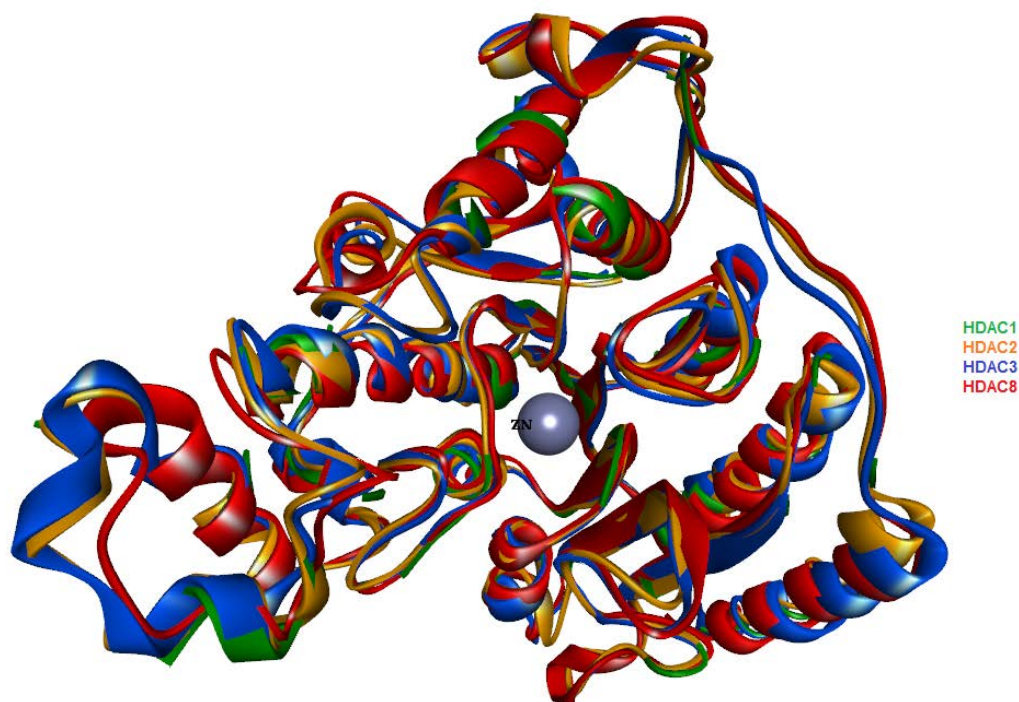
Figure 3. 3. Structural superimposition and alignment of class I HDACs. Each isoform is indicated in its respective color.
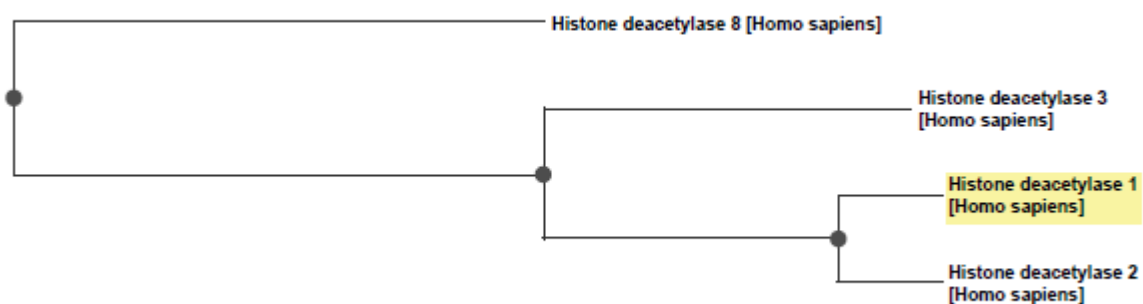
Figure 3. 4. Phylogenetic tress showing evolutionary relationship among Class I HDACs. The tree revealed that HDACs 1 and 2 are closely related, share ancestral origin with HDAC3 by 1 node and with HDAC8 by 2 nodes.

3.2 The Design of Isoform-selective HDAC Inhibitors by Scaffold Hopping

Virtual screening is a process of screening a large library of compounds to identify pharmacologically active compounds. It is automated to quickly evaluate a series of

"compounds based on their biological activity against a target protein. It is usually used to identify the initial compound (hit) for further optimization. In this study, our virtual screening of molecular fragment library on Otava database returned a fragment (Otava id; 5683342) with desirable activity against HDAC3. The library was screened against HDAC3 because our phylogenetic analysis of HDAC isoforms in question, using distance method, showed that HDAC3 share a sequence similarity with HDACs 1, 2 and 8 (Figure 3.4). Based on the general pharmacophore features of HDAC inhibitors, structural modifications were made by scaffold hopping in which various synthetically feasible groups were added and fragments replaced to achieve particular polar, hydrophobic or steric interactions around the entrance and vicinity of the catalytic channels (Figure 3.6). These interactions might enhance the binding affinity and selectivity considering the subtle difference in the amino acids at the highly conserved active sites of HDAC isoforms. The geometries of the ligands were optimized using and the atom potential types and partial charges were assigned with the Momany and Rone CHARMm force field.
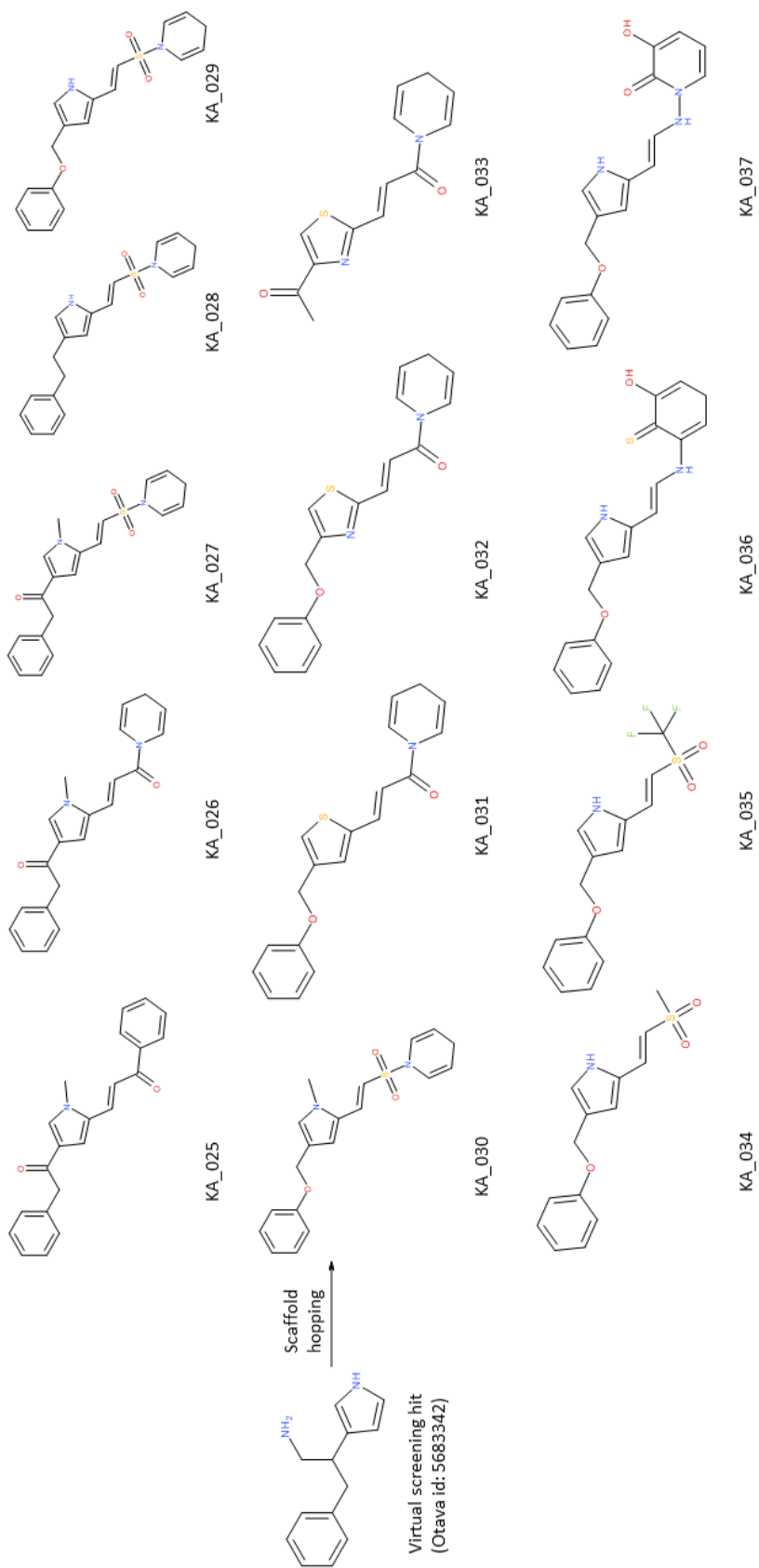
Figure 3. 5. The designed compounds KA_025 through KA_037 by hopping a common scaffold (Otava id: 56883342) identified through virtual screening.

3.3 Identification of Isoform-selective HDAC Inhibitors via Structure-Based Virtual Screening

3.3.1 Ligand setup

A total of 2,703,000 compounds available for screening were retrieved from Otava database (http://www.otavachemicals.com). For those compounds that reached molecular docking stage, their 3D geometries were optimized by generating all of the tautomers, and making sure that all of the ionizable groups were properly protonated, using Biovia DS 4.5 (Dassault Systèmes BIOVIA, 2017).

3.3.2 Pre-screening

rDock is a tool for high-throughput docking and virtual screening. The platform supports structure-based drug design process (Ruiz-Carmona et al., 2014) (http://rdock.sourceforge.net). In rDock Genetic algorithm converges very quickly to allow virtual screening – the global minimum is reached by multiple docking runs in which poor ligands are discarded early on. In this study, 2,703,000 compounds were screened against HDACs 1, 2, 3, 6 and 8. The procedure involved 3 steps: system definition using the available "prm" script, cavity detection using the binding pocket coordinates generated from Autodock4 and docking (50 runs were allowed per each compound). Based on rDock prediction of the activity (ranking of compounds according to rDock score) (Li et al., 2003), this large compound library was reduced to a total of **161,941** compounds (**43,302** for HDAC1; **42,221** for HDAsC2; **37,414** for HDAC3, and **39,004** for HDAC8).

3.3.3 Structure-based virtual screening protocol

Structure-based virtual screening is believed to be more effective at detecting novel chemical scaffolds and is more commonly used in the academic lab (Walters et al., 1998). AutoDock Vina, is a program used for structure-based virtual screening due to its

relative higher speed. It automatically calculates the grid maps and clusters the results in a way transparent to the user (Trott and Olson, 2010) (http://vina.scripps.edu). Here, because of the high sequence conservation and structural similarity among class I HDACs (de Ruijter et al., 2003), the **161,941** compounds that showed activity against class I HDACs at pre-screening stage, were further screened against each individual member of the class using Autodock Vina with grid and docking parameters given in Table 3.2.

3.3.4 Criteria for the selection of isoform-selective inhibitors

The selection of the selective compounds in the current study was guided by Bieliauskas and Pflum, (2008). In this article, the authors provided a detailed review of isoform-selectivity of HDAC inhibitors. PCI-34051 showed > 200-fold selectivity for HDAC8 over other HDAC isoforms and is therefore considered HDAC8 selective (Balasubramanian et al., 2008). A cyclic peptide mimic displayed modest selectivity within class I, with a 4-fold preference for HDAC1 over HDAC8 (Liu et al., 2007). Here, the selection of the selective compounds was made based on selectivity index value calculated as the ratio of inhibition constant (Ki) of an inhibitor against one isoform to Ki of the same inhibitor against any other isoforms (eg. Selectivity index of compound 1 for HDAC1 over HDAC2 = Ki of compound 1 against HDAC1÷ Ki of compound 1 against HDAC2). Those compounds that showed ≥ 5-fold selectivity for one isoform over the other isoforms were considered moderately selective and those that displayed ≥ 100-fold selectivity for one isoform over the others were considered highly selective. Those compounds with high binding affinity but failed to satisfy these criteria were counted out. Employing this extreme filtering reduced the number of detected compounds to a total of 41 compounds (12 for HDAC1; 11 for HDAC2; 9 for HDAC3 and 8 for HDAC8).

Table 3. 2. Grid mapping parameters used for virtual screening docking against respective enzymes.

Centre (Å)	HDAC1	HDAC2	HDAC3	HDAC8
X	-53.62	-53.553	42.753	39.175
Y	12.044	12.169	52.139	37.193
Z	-6.977	-6.907	19.416	39.979
Dimension (Å)				
X	53.056	52.196	53.665	55.227
Y	57.977	54.181	52.998	55.981
Z	58.976	59.827	55.674	55.274

3.3.5 Further molecular docking assay

To ascertain the selectivity of the total 45 compounds identified via structure-based virtual screening, each set of compounds was docked into the binding pocket of their respective isoform using Autodock 4.2 (Morris and Huey, 2009) (https://autodock.scripts.edu). The following energy grid box dimensions were used: 55_55_55 Å for HDACs 1, 2, 8 and 65_65_65 Å for HDACs 3 and 6. These parameters were chosen according to the size of the binding pocket of each isoform, so as to cover the entire binding site and its neighboring residues. The Lamarckian genetic algorithm was used for ligand conformational search. For each compound, 20 independent runs were performed, and the distinct ligand conformers were generated and docked randomly into the binding pocket of these enzymes. The program randomly assigned torsion angles to rotatable bonds. Fifteen million energy evaluations were allowed for each ligand. Three independent dockings were run for each complex and average of free energy of binding was computed. According to the Autodock 4.2's calculation of binding energy, a total of **36** compounds (**10** for HDAC1; **10** for HDAC2; **8** for HDAC3 and **8** for HDAC8) were found to show selectivity for their respective isoforms, whereas five compounds showed high binding affinity but failed to satisfy the criteria for selectivity despite repetitive docking runs.

3.3.6 Drug-likeness and ADMET prediction

Absorption, Distribution, Metabolism, Elimination and Toxicity (ADMET) properties are very important in current drug discovery and development. Nowadays, computational modeling is complementing *in vitro* and *in vivo* estimation of ADMET properties. *In silico* techniques have been applied to predict ADMET properties of compounds over the past decade. Here, drug likeness was predicted using ADMET Predictor (Simulation Plus Model) (http://www.simulations-plus.com) — these models include S+logP (octanol-water partition coefficient, log P); S+logD (octanol-water distribution coefficient, log D; calculated from pK_a and S+logP); MlogP (Moriguchi model of octanol-water partition coefficient, log P); Ruleof5 ('computational filter for oral absorption in human identical to the Lipinski's "Rule of Five"') (Owens and Lipinski, 2003; Lipinski, 2004; Bhal et al., 2007); molecular weight (dalton), sum of H-bond donors (S_HBD) and acceptors (S_NO), topological polar surface area (TPSA). Other ADMET properties were predicted using AdmetSAR server (http://lmmd.ecust.edu.cn/admetsar1). AdmetSAR program estimates properties based on substructure pattern recognition and then uses support vector machine algorithm to build a model (Shen et al., 2010). The chemical information of each of 1-36 compounds was input as "SMILE" and the corresponding ADMET properties estimated.
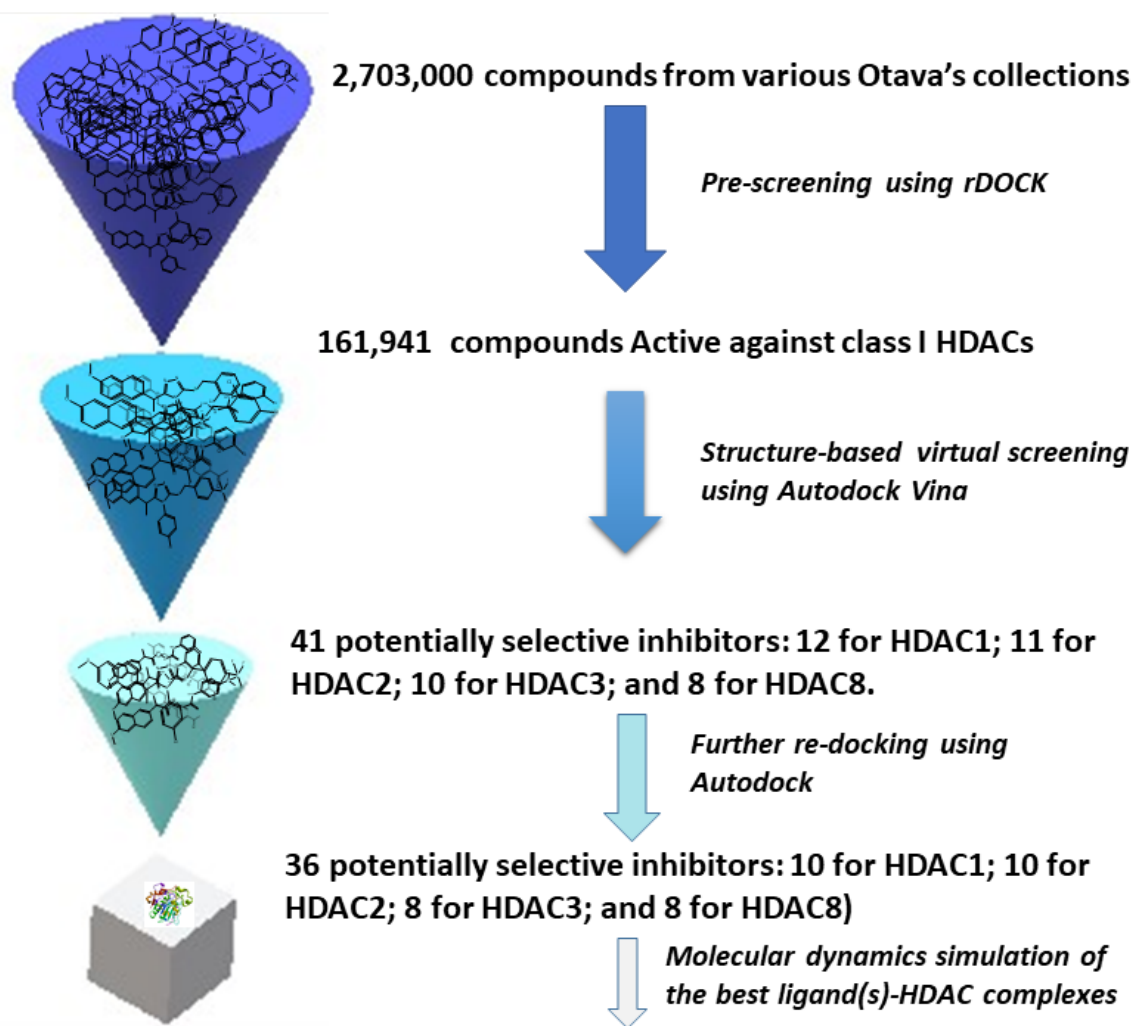
Figure 3. 6. Virtual screening workflow combined with molecular docking and dynamics simulation.

3.3.7 Molecular dynamics simulation

To study the structural dynamics and stability of HDAC-ligand complexes, both the free HDACs and their complexes with the respective best ligand identified via virtual screening were submitted to MD simulations using NAMD software (Phillips et al., 2005) (http://www.ks.uiuc.edu/Research/namd/). Input files for NAMD were generated using CHARMM GUI (CHARMM36) (Lee et al., 2016) (http://www.charmm.org). Ligand parameterization was carried out using CHARMM General Force Field (CGenFF) server (https://cgenff.paramchem.org/). CGenFF server was used to perform ligand atom typing and assignment of parameters and charges by analogy in a fully

automated fashion. During the input preparation, all the systems were solvated using the TIP3 water model and neutralized with KCl (ionic concentration, 0.2 M). The systems' energy was minimized for 1000 steps by steepest descent method (Bibi et al., 2013; Kausar et al., 2013). Following a 2 ns-equilibration run at constant number of particles, volume and temperature (NVT) ensemble, three parallel unrestrained 10 ns-production-MD simulations with different initial velocities were performed for each system at constant temperature and pressure (NPT) ensemble. During the production run, the time step and collection interval were set to 2 fs and 1 ps respectively. Structural stability of the systems was compared by analyzing the average values of potential energy, root-mean-squared deviation (RMSD) and root-mean-squared displacement (RMSF) profiles throughout the trajectories.

3.4 Selective Inhibitor Design for HDAC6

3.4.1 The search for HDAC6 relatives

To design selective inhibitors of HDAC6, a comparison of the binding affinity of candidate compounds against HDAC6 and its closest relatives needs to be carried out. To identify these relatives, the FASTA sequence of HDAC6 was retrieved from the National Center for Biotechnology Information (NCBI) Entrez sequence search. Following protein Basic Local Alignment Search Tool (BLASTp) run against the Protein Data Bank database, multiple sequences were returned, among which the most similar proteins were HDAC4 (AAH39904.1) (Strausberg el al, 2002); HDAC5 (NCBI Reference Sequence number: NP_001015053.1) (Hendrick et al., 2017); HDAC6 (GenBank accession number: AAH69243.1) (Strausberg el al, 2002); HDAC7 (GenBank accession number: AAH06453.2) (Strausberg el al, 2002); and HDAC9 (GenBank accession number: AAI11736.1) (Strausberg el al, 2002); HDAC10 (GenBank accession number: AAI25083.1) (Strausberg el al, 2002). These HDAC isoforms were re-aligned and a phylogenetic tree was then constructed from this alignment to gain insight into their evolutionary relationship.
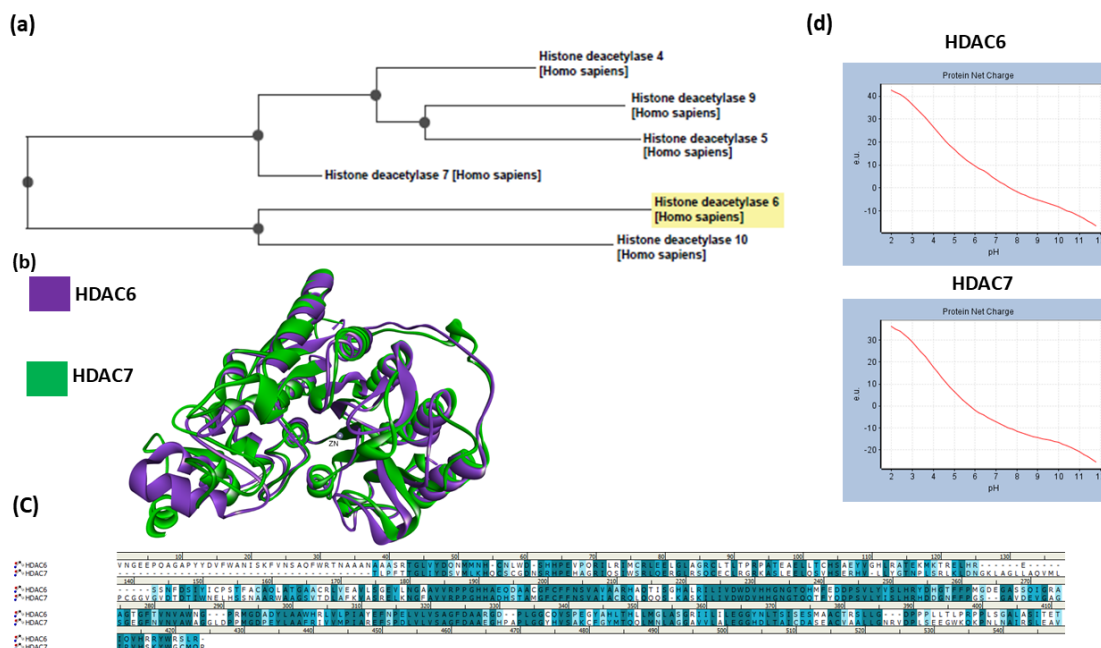
Figure 3. 7. A phylogenetic tree showing evolutionary relationship among Class II HDACs. The tree revealed that HDACs 6 and 10 are closely related, share ancestral origin with HDAC7 by 1 node. HDACs 5 and 9 are close relative and are distant from HDAC4 by 1 node (a). Structural superposition of HDACs 6 (in purple) and HDAC7 (in green) showed an RMSD of 1.003 Å (b). Sequence alignment between HDACs 6 and 7; identity and similarity, 41.1% and 55.8% respectively. Identity is indicated in dark bule, similarity in light blue and difference in white. Mostly, the indentical residues are located within the conserved active site of the two isoforms (c). Comparison of the two proteins' net charges at different pH (d).

3.4.2 Structure-based selective inhibitor design for HDAC6

Approximately, a library of 200,000 compounds was developed out of the 2,703,000 compounds studied above (**see section 3.3**). This library contains compounds with $\Delta G >$ 7.00 kcal/mol against class I HDACs. The idea was that these compounds showed no preference for class I HDACs and thus, some of them may show potential selectivity for HDAC6. Using Biovia DS 4.5 program (Dassault Systèmes BIOVIA, 2017), the molecules were filtered based on the elements of drug-likeness guided by Lipinski's rule of 5 (Lipinski, 2004): LogP < 5; S_HBD < 5; S_HBA < 10; and MW < 500 Da. A total of 72,461 were found to have satisfied these criteria. The geometries of these compounds were optimized by properly protonating all of the ionizable groups and by

50

energy minimization using CHARMM force filed, and then saved as PDB format for virtual screening (Dassault Systèmes BIOVIA, 2017).

3.4.3 Structure-based virtual screening protocol

Structure-based virtual screening is commonly used in the academic lab to identify novel drug candidates or scaffolds for lead optimization. Autodock Vina is a program used for structure-based virtual screening due to its relative higher speed than Autodock 4 and many other structure-based virtual screening programs. Autodock Vina uses a hybrid scoring function (empirical + knowledge-based). The exhaustiveness, which is the time spent on the search is already varied heuristically depending on the number of atoms, flexibility (Trott and Olson, 2010). It was used to screen the library of ~ 72 461 compounds against HDAC6 using the following grid box dimension: 60, 60, 60 Å; and grid box center: (X = -1.183), (Y = 8.752), (Z = 5.755) Å. First, the compounds were filtered based on their binding energy values ($\Delta G > 10$ kcal/mol), and a total of 9432 satisfied this criterion. Second, the top 100 protein-ligand complexes were analyzed for orientation of ligands in a binding site. By visual inspection, 20 compounds showed reasonable binding modes and were therefore manually selected for further analysis.

3.4.4 Molecular docking assay

For *in silico* selectivity evaluation, these 20 compounds were docked into the catalytic channels of HDACs 6 and 7. AutoDockTool (ADT) was used to assign Gasteiger partial charges to each atom of the PDB file to generate a pdbqt file, which was subsequently used to generate grid parameter file (gpf) and a docking parameter file (dpf). These gpf and dpf files were then used as input files of Autodock 4.2 for grid mapping and docking respectively (Morris et al., 1998). Also, for the sake of comparison of *in silico* performance, a series of known HDAC6 inhibitors were docked into the catalytic pockets of these enzymes. Energy grid boxes of the following dimension: 60, 60, 60 Å; and grid center near Zn^{2+} ion; (X = -1.183), (Y = 8.752), (Z = 5.755 Å) for HDAC6, and of dimension 60_60_60 Å and grid center near Zn^{2+} ion; (Z = -35.278) (Y = -27.984) (Z = -19.016) Å for HDAC7, were used to cover the entire active site of HDAC6 and

HDAC7. The search for ligand conformation in the active sites of these enzymes was carried out using the Lamarckian genetic algorithm. For each ligand, 20 independent runs were performed, and the distinct conformers generated were docked randomly into the catalytic pocket of the enzyme using 20,000,000 energy evaluation.

3.4.5 Drug-likeness and ADMET prediction

In silico techniques have been applied to predict Absorption, Distribution, Metabolism, Elimination, and Toxicity (ADMET) properties of compounds over the past decades. Herein, drug-likeness was predicted using ADMET Predictor (https://www.simulations-plus.com/). ADMET Predictor allows for the rapid and easy creation of high-quality Quantitative Structure-Activity Relationship (QSAR)/Quantitative Structure-Property Relationship (QSPR) models based on one's data. Complementarily, the ADMET properties were predicted using ADMET Structure–Activity Relationship (AdmetSAR) server (http://lmmd.ecust.edu.cn/admetsar1) AdmetSAR program estimates properties based on substructure pattern recognition and then uses support vector machine algorithm to build a model. The models were built using annotated data point from a large set of unique compounds from the literature (Shen et al., 2010).

3.4.6 Molecular dynamics simulation

To examine the stability of ligand binding mode, molecular dynamics (MD) simulations were performed for the free form of HDAC6 and its complexes with the 4 potentially selective inhibitors, using NAMD software (Phillips et al., 2005) Input files for NAMD were generated using CHARMM GUI (http://www.charmm-gui.org/)(Lee et al., 2016). Ligand parameterization was carried out using CHARMM General Force Field (CGenFF) server (https://cgenff.paramchem.org/) which performed ligand atom typing and assignment of parameters and charges by analogy in a fully automated fashion. All the systems were solvated using the TIP3 water model and neutralized by addition of KCl to an ionic concentration of 0.2 M. Minimization for 1 ps was carried out by steepest descent method and the system equilibrated for 2 ns in NVT ensemble. Unrestrained 10 ns-production-MD simulations were performed at constant temperature

(310 K) and pressure (1 atm) in (NPT) ensemble at time step and collection interval of 2 fs and 1 ps, respectively. The computational workflow is shown in Figure 3.8 below.

~ 72 461 druglike compounds retrieved from Otava database

Structure-based Virtual screening using Autodock Vina

100 compounds with ΔG ≥ 10 kcal/mol

Molecular docking using Autodock 4

20 compounds with good binding modes

Docking into HDACs 6 and 7 using Autodock 4

4 potential HDAC6-selective compounds

Molcular dynamics simulation Using NAMD

4 potential HDAC6-selective inhibitors with stable binding modes

Figure 3. 8. Virtual screening workflow for the identification of potential lead compounds for the design of HDAC6-selective inhibitors.

3.5 The Search for Selective Inhibitors of HDAC6 by Pharmacophore-Based Virtual Screening

3.5.1 Selection of the training set molecules

A total of 20 HDAC inhibitors with experimental activity (Ki) ranging from 4-400 nM, (Mann et al., 2007; A. et al., 2010; Bantscheff et al., 2011; Bertino and Otterson, 2011; Soragni et al., 2011; Tang et al., 2013; Salvador et al., 2013; Bjornsson et al., 2014; Bailey, Stenehjem and Sharma, 2015; Lee et al., 2015; Schölz et al., 2015; Vogl et al., 2017) were retrieved from CHEMBL database (https://www.ebi.ac.uk/chembl/). These include the approved drugs: Vorinostat, Belinostat and Panobinostat, and those at various stages of clinical trials: Mocetinostat, Entinostat, Tacedinaline, Ricolinostat, Abexinostat, Valproic acid, Butyric acid, Phenyl butyric acid, Droxinostat, Tubacin, Scriptaid, Nexturastat A, M344, MC1568, RGFP966, TMP269, and the natural inhibitor TSA. These inhibitors are well-validated representatives of different classes of HDAC inhibitors with diverse structures, and were therefore used as the training set to develop common feature 3D-pharmacophore models. The training set compounds are used to determine the quality of the pharmacophore hypotheses.

3.5.2 Pharmacophore model generation

Pharmacophore is the spatial configuration of essential features that enable a ligand molecule to interact with a specific target protein. Pharmacophore modeling enables ligand-based virtual screening to be performed using structural information on the known ligand of that protein (Dror et al., 2009). The approach has been successfully applied towards the identification of lead compounds in drug development. HipHop module, a method applied to generate pharmacophore hypotheses in this study, is a part of the Catalyst software package of Biovia DS 4.5 (Barnum et al., 1996; Clement and Mehl, 2000; Guner et al., 2004). It allows for feature-based alignment of a collection of compounds without considering their activity. The algorithm matches the chemical features of a molecule against drug candidate molecules. It produces a series molecular alignments from a collection of conformational models. A Configuration consists of a

set of relative locations in 3D space, and associated feature types used to align chemically important functional groups common to the training set and subsequently develop pharmacophoric hypotheses from these aligned structures. For a compound to match the configuration it should possess structural features that can be superimposed within a certain tolerance from the corresponding ideal locations (Clement and Mehl, 2000). In the current study, the docked pose of the most active compound, Panobinostat was considered as a reference compound and its principal and MaxOmitFeat values were respective, set to 2 and 0 whereas the principal and MaxOmitFeat values for the remaining training set compounds were set to 1 and 2, respectively, based on the pharmacophore model generated in a recent study (Luo et al., 2016). The minimum interference distance was adjusted to 1.00 Å to ensure close proximity of pharmacophoric features; excluded volume, 0; minimum features, 1; maximum features, 10; minimum feature point, 1; number of lead that may miss, 1; complete miss, 0 and superposition error, 1.0. Maximum number of conformers generated was 255, with the energy threshold of 20 kcal/mol from the global minimum.

2.5.3 Pharmacophore model validation

To evaluate the predictive ability of the pharmacophore models generated, another set of 20 known HDAC inhibitors including Resminostat, Pracinostat (SB939), Givinostat, CUDC-101, PCI-34051, Dacinostat, CHR-3996, BRD73954, Tubastatin A, AR-42, CAY10603, 4SC-202, BG45, LMK-235, Santacruzamate A (CAY10683), HPOB, Citarinostat (ACY-241), TMP195, Tucidinostat (Chidamide),   and   ACY-738 (experimenal activity (Ki) ranging from 2-1500 nM), (Bantscheff et al., 2011; Soragni et al., 2011; Tang et al., 2013; Bjornsson et al., 2014; Schölz et al., 2015) were used as the active molecules in the test set. For each of these compounds, 20 inactive forms (decoys) were generated using a Directory of Useful Decoys, Enhanced (DUD-E). (Mysinger et al., 2012) Hence, a database containing 420 compounds was developed and the Güner-Henry scoring method was applied to validate the pharmacophore hypotheses generated. In a quantitative manner, this method evaluated the predictive ability of the generated model by retrieving the active compounds from a database

containing 20 active and 400 inactive compounds. The GH score was computed using equations 1-4 below:

$$Y\% = \frac{H_a}{H_t} \times 100\% \tag{1}$$

$$\%A = \frac{H_a}{A} \times 100\% \tag{2}$$

$$E = \frac{H_a \times D}{H_t \times A} \tag{3}$$

$$GH = \frac{H_a(3A + H_t)}{4H_t A}\left(1 - \frac{H_t - H_a}{D - A}\right) \tag{4}$$

Where *D* is the total molecules in the database, *A* is the total number of active molecules in the database, H_t is the total hits in the database, H_a is the number of active hits, *Y%* is the percentage of active compounds obtained from the decoy set, *A%* is the percentage ratio of actives in the hits list, *E* is the enrichment factor, and *GH* is the goodness of hit score which is a measure of the quality of a model and is expected to range from 0.6 to 1 for an optimal pharmacophore model. (Guner et al., 2004).

3.5.4 Database search

To search for the new lead compound as HDAC6 inhibitors, Hypo1 was run against "DruglikeDiverse" database in the Biovia DS 4.5 (Dassault Systèmes BIOVIA, 2017). The molecules were filtered based on Lipinski's "Rule of 5" (Lipinski, 2004). This database was screened because, to the best of our knowledge, it has not been explored previously for the identification of HDAC6 inhibitors and it might contain novel scaffolds for HDAC6 inhibitor designs. The idea of screening this database of fewer than 10,000 compounds was to ascertain the robustness of the generated model through molecular docking and dynamics studies. Subsequently, a larger compound library such as National Cancer Institute and ZINC databases will be probed using the model for potential hit compounds.

3.5.5 Drug-likeness and ADMET prediction

Drug-likeness was predicted using ADMET Predictor (Simulation Plus Model) (http://www.simulations-plus.com) — these models include S+logP, S+logD, MlogP, MWt, S_HBD, S_NO, TPSA. The ADMET properties such as P(BBB+), P(HIA+), aqueous solubility Cacao-2 cell permeability, and rat acute toxicity, were predicted using AdmetSAR server (http://lmmd.ecust.edu.cn/admetsar1) (Shen et al., 2010).

3.5.6 Molecular docking assay

Docking input files were generated using AutoDockTools. (Morris and Huey, 2009) Gasteiger partial charges were assigned to each atom to generate gpf and dpf files. Energy grid boxes of dimensions 70, 70 and 70 Å for HDACs 3, 6 and 7; and of dimensions 60, 60 and 60 Å for HDACs 1, 2 and 8 were centered near Zn^{2+} ion, to cover the entire binding sites of the enzymes. The search for ligand conformation in the active sites of the enzymes was carried out using Lamarckian GA in Autodock4. For each ligand, 20 independent runs were performed, and the distinct conformers generated were docked randomly into the catalytic pocket of the enzyme using 20,000,000 energy evaluations.

3.5.7 Molecular dynamics simulation

To examine the stability of ligand binding modes MD simulations were performed for the free form of HDAC6 and its complexes with Panobinostat and the selective lead compounds (IBS399024 and ENA50196), using NAMD software (Phillips et al., 2005). Input files for NAMD were generated using CHARMM GUI (Lee et al., 2016). The energy of the systems was minimized for 1000 steps by steepest descent method and equilibrated for 2 ns in NVT ensemble. All the systems were submitted to 10 ns-production run in NPT ensemble, was performed. During this production run the time step and collection interval were set to 2 fs and 1 ps, respectively. The stability of ligand binding modes was assessed by comparative analyses of RMSD and RMSF throughout the trajectories, of the free form of HDAC6 and the complexes.

3.6 Homology Modeling of Human Histone Deacetylase 10

3.6.1 Template selection

Template selection is carried out by searching for homologous protein sequences and/or structures with tools such as BLAST (Basic Local Alignment Search Tool) and PSI-BLAST (https://blast.ncbi.nlm.nih.gov/Blast.cgi). Here, the recently-solved crystal structure of Danio rerio (zebrafish) HDAC10 (PDB ID; 5TD7, release date 24-05-2017) was retrieved from PDB and used as a template structure.

3.6.2 Alignment of the target sequence with the template sequence

Generally, when there is a minimum of 30% sequence identity between a target and a template, proteins are expected to have similar structures if the aligned region is long enough. When two proteins have more than 50% sequence identity the quality of the model is generally considered reliable (Pevsner, 2015). The target sequence (fasta format) was retrieved from UniProt databank (NP_114408.3) (http://www.uniprot.org/). The template sequence was displayed from the protein structure in BIOVIA DS 4.5 (http://accelrys.com/). The two sequences were aligned using "Align Sequences" toolkit of BIOVIA DS 4.5 (Figure 3.9).

3.6.3 Model building

The commonly used program, MODELLER (Webb and Sali, 2016) uses modeling by satisfaction of spatial restraints to translate sequence alignments into distance and chirality constraints, which are then used as input for distance geometry calculations. The model is calculated by an optimization method relying on conjugate gradients and molecular dynamics (Sali and Blundell, 1993). Generalized comparative modeling starts with predicting contacts and secondary structure for the template-aligned regions, and possibly for the unaligned regions and then searches the conformational space guided by

a distance geometry and clustering, to overcome alignment mistakes. (Kolinski et al., 2001). Here, 20 models were built using "Homology Modeling" protocol of BIOVIA DS 4.5. They were then verified with MODELLER plug-in. The best model (M0017), with the DOPE score and Normalized DOPE score of -78039.35938 and -0.814028 respectively, was then minimized using the "Clean Geometry" toolkit to avoid any further steric hindrance of amino acids side chains. Finally, the protein was prepared using "Prepare Protein" protocol and protonated at pH, 7.4.

3.6.4 Model validation

Assessment of the quality of protein structure (experimentally derived or homology model) based on general knowledge of protein structure principles (bond length, angle, peptide bonds, local environment for hydrophobic/hydrophilic residues, etc.) (Pevsner, 2015) is of paramount importance. In the current study, the web-based version of ProSA, ProSA-web was used to assess the quality of the best model (M0017). The overall quality score calculated by ProSA for M0017 is displayed in a plot that showed the scores of all experimentally determined protein chains currently available in the PDB (Berman et al., 2000).
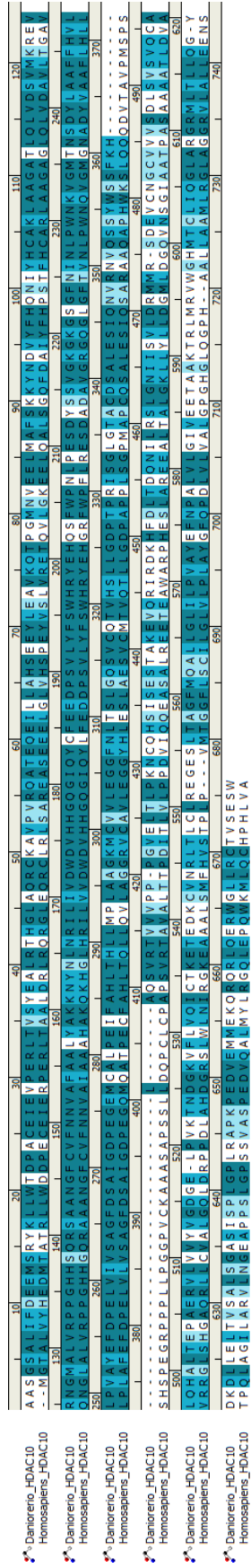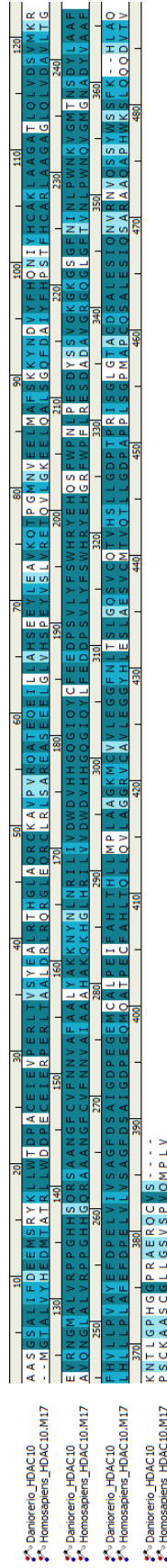
Figure 3. 9. The whole sequence alignment of *Danio rerio* (zebrafish) Histone deacetylase 10 and human histone deacetylase 10; identity (in dark blue) and similarity (in light blue) are 43.8% and 63.6% respectively (**a**). Catalytic domain alignment of *Danio rerio* Histone deacetylase 10 and human histone deacetylase 10; identity and similarity are 58.6% and 76.6% respectively (**b**).

3.6.5 Molecular docking

The protein was prepared using "Prepare Protein" protocol and protonated at pH, 7.4. The A series of HDAC10 inhibitors with known Ki (or IC50) values were retrieved from CHEMBL database. Their geometry was optimized, and prepared using "Prepare Ligand" protocol at pH, 7.4 (Dassault Systèmes BIOVIA, 2017). AutoDockTool (Morris et al., 1998) was used to assign Gasteiger partial charges to each atom of the protein in the PDB format to generate a pdbqt file, which was subsequently used to generate gpf and dpf files. These files were then used as input files for grid mapping and docking respectively. Energy grid box of dimension 60, 60, 60 Å was centered near Zn^{2+} metal ion, and covered the entire active site of HDAC6 and HDAC10. Autodock 4.2's Lamarckian Genetic Algorithm (Morris et al., 1998) with 10,000,000 energy evaluations were used for ligand conformational search. Twenty independent runs were performed for each ligand and the distinct conformers were generated and docked randomly into the binding pocket of these enzymes.

3.6.6 Ligand-based virtual screening

SwissSimilarity is a new web tool for rapid ligand-based virtual screening of small to unprecedented ultralarge libraries of small molecules (Zoete et al., 2016). Here, based on the Autodock 4.0's calculation, Quisinostat was found to have the highest affinity for hHDAC10. Quisinostat was therefore submitted to SwissSimilarity (superpositional 3D similarity) search against ZINC database containing 10,639,400 drug-like compounds. The top 100 hits were docked in the catalytic channel of hHDAC10 using Autodck 4.2 with the docking protocols described above (see **subsubsection 3.6.6**)

3.6.7 Molecular dynamics Simulations

The built homology model, M0017 and its complexes with Quisinostat and ZINC19749069 were submitted to MD simulation. The protocol used here is different from the MD simulation protocol used in our previous studies described above in that the minimization and production time periods were extended to 10,000 steps (10 ps) and

20 ns respectively (see **subsections 3.3.7, 3.4.6 and 3.5.7**). Input files for NAMD were generated using CHARMM GUI (Lee et al., 2016). All the systems were solvated using the TIP3 water model and neutralized by addition of NaCl to an ionic concentration of 0.2 M. NAMD (Phillips et al., 2005) was used for the simulation. The energy of the systems was minimized for 10000 steps (10 ps) by steepest descent method and equilibrated for 2 ns in NVT ensemble. Then, unrestrained production run was performed for 20 ns in NPT ensemble at time step and collection interval of 2 fs and 1 ps, respectively.

4. RESULTS

4.1 Sequence and Structural Analyses of Class I HDACs

The whole sequence alignment revealed that amino acid residues in the catalytic channels of class I HDACs are similar. They share 33.1% sequence identity and 57.8% sequence similarity. The HDACs' active site is conserved, especially among class I HDACs 1-3 — with sequence identity and similarity of 60.5% and 81.7% respectively. HDACs 1 and 2 share the highest sequence identity of 93.5% and similarity 97.8%. Structural superimposition of HDACs 1 and 2 showed the lowest RMSD while that of HDACs 3 and 6 showed the highest RMSD value (Table 4.1). Phylogenetic tree revealed that HDACs 6 and 8 were relatively distant from HDACs 1 and 2. HDAC3 shares sequence similarity with all the enzymes under study. These data implied that the subtle difference around their catalytic channel can be exploited to design selective inhibitors.

Table 4. 1. Main-chain RMSD below the diagonal (in yellow) and Number of Overlapping Residues above the diagonal (in blue) of class I HDACs and HDAC6.

RMSD (Å) (YELLOW)/NUMBER OF OVERLAPPED RESIDUES (BLUE)					
PROTEIN	HDAC1	HDAC2	HDAC3	HDAC8	HDAC6
HDAC1		366	364	337	260
HDAC2	0.892		364	337	260
HDAC3	0.989	0.927		337	260
HDAC8	1.192	1.179	1.114		260

,

	Carbon
	Oxygen
	Nitrogen
	Sulfur
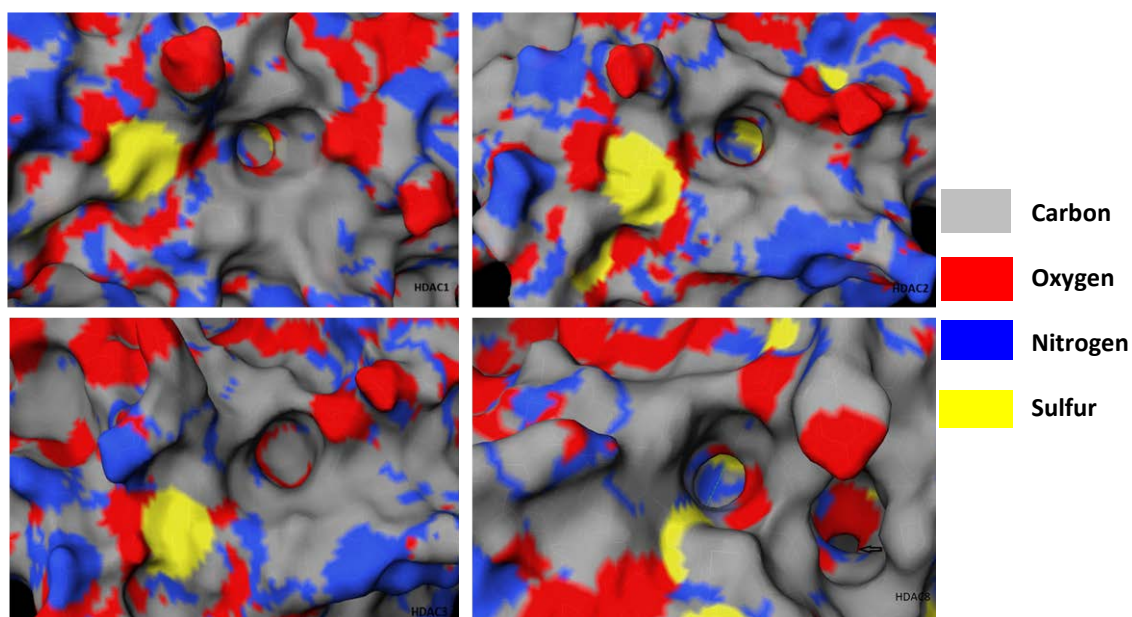
Figure 4. 2. Molecular surface representations of the catalytic pocket of class I HDACs.

Molecular surface representations of the catalytic channels of class I HDACs are juxtaposed in Figure 4.1. Class I HDACs share a long tunneled catalytic pocket containing polar residues deep inside near Zn^{2+} metal ion. Morphologically, they also share a surface entrance rich in hyrophobic residues. HDAC8 contains a unique acetate release channel (pointed by an arrow head) which presents a potential opportunity for achieving selectivity.

4.2 Design of Isoform-selective HDAC Inhibitors by Scaffold Hopping.

4.2.1 Binding affinity

The estimated free energy of binding and inhibition constant of our designed compounds are shown in Table 4.2 below. KA_025, KA_026, and KA_027 showed fthe highest binding affinity and selectivity for HDACs 1 and 2; KA_029 and KA_036 showed selectivity for HDAC1 and HDAC2 respectively. KA_028 showed selectivity

for class I HDACs. KA_030 through KA_035 and KA_037 were found to be nonselective. The selectivity fold values of the potential selective inhibitors are compared in Table 4.3.

KA_025, KA_026, and KA_027 spanned the catalytic channels of HDACs 1 and 2 in a similar mode. The predominant interactions common to the complexes of these compounds were π-π stacked, π-π T-shaped, π-alkyl, van der Waals, conventional H-bonds, and carbon-H-bonds (Figures 4.2-4). KA_029 formed an additional interaction (Metal-acceptor) between its sulfonyl oxygen and Zn^{2+} ion, coupled with π-sulfur interactions with HIS141 and HIS178 (Figure 4.5). However, such interactions were not observed with HDAC2 despite the catalytic channels similarity existing between HDACs 1 and 2. This is due to the conformational difference between the two isoforms that allowed the binding of this same compound to these homologous proteins with different modes. Interestingly, KA_036 bound to these isoforms with different orientations despite triplicate docking runs to ascertain its correct binding mode (Figure 4.6). Consequently, the set of interactions, and the binding affinity were different, higher being against HDAC2.
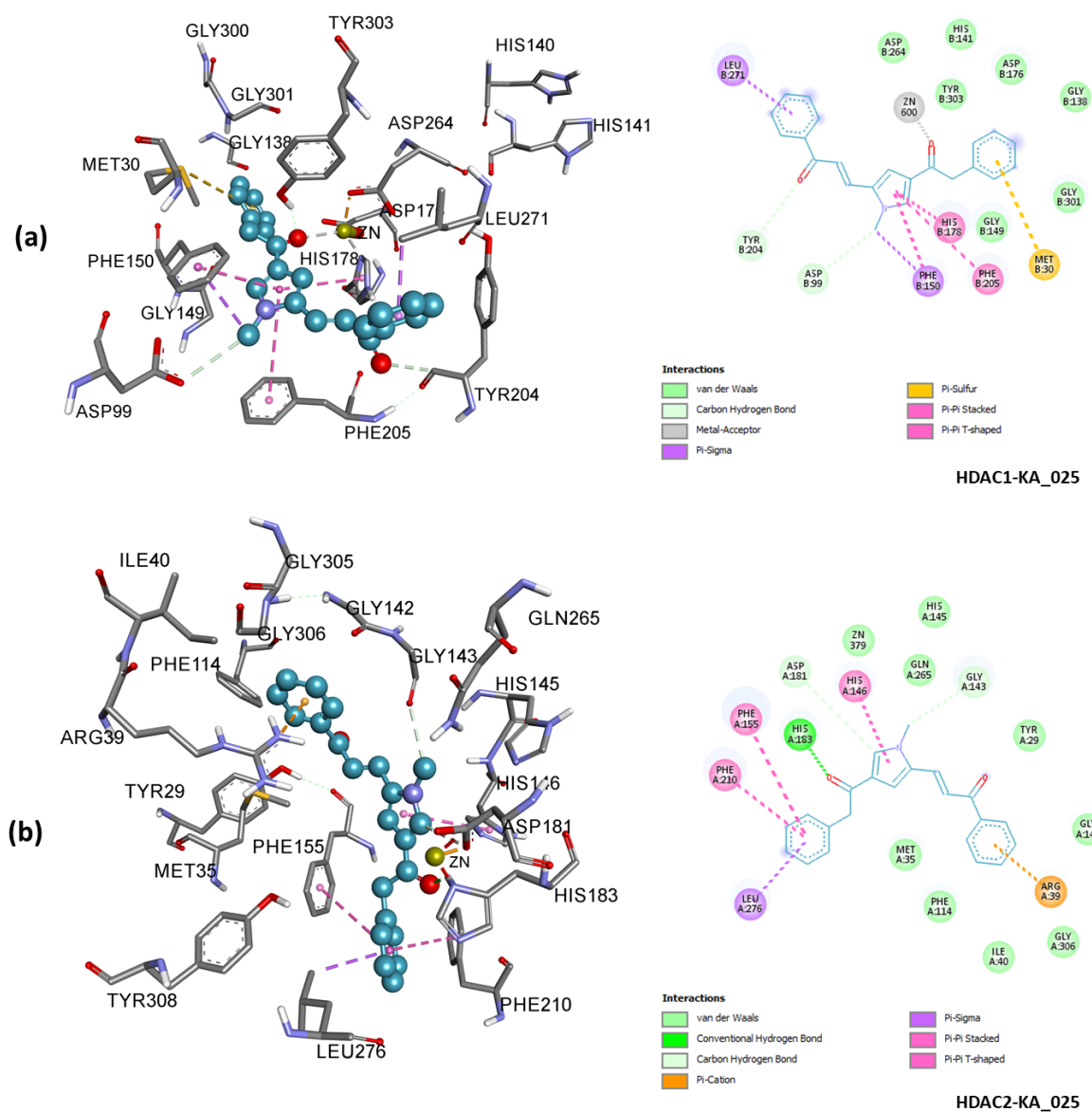
Figure 4. 3. 3D (left) and 2D (right) representations of the interaction between HDAC1 and KA_025 (a). 3D (left) and 2D (right) representations of the interaction between HDAC2 and KA_02; the types of non-bond interactions are indicated in their respective colors (b).
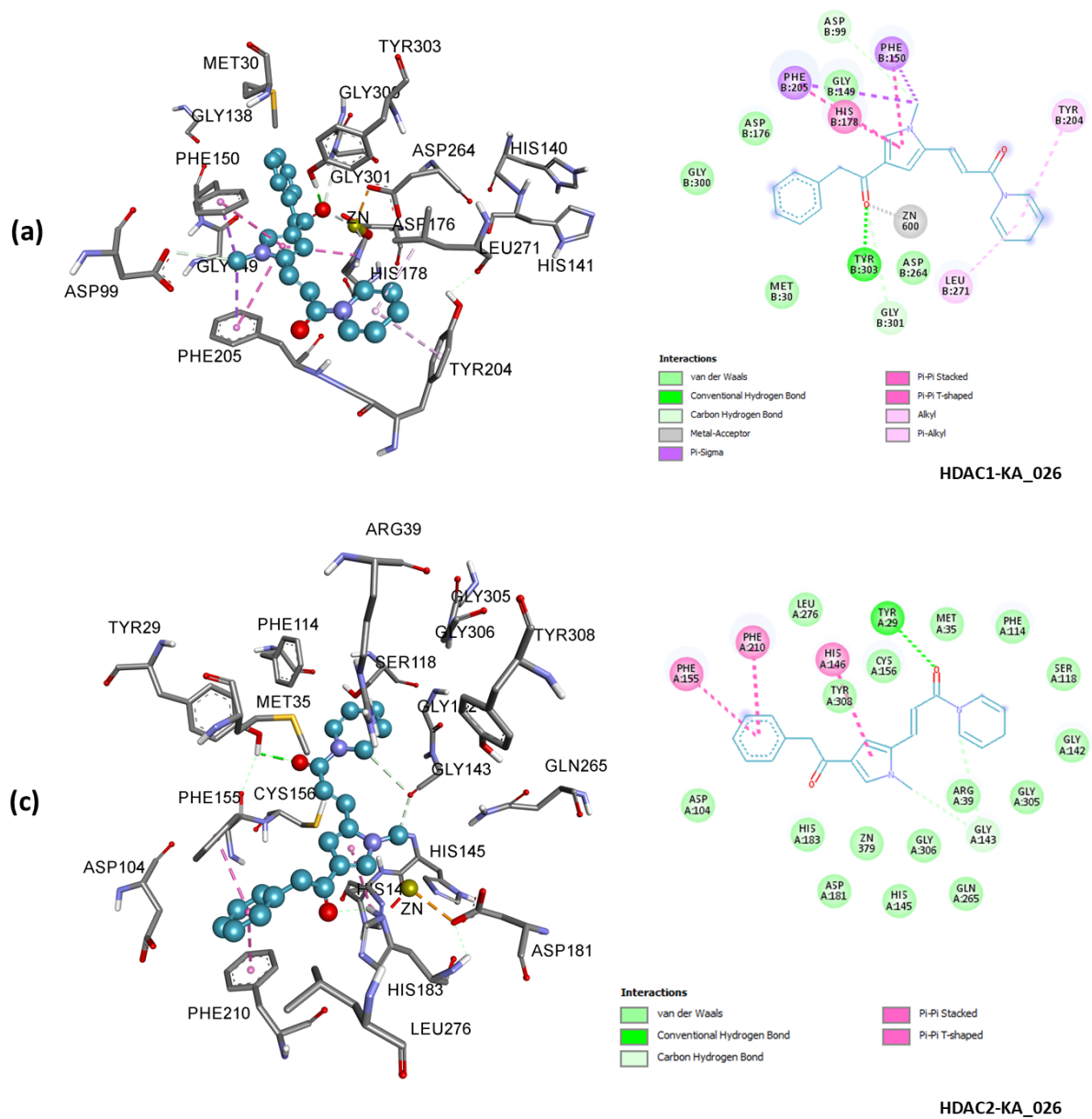
Figure 4. 4. 3D (left) and 2D (right) representations of the interaction between HDAC1 and KA_026 (a). 3D (left) and 2D (right) representations of the interaction between HDAC2 and KA_026; the types of non-bond interactions are indicated in their respective colors (b).
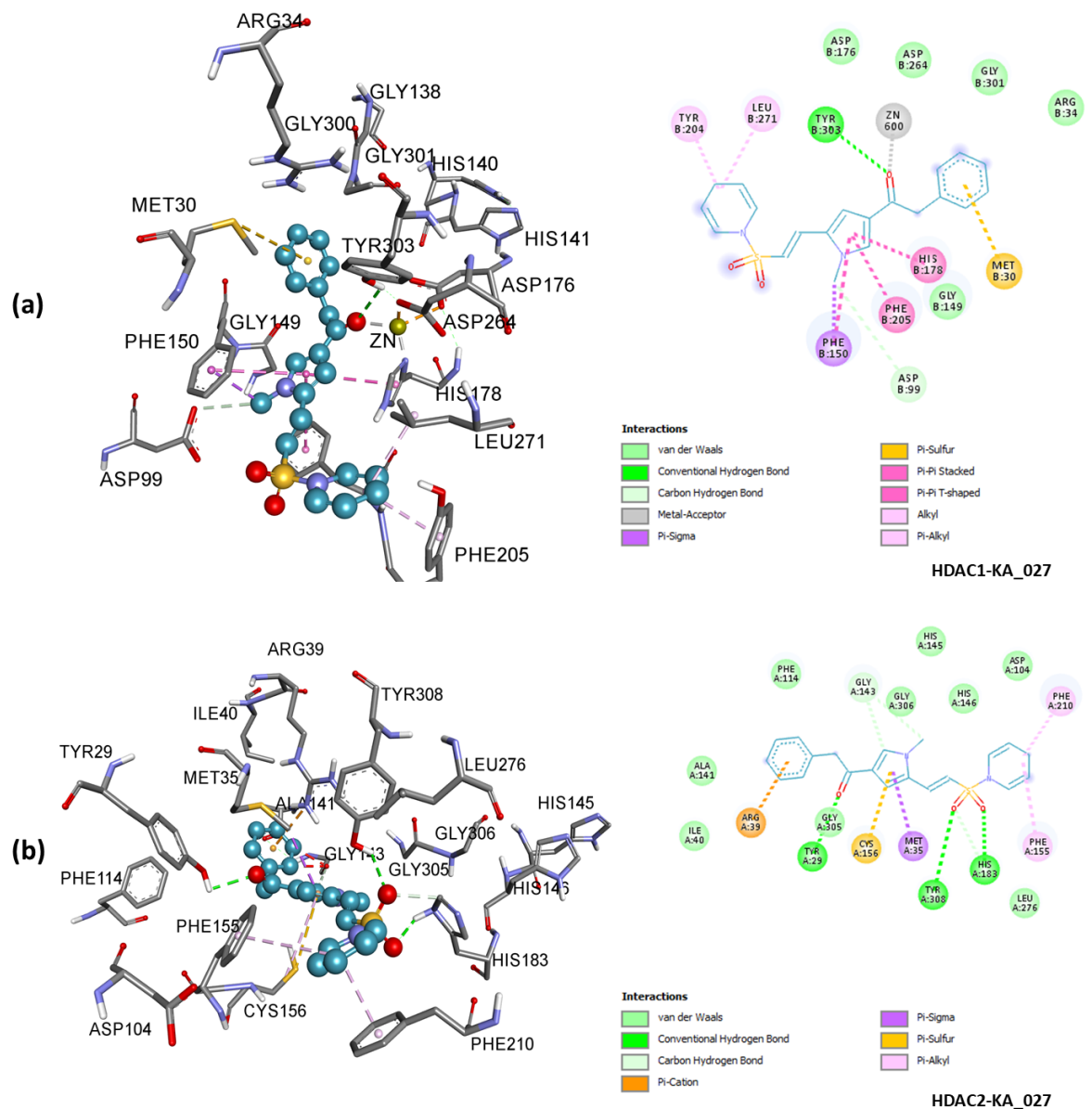
Figure 4. 5. 3D (left) and 2D (right) representations of the interaction between HDAC1 and KA_027 (a). 3D (left) and 2D (right) representations of the interaction between HDAC2 and KA_027; other types of non-bond interactions are indicated in their respective colors (b).

Figure 4. 6. 3D (upper) and 2D (lower) representations of the interaction between HDAC1 and KA_029; the types of non-bond interactions are indicated in their respective colors
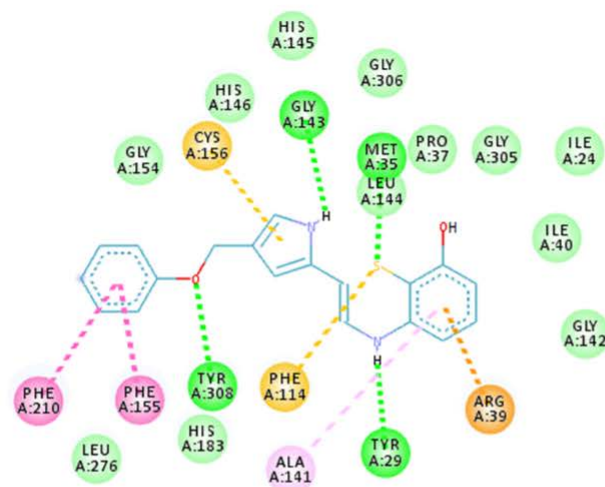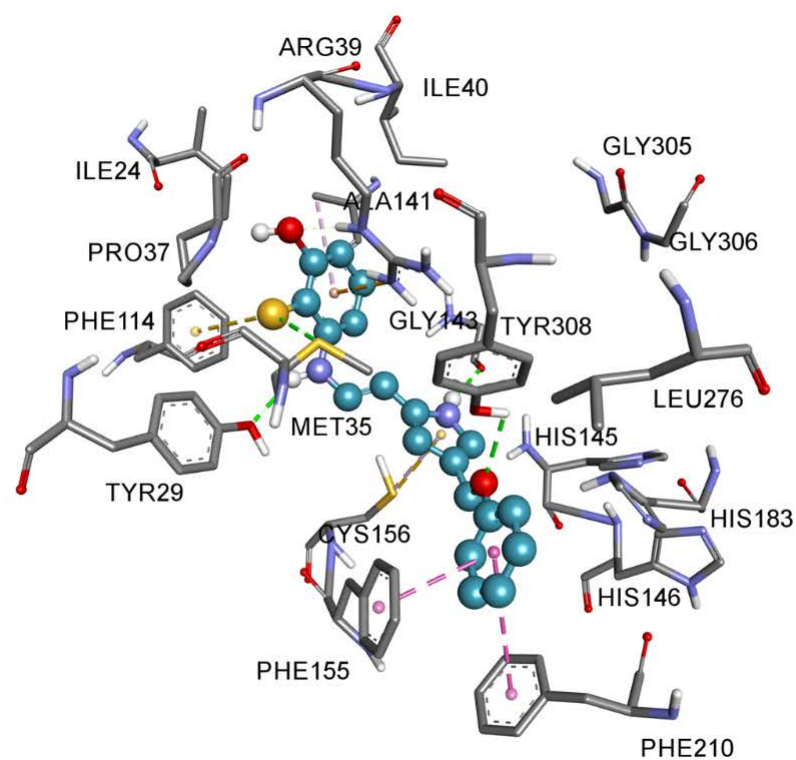
Figure 4. 7. 3D (upper) and 2D (lower) representations of the interaction between HDAC2 and KA_036; the types of non-bond interactions are indicated in their respective colors in the 2D scheme.

Table 4. 2. Estimated free energy of binding of KAs against Class I HDACs and HDAC6 compared with known HDAC inhibitors. The compounds are color-coded: known HDAC inhibitors (grey); HDACs 1- and 2-selective (green); HDAC1-selective (yellow); HDAC2-selective (purple) and nonselective inhibitors (orange).

Compound	ΔG (kcal/mol)				
	HDAC1	HDAC2	HDAC3	HDAC8	HDAC6
Vorinostat	-8.45	-8.64	-8.32	-8.42	-8.55
Belinostat	-9.62	-8.89	-9.44	-8.68	-8.02
Romidepsin	-8.22	-8.76	-8.44	-7.99	-7.34
Entinostat	-9.82	-9.86	-10.62	-7.16	-7.65
Tacedinaline	-8.62	-8.10	-9.08	-7.36	-7.82
Mocetinostat	-9.89	-9.44	-9.76	-6.44	-7.32
KA_025	-10.45	-10.31	-8.99	-8.53	-8.46
KA_026	-10.20	-9.82	-8.88	-8.64	-8.62
KA_027	-10.34	-10.21	-9.01	-8.93	-8.93
KA_028	-9.72	-9.52	-8.87	-8.39	-7.94
KA_029	-9.95	-8.02	-8.1	-7.71	-8.00
KA_030	-9.18	-8.41	-8.29	-7.90	-7.94
KA_031	-9.41	-8.98	-9.09	-8.43	-8.6
KA_032	-9.05	-8.35	-8.82	-7.66	-8.29
KA_033	-8.23	-8.14	-8.15	-7.70	-7.72
KA_034	-8.60	-7.79	-8.01	-8.22	-7.56
KA_035	-8.12	-7.33	-7.60	-7.72	-7.22
KA_036	-7.60	-9.03	-7.9	-7.81	-7.73
KA_037	-7.92	-8.11	-8.13	-7.81	-8.08

Table 4. 3. Selectivity index of HDAC1 compared with HDACs 2, 3, 6, 8; and HDAC2 compared with HDACs 1, 3, 6 and 8.

Compounds	HDAC1 Ki_1 (nM)	HDAC2 Ki_2 (nM)	HDAC3 Ki_3 (nM)	HDAC8 Ki_8 (nM)	HDAC6 Ki_6 (nM)	Selectivity Index				Selectivity
						Ki_2/Ki_1	Ki_3/Ki_1	Ki_8/Ki_1	Ki_6/Ki_1	
KA_025	21.85	27.49	384	678	689	1.26	17.57	31.03	31.53	HDAC1&2
KA_026	33.28	63.43	396	465.02	483.53	1.91	11	13.97	14.53	HDAC1&2
KA_027	26.25	32.82	246.21	282.7	284.26	1.25	9.34	10.77	10.83	HDAC1&2
KA_029	51.13	1271	1240	2220	1286	24.9	24.25	43.42	25.15	HDAC1
						Ki_1/Ki_2	Ki_3/Ki_2	Ki_8/Ki_2	Ki_6/Ki_2	
KA_036	2680	238.67	1619	1890	2160	11.23	6.78	7.92	9.05	HDAC2

4.2.2 ADMET analysis

The designed compounds were drug-like having passed the rule of 5 and other pharmacokinetic tests (Table 4.4). All the physicochemical parameters were found to be within the acceptable range for drug candidacy. An important measure of drug-likeness, topological polar surface (TPSA) area is an index which shows the likelihood of transporting a molecule through cell membranes – allows for the prediction of human intestinal absorption and blood-brain barrier penetration among others. The Descriptor sensitivity analysis of S+logP in response (TPSA) is shown in Figure 4.7. The slope of the curve corresponded to the value reflecting the hydrophilicity/hydrophobicity of the compounds. These compounds were predicted to have TPSA < 100, indicating their tendency for crossing the lipid bilayer. Caco-2 (human epithelial colorectal adenocarcinoma) permeability is another crucial property reflecting gastrointestinal permeability by measuring the rate of transport of a drug molecule across the Caco-2 cell line. It was studied *in vitro* (The et al., 2011) and *in silico* — QSAR model was applied to study Caco-2 permeability of dataset of 674 established compounds (Wang et al., 2000). The aqueous solubility is an important ADMET property influencing absorption and transport of a drug molecule in the body. Quantitative Structure-Property Relationship (QSPR) was applied to relate 150 drug and

organic molecules to their respective aqueous solubility (Ghasemi and Saaidpour, 2007).

Table 4. 4. Predicted Drug-like and ADMET properties of KA_025 through KA_037 using ADMET Predictor™ and AdmetSAR modeling programs.

Name	MlogP	S+logP	S+logD	MWt (Da)	M_NO	HBDH	T_PSA (Å²)	P(BBB+)	P(HIA+)	Aq. Sol. (LogS)	Caco-2 Perm. (cm/s)
KA_025	3.33	4.056	4.06	329	3	0	39.07	0.9935	0.9784	-3.6906	1.4943
KA_026	2.51	2.471	2.47	332	4	0	42.31	0.9882	0.9784	-3.2093	1.4537
KA_027	2.96	2.957	2.02	368	5	0	59.38	0.9031	1	-3.4582	0.9243
KA_028	2.2	3.943	3.94	340	4	1	53.17	0.9791	1	-3.4364	0.8404
KA_029	3.21	3.206	1.58	342	5	1	62.4	0.9575	1	-3.6458	1.0199
KA_030	1.68	3.449	3.45	356	5	0	51.54	0.9159	1	-3.7513	1.0197
KA_031	2.946	3.755	3.755	323.4	3	0	29.54	0.9943	1	-3.6109	1.505
KA_032	1.981	2.694	2.694	326.4	4	1	41.57	0.9824	0.965	-3.5817	1.3993
KA_033	0.62	0.929	0.929	262.3	4	1	49.41	0.9443	0.9272	-2.4127	1.4715
KA_034	0.589	2.105	2.105	277.3	4	1	59.16	0.9758	1	-2.6094	1.0467
KA_035	0.97	3.564	3.564	331.3	4	1	59.16	0.9758	1	-2.6094	1.0467
KA_036	3.99	3.989	2.81	322	3	2	37.05	0.7739	0.9225	-3.1637	1.0026
KA_037	2.323	2.719	2.7	322.4	5	2	67.25	0.8496	0.9682	-2.5174	0.9262

Note: The drug-like molecules should violate no more than one of the following 1-4 properties (Lipinski, 2004); 5-8 are other crucial ADMET properties:
1. MlogP (Moriguchi model of octanol–water partition coefficient, log P) (≤ 5).
   Or S + LogP (Simulation Plus Model of octanol–water distribution coefficient) ≤ 5.
   Or S + logD (Simulation Plus Model of octanol–water distribution coefficient, log D) ≤ 5.
2. MWt (Molecular weight) ≤ 500 Da.
3. S_HBD (Sum of H-bond donors, NH- and OH) ≤ 5
4. S_NO (Sum H-bond acceptors, N and O) ≤ 10.
5. T_PSA (Topological polar surface area) ≤ 140Å².
6. P(HIA+) (Probability for human intestinal absorption) > 0.6.
7. Aqueous Solubility (LogS > -5.7).
8. Caco-2 permeability (LogPapp, cm/s) (faster than 22 nm/s).

Figure 4. 8. Sensitivity curve of exponential of S+LogP versus topological polar surface area of compounds KA_025 (A), KA_029 (B) and KA_036 (C).

4.3. Identification of Potential Isoform-Selective Histone Deacetylase Inhibitors via Structure-Based Virtual Screening

4.3.1 Binding affinity

The calculated inhibition constant of the best-ranked compounds with remarkable isoform selectivity for their respective HDAC isoforms are given in Table 4.5. Compound 1 (Otava id; 3368838) was found to show ~ 25- to 200-fold moderate selectivity for HDAC1 compared with HDACs 2, 3 and 8. Similarly, compound 11 (otava id; P7020400743) was ~ 124- to 3630-fold highly selective for HDAC2 over rest of the class members. Compound 21 (Otava id; P7020350446) showed ~ 5- to 56-fold moderate selectivity for HDAC3 over the rest of the isoforms. Compound 29 (Otava id; P7019081225) showed ~ 180- to 680-fold high selectivity for HDAC8 over the rest of the class members.

Table 4. 5. Structures, calculated inhibition constant (Ki) of the best-ranked selective inhibitors of class I HDACs identified via structure-based virtual screening.

Ligand	Otava id	Structure	HDAC1 Ki (nM)	HDAC2 Ki(nM)	HDAC3 Ki(nM)	HDAC6 Ki(nM)	HDAC8 Ki(nM)	Selectivity
Compound 1	3368838		**6.77**	178.80	373.10	1088.5	1347.31	**HDAC1**
Compound 11	P7020400743		3.43	**0.55**	595.32	1997.50	847.82	**HDAC2**
Compound 21	P7020350446		9.97	154.80	**31.05**	1744.74	897.26	**HDAC3**
Compound 29	P7019081225		18.30	22.67	68.95	38.64	**0.10**	**HDAC8**

4.3.2 Drug-likeness and ADMET analysis

The drug-like and ADMET properties predicted are shown in Table 4.6. All the 36 compounds were found to be drug-like having obeyed the "Rule of 5" and displayed good physicochemical chemical properties. AdmetSAR, a program used in this study, estimates ADMET properties based on substructure pattern recognition and then uses support vector machine algorithm to build a model (Cheng et al., 2012). ADMET properties estimated including aqueous solubility (LogS$_w$) and Caco-2 permeability were within the normal range of drug candidacy.

Table 4. 6. Predicted drug-like and ADMET properties of compounds 1 through 36.

S/N	Otava code	MlogP	S+logP	S+logD	Ruleof5	Mwt (Da)	S_NO	S_HBD	TPSA (Å^2)	Aq. Sol. ($\log s_w$)	Caco-2 perm. (cm/s)
1	3368838	2.743	3.567	3.567	0	387.501	5	0	63.68	-3.6674	0.7903
2	P1167483	2.328	2.595	0.347	0	340.403	5	3	85.44	-3.9247	0.908
3	4562316	3.006	3.039	3.039	0	305.335	4	0	50.52	-3.588	0.7903
4	P0105480004	2.9	0.117	0.115	0	294.294	7	2	87.69	-3.1743	0.7726
5	P7012340203	1.358	4.409	1.07	0	339.418	5	2	75.11	-3.9352	0.906
6	P7016000027	0.815	1.051	0.172	0	360.418	8	2	117.28	-31015	1.2241
7	4562295	2.729	2.657	2.657	0	321.335	5	1	68.54	-2.9611	0.9342
8	P0217690002	2.182	1.562	1.497	0	282.304	6	3	90.9	-3.2046	0.7418
9	4562397	3.134	3.153	3.153	0	281.357	3	0	29.54	-2.7639	1.7487
10	P7013831126	2.593	3.465	0.085	0	376.436	5	1	72.19	-3.465	1.1189
11	P7020400743	2.108	2.419	-0.012	0	271.318	4	2	66.4	-4.1709	0.8802
12	P2194599	1.04	1.287	-1.451	0	303.32	7	2	105.32	-2.6568	-0.2524
13	P1146482	1.825	3.148	-0.266	0	220.204	4	2	65.98	-2.9419	0.8747
14	P7020090764	1.054	2.929	0.239	0	307.311	6	3	95.34	-2.9757	1.0673
15	P7020350445	0.831	0.569	-2.038	0	246.227	7	3	107.97	-2.1965	0.2993
16	1.25E+08	3.189	3.509	3.5	0	348.382	5	1	72.2	-4.5638	0.3963
17	4562375	2.916	2.984	0.882	0	340.425	5	1	62.55	-3.3815	1.1657
18	P1357221	1.99	3.164	-0.148	0	257.222	4	1	63.33	-4.4561	1.3197
19	P1688898	2.201	2.809	2.779	0	329.382	7	3	103.79	-2.8164	0.9713
20	4562294	2.901	3.435	3.435	0	318.378	4	1	43.26	-3.9688	1.5988
21	P7020350446	1.112	0.807	-2.047	0	260.254	7	3	107.97	-3.1165	0.4911
22	4562273	1.178	1.73	1.729	0	335.365	6	2	84.08	-3.6675	1.6083
23	4562274	1.618	2.284	2.284	0	319.365	5	1	64.11	-3.3149	0.8019
24	7.21E+09	3.805	4.161	4.155	0	312.368	3	1	41.99	-4.26	1.5715
25	1.15E+08	4.144	4.286	4.286	0	281.143	3	2	41.13	-5.3771	1.7059
26	P7016361082	1.595	1.924	1.414	0	324.791	6	2	87.74	-3.8428	1.221
27	1.06E+08	3.336	4	4	0	276.724	4	2	50.36	-4.7511	1.4481
28	1.27E+08	4.369	4.578	4.578	1	288.779	3	2	41.13	-5.5755	1.7277
29	P7019081225	1.305	3.4	-0.536	0	372.383	6	3	99.52	-3.945	0.129
30	P1364003	3.258	4.639	1.229	0	284.357	3	1	46.53	-4.0695	0.8467
31	P7017470060	1.342	2.754	0.141	0	296.281	5	1	76.74	-3.1626	0.0181
32	P0127442890	0.059	1.535	-0.766	0	331.349	6	1	89.63	-3.6986	0.5452
33	P7020420366	0.809	1.598	-1.029	0	231.253	4	2	70.16	-3.6044	0.3752
34	P1365606	1.983	3.912	0.701	0	237.26	3	2	53.09	-3.8013	0.6419

| 35 | P0108480094 | 3.576 | 3.478 | 3.478 | 0 | 415.517 | 5 | 1 | 61.77 | -3.8614 | 1.1606 |
| 36 | P7114490082 | 1.598 | 1.734 | -0.757 | 0 | 245.236 | 5 | 3 | 86.63 | -3.6044 | 0.3752 |

Note: The drug-like molecules should violate no more than one of the following 1-4 properties (Lipinski, 2004); 5-7 are other crucial ADMET properties:
1. MlogP (Moriguchi model of octanol–water partition coefficient, log P) ($\leq$ 5).
   Or S + LogP (Simulation Plus Model of octanol–water distribution coefficient) $\leq$ 5.
   Or S + logD (Simulation Plus Model of octanol–water distribution coefficient, log D) $\leq$ 5.
2. MWt (Molecular weight) $\leq$ 500 Da.
3. S_HBD (Sum of H-bond donors, NH- and OH) $\leq$ 5
4. S_NO (Sum H-bond acceptors, N and O) $\leq$ 10.
5. T_PSA (Topological polar surface area) $\leq$ 140Å^2
6. Aqueous Solubility (LogS > -5.7)
7. Caco-2 permeability (LogPapp, cm/s) (faster than 22 nm/s)

4.3.3 Molecular dynamics simulation analysis

RMSD: The stabilities of each free isoform and its complex with the respective best-ranked ligand were examined by analyzing simulation parameters. In drug design, RMSD can be used to measure the stability of a docked protein-ligand complex. For HDACs 1 and 2, the backbone RMSD profiles of both free and complexes were within the range of 0.6-1.6Å (Figures 4.8 (a) and (b)), with the complexes showing higher stabilities until the end of the simulation. In addition, the RMSD of the free form of HDAC2 was in synchrony with that of the complex between 3-6 ns. Similar trend (0.6-1.4Å) was observed with RMSD of the free and complex forms of HDAC3 until 9 ns — as the simulation progressed, the complex showed higher stability than the free enzyme (Figure 4.8 (c)). In the same manner, bound HDAC8 showed lower RMSD than its free form (Figures 4.8 (d)).
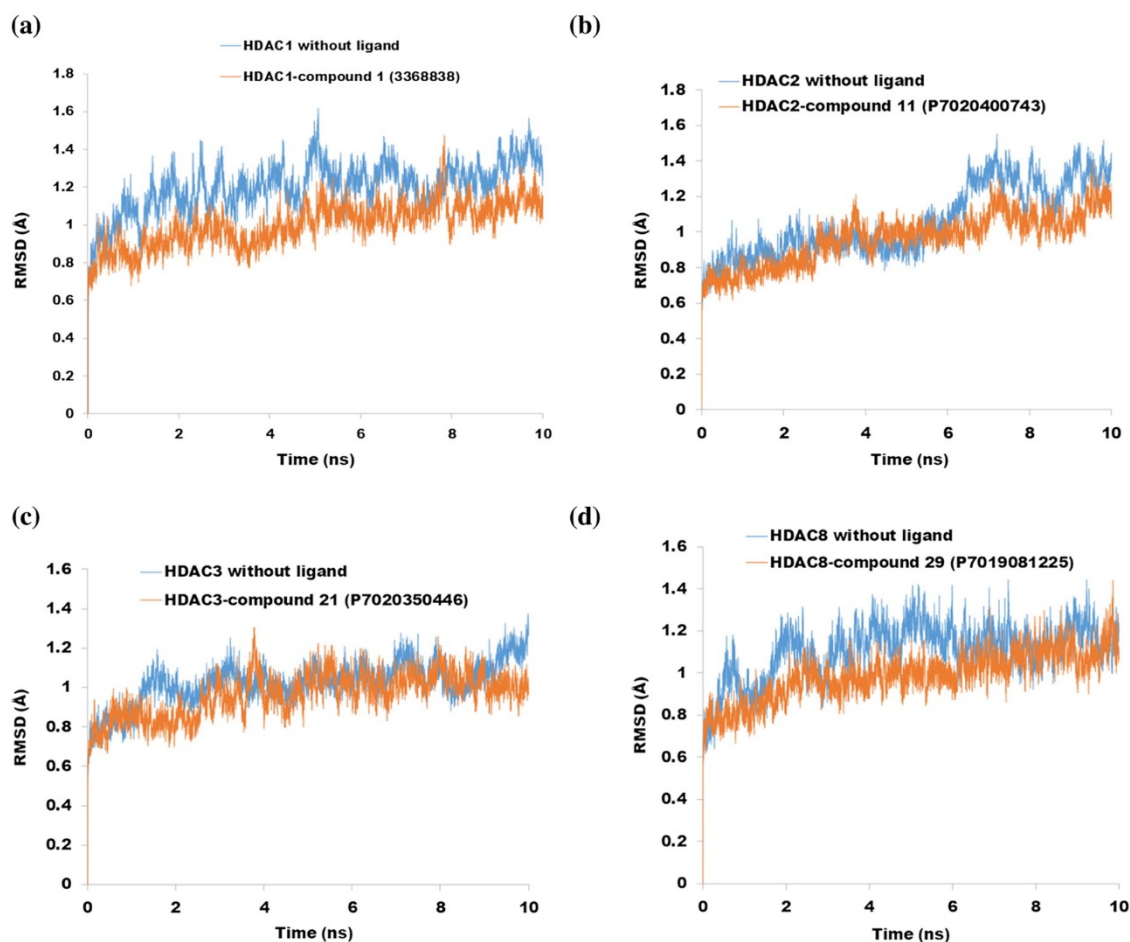
Figure 4. 9. 10 ns-MD simulation RMSD profiles of free and bound enzymes. HDAC1 without ligand (blue) and HDAC1-compound 1 (Otava id; 3368838) complex (orange) (a). HDAC2 without ligand (blue) and HDAC2-compound 11 (Otava id; P7020400743) complex (orange) (b). HDAC3 without ligand (blue) and HDAC3-compound 21 (Otava id; P7020350446) complex (orange) (c). HDAC8 without ligand and HDAC8-compound 29 (Otava id; P7019081225) complex (orange) (d).

Potential energy is another measure of protein-ligand complex stability. The potential energy of the complexes was lower and remained stable throughout the simulation time (Figure 4.9).
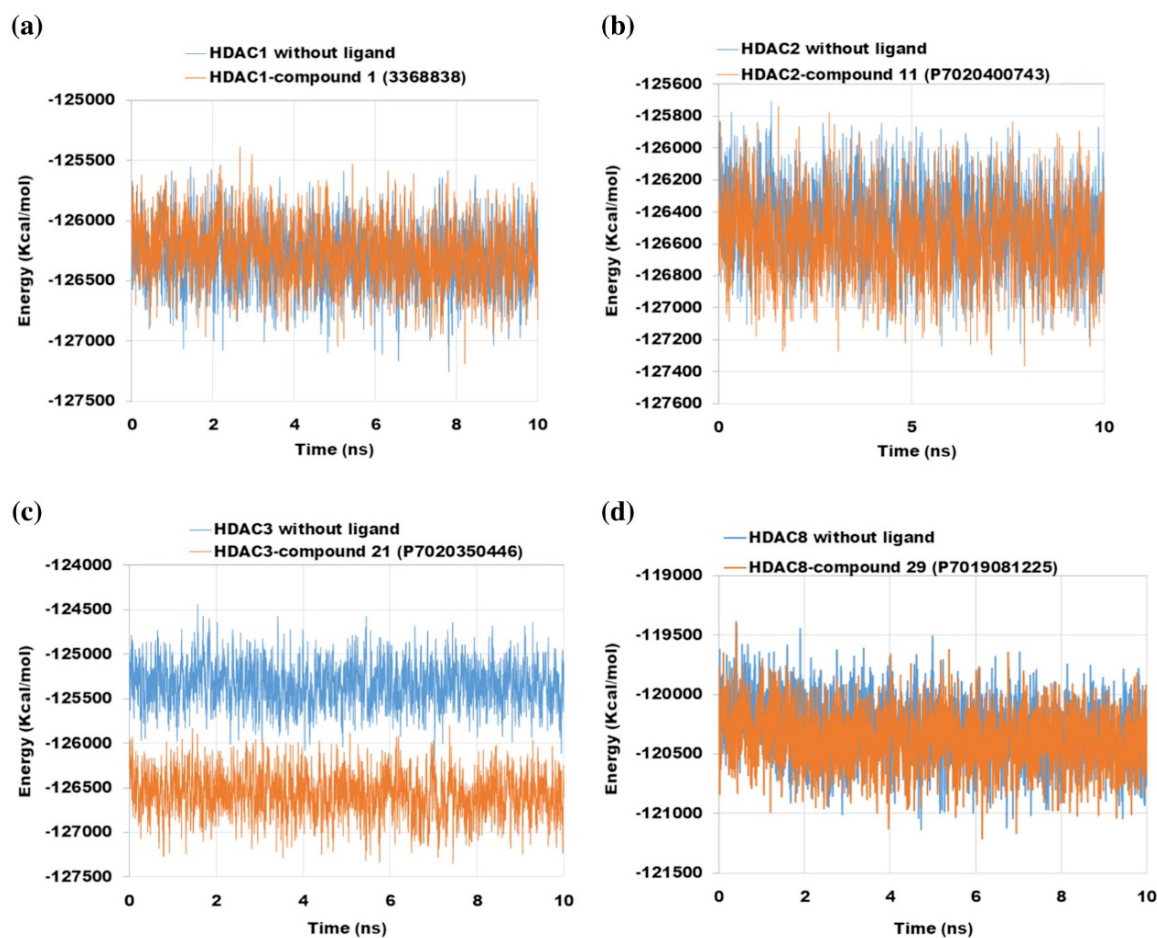
Figure 4. 10. 10 ns-MD simulation energy profiles of the free and bound enzymes. HDAC1 without ligand (blue) and HDAC1-compound 1 (Otava id; 3368838) complex (orange) (a). HDAC2 without ligand (blue) and HDAC2-compound 11 (Otava id; P7020400743) complex (orange) (b). HDAC2 without ligand (blue) and HDAC3-compound 21 (Otava id; P7020350446) (orange) (c). HDAC8 without ligand (blue) and HDAC8-compound 29 (Otava id; P7019081225) complex (orange) (d).

RMSF profile of a dynamic system shows residue fluctuation over time. Fewer residues in the complexes showed increased RMSFs compared with the free isoforms. In other words, those residues involved in interaction with inhibitors showed lower fluctuation, indicating the stability of the complexes (Figure 4.10).
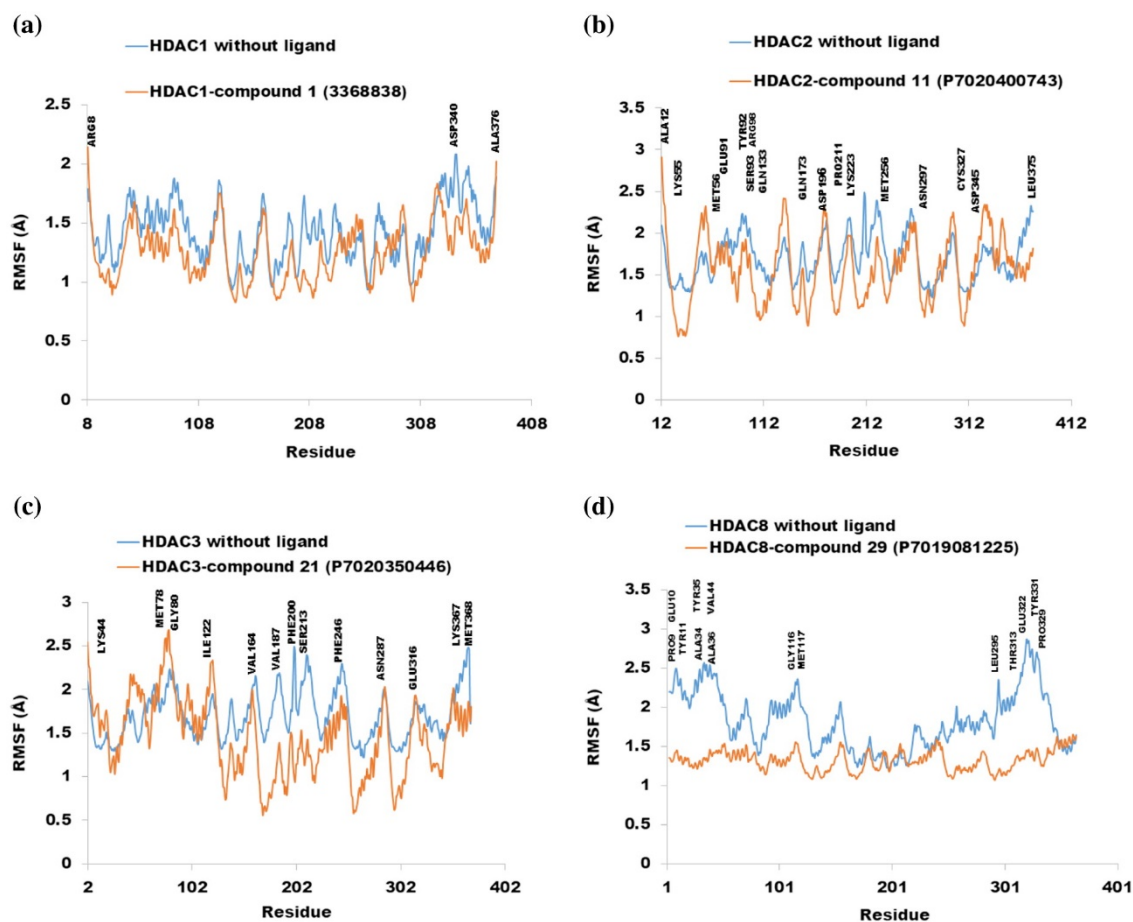
Figure 4. 11. RMSF profiles of the free and bound enzymes. HDAC1 without ligand (blue) and HDAC1-compound 1 (Otava id; 3368838) complex (orange) (a). HDAC2 without ligand (blue) and HDAC2-compound 11 (Otava id; P7020400743) complex (orange) (b). HDAC3 without ligand (blue) and HDAC3-compound 21 (Otava id; P7020350446) (orange) (c). HDAC8 without ligand (blue) and HDAC8-compound 29 (Otava id; P7019081225) complex (orange) (d). HDACs 1, 2 and 3 have their crystal structures starting with residues 8, 12 and 2 respectively.

4.4 The Design of Potential Selective Inhibitors of HDAC6

4.4.1 Interaction of known HDAC inhibitors with HDAC6 catalytic domain 2

The self-docking of TSA reproduced similar conformation to the experimental pose in the catalytic channel of HDAC6. TSA bound to the enzyme with its cap-linker-chelator pharmacophore feature; the hydroxamic acid group chelated Zn^{2+} and formed H-bond

interactions with HIS610 and GLY619, the carbonyl oxygen of the linker group also formed additional H-bond interaction with HIS651 along the tunnel, and van der Waals interaction were formed all over the channel (Figure 4.10 (a)). In a similar manner, Panobinostat bound with its cap-linker-chelator pharmacophore features with which Zn^{2+} ion was chelated via hydroxamic acid group and H-bond interactions were formed with HIS610 and GLY19. In contrast, the pyrrole moiety of indole ring (cap) engaged THR678 and MET682 via H-bond interactions and additional π-sulfur interaction (Figure 4.10 (b)). These additional interactions might account for the increased binding affinity observed with Panobinostat compared with the native ligand, TSA.

The binding modes of the remaining known HDAC inhibitors in the catalytic channel of HDAC6 are shown in Figures 4.12-19. All the hydroxamates showed similar binding mode — engaging Zn^{2+} ion via the hydroxamic acid group, spanning the enzyme's long tunnel with their aliphatic/aromatic linker, making various interactions via their capping group.
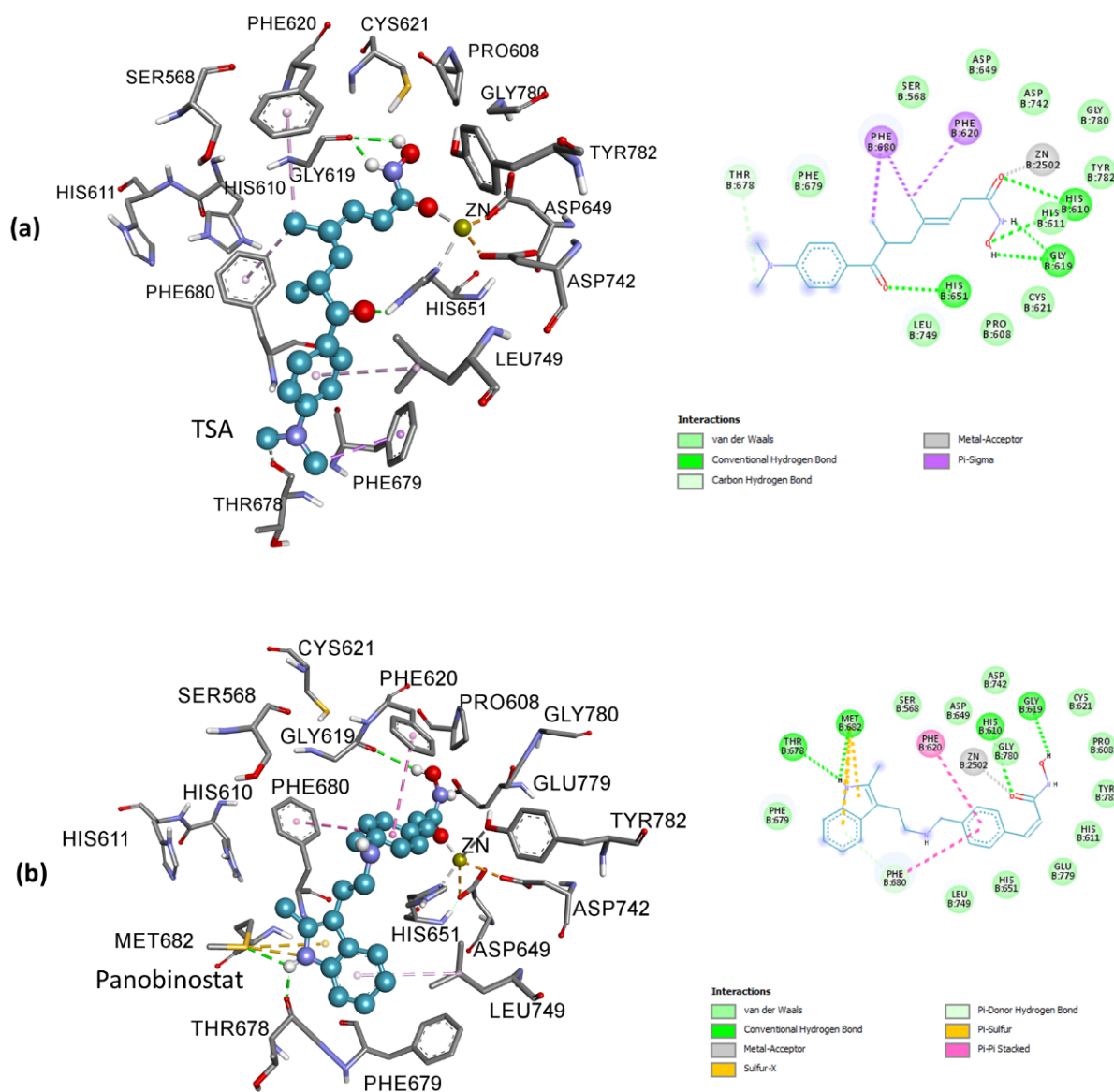
Figure 4. 12. 3D (left) and 2D (right) interaction diagrams between HDAC6 catalytic domain 2 and **Trichostatin A** (a), and **Panobinostat** (b). Panobinostat was found to have the highest binding affinity among the known HDAC inhibitors docked into the catalytic channel of the enzymes.

Figure 4. 13. 3D (a) and 2D (b) interaction diagrams between HDAC6 catalytic domain 2 and **Belinostat** ($\Delta G = 9.22$ kcal/mol; Ki = 175.22 nM).
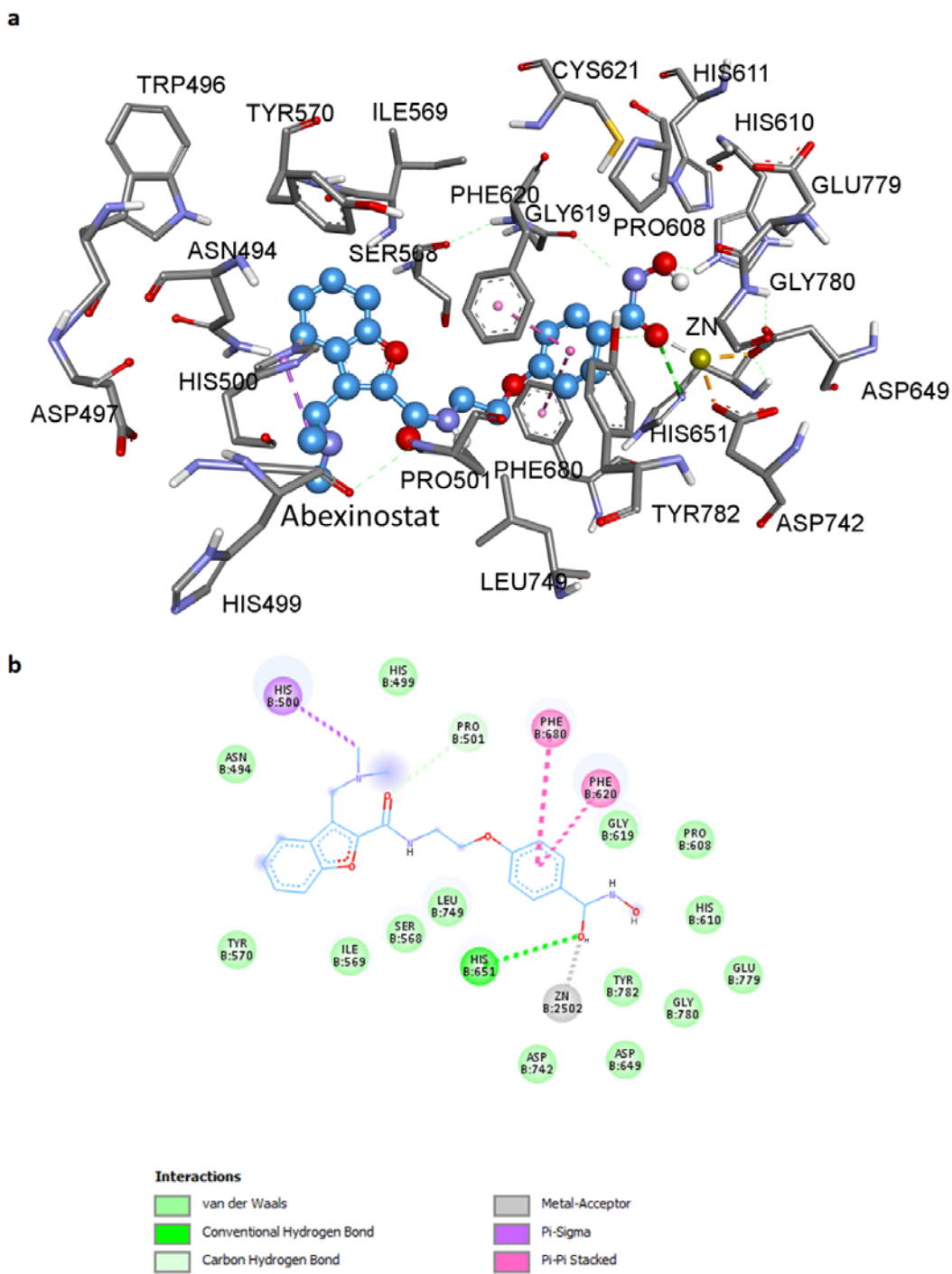
Figure 4. 14. 3D (a) and 2D (b) interaction diagrams between HDAC6 catalytic domain 2 and **Abexinostat** (ΔG = -8.42 kcal/mol; Ki = 678.28 nM).
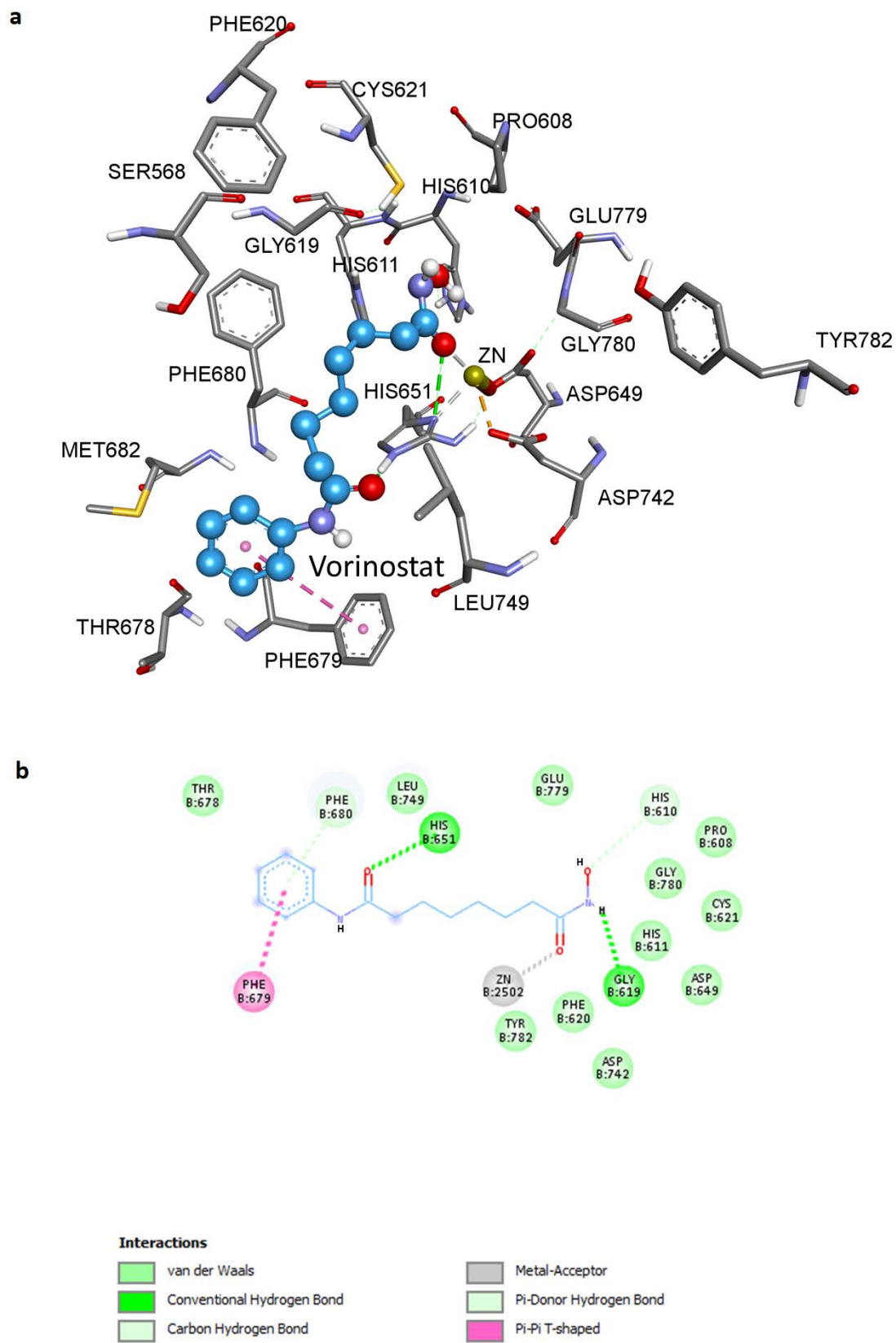
Figure 4. 15. 3D (a) and 2D (b) interaction diagrams between HDAC6 catalytic domain 2 and **Vorinostat** (ΔG = -8.40 kcal/mol; Ki = 691.30 nM).
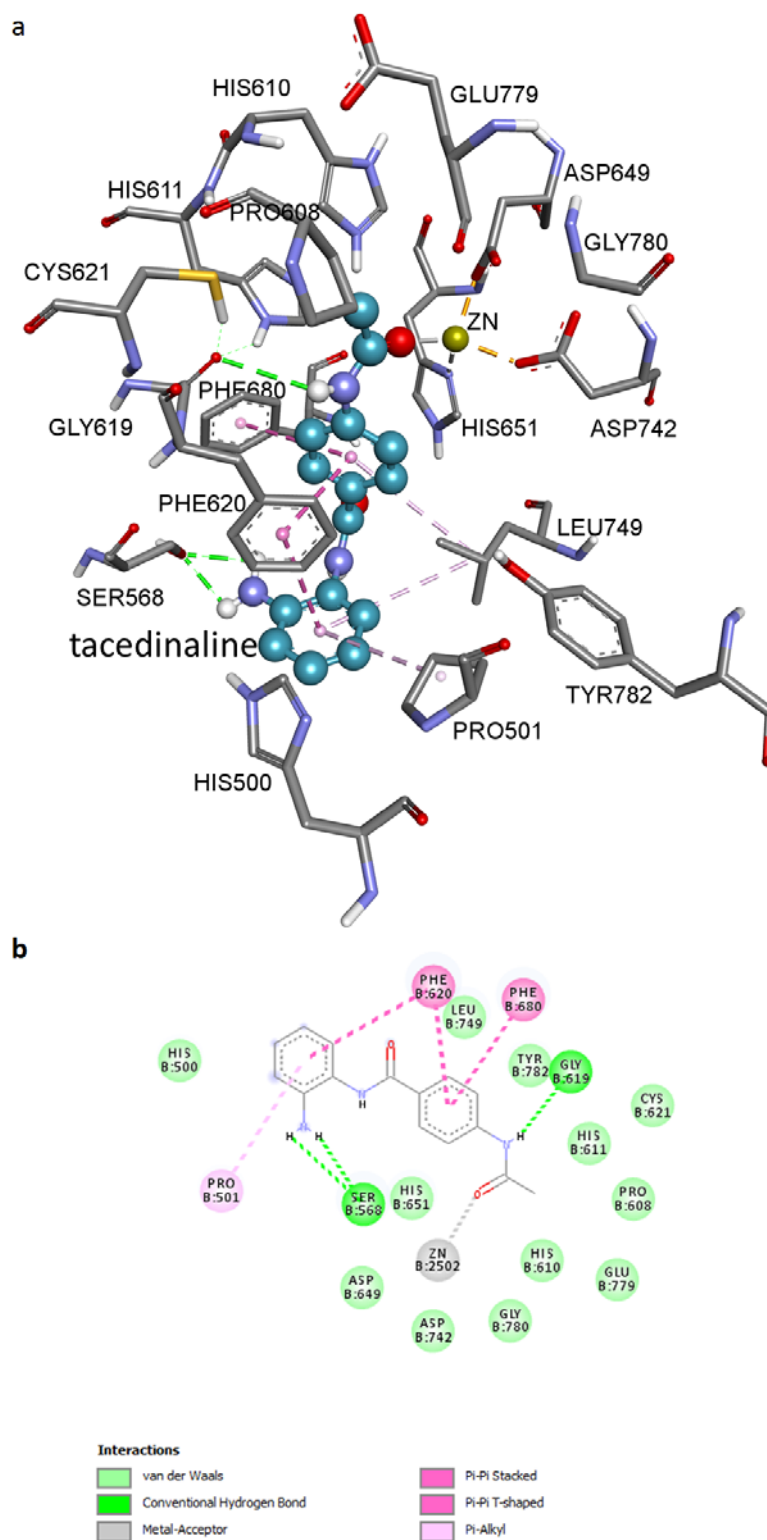
Figure 4. 16. 3D (a) and 2D (b) interaction diagrams between HDAC6 catalytic domain 2 and **Tacedinaline** (ΔG = -8.19 kcal/mol; Ki = 1.00 µM).
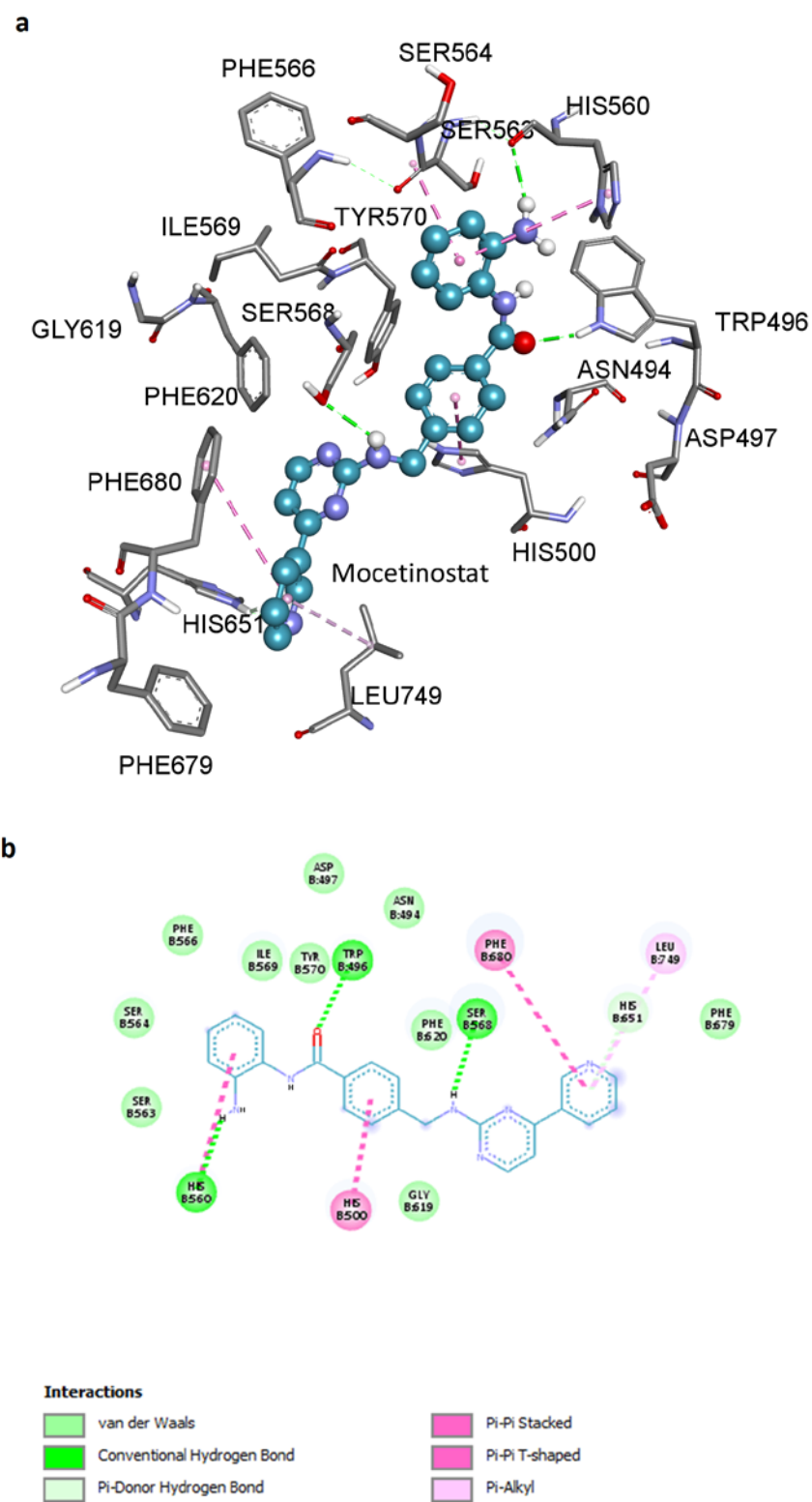
Figure 4. 17. 3D (a) and 2D (b) interaction diagrams between HDAC6 catalytic domain 2 and **Mocetinostat** (ΔG = -7.99 Kcal/mol; K i= 1.39 µM).
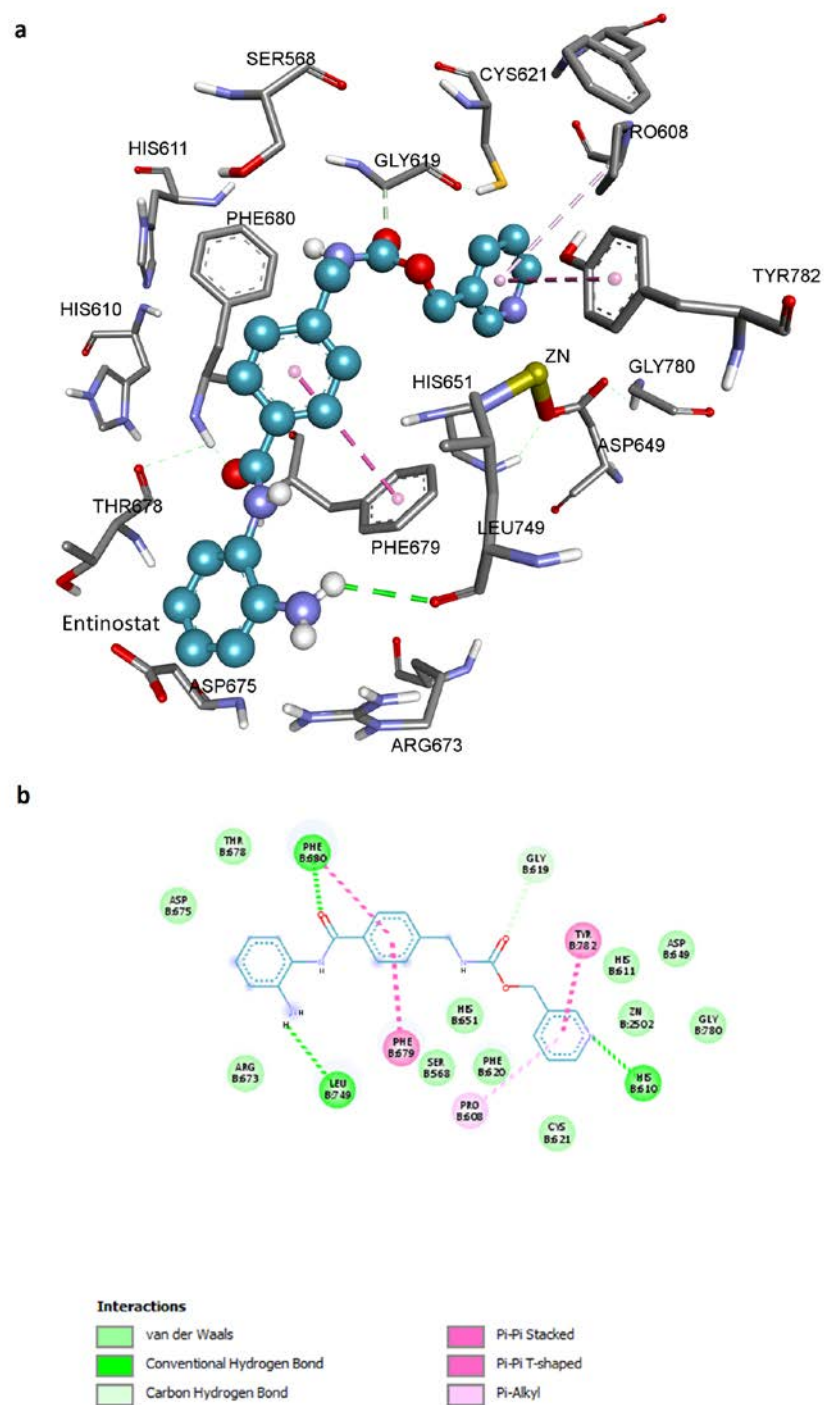
Figure 4. 18. 3D (a) and 2D (b) interaction diagrams between HDAC6 catalytic domain 2 and **Entinostat** (ΔG = -7.71 kcal/mol; Ki = 3.44 µM).

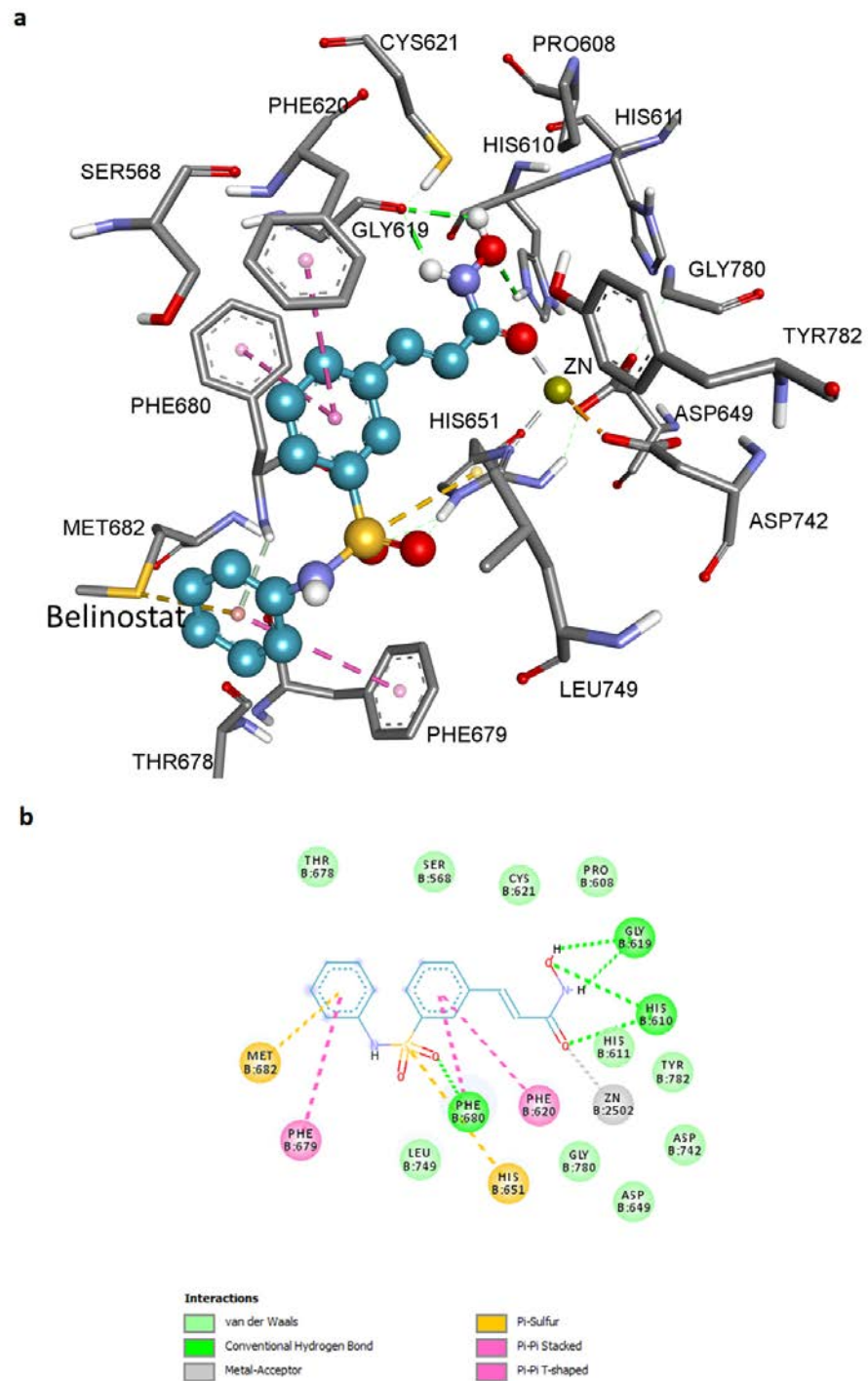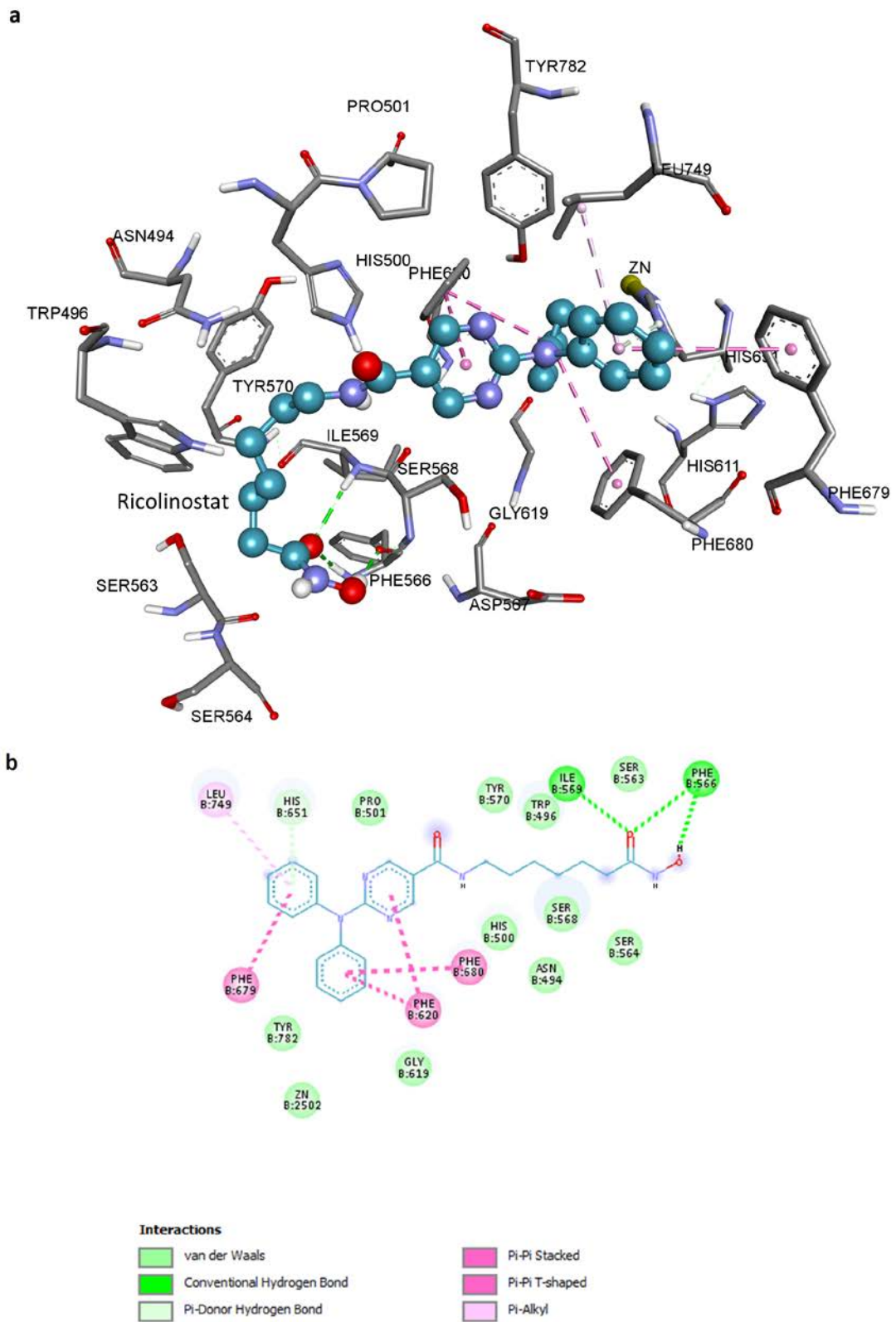Figure 4. 19. 3D (a) and 2D () interaction diagrams between HDAC6 catalytic domain 2 and **Ricolinostat** (ΔG = -7.71 kcal/mol; Ki = 2.24 μM).
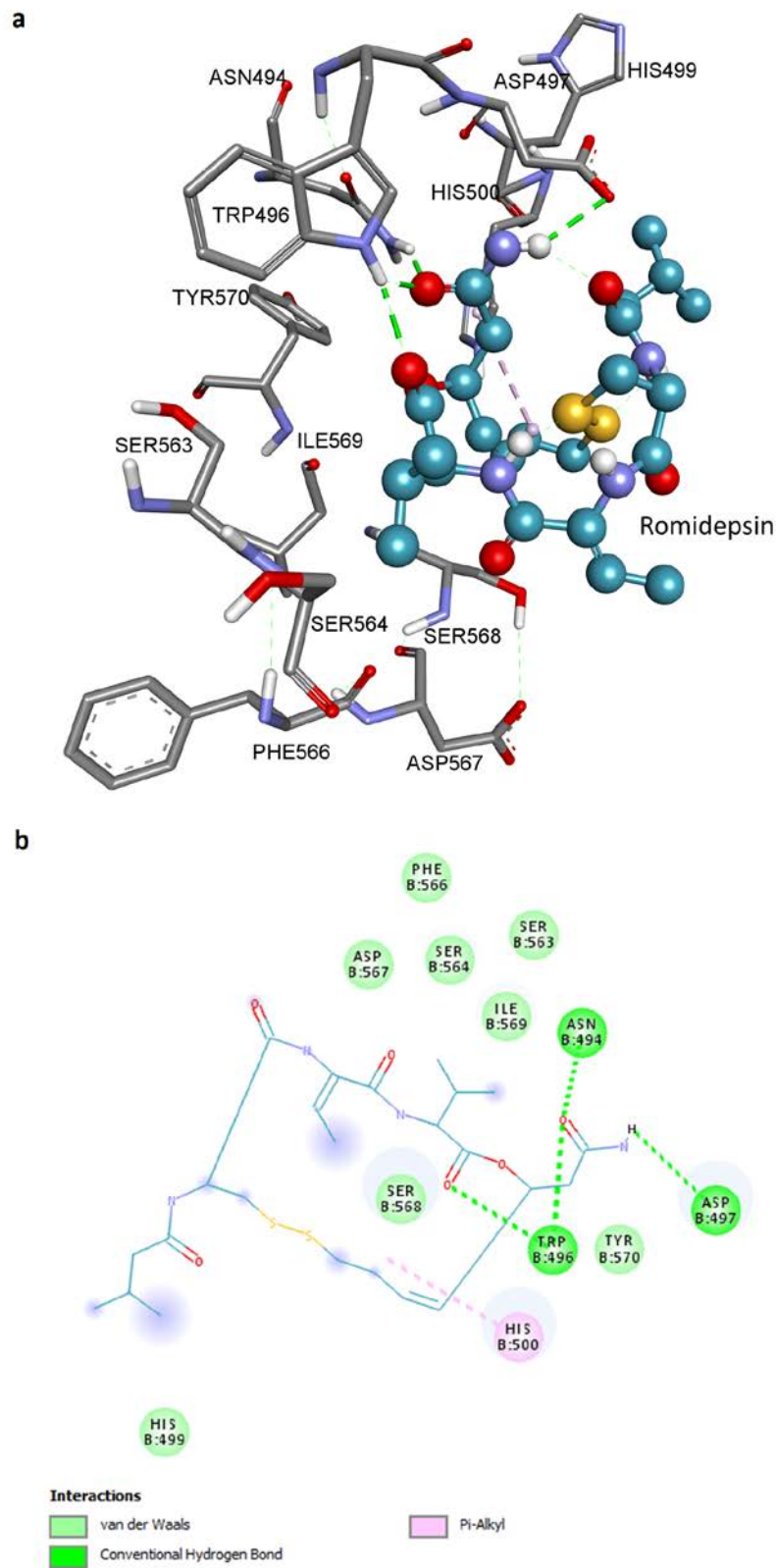
Figure 4. 20. 3D (upper) and 2D (lower) interaction diagrams between HDAC6 catalytic domain 2 and (ΔG= -5.84 kcal/mol; Ki = 52.73 µM).
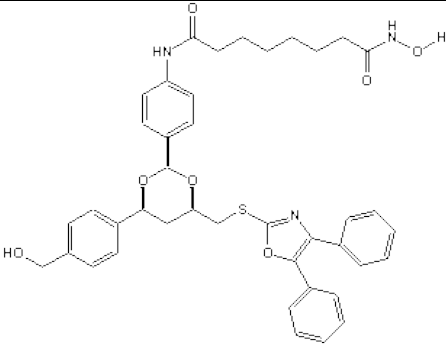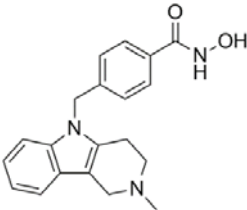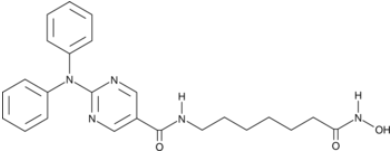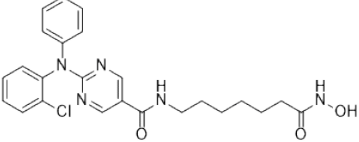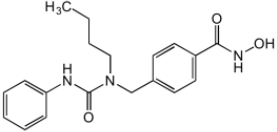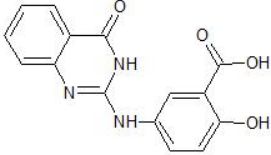
4.4.2 Identification of Potential Lead Compounds as HDAC6-Selective Inhibitors
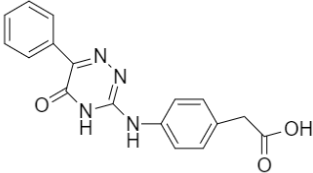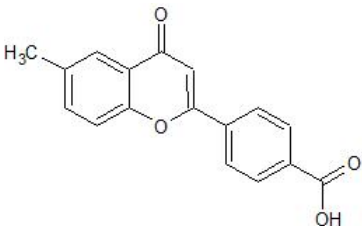
The predicted HDAC6 inhibitors, P7020527347, P2194879, P3823745, and P7715560117 showed ~ 60- to 400-fold selectivity for HDAC6 over HDAC7. P7020527347, P2194879 showed increased binding affinity for HDAC6 compared with all the known HDAC inhibitors studied here. Except for Citarinostat, the predicted inhibitors showed improved in silico performance which might be attributed to their ionizable carboxylic fragment (absent in the known HDAC6-selective inhibitors) (Table 2). The experimental values of these known inhibitors vary depending on the assay conditions, making their comparison with these *in silico* values difficult. Nonetheless, the range of this values have been provided here in the introduction section and the appropriate literature was cited.

These known inhibitors bound to HDAC6 with their pharmacophore model containing 3 features: heterocyclic aromatic ring as a capping group for the enzyme's surface recognition, aliphatic/aromatic linker group that spanned the long tunnel, and the hydroxamic acid moiety as a zinc-binding domain (Appendix B.3).

Like the above-described interaction pattern, the best-ranked compound, P7020527347 formed 2 H-bonds formed between carboxyl group (zinc-binding group) and HIS610, TRY782; and 1 H-bond between oxygen of the hydoxyphenyl group (linker) and HIS611 deep inside the channel; and 1 H-bond between the oxo group of the N-containing heterocyclic fused ring and HIS680. Other contributing forces include 5 Van der Waals interactions in the deep active site, and π-π stacked, π-π T-shaped and π-alkyl interactions at the entrance and along the tunnel (Figure 4.20 (a)). The binding of the same compound at the end of 10 ns-MD simulation was also analyzed. Its orientation remained the same in the 3D space, but the carboxyl group ionized and interacted with seemingly ionized ASP742 via H-bond in the deep channel as shown in 2D scheme (Figure 4.20 (b)).

Table 4. 7. Calculated binding energy (ΔG) and inhibition constant (Ki) of the 5-selected known selective inhibitors of HDAC6 compared with the 4 potential selective lead compounds (highlighted in bold) identified via structure-based virtual screening.

Structures	Compound	HDAC6		HDAC7	
		ΔG (kcal/mol)	Ki (nM)	ΔG (kcal/mol)	Ki (nM)
	Tubacin	-10.50	37.85	-9.08	220.31
	Tubastatin A	-10.19	34.12	-8.62	484.16
	Ricolinostat	-10.22	32.21	-9.11	209.95
	Citarinostat	-11.17	6.49	-8.08	1190
	Nexturastat A	-10.61	16.78	-9.53	103.09
	P7020527347	-13.16	0.23	-9.55	90.65

	P2194879	-11.79	2.29	-9.01	251.23
	P3823745	-10.62	16.52	-8.17	1110
	P7715560117	-10.56	18.21	-8.23	1094

The second 2nd-ranked compound is P2194879, with bulky aromatic cap group stacked at the entrance to the channel by forming π-π T-shaped with HIS500, and 2 π-alkyl interactions with PRO501 and LEU749. Deep inside the active site, 2 H-bonds were formed between the carboxyl group and HIS610, TRY782. The carbonyl oxygen also engaged Zn^{2+} ion via metal-acceptor interactions. Other types of non-bond interactions include 10 van der Waals interactions all over the channel (Figure 4.21 (a)). The binding mode of the same compound at the end of 10 ns-MD simulation showed that its orientation remained the same in the 3D space, but the carboxyl group ionized, and the H-bonds were retained but the set of van der Waals attraction were altered as shown in the 2D scheme (Figure 4.21 (b)).

P3823745 is the 3rd-ranked compound with similar binding mode to that of P2194879 described above. HIS500 and PRO501 were involved in π-sigma and π-π stacked interactions respectively, with the cap group. At the bottom of the pocket, 2 H-bonds were formed between the carboxyl group and HIS610, TRY782; with Zn^{2+} ion engaged via metal-acceptor interaction. Several van der Waals interactions were formed all over the active site (Figure 4.22 (a)). The binding of the same compound at the end of 10 ns-

MD simulation showed that its orientation remained the same in the 3D space but the carboxyl group ionized and formed H-bond with TYR782 instead of the seemingly ionized ASP742 in the docking complex, the carbonyl group of the cap moiety also formed H-bond with SER568 as shown in 2D scheme (Figure 4.22 (b)).

The 4th -ranked compound, P7715560117 apparently made no physical interaction with any amino acid residues at the entrance to the channel. Instead, van der Waals interactions were formed along the entire length of the tunnel. In a similar manner to the rest of the compounds, 2 H-bonds were formed between the carboxyl group and HIS610, TRY782; with Zn^{2+} ion engaged via metal-acceptor interaction (Figure 4.23 (a)). The binding of the same compound at the end of 10 ns-MD simulation revealed that its orientation remained the same in the 3D space, but the carboxyl group ionized and formed H-bond with TYR782 instead of the seemingly ionized ASP742 in the docking complex, as shown in 2D scheme (Figure 4.23 (b)).
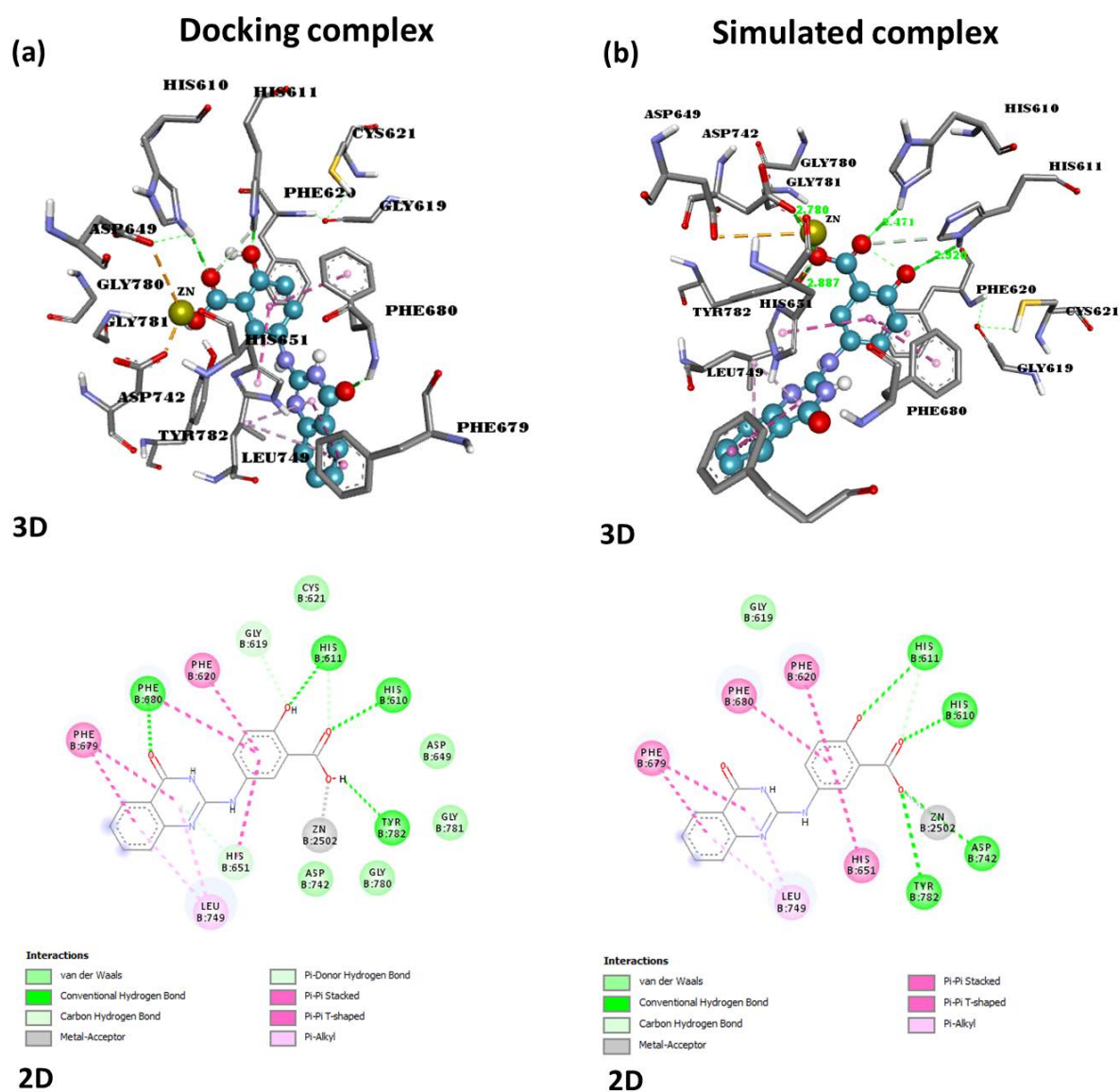
Figure 4. 21. Binding mode of P7020527347 to HDAC6; the compound engaged zinc metal ion deep inside the pocket via a strong metallic interaction with carboxylic group — the same carboxylic group formed 4 H-bonds with HIS610, 611 and ASP742, 782 in 3D space and the key for the non-bond interactions is given in the 2D scheme (a). The binding of the same compound at the end of 10 ns-MD simulation; its orientation remained the same in the 3D space, but the carboxyl group ionized and interacted with seemingly ionized ASP742 via H-bond in the deep channel as shown in 2D scheme (b).
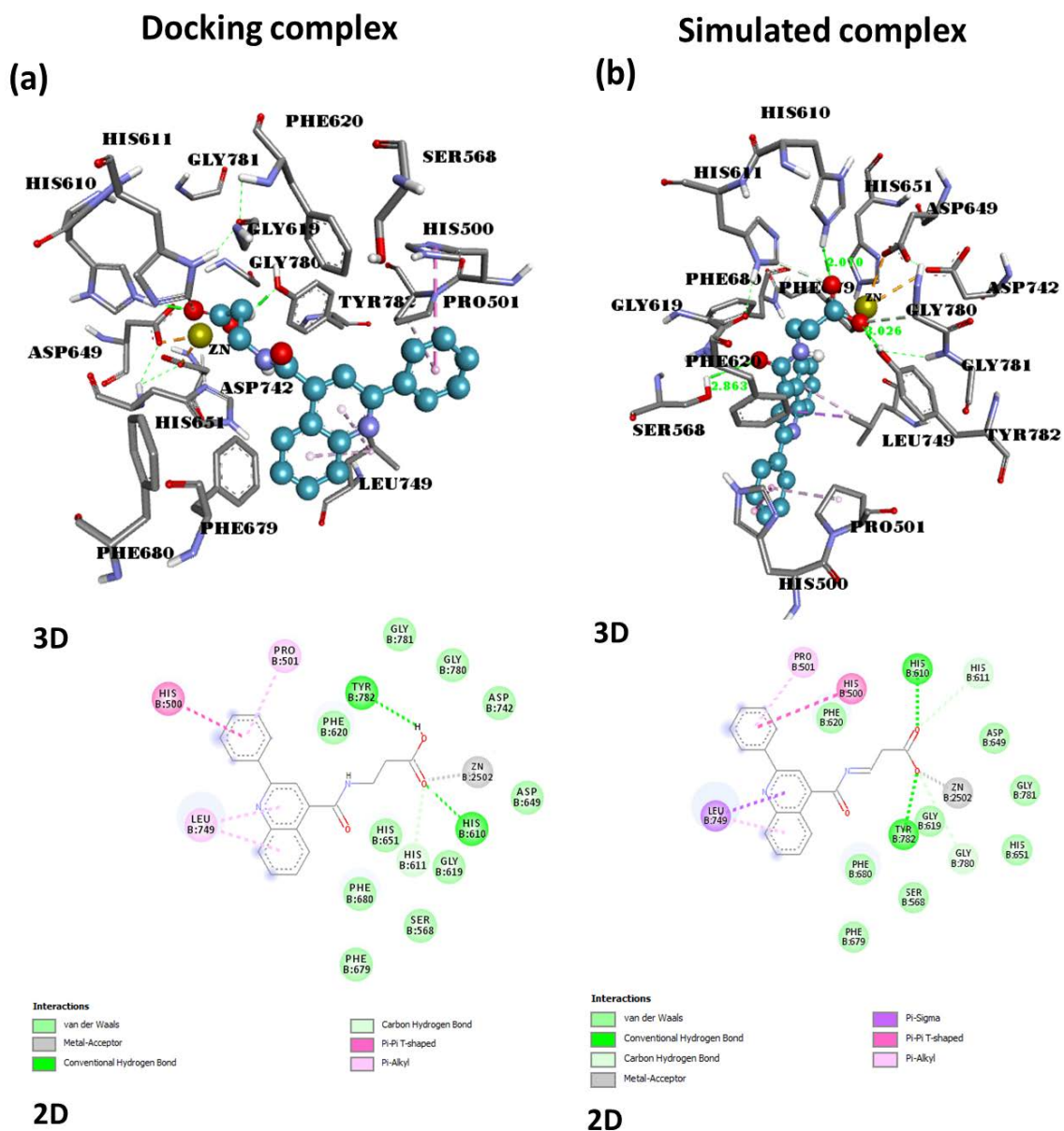
Figure 4. 22. P2194879 bound to HDAC6 with its bulky capping group stuck at the entrance to the channel and engaged zinc metal ion in the deep pocket via a strong metallic interaction with carboxylic group — the same carboxylic group formed H-bonds with HIS610 and TYR782 in 3D space and the key for the non-bond interactions is given in the 2D scheme (a). The binding of the same compound at the end of 10 ns-MD simulation; its mode remained the same in the 3D space, but the carboxyl group ionized, and the H-bonds were retained but the set of Van der Waals attraction were altered as shown in the 2D scheme (b).

97
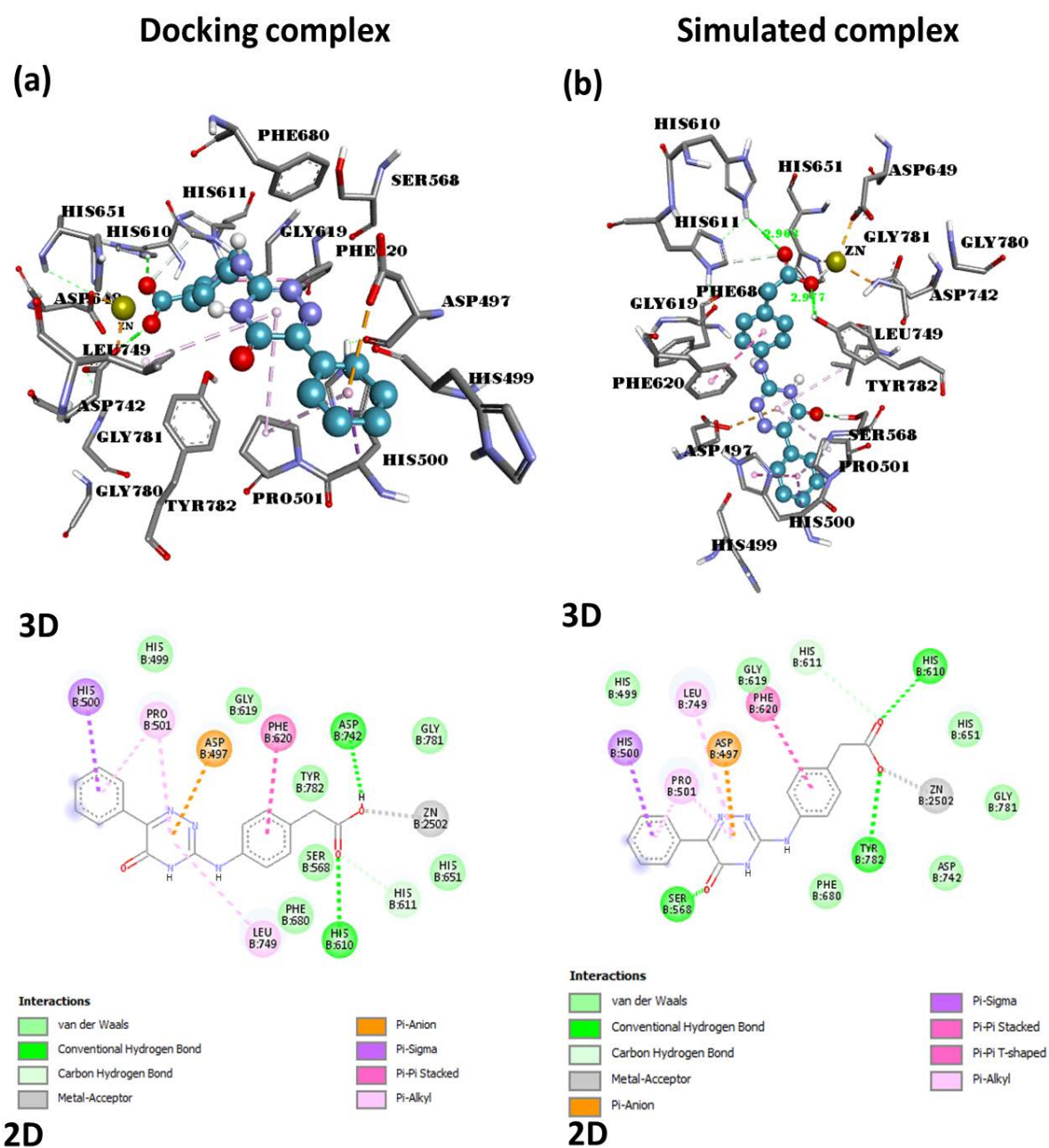
Figure 4. 23. P3823745 binding mode to HDAC6; the compound engaged zinc ion deep inside the pocket via a strong metallic interaction with carboxylic group — the same carboxylic group formed H-bonds with HIS610 and ASP742 in 3D in 3D space and the key for the non-bond interactions is given in the 2D scheme (a). The binding of the same compound at the end of 10 ns-MD simulation; its orientation remain the same in the 3D space but the carboxyl group ionized and formed H-bond with TYR782 instead of the seemingly ionized ASP742 in the docking complex, the carbonyl group of the cap moiety also formed H-bond with SER568 as shown in 2D scheme (b).

Docking complex

(a)

Simulated complex

(b)
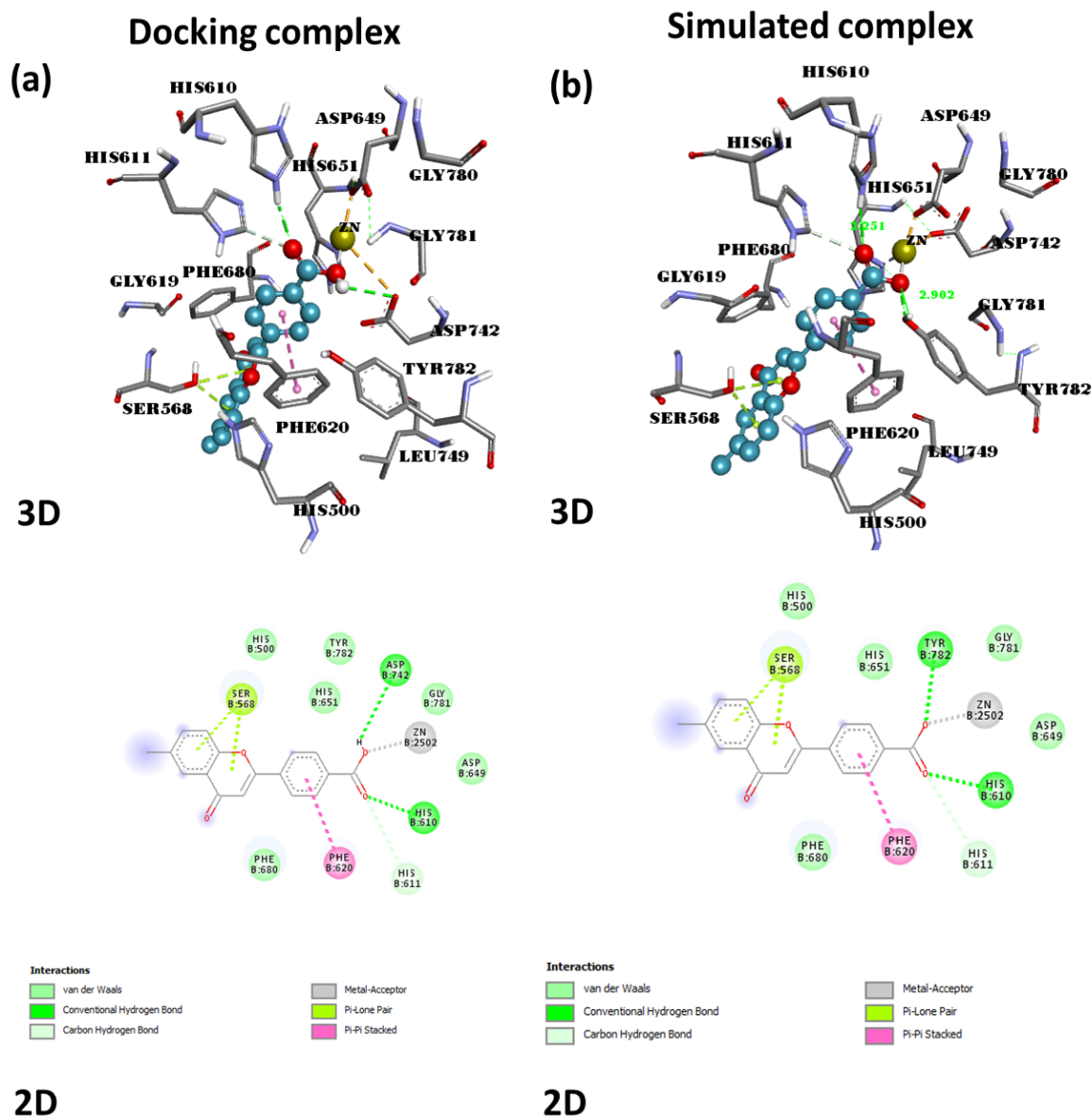
Figure 4. 24. Binding mode of P7715560117 to HDAC6; the compound engaged zinc ion deep inside the pocket via strong metallic interaction with carboxylic group — the same carboxylic group formed H-bonds with HIS610 and ASP742 in 3D space and the key for the non-bond interactions is given in the 2D scheme (a). The binding of the same compound at the end of 10 ns-MD simulation; its orientation remained the same in the 3D space, but the carboxyl group ionized and formed H-bond with TYR782 instead of the seemingly ionized ASP742 in the docking complex, as shown in 2D scheme (b).

The predicted drug-like and ADMET properties of the 4 potentially selective inhibitors of HDAC6 are given in Table 1. These descriptors are: S + logP; S + log D; MlogP; MWt; S_HBD and S_NO. Any compound violating more than 1 of these properties is likely to have poor absorption and oral bioavailability (Lipinski, 2004). Other

physicochemical properties including probability for human Intestinal absorption and Cacao-2 permeability, aqueous solubility and rat acute toxicity values were also found to be within the normal range of drug molecule.

Table 4. 8. Drug-like and ADMET properties of the 4 potentially selective inhibitors of HDAC6 predicted using ADMET Predictor[TM] and admetSAR.

Otava id	MlogP	S+logP	S+logD	MWt (Da)	S_NO	T_PSA (Å^2)	S_HBD	P(HIA+)	Aqueous Solubility (LogS)	Caco-2 permeability (LogPapp, cm/s)	R.A.T. (LD50, mol/kg)
Tubastatin A	2.39	1.996	1.326	335.408	5	57.5	2	0.9953	-2.8888	0.5832	2.6938
Ricolinostat	3.259	3.288	3.285	433.513	8	107.45	3	0.9509	-3.2847	0.3808	2.5013
Citarinostat	3.467	3.92	3.916	467.958	8	107.45	3	0.9545	-3.9177	0.5666	2.5652
Nexturastat	3.344	2.513	2.501	341.413	6	81.67	3	0.9914	-3.8825	0.7331	2.3276
P7020527347	0.614	1.732	-1.245	297.272	7	115.31	4	0.8	-3.8034	0.681	2.4787
P2194879	1.95	2.413	-0.482	320.35	5	79.29	2	0.97	-3.0952	0.2519	2.0093
P3823745	2.443	2.025	-1.038	322.325	7	107.97	3	0.98	-3.2017	0.4935	2.38
P7715560117	2.13	3.893	0.546	280.282	4	67.51	1	1	-3.3279	0.7413	2.9342

Note: The drug-like molecules should violate no more than one of the following 1-4 properties (Lipinski, 2004); 5-8 are other crucial ADMET properties:
1. MlogP (Moriguchi model of octanol–water partition coefficient, log P) ($\leq$ 5).
   Or S + LogP (Simulation Plus Model of octanol–water distribution coefficient) $\leq$ 5.
   Or S + logD (Simulation Plus Model of octanol–water distribution coefficient, log D) $\leq$ 5.
2. MWt (Molecular weight) $\leq$ 500 Da.
3. S_HBD (Sum of H-bond donors, NH- and OH) $\leq$ 5.
4. S_NO (Sum H-bond acceptors, N and O) $\leq$ 10.
5. T_PSA (Topological polar surface area) $\leq$ 140Å^2.
6. P(HIA+) (Probability for human intestinal absorption) > 0.6.
7. Aqueous Solubility (LogS > -5.7).
8. Caco-2 permeability (LogPapp, cm/s) (faster than 22 nm/s).

Comparative analysis of the MD simulation results showed that the RMSD of both the free enzyme and the 4 complexes started out slightly in synch until around 0.2 ns, beyond which each system behaved differently until the end of the simulation. HDAC6-P3823745 complex deviated from 0.6-1.3 Å until around 4 ns, beyond which it stabilized (between 0.80-1.00 Å) until the end of the simulation. The complexes with of HDAC6 with P7715560117, P2194879 and P7020527347 showed a similar trend but slightly higher deviation (between 0.90-1.40 Å) towards the end of the simulation. Overall, all the complexes showed slightly higher stability compared with the free enzyme (Figure 4.24 (a)). In agreement with the RMSD distribution, the non-bond

distance between HDAC6 and P3823745 was found to be the shortest throughout the simulation time. Except for HDAC6-P7715560117, all the non-bond distances varied by < 1 Å over the entire trajectory (Figure 4.24 (b)) Radius of gyration (Rg) is another important parameter used to examine the structural stability of proteins and protein-ligand complexes over time. Here, the Rg profiles of the free HDAC6 and complexes were found to be within the range of 1.33-1.42 Å, indicating the potential stability of the complexes over time of the simulation (Figure 4.24 (c)).
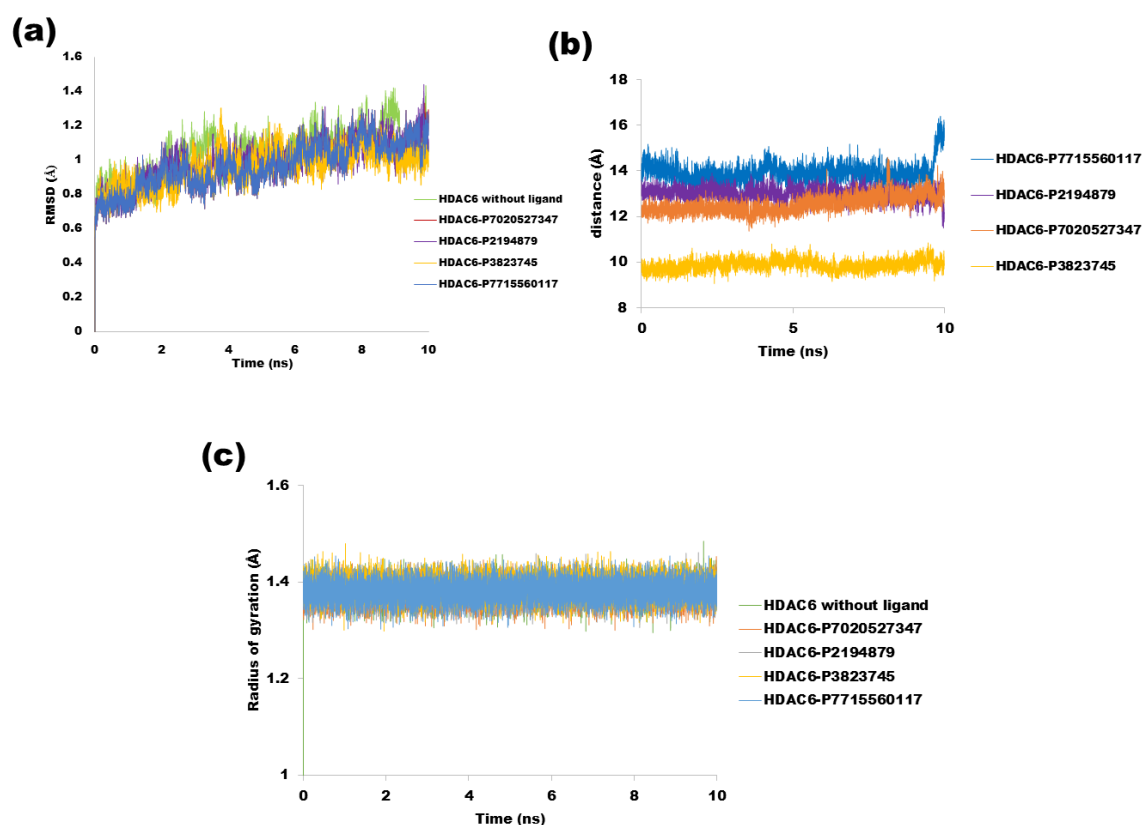
Figure 4. 25. Root-Mean-Squared Deviation (RMSD) profiles of HDAC6-CD2 without ligand (green) and the complexes of HDAC6-CD2 with P7020527347 (red), P2194879 (purple), P3823745 (yellow), and P7715560117 (blue). The complex of HDAC6-CD2 with P3823745 (yellow) displayed the highest stability over time of the simulation.

4.4.3 Pharmacophore hypotheses generated

Even though the 10 hypotheses generated contain the same features; 1 H-bond donor, 1 H-bond acceptor, 2 hydrophobic (aliphatic/aromatic) groups (Figure A1.1), Hypo1 was found to be most statistically valuable, having the highest rank value (Table 4.6), enrichment factor (16.23), and GH score (0.78) (Table 4.7). The 4 pharmacophore features mapped very well onto the following known HDAC inhibitors: Belinostat, Abexinostat, Panobinostat, Vorinostat and Entinostat, among the training set compounds. The hydrophobic (aromatic) feature mapped onto different cap groups; the H-bond donor feature also mapped onto cap groups in Panobinostat, and Entinostat, and onto the linker regions in Belinostat, Abexinostat and Vorinostat; the H-bond acceptor feature mapped mainly, onto carbonyl oxygen of the hydroxamic acid and amide groups

(Figure 4.25). Interestingly, although diverse in stuctures, the 10 best-fitting compounds retrieved by hypo1 satisfied the geometric constraints of the hypothesis — they all showed fit value > 3, and mapped onto hypo1 well with their distinct scaffolds (Figure 4.26).

Table 4. 9. Characteristic features of the 10 pharmacophore hypotheses generated by HipHop approach.

Hypotheses	Feature[a]	Rank	Max. Fit
1	HHDA	89.275	4
2	HHDA	86.538	4
3	HHDA	84.688	4
4	HHDA	83.972	4
5	HHDA	83.848	4
6	HHDA	83.755	4
7	HHDA	82.540	4
8	HHDA	81.143	4
9	HHDA	81.116	4
10	HHDA	76.878	4

[a] Feature: A: H-bond acceptor; D: H-bond donor: H: Hydrophobic (aliphatic/aromatic) group.

Table 4. 10. Pharmacophore hypotheses validation using Guner-Henry scoring method.

Hypotheses	Ha	A	D	Ht	%Y	%A	E	GH
1	17	20	420	22	77.27	85.00	16.23	0.7821
2	16	20	420	25	64.00	80.00	13.44	0.6647
3	15	20	420	22	68.18	75.00	14.32	0.6866
4	16	20	420	22	72.73	80.00	15.27	0.7343
5	16	20	420	25	64.00	80.00	13.44	0.6647
6	15	20	420	26	57.69	75.00	12.12	0.6031
7	14	20	420	20	70.00	70.00	14.70	0.6895
8	15	20	420	26	57.69	75.00	12.12	0.6031
9	15	20	420	25	60.00	75.00	12.60	0.6216
10	14	20	420	21	66.67	70.00	14.00	0.6632

D is the total molecules in the database
A is the total number of active molecules in the database
H_t is the total hits in the database,
H_a is the number of active hits
$Y\%$ is the percentage of active compounds obtained from the decoy set
$A\%$ is the percentage ratio of actives in the hits list, E is the enrichment factor
GH is the goodness of hit (Güner-Henry) score
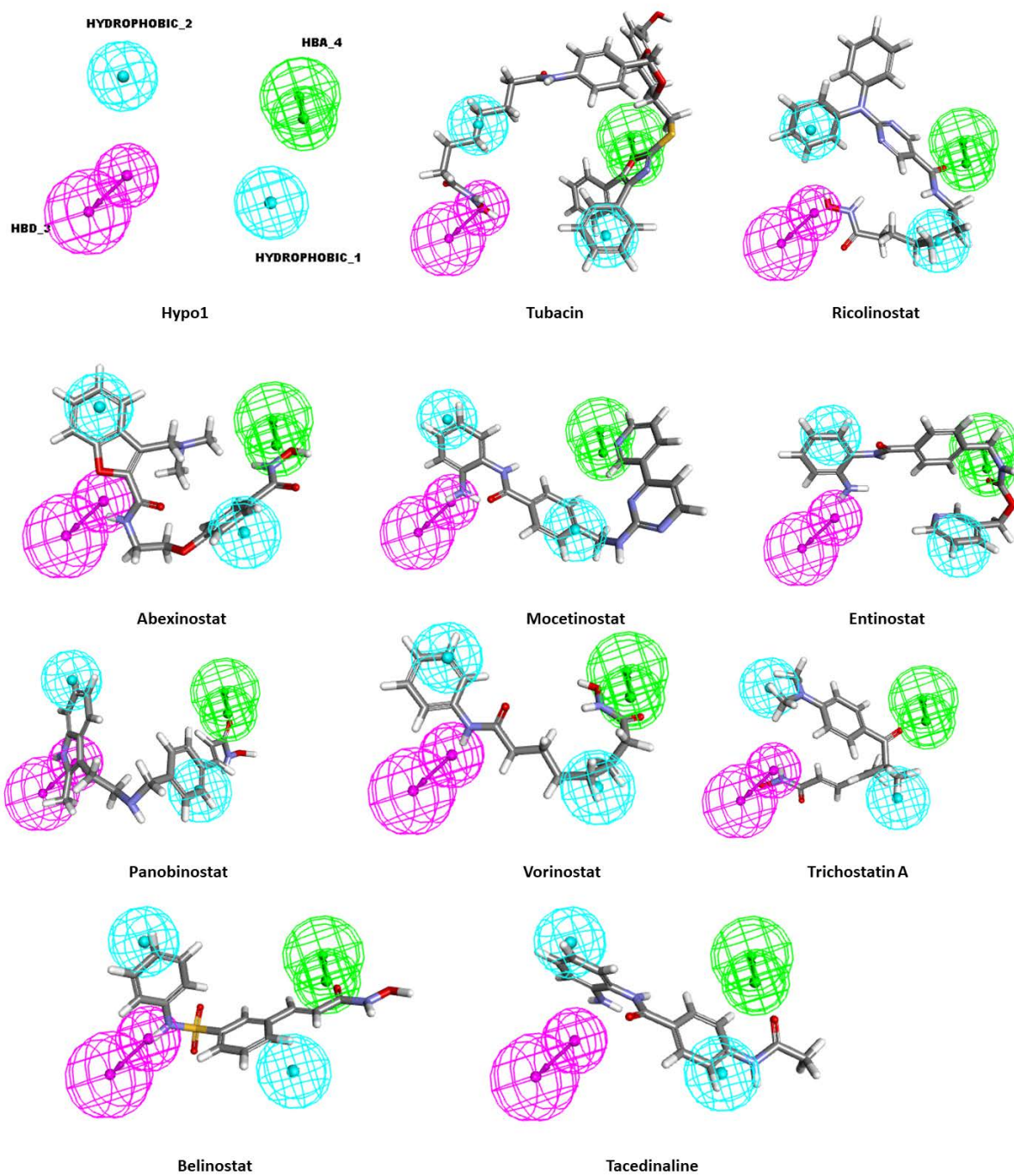
Figure 4. 26. Mapping of pharmacophore hypothesis 1 (Hypo1) to some selected compounds among the training set molecules.
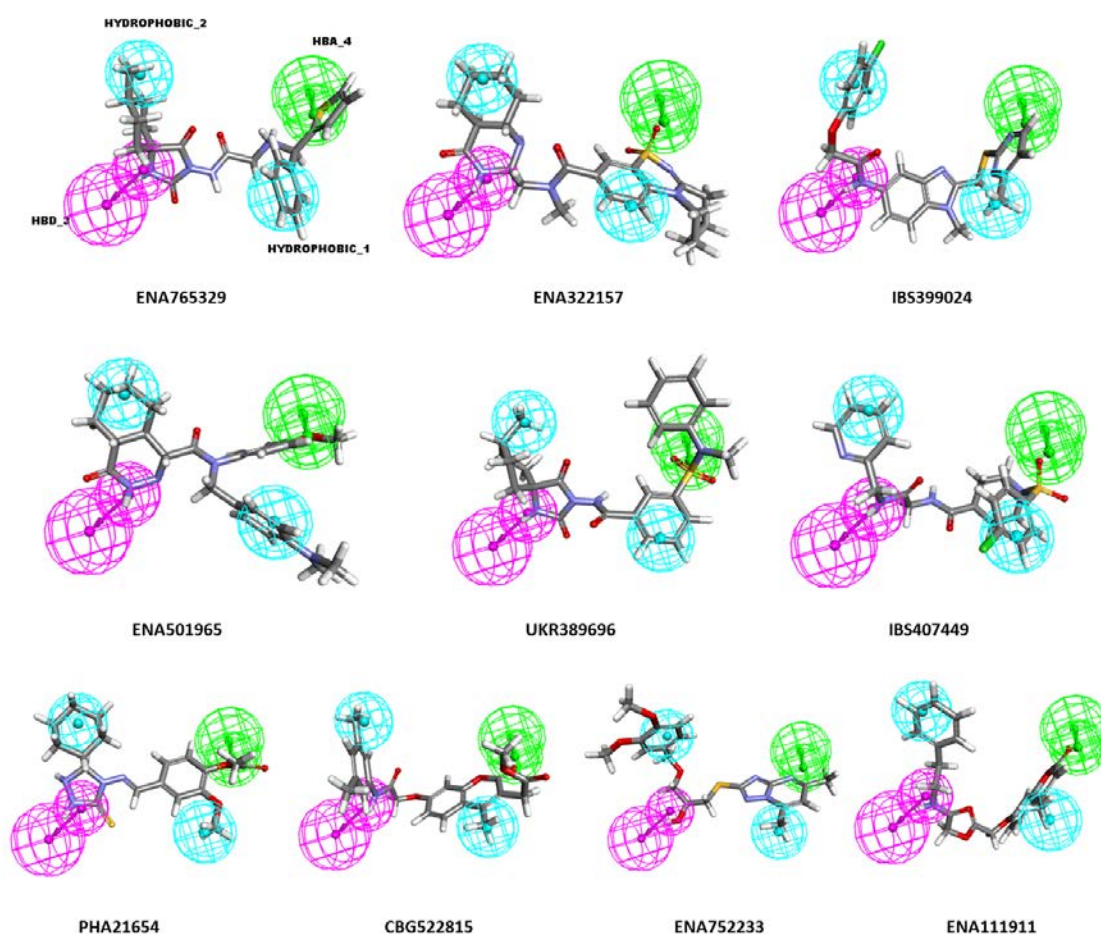
Figure 4. 27. 10 best-fitting lead compounds that satisfied the geometric constraints of Hypo1 identified by 3D query against "DruglikeDiverse" Database in Biovia DS 4.5.

ADMET Analysis: The ADMET properties of the top 10 lead compounds are presented in Table 4.8. These properties were found to be within the normal range of drug candidacy. According to the "rule of 5", poor passive absorption or permeability is more likely if the compound violates two or more of the following conditions: LogP $\leq$ 5, MWt $\leq$ 500 Da, S_HBD $\leq$ 5, S_HBA $\leq$ 10. Other ADMET properties such as blood brain barrier crossing and human intestinal absorption were given as probability; caco-2 permeability and aqueous solubility of our designed compounds were in agreement with the widely-followed "Jorgensen Rule-of-Three" which states that "the aqueous solubility measured as logS should be greater than -5.7, the apparent caco-2 cell permeability should be faster than 22 nm/s and the number of primary metabolites

should be less than 7; these limits are based on the properties of 90% of 1700 oral drugs" (Di and Kerns, 2016).

Table 4. 11. Drug-like and ADMET properties of the top 10 hit compounds predicted using ADMET Predictor[TM] and admetSAR programs.

Compound id	S+logP	S+logD	Mw(Da)	S_HBD	S_NO	TPSA (Å^2)	P(HIA+)	Aq sol (LogS)	Caco-2 perm (LogPapp, cm/s)
ENA765329	1.802	1.798	426.54	3	7	90.54	0.8938	-3.4892	0.3097
ENA322157	-3.035	-3.044	475.61	4	9	117.5	0.9034	-3.6409	-0.4585
IBS399024	3.687	3.686	453.95	1	7	81.93	0.9887	-4.0501	1.3814
ENA501965	4.717	4.717	434.54	0	7	74.57	0.8812	-3.6258	0.7037
UKR389696	2.629	2.62	470.55	2	9	115.89	0.9215	-3.4524	0.4228
IBS407449	0.828	0.828	450.95	2	8	108.47	0.9647	-3.7963	0.1817
PHA21654	2.645	2.645	376.48	2	7	75.19	0.9421	-3.3819	0.6714
CBG522815	3.415	3.415	409.44	1	7	94.84	0.8796	-3.5931	0.768
ENA752233	3.134	3.1	406.51	2	8	93.89	0.8398	-3.3346	0.7087
EN111911	2.952	2.952	395.42	1	7	94.84	0.9701	-3.2998	0.4732

Note: The drug-like molecules should violate no more than one of the following 1-4 properties (Lipinski, 2004); 5-8 are other crucial ADMET properties:
1. S + LogP (Simulation Plus Model of octanol–water distribution coefficient) ≤ 5.
   Or S + logD (Simulation Plus Model of octanol–water distribution coefficient, log D) ≤ 5.
2. MWt (Molecular weight) ≤ 500 Da.
3. S_HBD (Sum of H-bond donors, NH- and OH) ≤ 5
4. S_NO (Sum H-bond acceptors, N and O) ≤ 10.
5. T_PSA (Topological polar surface area) ≤ 140 Å^2
6. P(HIA+) (Probability for human intestinal absorption) > 0.6
7. Aqueous Solubility (LogS > -5.7)
8. Caco-2 permeability (LogPapp, cm/s) (faster than 22 nm/s)

Binding Affinity of the 10 Best-fitting Lead Compounds Retrieved by Hypothesis 1: The pharmacophore fit values and calculated binding energy of the best-fitting compounds against HDAC6 in comparison with class I HDACs and HDAC7 are given in Table 4.9. ENA501965 and IBS399024 displayed the highest binding affinity and selectivity for HDAC6 CD2 over class I HDACs and HDAC7. In addition, these two potentially

selective lead compounds were found to have lower binding energy compared to Panobinostat — the lowest-energy-binding compound among the training set.

Table 4. 12. Structures, fit values and calculated binding energy of the top 10 lead compouds against HDAC6 compared with class I HDACs and HDAC7.

Rank	DruglikeDiverse id	Fit values	ΔG (kcal/mol)					
			HDAC6	HDAC1	HDAC2	HDAC3	HDAC8	HDAC7
1	ENA765329	3.64833	-9.43	-8.22	-8.54	-7.88	-8.67	-8.34
2	ENA322157	3.57888	-8.97	-7.36	-7.75	-8.11	-6.99	-8.44
3	IBS399024	3.57652	-10.86	-7.24	-7.56	-6.78	-7.67	-8.01
4	ENA501965	3.51523	-11.64	-6.85	-7.32	-7.43	-8.09	-8.34
5	UKR389696	3.51467	-8.16	-8.51	-7.87	-8.42	-8.67	-8.21
6	IBS407449	3.47151	-8.08	-7.49	-7.81	-8.11	-7.89	-7.44
7	PHA21654	3.46511	-8.66	-8.28	-8.27	-7.31	-7.44	-7.89
8	CBG522815	3.43677	-8.76	-8.41	-7.96	-8.23	-8.41	-8.16
9	ENA752233	3.43067	-9.5	-7.87	-8.31	-8.25	-8.67	-8.44
10	EN111911	3.36412	-9.11	-8.02	-8.24	-7.77	-7.86	-8.09

Binding Mode of ENA501965 and IBS399024

The binding modes and interaction patterns of ENA501965 and IBS399024 with HDAC6 were analyzed using Biovia DS 4.5 visualizer. ENA501965 fitted well in the catalytic channel of HDAC6 with its fused heterocyclic ring serving as a capping group for surface recognition, which formed 2 H-bond interaction with ionized OH group of SER568; 1 H-bond interaction with HIS500; and 1 H-bond interaction with HIS651; alkyl interactions with PRO501, PHE620 and LEU749 at the entrance to the channel. The amide-containing linker of ENA501965, via its dimethylaminophenyl substituent, filled a small cavity along the middle of the tunnel by apparent steric clashes and 1 π-alkyl interaction with PHE679. Interestingly, contrary to the traditional hydroxamic acid group as zinc-binding moiety, the methoxyphenyl group chelated Zn^{2+} ion via methoxyl oxygen and induced van der Waals attraction with HIS611, ASP742, TYR782, and GLY780 deep inside the channel (Figure 4.27 (a)); where "charge relay" mechanism of histone deacetylation takes place (Hai and Christianson, 2016).

Intriguingly, IBS399024 bound HDAC6 with different mode from those of the known HDAC inhibitors and ENA501965. IBS399024 did not obey the cap-linker-chelator feature of zinc-binding HDAC inhibitors. Instead, it bound with the conformation that enabled it to fit into the enzyme's catalytic channel. The chlorophenyl group serving as a capping group, was buried in the interior of the tunnel and formed a halogen interaction with SER568 in addition to the other types of interaction. The linker group of IBS399024 formed 2 H-bond interactions with HIS500 and ASN494. Deep inside the channel, Zn^{2+} ion engaged in van der Waals interaction with N-containing heterocyclic ring, HIS651 via H-bond, while HIS61 & 611, LEU749, TYR782 interacted via π-alkyl; PHE620 via π-π stacked, PHE680 via π-π T-shaped interaction (Figure 4.27 (b)).

Intriguingly, IBS399024 bound HDAC6 with different mode from those of the known HDAC inhibitors and ENA501965. IBS399024 did not obey the cap-linker-chelator feature of zinc-binding HDAC inhibitors. Instead, it bound with the conformation that enabled it to fit into the enzyme's catalytic channel. The chlorophenyl group, thought to serve as a linker group, was buried in the interior of the tunnel. HIS500, PRO501 and SER568, residues found to interact with the cap group of ENA501965, interacted with the perceived linker group of IBS399024 near the entrance to the channel. Deep inside the channel, HIS610 611 & 651, PHE680, TYR782 interacted via π-alkyl, π-sigma, and π-π T-shaped interactions — instead of which van der Waals interactions were observed with ENA501965. Nevertheless, Zn^{2+} ion was involved via van der Waals interaction by N-containing heterocyclic ring (Figure 4.27 (b)).
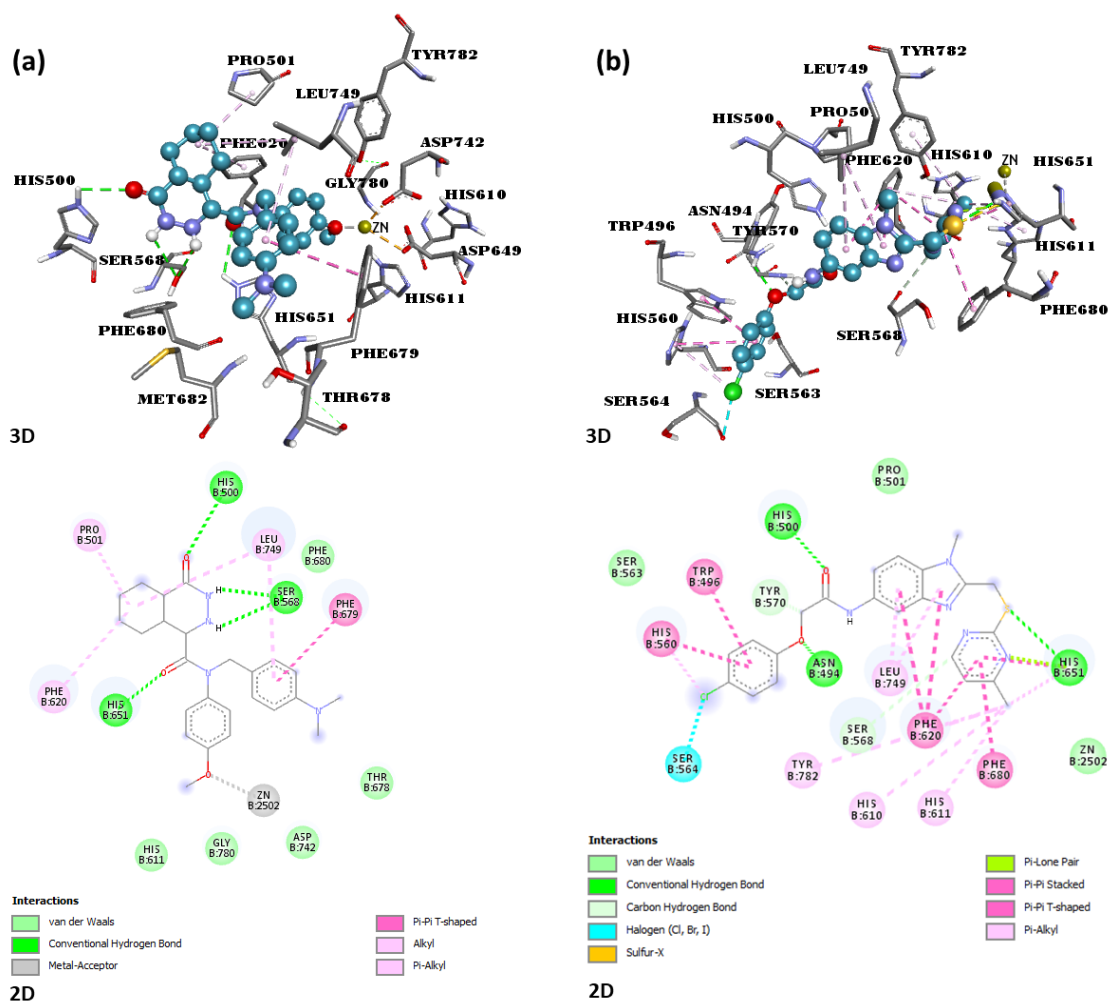
Figure 4. 28. 3D (left) and 2D (right) interaction diagram between HDAC6 catalytic domain 2 and compounds 4 (DruglikeDiverse id; ENA50196) (a) and compounds 3 (DruglikeDiverse id; IBS399024) (b).

Molecular Dynamics Simulation Analysis: Structural stability of docking complexes of HDAC6 with panobionstat, IBS399024 and ENA50196 was examined by 10 ns-MD simulation. All the systems showed similar behavior until around 1 ns, beyond which the backbone RMSD of the free enzyme started to increase higher than those of the complexes until the end of the simulation. RMSD profiles of the complexes remained in synchrony until around 1.3 ns, after which HDAC6-IBS399024 complex started to increase higher than those of the other two complexes and then stabilized until the end of the simulation. The complexes of HDAC6 with Panobinostat and ENA501965 showed similar trend until around 3.3 ns, then each complex continued to deviate and later stabilized until the end of the simulation. Of the 4 systems simulated, HDAC6-

109

ENA501965 complex showed the lowest RMSD profile and thus highest stability over time of the simulation (Figure 4.28 (a)).

Similarly, HDAC6-Panobinostat and HDAC6-ENA501965 complexes showed relatively lower residue fluctuations compared with HDAC6-IBS399024 complex, and to the free enzyme. Nevertheless, few residues in both the free enzyme and the complexes fluctuated above 1.7 Å, indicating the structural stability of the systems over time of the simualation (Figure 4.28 (b)). These parameters were in agreement with one another, and were consistent with the MD results of our recent study examining the stability of ligand mode to HDAC6 CD2 (Uba and Yelekçi, 2018).
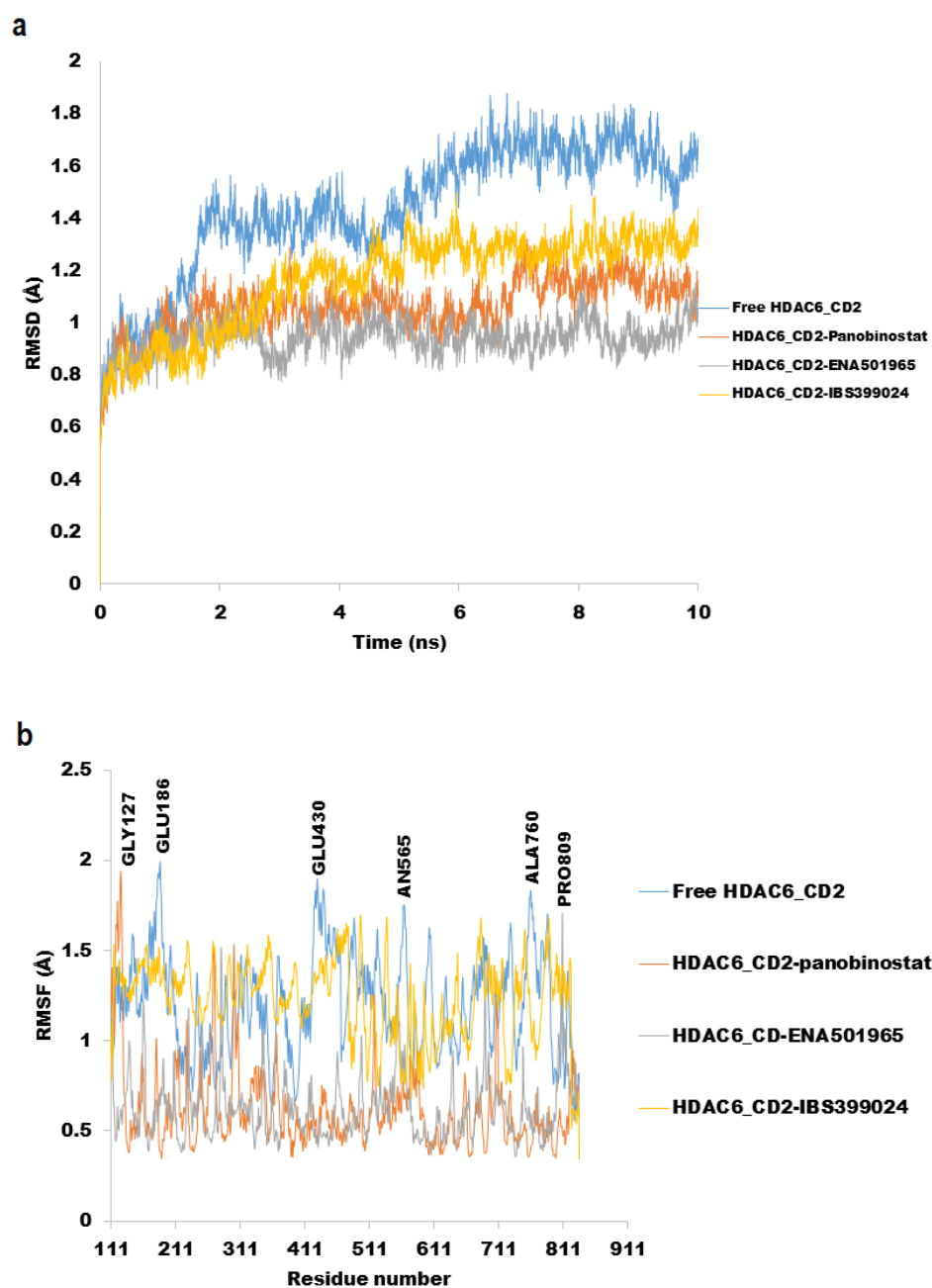
Figure 4. 29. RMSD profiles of the free form of HDAC6 and its docking complexes with, Panobinostat, ENA501965 and IBS399024; HDAC6-ENA501965 complex showed the lowest RMSD and thus highest stability over time of the simulation (a). RMSF profiles of HDAC6 and its docking complexes with, panobinostat, ENA501965 and IBS399024; HDAC6-ENA501965 and HDAC6-Panobinostat complexes showed lower fluctuation compared to the free enzyme and HDAC6-IBS399024 complex.

4.5. Homology Modeling of Human Histone Deacetylase 10

4.5.1 Built homology models

The 20 built models of human HDAC10 were shown in Figure 4.24 (a). The models differed slightly in their loop region — this region appeared to be of higher energy compared with the rest of the structure. The variable regions usually come from loops and turns located further away from the binding site. Model 17 (M0017) found to be the best having the lowest normalized DOPE score (Table 13). The catalytic domain of M0017 was therefore extracted (Figure 4.24 (b)) and aligned to the experimental crystal structure of *Danio rerio* HDAC10. The two structures were perfectly aligned with very low RMSD value (0.23 Å) (Figure 4.24 (c)). This is as a result of the high sequence identity (58.6%) and similarity (76.6%) between *Danio rerio* HDAC10 and human HDAC10.

4.5.2. Model Structure Validation

M0017 was found to have z-score value -5.00, which is within the range of native conformation (Figure 4.30 (a)). The energy plot shows the local model quality by plotting energies as a function of amino acid residue position i – positive values correspond to erroneous parts of a model (Figure 4.30 (b)). In addition, Ramachandran plot was generated which showed the energetically allowed regions of the protein backbone. These are the regions of alpha-helical and beta-sheet conformations with no steric clashes upon rotation around torsion angles phi and psi (Figure 4.30 (c)).
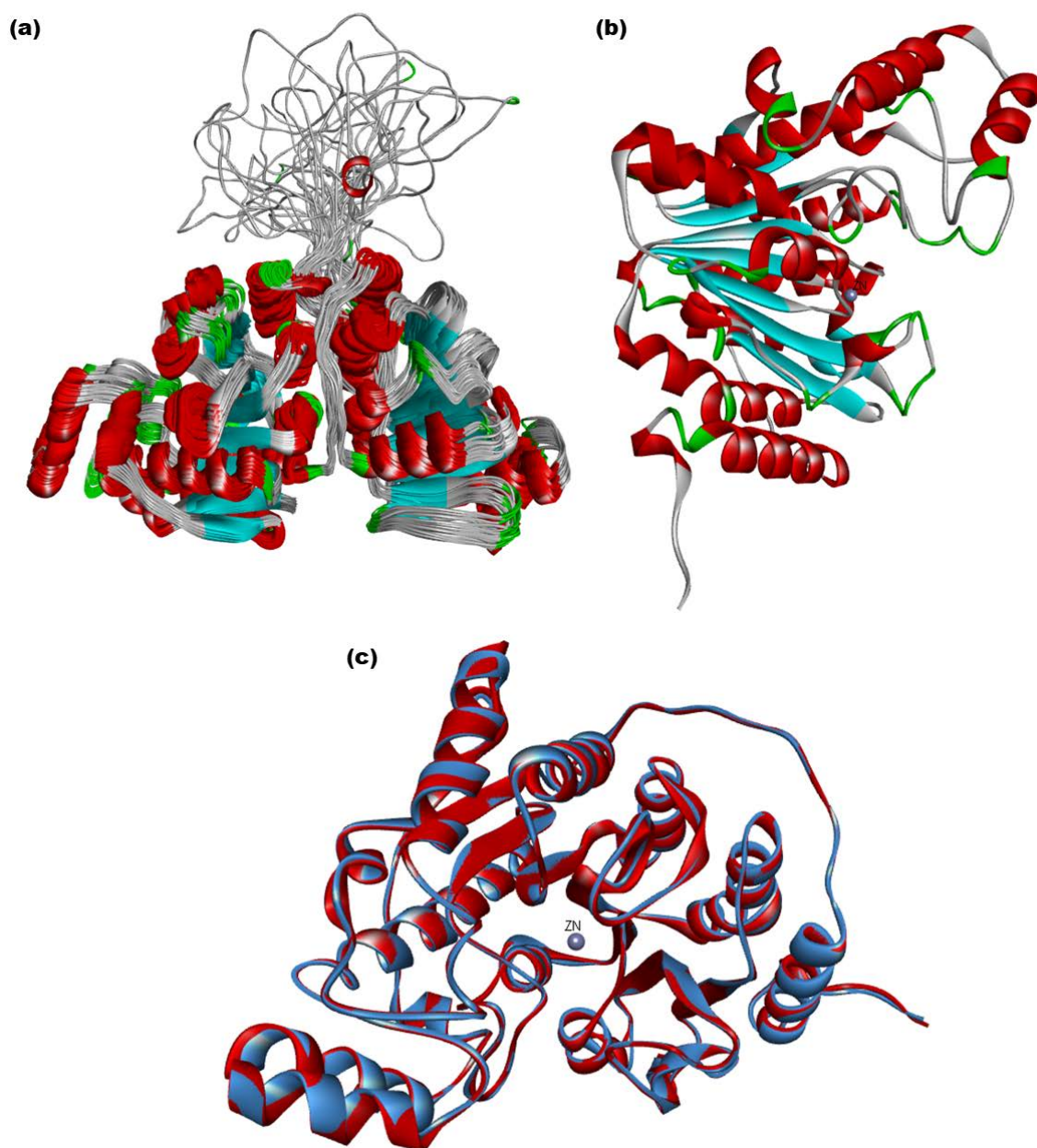
Figure 4. 30. Twenty models of human histone deacetylase 10 built using Danio rerio (zebrafish) histone deacetylase-10 X-ray crystal structure (5TD7) as a template (a). The 3D structure of the cataltytic domain of the best model (M0017)
(Normalized DOPE Score:-0.814028) (b). The alignment of M0017 (red) to zebrafish HDAC10 (blue) (c).

Table 4. 13. DOPE Score and Normalized DOPE Score (from modeler) of the 20 built models. The best model (M0017) is highlighted in yellow.

Model	DOPE Score	Normalized DOPE Score
M0009	-77825.51563	-0.791391
M0001	-77740.39844	-0.78238
M0020	-77405.42188	-0.746919
M0013	-77796.80469	-0.788351
M0019	-77845.39063	-0.793495
M0002	-77654.78125	-0.773316
M0004	-77812.5625	-0.790019
M0003	-77808.5625	-0.789596
M0018	-77785.17188	-0.78712
M0015	-77799.80469	-0.788669
M0014	-77005.67969	-0.704601
M0017	-78039.35938	-0.814028
M0005	-77874.83594	-0.796612
M0006	-77968.65625	-0.806544
M0008	-77377.20313	-0.743931
M0007	-77369.35156	-0.7431
M0011	-76650.96094	-0.66705
M0012	-76912.98438	-0.694788
M0010	-77877.89844	-0.796936
M0016	-77678.02344	-0.775777
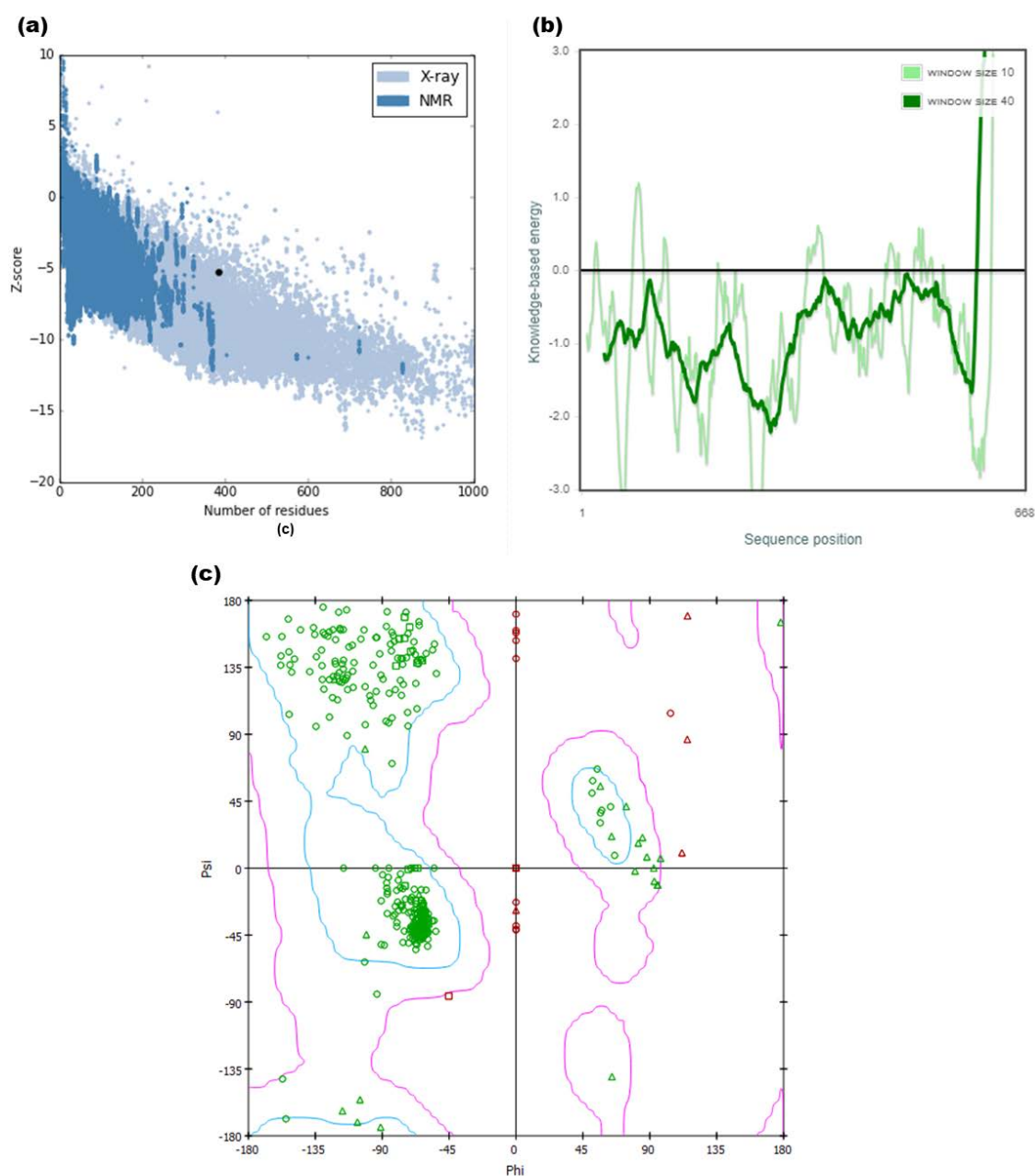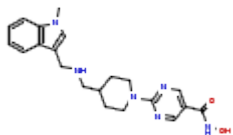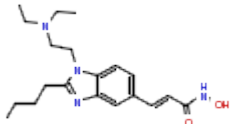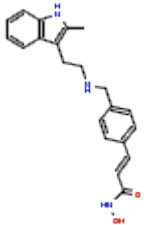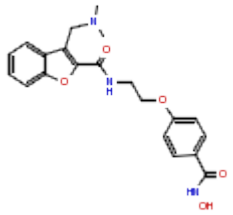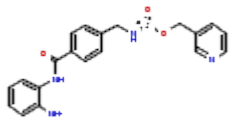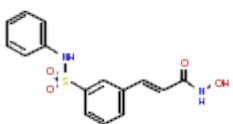
Figure 4. 31. Structural validation of the best model (M0017). ProSA-web z-scores of all protein chains in PDB determined by X-ray crystallography (light blue) or NMR spectroscopy (dark blue) with respect to their length. The plot showed that M0017 (black spot) with z-score value -5.00 is within the range of native conformation (a). Energy plot showing the local model quality by plotting energies as a function of amino acid sequence position i; positive values correspond to erroneous parts of the model (b). Ramachandran plot showing the energetically allowed region the model structure (c).

4.5.3 Molecular docking results

The docking calculation results of the known HDAC10 inhibitors are compared with their respective Ki (or IC50) values from the literature (Hutt et al., 2010; Wang et al., 2011; Rajak et al., 2012) in Table 4.14. Although these experimental values were not exactly reproduced *in silico*, the docking calculation accurately predicted the activity of these compounds against HDAC10. The difference might have resulted from the difference between protocols used to assay the experimental activity and Autodock's binding energy calculation. Among the promising compounds retrieved from ZINC database, ZINC37433253 was found to show preference for HDAC6 over HDAC10 despite the fact that the same compound bound to the two isoforms with similar binding mode and similar set of interactions deep inside the channels. The binding mode is shown in the 3D scheme, and the key for the non-bond interaction is shown in the 2D schemes (Figure 4.32). Fitting ZINC37433253 into the general pharmacophore features of the typical HDAC inhibitor, the N-methyl-indole ring could serve as a capping group channeling the ionized carboxyl group, via a short amide-containing linker group, into the deep channels of both the isoforms forming a strong electrostatic interaction with Zn^{2+} ion. Other interactions formed in the deep channels of both isoforms include electrostatic attraction, H-bond, alkyl, π-alkyl, and van der Waals interactions. The unique π-sigma interaction formed between the cap group and LEU749 of HDAC6 and π-lone pair interaction between the linker's carbonyl oxygen and PHE680 might have aided in the potential selectivity of ZINC37433253 for HDAC6 (-11.96 kcal/mol) over HDAC10 (-8.85 kcal/mol) (Table C.1)

Another potential lead compound, ZINC19749069 preferentially bound to HDAC10 (-9.68 kcal/mol) over HDAC6 (-7.91 kcal/mol) (Table C.1). ZINC19749069 formed 2 H-bonds (along the tunnel with GLU272, and deep inside with HIS174), π-cation interaction with GLU272 along the tunnel, a π-anion interaction with HIS135 in the deep channel, an alkyl and a π-alkyl interactions near the entrance and middle of the channel respectively, a π-π T-shaped interaction deep inside, and van der Waals interactions all over the channel (Figure 4.33).

116

Table 4. 14. Calculated binding affinity of the known HDAC inhibitors in comparison with their experimental (Exptl.) Ki or IC50 values.

Compound	Structure	Calculated ΔG (kcal/mol)	Calculated Ki (nM)	Exptl. Ki (nM)	Exptl. IC50 (nM)
Quisinostat		-11.73	2.54	0.50	-
Pracinostat		-10.46	21.53	23.00	-
Panobinostat		-10.05	42.91	31	-
Abexinostat		-10.24	31.15	24	-
Entinostat		-9.40	129.40	-	11100
Belinostat		-9.72	74.64	59	-

Tubacin		-9.76	69.76	373.7	-
PCI34051		-10.6	17.02	-	13
CUDC-101		-10.2	33.64	-	26.1
Vorinostat		-9.74	72.38	60	-
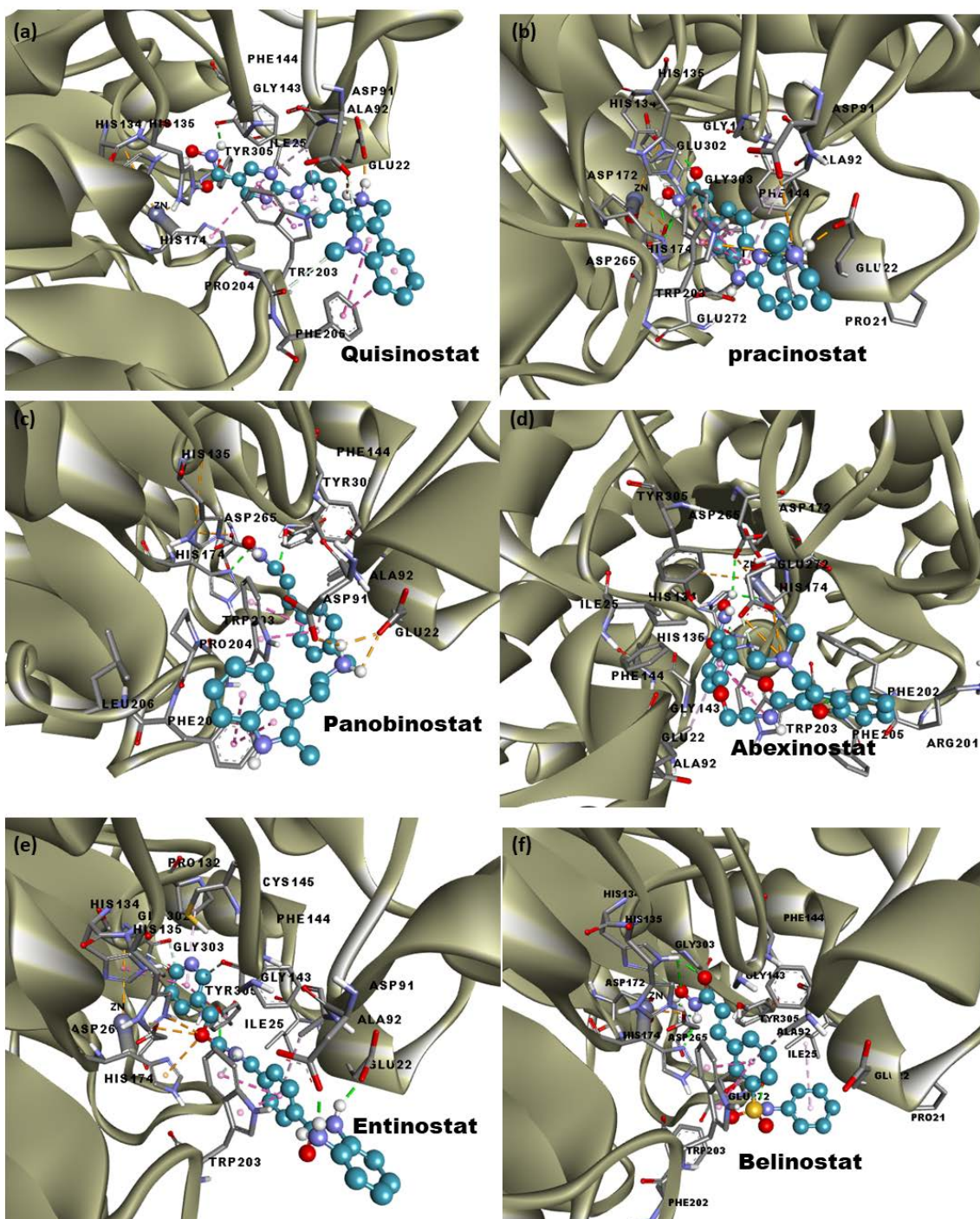
Figure 4. 32. Binding modes of known HDAC10 inhibitors to human HDAC10 model (M0017); Quisinostat (a), Practinostat (b), Panobinostat (c), Abexinostat (d), Entinostat (e), Belinostat (f).
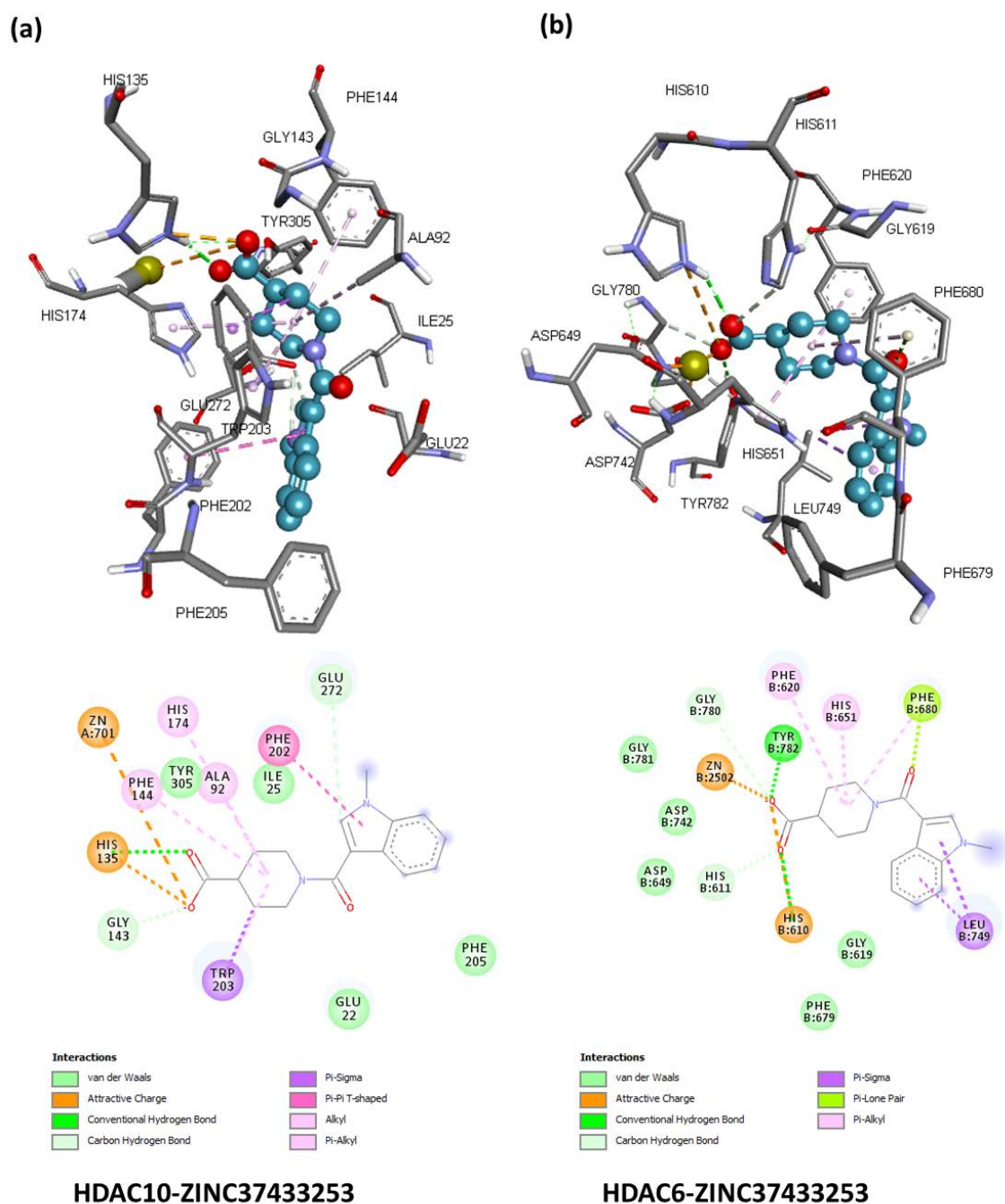
Figure 4. 33. Binding mode of ZINC37433253 to HDAC10 (a) and HDAC6 (b). Although the compound bound to the two isoforms with similar binding mode and similar set of interactions deep inside the channels preferential binding to HDAC6 was observed. The key for the non-bond interaction is shown in the 2D scheme.
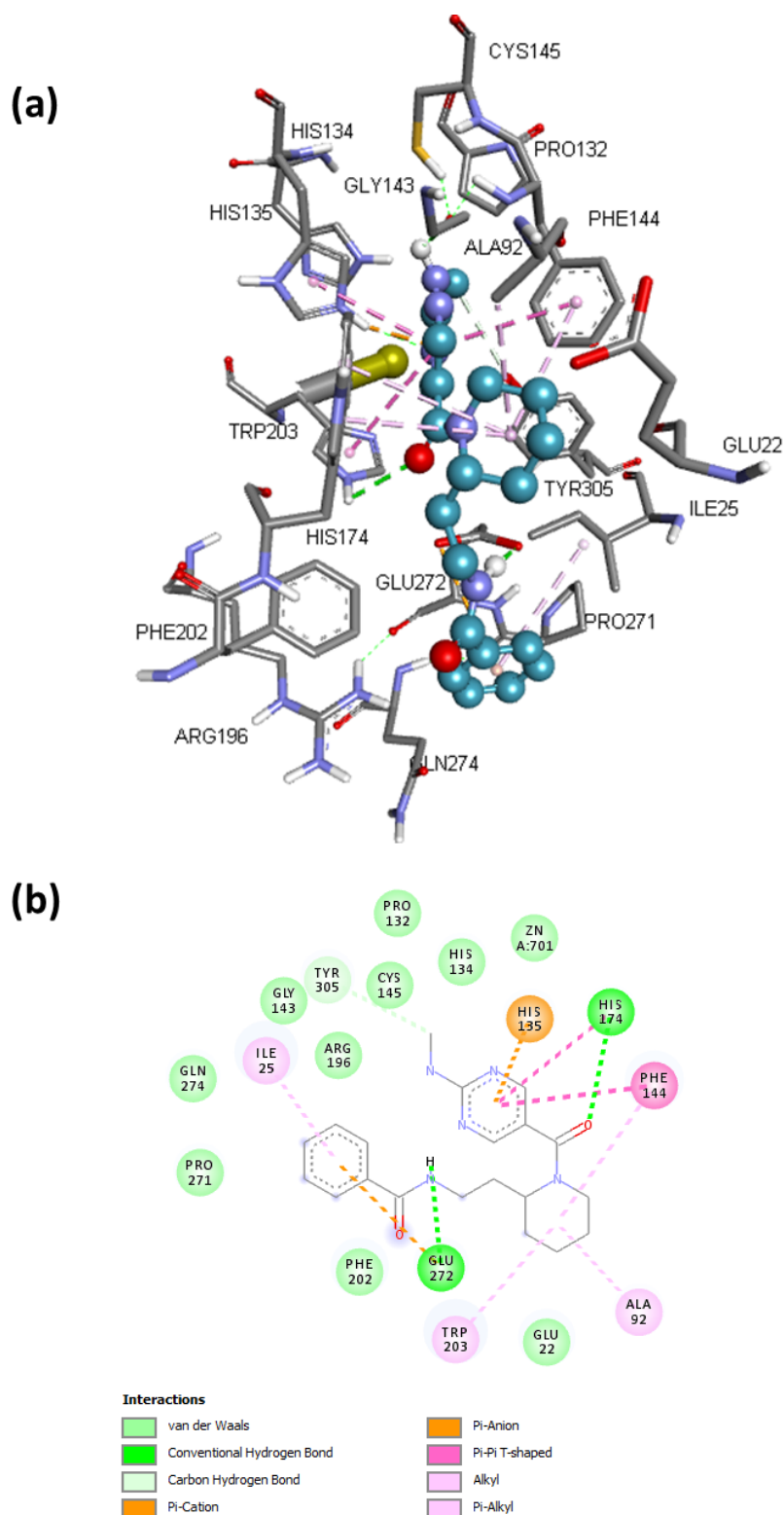
HDAC10-ZINC19749069

Figure 4. 34. Binding mode of ZINC19749069 to HDAC10 in the 3D space (a), and the interaction pattern shown in the 2D scheme (b).

4.5.4 Molecular dynamics simulation Results Analysis

The RMSD of the free HDAC10 rose to 5.3 Å at round 4 ns, and then fell down to 3 Å and stabilized at around 12 ns (between 2.9 Å and 3.3 Å) until the end of the 20 ns-MD simulation. Similarly, the RMSD of HDAC10-Quisinostat complex increased to about 5.8 Å from the starting configuration until around 10 ns, and then fell down to about 4.1 Å, and stabilized (between 3.8 Å and 4.4 Å) until the end of the 20 ns-MD simulation (Figure 4.33 (a)) The RMSD of HDAC10-ZINC19749069 started to stabilize at round 4 ns and converged around 7 ns until the end of the simulation.

RMSF analysis showed that the amino acid residues in both the free HDAC10 and the complexes fluctuated low. However, residues 361-386 were within the loop region outside the active site, and thus showed higher fluctuation (between 3.9 Å and 16 Å) in all the 3 systems. Loops are generally hard to model because of their flexibility (Figure 4.33 (b)).

The radius of gyration (Rg) of a protein is a measure of its compactness. If a protein is stably folded, it will likely maintain a relatively steady value of Rg. If a protein unfolds, its Rg will change over time. The Rg of free HDAC10 and the complexes remained stabilized between 1.30 Å and 1.48 Å, suggesting stability over time (Figure 4.33 (c)).

Another parameter evaluated is the total energy of the system which is not useful for much of anything aside from proving that the simulation was physically valid. Here, the total energy refers to the potential energy, and was found to be consistent with the RMSD, RMSF and Rg profiles throughout the simulation in all the 3 systems (Figure 4.33 (d)).

Thus, ZINC19749069 displayed the highest binding mode stability over time, suggesting its potential selectivity for HDAC10.
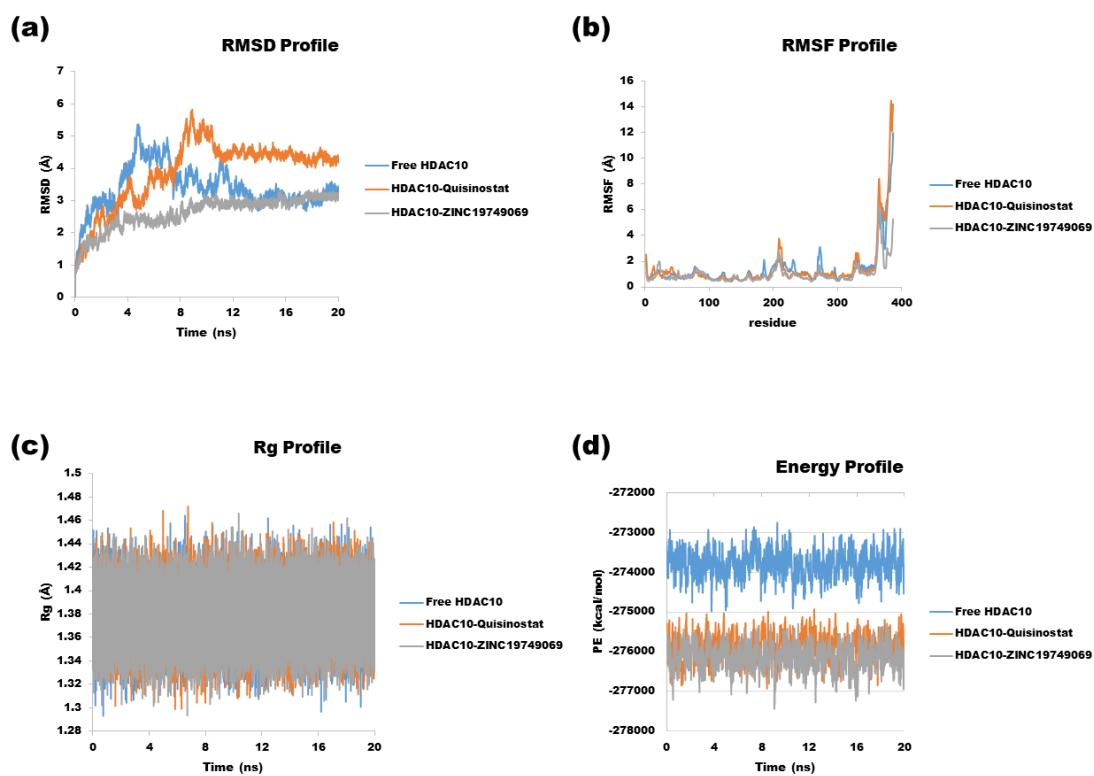
Figure 4. 35. Root-mean-squared deviation (RMSD) (a), Root-mean-squared fluctuation (RMSF) (b), Radius of gyration of free HDAC10 (blue), HDAC10-Quisinostat (orange), and HDAC10-ZINC19749069 (grey) complexes. HDAC10-ZINC19749069 displayed the highest stability over time.

5. DISCUSSION

5.1 Design of Isoform-Selective HDAC Inhibitors by Scaffold Hopping

Compared with the approved HDAC inhibitors (Vorinostat, Belinostat and Romidepsin) and well-studied HDAC inhibitors in clinical trials (Entinostat, Tacedinaline and Mocetinostat), KA_025, KA_026 and KA_027 displayed increased potency and selectivity (with the exception of Entinostat which showed higher binding affinity for HDAC3; ΔG = -10.62 Kcal/mol) (Table 4.2). Entinostat binds selectively to the class I HDACs 1-3 and modestly, to HDAC8, currently in clinical development for the treatment of human colorectal cancer lines (Bracker et al., 2009). Similarly, Tacedinaline show preference for class I HDACs 1-3 with modest activity against HDAC8, inhibits the growth of lung and breast cancers, lymphoblastic leukemia and more (Mottamal et al., 2015). Mocetinostat displays 2-10 folds higher selectivity for HDAC1 over HDACs 2, 3 and 11 (Boumber et al., 2011). Therefore, these known inhibitors were used as reference compounds to guide the selection of potent and selective inhibitors in the current study. The thresholds for potency and selectivity index were > 9.00 Kcal/mol and ≥ 7 respectively.

Generally, the removal of the acetyl group from a substrate occurs through a "charge-relay system" consisting of two adjacent histidine residues, two aspartic residues, and one tyrosine residue deep inside HDACs catalytic pocket. A cation binds near the bottom of the pocket to be coordinated by two additional aspartates, one histidine and a water molecule (Finnin et al., 1999). HDAC inhibitors function by chelating the Zn^{2+}, making the charge-relay system dysfunctional. In the complexes of HDAC1 with KA_025, KA_026, and KA_027, zinc was involved in metal-acceptor interaction via carbonyl oxygen of the linker group, however, such interaction was not observed in the complexes of HDAC2 with these compounds, rather, van der Waals interaction. Moreover, the two adjacent histidine residues (HIS140 and HIS141 for HDAC1 and HIS145 and HIS146 for HDAC2) and two aspartic acid residues (ASP176 and ASP264

for HDAC1) and one (ASP183 in HDAC2) interacted with KA_025, KA_026, and KA_027. These findings were consistent with a study by Fournel et al. (2002), in which sulfonamide anilides exhibited antiproliferative activity against human tumor without chelating zinc from the active site of HDACs. Here, although it is not clear what exactly brought about the selectivity of KA_025, KA_026, and KA_027 for HDACs 1 and 2 given their similarity in structure with the other nonselective inhibitors, we speculate that their unique carbonyl group near the cap might have changed the set of interactions in the deep active site, and consequently led to their selectivity for HDACs 1 and 2.

Interestingly, KA_029 interacted with HDAC1 in the typical way HDAC inhibitors bind zinc-containing HDACs. Zinc ion was chelated by one sulfonyl oxygen via metal-acceptor interaction and the catalytically essential amino acid residues, HIS140, HIS141, HIS178, ASP176, ASP264, and TR303 also interacted mainly with sulfonyl group. This result is partly in agreement with findings by Noor et al. (2015), in which Zn^{2+} ion was chelated by sulfonyl oxygen of class I selective inhibitor.

In case of HDAC2-KA_036 complex, various non-covalent interactions including van der Waals, π-sulfur, π-alkyl, π-π stacked and 4 H-bonds were formed. Interestingly, the oxygen bridge of the linker group engaged TRY308 via one H-bond. TRY308 is a component of charge-relay system of HDAC2 catalysis. These interactions added up to contribute to the overall stability of the complex.

These findings are especially important given the lack of specificity of the many HDAC inhibitors in clinical use and trials. It is particularly challenging to achieve isoform selectivity among class I HDACs due to their highly conserved active site. It is believed that, the continued identification of isoform-selective inhibitors will remain a major challenge to HDAC inhibitor development. Theoretically, the isoform-selective HDAC inhibitors might be more effective if the specific HDAC is a component of a repressive complex that is crucial for tumorigenesis (Lane and Chabner, 2009). In this study, class I HDACs and HDAC6 were targeted considering findings that histone acetylation is thought to be primarily regulated by HDACs 1-3, whereas the acetylation of tubulin and Hsp90 is specifically regulated through HDAC6 (Newbold et al., 2013). That, HDACs

1-3 are frequently upregulated in a variety of human cancers including breast, colon, lung cancers and more and thus their individual pharmacological blockade induces apoptosis and cell cycle arrest. That, HDACs 1, 2 are key components of CoREST, NuRD, and Sin3 corepressor complexes while HDAC3 is a component of N-CoR complex (Ahringer, 2000). That, the aberrant recruitment of these complexes to the promoter of the tumor suppressor, p53 epigenetically represses transcriptional activity of the gene (Luo et al., 2000). That, the antitumor effect of HDAC inhibitors is widely linked to class I inhibition (Dejligbjerg et al., 2008). These provide strong rationales for selective inhibition of these individual isoforms in cancer. The search for isoform-selective HDAC inhibitors is being carried out using both computational and experimental approaches. Computational procedures are indispensable components of rational drug design. Therefore, these predicted HDAC inhibitors can be potentially isoform-selective, warranting further modeling-based and experimental studies towards validation of their bioactivity.

5.2. Isoform-selective Histone Deacetylase Inhibitors Identified via Structure-Based Virtual Screening and Molecular Dynamics Simulation

In the present study, exhaustive structure-based virtual screening of a chemical database containing ~ 2.7 million compounds, against class I HDACs, was carried out. This is in line with the fact that, the emerging trend suggests that, subtle differences in the catalytic channels of HDAC isoforms can be explored to achieve selectivity (Bieliauskas and Pflum, 2008).

Compound 1 (a sulfonamide derivative) displayed many folds selectivity for HDAC1 over the reported compounds of the same class (Fournel et al., 2002; Bouchain and Delorme, 2003). Compound 1 spanned the catalytic channel of HDAC1 by forming various interactions along the pocket entrance with PHE205, PHE150, and ASP99 and more amino acid residues.

At the bottom of the pocket near Zn^{2+} metal ion, the sulfonyl and other polar groups on the compound interacted with HIS140, HIS141, ASP176, TRY303 (Figure 5.1).

Together with ASP264 (not found to be involved in the interaction here), ASP176, HIS140, and HIS141 act as general acid-base catalytic pairs – coupled with Zn^{2+} metal ion coordination, TRY303 stabilizes the oxyanion of the tetrahedral intermediate formed in the "charge relay system" of HDAC1 catalysis (Lombardi et al., 2011). Hence, disrupting this system of catalysis may lead to the blockade of the enzymatic activity. Other top-ranking inhibitors of HD AC1 identified were amide and carboxylic acid derivatives (Table A 1.1-5).
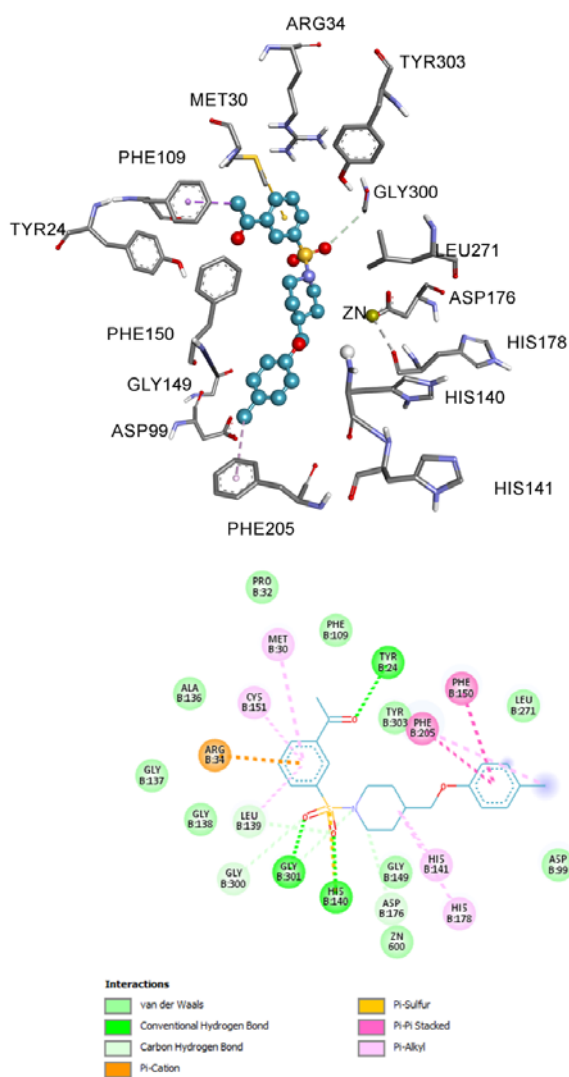
Figure 5. 1. 3D representation of a complex of HDAC1 with compound 1 (Otava code; 3368838).

In HDAC2-compound 11 complex, the naphthalenyl moiety served as surface recognition group channeling the carboxyl group, via amide linker, to the bottom of the pocket towards zinc coordinate.
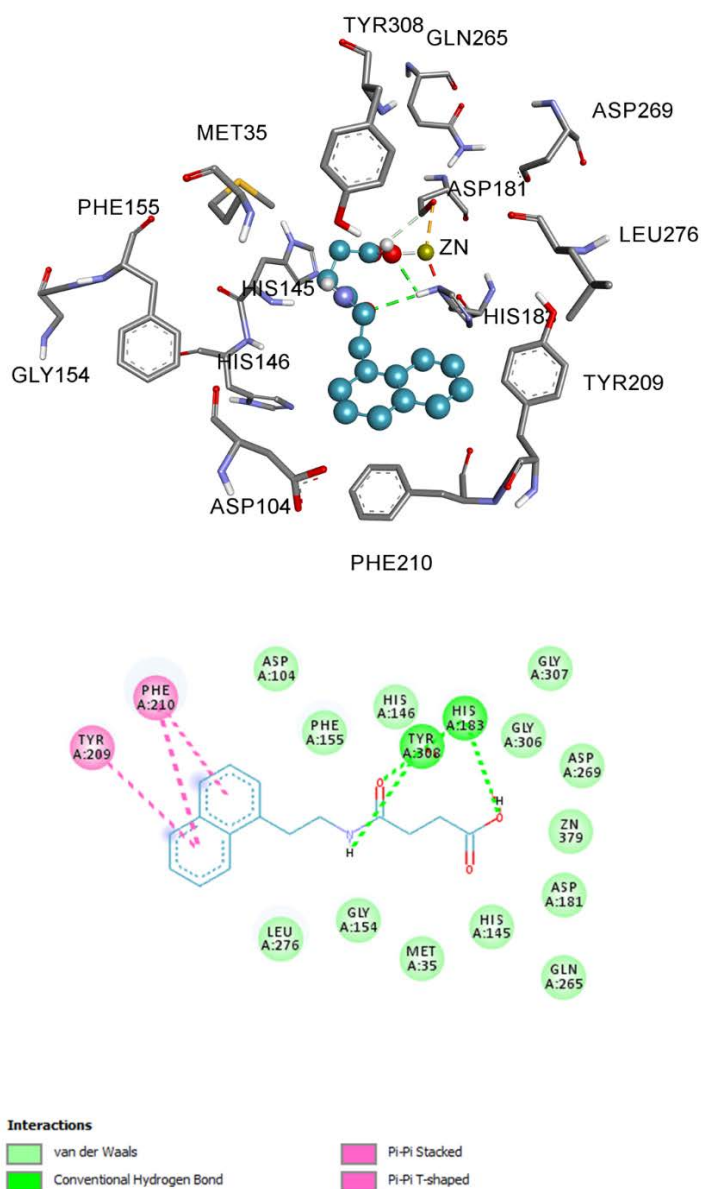
Figure 5. 2. 3D representation of a complex of HDAC2 with compound 11 (Otava id; P7020400743).

Compound 11 interacted with HIS145, HIS146, ASP266, TRY308 and more residues deep inside HDAC2 catalytic pocket via mainly, carbonyl oxygen (Figure 5.2).
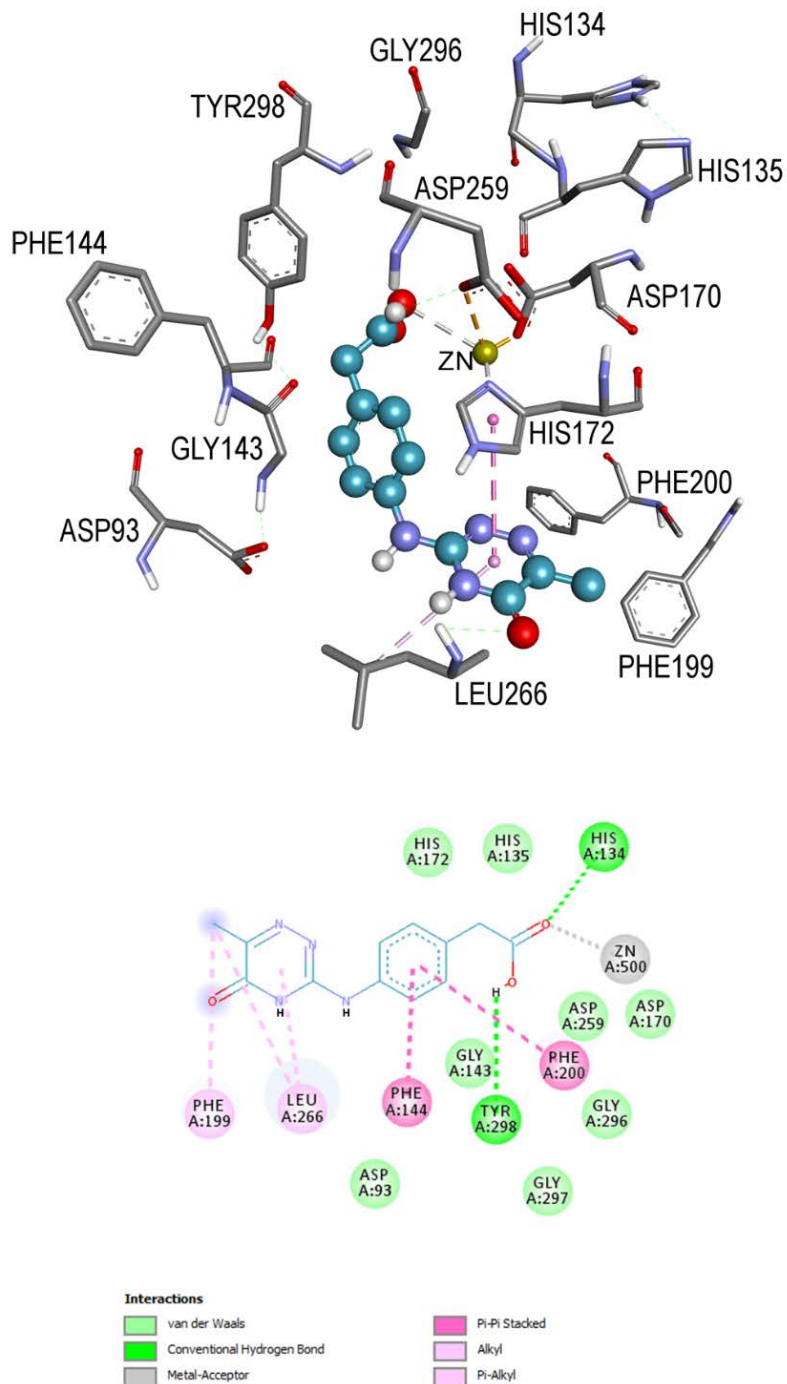
Figure 5. 3. 3D representation of a complex of HDAC3 with compound 21 (Otava id; P7020350446).

Interestingly, of all the 36 compounds identified, compound 29 was found to have the highest binding affinity and showed high selectivity for HDAC8 (Table 5.1). Compound 29 is a carboxylic acid derivative with a bulky cap (substituted phenanthrenyl moiety) and an amine-containing aromatic linker involved mainly, in π interactions with aromatic groups of different side chains. The zinc binding moiety, carboxyl group chelated Zn^{2+} ion via carbonyl oxygen and formed 3 H-bond interactions with HIS129, HIS130, and TYR293 (Figure 5.4). In addition, various more interactions formed along the entrance and the interior of the channel resulted in the complete burial of compound 29 in HDAC8 active site. HDAC8 exhibits an acetate release channel different from that of HDACs 1–3, and a unique lateral internal channel — these features could be exploited to achieve isoform selectivity (Micelli and Rastelli, 2015). Whitehead et al. (2011) achieved selectivity for HDAC8 by exploiting acetate release channel with a small molecule.
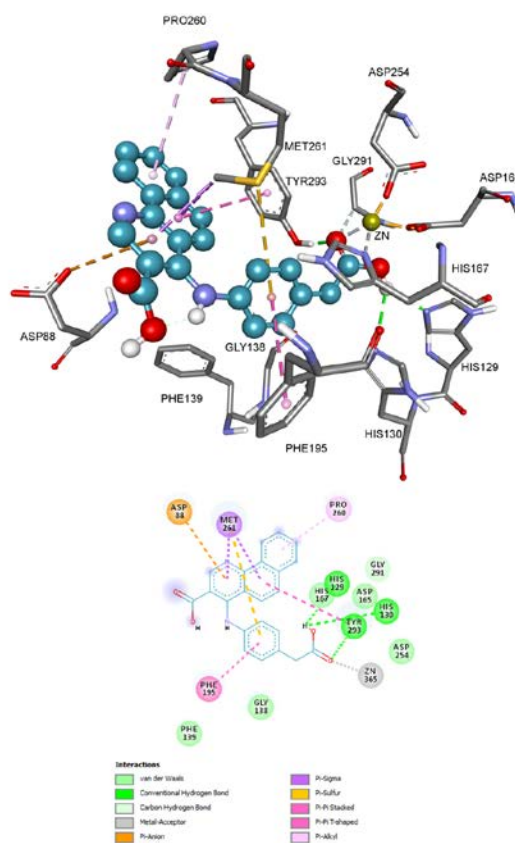
Figure 5. 4. 3D representation of a complexes of HDAC8 with compound 29 (Otava code; P7019081225).

Overall, although the detected compounds were structurally diverse, most of them contain carboxyl groups. Abdel-Atty et al. (2014) reported carboxylic acid derivatives to have HDAC inhibition and cytotoxic activities against HepG2 human cancer cell lines by *in vitro*, 3D pharmacophore QSAR, and molecular docking studies — however, no isoform selectivity was shown. In another activity and docking studies, carboxylic acid derivatives were modified yielding potent and selective inhibitors of HDAC8 (Bora-Tatar et al., 2009).

The structurally-related short-chain fatty acids, such as Valproic acid, butyric acid, and phenylbutyric acid possess weak inhibition against classes I and II HDACs. Valproic acid, already in clinical use for the treatment of epilepsy (Phiel et al., 2001), causes hyperacetylation of histones in cultured cells and *in vivo* – most probably, by inhibiting HDACs, which induces differentiation of carcinoma cells, transformed hematopoietic progenitor cells and leukemic blasts (Göttlicher et al., 2001).

In the context of pharmacophore features of the compounds identified in the present study, their capping groups might have aided in their isoform selectivity. Compounds 1 and 11 contain an aromatic and a fused aromatic ring respectively. Compounds 21 and 29 harbor heterocyclic and fused heterocyclic 3-membered rings respectively. These bulky capping groups formed various interactions, in addition to the steric clashes, with the amino acid residues the entrance to the channel of their respective target. Although it is difficult to precisely predict the specific features of the capping group required for selectivity (Bieliauskas and Pflum, (2008), the cap have been explored to achieve selectivity in HDAC inhibitors due to the subtle differences in the amino acid residues around the entrance to the HDACs catalytic channels. Whitehead et al. (2011) achieved selectivity within class I HDACs with a non-hydroxamate compounds bearing aromatic heterocyclic indole ring as the capping group. Butler et al. (2010) investigated the structural basis of HDACs selectivity by incorporating steric bulk into the capping group of their designed HDAC inhibitors. High plasticity of the HDAC8 catalytic channel is thought to enable binding of an inhibitor otherwise unable to fit the more rigid channel of other HDACs (Micelli and Rastelli, 2015). This might be why

compound 29 bearing a bulky capping group, selectively fitted in the flexible channel of HDAC8 compared over rest of the class members.

Furthermore, the binding mode stability of the best-ranked ligands was examined by MD simulation. At physiological condition, the inhibitors remained bound to their respective target enzymes throughout the simulation. MD simulation has been successfully applied to examine the binding mode stability of HDAC inhibitors. Thangapandian et al. (2012) investigated inhibitor selectivity across classes of HDACs by a 5 ns-MD simulation. Tambunan et al. (2013) designed HDAC inhibitors whose affinity was comparable with that of Vorinostat against class II HDACs, and studied their binding mode stability by a 5 ns-MD simulation. Noor et al. (2015) extended their simulation time period to 12 ns in an attempt to explore the binding modes of their designed potential inhibitors against HDACs 2 and 8. Here, the free and ligand-HDAC complexes were submitted to 10 ns-production-MD simulation. The MD simulation results of the current study were consistent with the findings of the studies cited above, as the potential energy profiles of the complexes were lower and in agreement with RMSD and RMSF distributions throughout the simulation time.

Despite increasing research effort in this field, very few truly isoform-selective inhibitors have been reported in the literature (Thaler and Mercurio, 2014; Zhang et al., 2015). Majority of HDAC inhibitors are either pan-inhibitors or class selective. The compounds reported here showed high and moderate isoform selectivity with good. According to Otava's catalogue, compound 1 is under the category of 'tangible' compounds. 'Tangible' compounds are those compounds with a high likelihood of being synthesized. Compounds 11, 21 and 29 are in the screening collection for prompt delivery. Compounds in this collection underwent quality control for structural confirmation. Therefore, the availability of these candidate compounds eliminates the possible setback issues associated with chemical synthesis. The may also serve as scaffolds for further optimization towards the design of isoform-selective HDAC inhibitors. Further studies are recommended for *in-vitro* and *in-vivo* validation of inhibitory effects of these proposed inhibitors.

5.3 Structure-Based Virtual Screening for Identification of HDAC6-Selective Inhibitors

Structure-based virtual screening has been an important source of novel molecular scaffolds for HDAC inhibitor design (Park et al., 2010; Uba and Yelekçi, 2017b). To the best of our knowledge, the recently solved crystal structure of HDAC6 has not been explored via structure-based virtual screening even though few attempts have been made since the release of the structure to discover new HDAC6 inhibitors (Negmeldin et al., 2017). Additionally, until recently, homology models were used to search for the conformational complexity of the enzymes and inhibitor binding properties (Sixto-López et al., 2017). Therefore, this study attempted to identify potentially selective inhibitors of this crucial cancer target by the combination of other *in silico* approaches along with the structure-based virtual screening.

To accomplish this goal, compounds were filtered not only based on their binding affinity but also and much more importantly, based on their potential selectivity for HDAC6 over the structurally related isoform, HDAC7. Out of the top 20 compounds evaluated, only 4 compounds were found to display potential selectivity for HDAC6, whereas the remaining compounds were excluded from further processing despite their high binding affinity. These 4 compounds were also predicted to have good drug-like and ADMET properties consistent with the widely followed "Rule of 5" and "Jorgensen Rule-of-Three". Lipinki's "Rule of 5" states that drug-like or orally available molecules should have no more than 1 violation of the following: MWt $\leq$ 500 Da; log P $\leq$ 5; S_HBD $\leq$ 5 and S_NO $\leq$ 10 (Lipinski, 2004). "Jorgensen Rule-of-Three "states that "the aqueous solubility measured as logS should be greater than –5.7, the apparent Caco-2 cell permeability should be faster than 22 nm/s and the number of primary metabolites should be less than 7; these limits are based on the properties of 90% of 1700 oral drugs" (Di and Kerns, 2016).

Structural analysis of these compounds revealed important information about their pharmacophoric features that might have aided their selectivity for HDAC6. They all share aromatic cap groups bound to the surface of the catalytic channel with common

interacting residues, HIS500 and LEU749 (except for P7020527347). Also, they all contain aromatic linker groups (except for P2194879), and a common carboxyl acid functional group as a zinc-binding domain. The capping group is responsible for enzyme surface recognition and various cap features of HDAC inhibitors have been explored to achieve selectivity, taking advantage of the subtle variation around the region. Butler et al. (2010) incorporated steric bulk into the cap of inhibitors and specifically blocked HDAC6. Shultz et al. (2011) designed isoindoline-based hydroxamates to achieve selectivity among HDACs. Towards a similar goal, Whitehead et al. (2011) designed HDAC inhibitors with aromatic heterocyclic indole ring. Surprisingly, very recently, "capless" inhibitors exhibited appreciable HDAC6 selectivity, and this was shown to be contributed by favorable binding entropy of the inhibitors to HDAC6 (Porter et al., 2018). Tubastatin A, a well-established HDAC6-selective inhibitor (Vishwakarma et al., 2013), closely resembles P2194879 in terms of capping group, and the rest of the 3 compounds, in terms of the aromatic linker group. Although all the 4 compounds are structurally diverse, they were found to be carboxylic acid derivatives. Carboxylic acid derivatives have been shown to strongly inhibit HDACs due to their ability to form a strong metal-acceptor interaction with Zn^{2+} metal ion (Bora-Tatar et al., 2009; Abdel-Atty et al., 2014). Moreover, the structurally related derivatives of carboxylic acid, valproic acid and other short chain fatty acids have already become well established as HDAC inhibitors (Göttlicher et al., 2001; Lu et al., 2004).

To overcome the protein flexibility issues associated with our rigid docking protocol, we submitted both the free HDAC6 and its complexes with these 4 predicted inhibitors to brief MD simulations, to examine the stability of ligand binding modes and the whole complex structural stability. The complex of HDAC6 with the 3rd-ranked compound (P3823745) was found to display the highest stability over time of the simulation. All the ligands remained in the active sites of the enzyme throughout the simulation and showed slightly higher stability compared with the free enzyme. Analysis of the last snapshot from each simulated system revealed that the ionized carboxyl fragments of all the 4 compounds formed strong metallic bond with Zn^{2+} ion and H-bond interactions with polar residues (mainly, ASP and TYR). This might justify their higher binding

affinity compared with the known selective inhibitors of HDAC6 (except for Citarinostat) The parameters analysed following the MD simulation were, to some extent, in agreement with our recent study examining the stability of ligand-HDAC binding modes via 10 ns-MD simulation (Uba and Yelekçi, 2017a), and with previous study by other group assessing structural stability of HDAC complexes via 5 ns-MD simulation (Thangapandian et al., 2012). However, the 10 ns-MD simulation time used by the current study may not be sufficient to fully examine the structural stability of these complexes — the trend of the RMSD might change at longer time. Nevertheless, being one of the early *in silico* studies on this newly-resolved crystal structure, our MD simulation may provide evidence of requiring a longer time for examining the stability of ligand binding modes.

The predicted compounds identified in the current study displayed both high potency and potential HDAC6 selectivity based on *in silico* assessment. In addition, according to Otava's categorization of this collection, they are compounds that have undergone quality control for structural confirmation and safety evaluation. Therefore, we propose that they may be used as lead compounds for further optimization towards the design of HDAC6 inhibitors with improved selectivity.

5.4 The Design of Selective Inhibitors of HDAC6 via Pharmacophore Modeling

Pharmacophore modeling in combination with other in silico procedures has become essential tools in the current computer-aided drug designs. The HipHop hypotheses method applied in this study, has been successful in identifying potential inhibitors of various biological targets. (Clement et al., 2003; Kim et al., 2008; Yilmaz et al., 2014; Ataei et al., 2015) Although all the 10 hypotheses developed in the current study consisted of the same features, their spatial locations in 3D space were different (Figure A1). All the hypotheses were subjected to evaluation using Güner-Henry scoring method. Hypo1 was found to be statistically valuable, as it successfully retrieved 85% of the active compounds with the enrichment factor (16.23), GH score (0.78). GH score of 0.78 indicates the soundness and reliability of the model.

The "DruglikeDiverse" database screening against Hypo1 returned a total of 1056 compounds. The Catalyst software imbedded in Biovia DS 4.5 automatically ranked these compounds according to their pharmacophore fit values. The top 10 best-fitting compounds with fit values >3 were selected for further studies. These fit values were consistent with those of polo-box domain inhibitors identified via multi-pharmacophore modeling. (Sakkiah et al., 2014) As the database name suggests, these compounds were drug-like and diverse in structure. "DruglikeDiverse" database has been directly explored for identification of new inhibitors of Topoisomerase I (Ataei et al., 2015) and very recently used as a guide towards the development of linear peptides for targeting αvβ3 integrin for cancer diagnosis (Ma et al., 2017). Therefore, this database could be an important repatoir of useful lead compounds against diverse biological targets. Its small size (~ 6000 compounds) allowed for a rapid search for lead compounds whose binding affinity were predicted by molecular docking, and the stability of binding mode by MD simulation. The pharmacophore model was sound, therefore can be used to search larger databases for better chemically diverse potential HDAC6-specific inhibitors.

Hypo1 was also consistent with the general pharmacophoric features of HDAC inhibitors known from literature (Mottamal et al., 2015). The cap-linker-chelator feature of zinc-binding HDACs inhibitors was well represented by hypo1. Considering the two FDA's approved drugs, vorinostat, and belinostat, the aromatic ring feature mapped onto the cap, the H-bond donor feature, and the second hydrophobic feature mapped onto the linker, and the H-bond acceptor feature mapped onto the chelator region. This is in agreement with ligand features essential for HDACs inhibitors previously studied by pharmacophore modeling (Beckers et al., 2007; Chen et al., 2008; Noureen et al., 2010).

Furthermore, the top 10 lead compounds were found to be drug-like, having passed the ADMET prediction and "Rule of 5" tests using two independent ADMET prediction tools, ADMET predictor[TM] and AdmetSAR server. Among the descriptors analyzed, specifically, aqueous solubility of a drug molecule influences absorption and transport of a drug molecule in the body. QSPR has been successfully applied to relate drug and

organic molecules to their respective aqueous solubility (Chen et al., 2002). Caco-2 permeability is another property reflecting gastrointestinal permeability by measuring the rate of transport of a drug molecule across the Caco-2 cell line. Caco-2 permeability of several drug molecules and drug candidates has been studied both *in vitro* (Yee, 1997; Ranaldi et al., 2003; Press and Di Grandi, 2008) and *in silico* (Guangli and Yiyu, 2006; The et al., 2011) These predicted physicochemical properties of the top 10 Hit compounds were consistent with those of drug molecules.

Moreover, ENA501965 and IBS399024 showed increased binding affinity and selectivity for HDAC6 CD2 over class I HDACs and HDAC7. ENA501965 bound HDAC6 CD2 with interesting mode — chelating Zn^{2+} ion via methoxyl oxygen of the methoxyphenyl substituent and filling the small cavity in the middle of the tunnel with dimethylnitrophenyl substituent on an amide-containing linker. The unique phthalazone cap of ENA501965 interacting with polar residues near the entrance to the channel might have aided the selectivity shown by the compound. Butler et al. (Butler et al., 2010) achieved HDAC6 selectivity by varying the cap features of hydroxamic acid containing HDAC inhibitors. Whitehead et al. (2011) added an aromatic heterocyclic indole ring to a non-hydroxamate compounds and achieved selectivity within class I HDACs. Findings of the current study are important given the poor pharmacokinetics and toxicity of hydroxamic acid-containing pan-HDAC inhibitors, prompting the search for non-hydroxamate HDAC inhibitors. (Suzuki and Miyata, 2005) On the other hand, IBS399024 bound with different mode and yet engaged Zn^{2+} ion via van der Waals interaction.

The stability of binding modes of Panobinostat, ENA501965, and IBS399024 was examined by 10 ns-production-MD simulation. In the presence of H_2O molecules and ions, these ligands remained bound to the enzyme throughout the simulation time. All the 3 complexes showed relatively higher structural stability than the free enzyme. HDAC6 CD2-ENA501965 complex was found to show the lowest RMSD profile (0.55-1.17 Å), followed by HDAC6 CD2-Panobinostat complex (0.58-1.20 Å) and HDAC6 CD2-IBS399024 complex (0.56-1.40 Å). These results were consistent with the molecular docking results of these complexes, also in agreement with the previous

results of our study examining the stability of ligand-HDAC complexes via 10 ns-MD simulation (Uba and Yelekçi, 2017a), and via 5 ns-MD simulation by another group (Thangapandian et al., 2012). Similar to the present study, Yu et al. (2009), successfully developed 3D pharmacophore model based on 24 hydroxamates to discover new HDAC1 inhibitors. Recently, Choubey et al. (2016), combined pharmacophore modeling, 3D-QSAR analysis, *in silico* screening and density functional theory (DFT) approaches towards identification of HDAC1 inhibitors. Class I HDACs were also targeted by pharmacophore modeling combined with other *in silico* procedures (Gupta et al., 2014). Here, only HDAC inhibitors in clinical use and trials were included in the training and test sets. In addition, the Hit compounds identified were subjected to selectivity assessment for other HDACs sharing structural similarity with HDAC6. Selectivity of HDAC inhibitors is increasingly attracting the attention of researchers working in this field in the wake of cytotoxicity associated with many of the HDACs inhibitors in clinical use and trials. Essentially, this study identified not only potential lead compounds for further optimization but also candidate molecules for possible selectivity towards HDAC6. Thus, the present study may provide additional information on the structural features necessary for the design of HDAC6 CD2 inhibitors, creating avenues for further *in silico* and experimental studies towards the improvement of potency and selectivity.

5.5 Homology Modeling of Human HDAC10 and the Design of Selective Inhibitor

The assessment of the accuracy and reliability of protein structures determined experimentally or by homology modeling is a necessary task that needs to be addressed. ProSA is a tool widely used to check 3D models of protein structures for potential errors (Wiederstein and Sippl, 2007). The web-based version of ProSA, ProSA-web was used to assess the quality of M0017 in the current study. The overall quality score calculated by ProSA for M0017 is displayed in a plot that showed the scores of all experimentally determined protein chains currently available in the PDB (Berman et al., 2000). This feature relates the score of a specific model to the scores computed from all experimental structures deposited in PDB. The z-score shows the overall model quality and measures the deviation of the total energy of the structure with respect to an energy

distribution derived from random conformations (Sippl, 1993; Sippl, 1995). Z-score outside a range characteristic for native proteins indicates erroneous structures. M0017 was found to have a z-score value -5.00, which corresponded to the native conformation.

Molecular docking of the known HDAC10 inhibitors was carried out to further validate the quality of the model as the calculated Ki values were in agreement with the experimental Ki (or IC50) values. In addition, all the compounds bound to the enzyme with reasonable orientations. This showed that the model could be used as a target structure for the design of selective inhibitors of HDAC10. Therefore, the most active compound, Quisinostat was run against ZINC database and druglike compounds with similar structure were retrieved. The top hit were docked into the catalytic channel of HDAC10 and HDAC6 CD2.

6. CONCLUSIONS

In this dissertation, the attempts made to design potential isoform-selective HDAC inhibitors for cancer therapy are reported. Class I HDACs are Zn^{2+}-dependent, primarily located in the nucleus, show the strongest enzymatic activity on histone, and are overexpressed in a variety of cancer types. Class I HDACs 1-3, components of corepressor complexes, are implicated in cancer progression through epigenetic repression of p53 gene. HDAC6, also a Zn^{2+}-dependent class IIb member, deacetylates tubulin, HSP90 and other non-histone proteins thereby regulating microtubule dynamics and promotes cancer cell invasion. The present study was aimed at designing potentially specific inhibitors of these individual isoform by a combination of various in silico approaches.

To achieving this aim, different molecular modeling procedures including sequence and structural alignments, topology-based scaffold hopping, molecular docking and dynamics simulation, and ADMET prediction were applied. The high sequence similarity and active sites conservation among HDAC (which poses difficulty in achieving isoform selectivity) were analyzed. HDACs 1 and 2 show the highest sequence and structural conservation of the catalytic domains, making the design of isoform-selective inhibitors particularly challenging between the two isoforms. The catalytic channel of HDAC3 is very similar to those of HDACs 1 and 2, while HDAC8, being a distant relative, displays active site plasticity and harbors acetate release channel, providing an avenue for achieving selectivity.

For validation purpose, a series of known HDAC inhibitors in clinical use and trials were studied and their binding affinities were consistent with their experimental Ki values. Also, for the sake of comparison of the binding modes and affinities of these established inhibitors with those of the predicted inhibitors designed in the current study.

To design isoform-selective inhibitors, molecular modification on a fragment retrieved from Otava database was performed by topology-based scaffold hopping and a library of compounds was developed. Thirteen compounds from this library, denoted KA_025 through KA_037, passed ADMET prediction test. *In silico* selectivity evaluation revealed 5 compounds (KA_025, KA_026, KA_027, KA_029, and KA_036) to have increased selectivity for HDACs 1 and 2 compared with HDACs 3, 6 and 8. They were found to display increased binding affinities compared with those of some selected HDAC inhibitors in clinical use and trials. Furthermore, their interaction patterns with amino acid residues in the active sites of HDACs 1 and 2 were examined and the structural basis of their selectivity was rationalized.

To circumvent difficulty in compound synthesis, structure-based virtual screening of ~ 2.7 million compounds retrieved from Otava database, was carried out against class I HDACs. By employing selectivity criteria used by previous studies on HDAC inhibitor selectivity, a total of 36 compounds (10 for HDAC1; 10 for HDAC2; 8 for HDAC3; and 8 for HDAC8) were found to show selectivity for their respective isoforms. To examine the stability of ligand binding modes, the complex of each isoform with its respective best-ranked ligand was submitted to MD simulation. At the end of a10 ns-MD simulation, the ligands remained bound to these targets in the presence of H_2O and ions. Comparative analyses of the potential energy, RMSD and RMSF profiles of the free and bound HDACs suggested that the complexes were more stable over time of the simulation.

While undertaking this research work, the crystal structure of HDAC6 catalytic domain 2 (CD2) was solved and deposited on the protein data bank (release date: 2016-07-27). Previous studies used homology models of the enzyme to design HDAC6 inhibitors. Here, the interaction patterns of this newly-resolved crystal structure with the established HDAC inhibitors were analyzed in order to gain insight into their modes of interaction.

In our continuous effort to search for selective HDAC6 inhibitors, we identified a total of 4 potential HDAC6-selective inhibitors via structure-based virtual screening of ~ 72 461 compounds retrieved from Otava database. These inhibitors belonging to carboxylic acid derivatives class, were found to be drug-like with good ADMET profiles. Their binding affinity and modes were analyzed by molecular docking assay. To examine the structural stability of these docking complexes, a 10 ns-MD simulation was performed for each complex. The results showed that these ligands remained bound to the enzyme in the presence of H_2O and ions, throughout the simulation time. These data may serve as additional lead compounds for further optimization towards the design of HDAC6-selective inhibitors.

Furthermore, to search for more diverse scaffolds for HDAC6-selective inhibitor design, 3D-common-feature (HipHop) hypotheses were developed and validated using Güner-Henry scoring method. Hypothesis 1 (Hypo1), consisting of 1 H-bond acceptor, 1 H-bond donor and 2 hydrophobic (aliphatic/aromatic) features, retrieved 85% of the active compounds with the enrichment factor (16.23) and goodness of the hit score (0.78). Using Hypo1, the search for new potential inhibitors of HDAC6 CD2 was performed by 3D-search query against "DruglikeDiverse" database. The top 10 best-fitting compounds subjected to ADMET prediction were found to be drug-like, with good ADMET profiles. Their binding affinity against HDAC6 CD2 in comparison with class I HDACs and HDAC7 was assessed by molecular docking. The stability of binding modes of the high-affinity and selective compounds (IBS399024 and ENA50196) was examined by 10 ns-MD simulation using NAMD software. RMSD and RMSF analyses revealed that both lead compounds might be stable in the active site of the enzyme over time of the simulation. These results showed that the pharmacophore model is robust, and can be used to search larger compound libraries retrieved from the National Cancer Institute (NCI) database.

Towards the completion of this research work the X-ray crystal structure of zebrafish HDAC10 was released. This structure was used as a template to model the 3D structure of human HDAC10 because of their high sequence similarity, especially around their

catalytic domain. The best model built was validated by 3D structural confirmation, and later by docking of a series known HDAC10 inhibitors into its catalytic pocket. To identify potential selective inhibitors, the highest-affinity compound, Quisinostat, was run against ZINC database containing 10,639,400 drug-like compounds, using SwissSimilarity sever. The top 100 hits with similar scaffolds to Quisinostat were retrieved whose binding mode was further predicted by molecular docking into HDAC10 and HDAC6 CD2. This homology modeled strucuture may allow the design of selective inhibitors of HDAC10 and may also aid in the understanding of the structural dynamics of the isoform. Thus, the strtuctural dynamics of the homology modeled protein and its complexes with Quisinostat and ZINC19749069 was studied by MD simulation. Analysis of MD simulation parameters showed that ZINC19749069 displayed the highest stability in the active site of the enzyme over time.

Taken together, those predicted inhibitors identified via structure-based virtual screening were found to be mainly carboxylic acid and amide derivatives, displayed higher binding affinity, increased selectivity, safer ADMET profile and more stable binding modes compared with the fragment-based designed inhibitors and those identified via pharmacophore-based virtual screening. On the other hand, fragment-based inhibitor designs allowed for the discovery of compounds with diverse functional groups as zinc-binding domains. Similarly, pharmacophore-based virtual screening retrieved non-hydroxamate compounds that were able to coordinate with Zn^{2+} ion, thereby eliminating the toxicity associated with the use of hydroxamates as HDAC inhibitors. In a nutshell, these results show direction for synthesis and biological testing of novel histone deacetylase inhibitors.

The future work will involve further virtual screening with larger compound libraries to retrieve more chemically diverse potential selective inhibitors of the individual HDAC isoform under study. In addition, longer MD simulation will be performed to ascertain the binding mode stability over time of simulation. Furthermore, for safety evaluation, the experimental models of Pharmacokinetic and Pharmacodynamic studies will be carried out to ascertain the drug candidacy of the potential selective inhibitors designed in this study. Similarly, for validation of the biological activity, *in vitro* testing against

panels of both solid and non-solid cancers will be performed. Furthermore, pathway analysis using molecular biology tools, following selective HDAC inhibition, will provide more insight into the role of the individual HDAC isoform in a given cancer pathology.

Herein, structure-based drug design has been shown to be a powerful technique for the rapid identification of small molecules against the 3D structure of the HDAC isoforms derived either by X-ray crystallography, or homology model.

REFERENCES

Abd El-Karim SS, Anwar MM, Mohamed NA, Nasr T, Elseginy SA (2015) Design, synthesis, biological evaluation and molecular docking studies of novel benzofuran-pyrazole derivatives as anticancer agents Bioorganic Chemistry 63: 1–12. doi: 10.1016/j.bioorg.2015.08.006.

Abdel-Atty MM, Farag NA, Kassab SE, Serya RAT, Abouzid KAM (2014) Design, synthesis, 3D pharmacophore, QSAR, and docking studies of carboxylic acid derivatives as Histone Deacetylase inhibitors and cytotoxic agents. Bioorganic Chemistry 57: 65–82. doi: 10.1016/j.bioorg.2014.08.006.

Ahringer J (2000) NuRD and SIN3: Histone deacetylase complexes in development Trends in Genetics 16: 351–356. doi: 10.1016/S0168-9525(00)02066-7.

Ai J, Wang Y, Dar JA, Liu J, Liu L, Nelson JB, Wang Z (2009) HDAC6 Regulates Androgen Receptor Hypersensitivity and Nuclear Localization via Modulating Hsp90 Acetylation in Castration-Resistant Prostate Cancer. Molecular Endocrinology, 23: 1963–1972. doi: 10.1210/me.2009-0188.

Allen WJ, Balius TE, Mukherjee S, Brozell SR, Moustakas DT, Lang PT, Case DA, Kuntz ID, Rizzo RC (2015) DOCK 6: Impact of new features and current docking performance. Journal of Computational Chemistry 36: 1132-56.

Alexandrov LB, Nik-Zainal S, Wedge DC, Aparicio SaJR, Behjati S, Biankin AV, Bignell GR, Bolli N, Borg A, Børresen-Dale A-L et al. (2013) Signatures of mutational processes in human cancer. Nature 500: 15–21. doi: 10.1038/nature12477.

Alonso H, Bliznyuk AA, Gready JE (2006) Combining docking and molecular dynamic simulations in drug design. Medicinal Research Reviews 26: 531–568. doi: 10.1002/med.20067.

Aqvist J, Luzhkov VB, Brandsdal BO (2002) Ligand binding affinities from MD simulations. Accounts of Chemical Research 35: 358–365. doi: 10.1021/ar010014p.

Arabsolghar R, Azimi T, Rasti M (2013) Mutant p53 binds to estrogen receptor negative promoter via DNMT1 and HDAC1 in MDA-MB-468 breast cancer cells Molecular Biology Reports 40: 2617–2625. doi: 10.1007/s11033-012-2348-7.

Armstrong L (2013) Epigenetics, Garland Science 23: 1022–1033. doi: 10.1016/j.cmet.2016.05.019

Ashktorab H, Belgrave K, Hosseinkhah F, Brim H, Nouraie M, Takkikto M, Hewitt S, Lee EL, Dashwood RH, Smoot D (2009). Global histone H4 acetylation and HDAC2 expression in colon adenoma and carcinoma. Digestive Diseases and Sciences 54: 2109–2117. doi: 10.1007/s10620-008-0601-7.

Ataei S, Yilmaz S, Ertan-Bolelli T, Yildiz I (2015) Generated 3D-Common Feature Hypotheses Using the HipHop Method for Developing New Topoisomerase i Inhibitors. Archiv der Pharmazie 348: 498–507. doi: 10.1002/ardp.201500045.

Bae HJ, Jung KH, Eun JW, Shen Q, Kim HS, Park SJ, Shin WC, Yang HD, Park WS, Lee JY et al. (2015) MicroRNA-221 governs tumor suppressor HDAC6 to potentiate malignant progression of liver cancer. Journal of Hepatology 63: 408–419. doi: 10.1016/j.jhep.2015.03.019.

Bailey H, Stenehjem DD, Sharma S (2015) Panobinostat for the treatment of multiple myeloma: The evidence to date. Journal of blood medicine 6: 269–276. doi: 10.2147/JBM.S69140.

Bajorath J (2002) Integration of virtual and high-throughput screening. Nature Reviews: Drug Discovery 1: 882–894. doi: 10.1038/nrd941.

Banerji U, Van Doorn L, Papadatos-Pastos D, Kristeleit R, Debnam P, Tall M, Stewart A, Raynaud F, Garrett MD, Toal M et al. (2012) A phase I pharmacokinetic and pharmacodynamic study of CHR-3996, an oral class I selective histone deacetylase inhibitor in refractory solid tumors. Clinical Cancer Research 18: 2687–2694. doi: 10.1158/1078-0432.CCR-11-3165.

Bantscheff M, Hopf C, Savitski MM, Dittmann A, Grandi P, Michon AM, Schlegl J, Abraham Y, Becher I, Bergamini G et al. (2011) Chemoproteomics profiling of HDAC inhibitors reveals selective targeting of HDAC complexes. Nature Biotechnology 29: 255–265. doi: 10.1038/nbt.1759.

Barneda-Zahonero B, Parra M (2012) Histone deacetylases and cancer. Molecular Oncology 6: 579–589. doi: 10.1016/j.molonc.2012.07.003.

Barnum D, Greene J, Smellie A, Sprague P (1996) Identification of common functional configurations among molecules. Journal of chemical information and computer sciences 36: 563–571. doi: 10.1021/ci950273r.

Bauer B, Siebert R and Traulsen, A. (2014) Cancer initiation with epistatic interactions between driver and passenger mutations. Journal of Theoretical Biology 358: 52–60. doi: 10.1016/j.jtbi.2014.05.018.

Bazzaro M, Lin Z, Santillan A, Lee MK, Wang MC, Chan KC, Bristow RE, Mazitschek R, Bradner J, Roden RBS (2008) Ubiquitin proteasome system stress underlies synergistic killing of ovarian cancer cells by bortezomib and a novel HDAC6 inhibitor. Clinical Cancer Research 14: 7340–7347. doi: 10.1158/1078-0432.CCR-08-0642.

Beckers T, Burkhardt C, Wieland H, Gimmnich P, Ciossek T, Maier T, Sanders K (2007) Distinct pharmacological properties of second generation HDAC inhibitors with the benzamide or hydroxamate head group. International Journal of Cancer 121: 1138–1148. doi: 10.1002/ijc.22751.

Beerenwinkel N, Antal T, Dingli D, Traulsen A, Kinzler KW, Velculescu VE, Vogelstein B, Nowak MA (2007) Genetic progression and the waiting time to cancer. PLoS Computational Biology 3: 2239–2246. doi: 10.1371/journal.pcbi.0030225.

Bendell JC, Patel MR, Infante JR, Kurkjian CD, Jones, SF, Pant S, Burris HA., Moreno O, Esquibel V, Levin W, Moore KN (2015) Phase 1, open-label, dose escalation, safety, and pharmacokinetics study of ME-344 as a single agent in patients with refractory solid tumors. Cancer 121: 1056–1063. doi: 10.1002/cncr.29155.

Benz RD (2007) Toxicological and clinical computational analysis and the US FDA/CDER Expert Opinion on Drug Metabolism & Toxicology, 3: 109–124. doi:10.1517/17425255.3.1.109.

Berman HM, Westbrook J, Feng Z, Gilliland G, Bhat TN, Weissig H, Shindyalov IN, Bourne PE (2011) The Protein Data Bank. Nucleic Acids Research, 28: 235-242. doi:10.1093/nar/28.1.235

Bernstein BE, Tong JK, Schreiber SL (2000) Genomewide studies of histone deacetylase function in yeast. Proceedings of the National Academy of Sciences 97: 13708–13713. doi: 10.1073/pnas.250477697.

Bertino EM, Otterson GA (2011) Romidepsin: a novel histone deacetylase inhibitor for cancer Expert Opinion on Investigational Drugs 20: 1151–1158. doi: 10.1517/13543784.2011.594437.

Bertos NR, Wang AH, Yang, XJ (2001) Class II histone deacetylases: structure, function, and regulation. Biochemistry and cell biology = Biochimie et biologie cellulaire 79: 243–52. doi: 10.1139/bcb-79-3-243.

Bhal SK, Kassam K, Peirson IG, Pearl GM (2007) The rule of five revisited: Applying log D in place of log P in drug-likeness filters. Molecular Pharmaceutics, 4: 556–560. doi: 10.1021/mp0700209.

Bibi N, Parveen Z, Rashid S (2013) Identification of Potential Plk1 Targets in a Cell-Cycle Specific Proteome through Structural Dynamics of Kinase and Polo Box-Mediated Interactions. PLoS ONE 8: e70843oi: 10.1371/journal.pone.0070843.

Bieliauskas AV, Pflum MKH (2008) Isoform-selective histone deacetylase inhibitors. Chemical Society Reviews, 37: 1402. doi: 10.1039/b703830p.

Biswas D, Roy S, Sen S. (2006) A simple approach for indexing the oral drug-likeness of a compound: Discriminating drug-like compounds from nondrug-like ones. Journal of Chemical Information and Modeling 46: 1394–1401. doi: 10.1021/ci050459i.

Bjornsson HT, Benjamin JS, Zhang L, Weissman J, Gerber EE, Chen Y-C, Vaurio RG, Potter M C, Hansen KD, Dietz HC. (2014) Histone deacetylase inhibition rescues structural and functional brain deficits in a mouse model of Kabuki syndrome. Science Translational Medicine, 6: 256ra135-256ra135. doi: 10.1126/scitranslmed.3009278.

Böhm HJ, Flohr A, Stahl, M. (2004) Scaffold hopping. Drug Discovery Today: Technologies 1: 217–224. doi: 10.1016/j.ddtec.2004.10.009.

Bolden JE, Peart MJ, Johnstone RW (2006). Anticancer activities of histone deacetylase inhibitors. Nature reviews. Drug discovery 5: 769–84. doi: 10.1038/nrd2133.

Bora-Tatar G, Dayangaç-Erden D, Demir AS, Dalkara S, Yelekçi K, Erdem-Yurter H (2009) Molecular modifications on carboxylic acid derivatives as potent histone deacetylase inhibitors: Activity and docking studies. Bioorganic & Medicinal Chemistry 17: 5219–5228. doi: 10.1016/j.bmc.2009.05.042.

Bosch-Presegue L, Vaquero A (2011) The Dual Role of Sirtuins in Cancer. Genes & Cancer 2: 648–662. doi: 10.1177/1947601911417862.

Botrugno OA, Santoro F, Minucci S (2009) Histone deacetylase inhibitors as a new weapon in the arsenal of differentiation therapies of cancer. Cancer Letters 280: 134–144. doi: 10.1016/j.canlet.2009.02.027.

Bottomley MJ, Surdo PL, Giovine PD, Cirillo A, Scarpelli R, Ferrigno F, Jones P, Neddermann P, Francesco RD, Steinku C, Gallinari P, Carfi A (2008) Structural and Functional Analysis of the Human HDAC4. Journal of Biological Chemistry 283: 26694–26704. doi: 10.1074/jbc.M803514200.

Bouchain G, Delorme D (2003). Novel hydroxamate and anilide derivatives as potent histone deacetylase inhibitors: synthesis and antiproliferative evaluation. Current medicinal chemistry, 10: 2359–72. doi: 10.2174/0929867033456585.

Boyault C, Gilquin B, Zhang Y, Rybin V, Garman E, Meyer-Klaucke W, Matthias P, Müller C W. and Khochbin S (2006) HDAC6–p97/VCP controlled polyubiquitin chain turnover. The EMBO Journal 25: 3357–3366. doi: 10.1038/sj.emboj.7601210.

Boyault C, Sadoul K, Pabion M, Khochbin S (2007). HDAC6, at the crossroads between cytoskeleton and cell signaling by acetylation and ubiquitination. Oncogene, 26: 5468–76. doi: 10.1038/sj.onc.1210614.

Bradbury CA, Khanim FL, Hayden R, Bunce CM, White DA, Drayson MT, Craddock C, Turner BM (2005) Histone deacetylases in acute myeloid leukaemia show a distinctive pattern of expression that changes selectively in response to deacetylase inhibitors. *Leukemia*, 19(10), pp. 1751–1759. doi: 10.1038/sj.leu.2403910.

Brint AT, Willett P (1987) Algorithms for the identification of three-dimensional maximal common substructures. Journal of Chemical Information and Modeling 27; 152–158. doi: 10.1021/ci00056a002.

Brosch G, Loidl P, Graessle S (2008) Histone modifications and chromatin dynamics: A focus on filamentous fungi. FEMS Microbiology Reviews 32: 409–439. doi: 10.1111/j.1574-6976.2007.00100.x.

Brunmeir R, Lagger S, Seiser C (2009) Histone deacetylase HDAC1/HDAC2-controlled embryonic development and cell differentiation. Intional Journal of Developmental Biology 53: 275-289. doi: 10.1387/ijdb.082649rb.

Brunsteiner M, Petukhov PA (2012) Insights from comprehensive multiple receptor docking to HDAC8. Journal of Molecular Modeling 18: 3927–3939. doi: 10.1007/s00894-011-1297-8.

Buchwald M, Krämer OH, Heinzel T (2009) HDACi - Targets beyond chromatin. Cancer Letters 280: 160–167. doi: 10.1016/j.canlet.2009.02.028.

Burdelski C, Ruge OM, Melling N, Koop C, Simon R, Steurer S, Sauter G, Kluth M, Hube-Magg C, Minner S, et al. (2015) HDAC1 overexpression independently predicts biochemical recurrence and is associated with rapid tumor cell proliferation and genomic instability in prostate cancer. Experimental and Molecular Pathology 98: 419–426. doi: 10.1016/j.yexmp.2015.03.024.

Burkhard P, Taylor P, Walkinshaw MD (1998) An example of a protein ligand found by database mining: description of the docking method and its verification by a 2.3 A X-ray structure of a thrombin-ligand complex. Journal of molecular biology 277: 449–66. doi: 10.1006/jmbi.1997.1608.

Burns SS, Akhmametyeva EM, Oblinger JL, Bush ML, Huang J, Senner V, Chen CS, Jacob A, Welling DB, Chang LS (2013) Histone deacetylase inhibitor AR-42 differentially affects cell-cycle transit in meningeal and meningioma cells, potently inhibiting NF2-deficient meningioma growth. Cancer Research 73: 792–803. doi: 10.1158/0008-5472.CAN-12-1888.

Burrell RA, McGranahan N, Bartek J, Swanton C (2013) The causes and consequences of genetic heterogeneity in cancer evolution. Nature 501: 338–45. doi: 10.1038/nature12625.

Butler KV, Kalin J, Brochier C, Vistoli G, Langley B, Kozikowski AP (2010) Rational design and simple chemistry yield a superior, neuroprotective HDAC6 inhibitor, tubastatin A. Journal of the American Chemical Society 132: 10842–10846. doi: 10.1021/ja102758v.

Byrd JC, Marcucci G, Parthun MR, Xiao JJ, Klisovic RB, Moran M, Lin TS, Liu S, Sklenar AR, Davis ME (2005) A phase 1 and pharmacodynamic study of depsipeptide (FK228) in chronic lymphocytic leukemia and acute myeloid leukemia. Blood 105: 959–967. doi: 10.1182/blood-2004-05-1693.

Cacan E, Ali MW, Boyd NH, Hooks SB, Greer SF (2014) Inhibition of HDAC1 and DNMT1 modulate RGS10 expression and decrease ovarian cancer chemoresistance. PLoS ONE 9: e87455 doi: 10.1371/journal.pone.0087455.

Cai M-H, Xu X-G, Yan SL, Sun Z, Ying Y, Wang B-K, Tu Y-Z (2018) Depletion of HDAC1, 7 and 8 by Histone Deacetylase Inhibition Confers Elimination of Pancreatic Cancer Stem Cells in Combination with Gemcitabine. Scientific Reports 8, Article number: 1621. doi:10.1038/s41598-018-20004-0

Camphausen K, Tofilon PJ (2007) Inhibition of histone deacetylation: A strategy for tumor radiosensitization. Journal of Clinical Oncology 26: 4051–4056. doi: 10.1200/JCO.2007.11.6202.

Cartron PF, Blanquart C, Hervouet E, Gregoire M, Vallette FM (2013) HDAC1-mSin3a-NCOR1, Dnmt3b-HDAC1-Egr1 and Dnmt1-PCNA-UHRF1-G9a regulate the NY-ESO1 gene expression. Molecular Oncology 7: 452–463. doi: 10.1016/j.molonc.2012.11.004.

Chalkiadaki A, Guarente L (2015) The multifaceted functions of sirtuins in cancer. Nature Reviews Cancer 15: 608–624. doi: 10.1038/nrc3985.

Chang CC, Lin BR, Chen ST, Hsieh TH, Li YJ, Kuo MYP (2011) HDAC2 promotes cell migration/invasion abilities through HIF-1α stabilization in human oral squamous cell carcinoma. Journal of Oral Pathology and Medicine 40: 567–575. doi: 10.1111/j.1600-0714.2011.01009.x.

Chavez-Blanco A, Segura-Pacheco B, Perez-Cardenas E, Taja-Chayeb L, Cetina L, Candelaria M, Cantu D, Gonzalez-Fierro A, Garcia-Lopez P, Zambrano P, Perez-Plasencia C (2005) Histone acetylation and histone deacetylase activity of magnesium valproate in tumor and peripheral blood of patients with cervical cancer. A phase I study. Molecular cancer 4: 22. doi: 10.1186/1476-4598-4-22.

Chen XQ, Cho SJ, Li Y, Venkatesh S (2002) Prediction of aqueous solubility of organic compounds using a quantitative structure-property relationship. Journal of Pharmaceutical Sciences 91: 1838–1852. doi: 10.1002/jps.10178.

Chen YD, Jiang YJ, Zhou JW, Yu QS, You, QD (2008) Identification of ligand features essential for HDACs inhibitors by pharmacophore modeling. Journal of Molecular Graphics and Modelling 26: 1160–1168. doi: 10.1016/j.jmgm.2007.10.007.

Cheng F, Li W, Liu G, Tang Y (2013). In silico ADMET prediction: recent advances, current challenges and future trends. Current Topics in Medicinal Chemistry 13: 1273–89. doi: 10.2174/15680266113139990033.

Cheng F, Li W, Zhou Y, Shen J, Wu Z, Liu G, Lee PW, Tang Y (2012) AdmetSAR: A comprehensive source and free tool for assessment of chemical ADMET properties.

Journal of Chemical Information and Modeling 52: 3099–3105. doi: 10.1021/ci300367a.

Choudhary C, Kumar C, Gnad F, Nielsen ML, Rehman M, Walther TC, Olsen JV, Mann M (2009) Lysine acetylation targets protein complexes and co-regulates major cellular functions. Science 325: 834-840. doi: 10.1126/science.1175371.

Choubey SK, Mariadasse R, Rajendran S, Jeyaraman J (2016) Identification of novel histone deacetylase 1 inhibitors by combined pharmacophore modeling, 3D-QSAR analysis, in silico screening and Density Functional Theory (DFT) approaches. Journal of Molecular Structure 1125: 391–404. doi: 10.1016/j.molstruc.2016.06.082.

Corbeil CR, Williams CI, Labute PJ (2012) Variability in docking success rates due to dataset preparation. Computer Aided Molecular Design 26: 775-86.

Cozza G (2017) The Development of CK2 Inhibitors: From Traditional Pharmacology to in Silico Rational Drug Design. Pharmaceuticals 10: 26. doi:10.3390/ph10010026.

Chu QSC, Nielsen TO, Alcindor T, Gupta A, Endo M, Goytain A, Xu H, Verma S, Tozer R, Knowling M et al. (2015) A phase II study of SB939, a novel pan-histone deacetylase inhibitor, in patients with translocation associated recurrent/metastatic sarcomas-NCIC-CTG IND 200. Annals of Oncology 26: 973–981. doi: 10.1093/annonc/mdv033.

Clark KP (1995) Flexible ligand docking without parameter adjustment across four ligand-receptor complexes. Journal of Computational Chemistry 16: 1210–1226. doi: 10.1002/jcc.540161004.

Clement OO, Freeman CM, Hartmann RW, Handratta VD, Vasaitis TS, Brodie AMH, Njar VCO (2003) Three dimensional pharmacophore modeling of human CYP17 inhibitors. Potential agents for prostate cancer therapy. Journal of Medicinal Chemistry 46: 2345–2351. doi: 10.1021/jm020576u.

Clement O.A., Mehl A.T. (2000) HipHop: pharmacophores based on multiple common-feature alignments. In: Güner OF, editor. Pharmacophore Perception, Development, and Use in Drug Design. International University Line, pp. 69–84, La Jolla (CA), USA.

Cooper GM, Hausman RE (2007) The Cell: A Molecular Approach, 2nd edition. Sinauer Associates, Sunderland (MA), USA. doi: 10.1017/CBO9781107415324.004.

Cornell WD, Cieplak P, Bayly CI, Gould IR, Merz KM, Ferguson DM, Spellmeyer DC, Fox T, Caldwell JW, Kollman, PA (1995) A second generation force field for the simulation of proteins, nucleic acids, and organic molecules. Journal of the American Chemical Society 117: 5179–5197. doi: 10.1021/ja00124a002.

Cruciani G, Milletti F, Storchi L, Sforna G, Goracci L (2009) In silico pKa prediction and ADME profiling. Chemistry and Biodiversity 6: 1812–1821. doi: 10.1002/cbdv.200900153.

Dassault Systèmes BIOVIA (2017). BIOVIA Discovery Studio 2017 R2: A comprehensive predictive science application for the Life Sciences. San Diego, CA, USA.

Dearden JC (2007) In silico prediction of ADMET properties: how far have we come?. Expert Opinion on Drug Metabolism & Toxicology 3: 635–639. doi: 10.1517/17425255.3.5.635.

Dejligbjerg M, Grauslund M, Litman T, Collins L, Qian X, Jeffers M, Lichenstein H, Jensen PB, Sehested M (2008) Differential effects of class I isoform histone deacetylase depletion and enzymatic inhibition by belinostat or valproic acid in HeLa cells. Molecular cancer 7: 70. doi: 10.1186/1476-4598-7-70.

Derynck R, Akhurst RJ, Balmain A (2001) TGF-beta signaling in tumor suppression and cancer progression. *Nature genetics* 29: 117–29. doi: 10.1038/ng1001-117.

DesJarlais RL, Sheridan RP, Dixon JS, Kuntz ID, Venkataraghavan R (1986) Docking flexible ligands to macromolecular receptors by molecular shape. Journal of medicinal chemistry 29: 2149–53. doi: 10.1021/jm00161a004.

Dhanyamraju PK, Holz PS, Finkernagel F, Fendrich V, Lauth M (2015) Histone Deacetylase 6 Represents a Novel Drug Target in the Oncogenic Hedgehog Signaling Pathway. Molecular Cancer Therapeutics 14: 727–739. doi: 10.1158/1535-7163.MCT-14-0481.

Di L., Kerns E.H. (2016) Drug-like Properties: Concepts, Structure Design and Methods from ADME to Toxicity Optimization, Drug-like Properties: Concepts, Structure Design and Methods from ADME to Toxicity Optimization, 2nd Edition. Elsevier, Burlington, (MA), USA. doi: 10.1016/C2013-0-18378-X.

Diller DJ, Merz KM (2001) High throughput docking for library design and library prioritization. Proteins: Structure, Function and Genetics 43: 113–124. doi: 10.1002/1097-0134(20010501)43:2<113::AID-PROT1023>3.0.CO;2-T.

Ding G, Liu HD, Huang Q, Liang HX, Ding ZH, Liao ZJ, Huang G (2013) HDAC6 promotes hepatocellular carcinoma progression by inhibiting P53 transcriptional activity. FEBS Letters 587: 880–886. doi: 10.1016/j.febslet.2013.02.001.

Dobson PD, Patel Y, Kell DB (2009) "Metabolite-likeness" as a criterion in the design and selection of pharmaceutical drug libraries. Drug Discovery Today 14: 31–40. doi: 10.1016/j.drudis.2008.10.011.

Dokmanovic M, Clarke C, Marks PA (2007) Histone deacetylase inhibitors: overview and perspectives. Molecular Cancer Research 5: 981–989. doi: 10.1158/1541-7786.MCR-07-0324.

Dovey OM, Foster CT, Cowley SM (2010) Histone deacetylase 1 (HDAC1), but not HDAC2, controls embryonic stem cell differentiation. Proceedings of the National Academy of Sciences 107: 8242–8247. doi: 10.1073/pnas.1000478107.

Dowling DP, Gantt SL, Gattis SG, Fierke CA, Christianson DW (2008) Structural studies of human histone deacetylase 8 and its site-specific variants complexed with substrate and inhibitors. Biochemistry 47: 13554–13563. doi: 10.1021/bi801610c.

Dror O, Schneidman-Duhovny D, Inbar Y, Nussinov R, Wolfson HJ (2009) Novel approach for efficient pharmacophore-based virtual screening: Method and applications. Journal of Chemical Information and Modeling 49: 2333–2343. doi: 10.1021/ci900263d.

Drummond DC, Noble CO, Kirpotin DB, Guo Z, Scott GK, Benz CC (2005) Clinical development of histone deacetylase inhibitors as anticancer agents. Annual review of pharmacology and toxicology 45: 495–528. doi: 10.1146/annurev.pharmtox.45.120403.095825.

Duenas-Gonzalez A, Coronel J, Cetina L, Gonzalez-Fierro A, Chavez-Blanco A, Taja-Chayeb, L (2014) Hydralazine-valproate: a repositioned drug combination for the epigenetic therapy of cancer. Expert Opinion in Drug Metabolism & Toxicology 10: 1433–1444. doi: 10.1517/17425255.2014.947263.

Durrant JD, McCammon JA (2011) Molecular dynamics simulations and drug discovery. BMC Biology 9: 71. doi: 10.1186/1741-7007-9-71.

Eccleston A, DeWitt N, Gunter C, Marte B, Nath D (2007) Epigenetics. Nature 447: 395–395. doi: 10.1038/447395a.

Egan WJ (2010) Predicting ADME properties in drug discovery. In K. Merz, Jr, D. Ringe, & C. Reynolds (Eds.). Cambridge University Press 165–178, Cambridge, UK. doi:10.1017/CBO9780511730412.013

Egger G, Liang G, Aparicio A, Jones PA (2004) Epigenetics in human disease and prospects for epigenetic therapy. Nature 429: 457–63. doi: 10.1038/nature02625.

Ehrlich P (1909) Ueber den jetzigen Stand der Chemotherapie. Berichte der Deutschen Chemischen Gesellschaft 42: 17-47.

Eke I, Schneider L, Förster C, Zips D, Kunz-Schughart LA, Cordes N (2013) EGFR/JIP-4/JNK2 signaling attenuates cetuximab-mediated radiosensitization of squamous cell carcinoma cells. Cancer Research 73: 297–306. doi: 10.1158/0008-5472.CAN-12-2021.

Ekins S, Waller CL, Swaan PW, Cruciani G, Wrighton SA, Wikel JH (2000) Progress in predicting human ADME parameters in silico. Journal of Pharmacological and Toxicological Methods 44: 251–272. doi: 10.1016/S1056-8719(00)00109-X.

Ellis L, Pili R (2010) Histone deacetylase inhibitors: Advancing therapeutic strategies in hematological and solid malignancies. Pharmaceuticals 3: 2441–2469. doi: 10.3390/ph3082441.

Esteller M (2008) Epigenetics in cancer. - main article. New England Journal of Medicine 358: 1148–1159. doi: 10.1056/NEJMra072067.

Ewing TJA, Makino S, Skillman AG, Kuntz ID (2001) DOCK 4.0: Search strategies for automated molecular docking of flexible molecule databases. Journal of Computer-Aided Molecular Design 15: 411–428. doi: 10.1023/A:1011115820450.

Fang Y (2012) Ligand–receptor interaction platforms and their applications for drug discovery Expert Opinion on Drug Discovery 7: 969–988. doi: 10.1517/17460441.2012.715631.

Feinberg AP, Koldobskiy MA, Göndör A (2016) Epigenetic modulators, modifiers and mediators in cancer aetiology and progression. Nature reviews. Genetics 17: 284–99. doi: 10.1038/nrg.2016.13.

Feinberg AP, Ohlsson R, Henikoff S (2006) The epigenetic progenitor origin of human cancer. Nature reviews Genetics 7: 21–33. doi: 10.1038/nrg1748.

Feinberg, AP, Tycko B (2004) The history of cancer epigenetics. Nature Reviews Cancer 4: 143–153. doi: 10.1038/nrc1279.

Finnin MS, Donigian JR, Cohen A, Richon VM, Rifkind R A, Marks PA, Breslow R, Pavletich NP (1999). Structures of a histone deacetylase homologue bound to the TSA and SAHA inhibitors. Nature 401: 188–193. doi: 10.1038/43710.

Fischer D, Norel R, Wolfson H, Nussinov R (1993) Surface motifs by a computer vision technique: searches, detection, and implications for protein-ligand recognition. Proteins, 16: 278–292. doi: 10.1002/prot.340160306.

Fischer E (1894) Einfluss der Configuration auf die Wirkung der Enzyme. Berichte der Deutschen Chemischen Gesellschaft 27: 2985–2993. doi: 10.1002/cber.18940270364.

Fournel M, Trachy-Bourget MC, Yan PT, Kalita A, Bonfils C, Beaulieu C, Frechette S, Leit S, Abou-Khalil E, Woo SH, Delorme D, MacLeod AR, Besterman JM, Li Z (2002) Sulfonamide anilides, a novel class of histone deacetylase inhibitors, are antiproliferative against human tumors. Cancer Research 62: 4325–4330.

Fraga MF, Ballestar E, Villar-Garea A, Boix-Chornet M, Espada J, Schotta G, Bonaldi T, Haydon C, Ropero S, Petrie K et al. (2005) Loss of acetylation at Lys16 and trimethylation at Lys20 of histone H4 is a common hallmark of human cancer. Nature genetics 37: 391–400. doi: 10.1038/ng1531.

Furuta E, Okuda H, Kobayashi A, Watabe K (2010) Metabolic genes in cancer: their roles in tumor progression and clinical implications. Biochimica et Biophysica Acta 1805: 141–152. doi: 10.1016/j.bbcan.2010.01.005.

Galloway TJ, Wirth LJ, Colevas AD, Gilbert J, Bauman JE, Saba NF, Raben D, Mehra R, Ma AW, Atoyan R et al. (2015) A phase I study of CUDC-101, a multitarget inhibitor of HDACs, EGFR, and HER2, in combination with chemoradiation in patients with head and neck squamous cell carcinoma. Clinical Cancer Research 21: 1566–1573. doi: 10.1158/1078-0432.CCR-14-2820.

Garcia-Manero G, Assouline S, Cortes J, Estrov Z, Kantarjian H, Yang H, Newsome WM, Miller WH, Rousseau C, Kalita A et al. (2008) Phase 1 study of the oral isotype specific histone deacetylase inhibitor MGCD0103 in leukemia. Blood 112: 981–989. doi: 10.1182/blood-2007-10-115873.

Garcia-Manero G, Yang H, Bueso-Ramos C, Ferrajoli A, Cortes J, Wierda WG, Faderl S, Koller C, Morris G, Rosner G et al. (2008) Phase 1 study of the histone deacetylase inhibitor vorinostat (suberoylanilide hydroxamic acid [SAHA]) in patients with advanced leukemias and myelodysplastic syndromes. Blood 111: 1060–1066. doi: 10.1182/blood-2007-06-098061.

Gardiner EJ, Holliday JD, O'Dowd C, Willett P (2011) Effectiveness of 2D fingerprints for scaffold hopping. Future medicinal chemistry 3: 405–14. doi: 10.4155/fmc.11.4.

Gerelchuluun A, Maeda J, Manabe E, Brents CA, Sakae T, Fujimori A, Chen DJ, Tsuboi K, Kato TA (2018) Histone Deacetylase Inhibitor Induced Radiation Sensitization Effects on Human Cancer Cells after Photon and Hadron Radiation Exposure. International Journal of Molecular Sciences 19: E496. doi: 10.3390/ijms19020496.

Ghasemi J, Saaidpour S (2007). QSPR prediction of aqueous solubility of drug-like organic compounds. Chemical & pharmaceutical bulletin 55: 669–674. doi: 10.1248/cpb.55.669.

Glaser K, Li J, Staver M, Wei R, Albert D, Davidsen S (2003) Role of class I and class II histone deacetylases in carcinoma cells using siRNA. Biochemical and Biophysical Research Communications 310: 529–36.

Godman CA, Joshi R, Tierney BR, Greenspan E, Rasmussen TP, Wang HW, Shin DG, Rosenberg DW, Giardina C (2008) HDAC3 impacts multiple oncogenic pathways in colon cancer cells with effects on Wnt and vitamin D signaling. Cancer Biology and Therapy 7: 1570–1580. doi: 10.4161/cbt.7.10.6561.

Gojo I, Jiemjit A, Trepel JB, Sparreboom A, Figg WD, Rollins S, Tidwell ML, Greer J, Eun JC, Lee MJ et al. (2007) Phase 1 and pharmacologic study of MS-275 a histone deacetylase inhibitor, in adults with refractory and relapsed acute leukemias. Blood 109: 2781–2790. doi: 10.1182/blood-2006-05-021873.

Goldberg AL, Cascio P, Saric T, Rock KL (2002) The importance of the proteasome and subsequent proteolytic steps in the generation of antigenic peptides. Molecular Immunology 39: 147–164. doi: 10.1016/S0161-5890(02)00098-6.

Goodsell DS, Lauble H, Stout CD, Olson AJ (1993). Automated docking in crystallography: analysis of the substrates of aconitase. Proteins 17: 1–10. doi: 10.1002/prot.340170104.

Goodsell D, Olson AJ (1990) Automated docking of substrates to proteins by simulated annealing. Proteins 8: 195–202. doi: 10.1002/prot.340080302.

Gregoretti IV, Lee YM, Goodson HV (2004). Molecular evolution of the histone deacetylase family: Functional implications of phylogenetic analysis. Journal of Molecular Biology 338: 17–31. doi: 10.1016/j.jmb.2004.02.006.

Grozinger CM, Hassig CA, Schreiber SL (1999) Three proteins define a class of human histone deacetylases related to yeast Hda1p. Proceedings of the National Academy of Sciences of the United States of America 96: 4868–4873. doi: 10.1073/pnas.96.9.4868.

Guardiola AR, Yao TP (2002) Molecular cloning and characterization of a novel histone deacetylase HDAC10. The Journal of biological chemistry 277: 3350–3356.

Guangli M, Yiyu C (2006) Predicting Caco-2 permeability using support vector machine and chemistry development kit. Journal of Pharmaceutical Sciences 9: 210–221.

Guenther MG, Barak O, Lazar MA (2001) The SMRT and N-CoR corepressors are activating cofactors for histone deacetylase 3. Molecular and Cellular Biology 21: 6091-101.

Guner O, Clement O, Kurogi Y (2004) Pharmacophore Modeling and Three Dimensional Database Searching for Drug Design Using Catalyst: Recent Advances. Current Medicinal Chemistry 11: 2991–3005. doi: 10.2174/0929867043364036.

Gupta N, Sitwala N, Patel K (2014) Pharmacophore modelling, validation, 3D virtual screening, docking, design and in silico ADMET simulation study of histone deacetylase class-1 inhibitors. Medicinal Chemistry Research 23: 4853–4864. doi: 10.1007/s00044-014-1057-2.

Haberland M, Montgomery RL, Olson EN (2009) The many roles of histone deacetylases in development and physiology: implications for disease and therapy. Nature Reviews Genetics 10: 32-42. doi: 10.1038/nrg2485.

Haberland M, Johnson A, Mokalled MH, Montgomery RL, Olson EN (2009). Genetic dissection of histone deacetylase requirement in tumor cells. Proceedings of the National Academy of Sciences 106: 7751–7755. doi: 10.1073/pnas.0903139106.

Haberland M, Montgomery RL, Olson EN (2009) The many roles of histone deacetylases in development and physiology: implications for disease and therapy. Nature Reviews Genetics 10: 32–42. doi: 10.1038/nrg2485.

Haggarty SJ, Koeller KM, Wong JC, Butcher RA, Schreiber SL (2003) Multidimensional chemical genetic analysis of diversity-oriented synthesis-derived deacetylase inhibitors using cell-based assays. Chemistry and Biology 10: 383–396. doi: 10.1016/S1074-5521(03)00095-4.

Haggarty SJ, Koeller KM, Wong JC, Grozinger CM, Schreiber SL (2003) Domain-selective small-molecule inhibitor of histone deacetylase 6 (HDAC6)-mediated tubulin deacetylation. Proceedings of the National Academy of Sciences 100: 4389–4394. doi: 10.1073/pnas.0430973100.

Hai Y, Christianson DW (2016) Histone deacetylase 6 structure and molecular basis of catalysis and inhibition. Nature Chemical Biology 12: 741-7. doi: 10.1038/nchembio.2134 (doi: 10.2210/PDB5EDU/PDB).

Hai Y, Shinsky SA, Porter NJ, Christianson DW (2017). Histone deacetylase 10 structure and molecular function as a polyamine deacetylase. Nature Communications 8: Article number: 15368. doi:10.1038/ncomms15368.

Halgren TA, Murphy RB, Friesner RA, Beard HS, Frye LL, Pollard, WT, and Banks JL (2004) Glide: A New Approach for Rapid, Accurate Docking and Scoring. 2. Enrichment Factors in Database Screening. Journal of Medicinal Chemistry 47: 1750–1759. doi: 10.1021/jm030644s.

Halkidou K, Gaughan L, Cook S, Leung HY, Neal DE, Robson CN (2004) Up-regulation and nuclear recruitment of HDAC1 in hormone refractory prostate cancer. The Prostate 59: 177–189. doi: 10.1002/pros.20022.

Hart TN, Read RJ (1992) A multiple-start Monte Carlo docking method. Proteins: Structure, Function and Genetics 13: 206–222. doi: 10.1002/prot.340130304.

Hasanov E, Chen G, Chowdhury P, Weldon J, Ding Z, Jonasch E, Sen S, Walker CL, Dere R (2017) Ubiquitination and regulation of AURKA identifies a hypoxia-independent E3 ligase activity of VHL. Oncogene 36: 3450–3463. doi: 10.1038/onc.2016.495.

Hassig CA, Fleischer TC, Billin AN, Schreiber SL, Ayer DE (1997) Histone deacetylase activity is required for full transcriptional repression by mSin3A. Cell 89: 341–347.

Hendrick E, Peixoto P, Blomme A, Polese C, Matheus N, Cimino J, Frère A, Mouithys-Mickalad A, Serteyn D, Bettendorff L, Elmoualij B et al. (2017). Metabolic inhibitors accentuate the anti-tumoral effect of HDAC5 inhibition. Oncogene 36: 4859-4874. doi: 10.1038/onc.2017.103.

Hou T, Wang J (2008) Structure-ADME relationship: still a long way to go? Expert opinion on drug metabolism & toxicology 4: 759–770. doi: 10.1517/17425255.4.6.759.

Hsieh CL, Ma HP, Su CM, Chang YJ, Hung WY, Ho YS, Huang WJ, Lin RK (2016) Alterations in histone deacetylase 8 lead to cell migration and poor prognosis in breast cancer. Life Sciences 151: 7–14. doi: 10.1016/j.lfs.2016.02.092.

Hu Y, Stumpfe D, Bajorath J (2016) Computational Exploration of Molecular Scaffolds in Medicinal Chemistry. Journal of Medicinal Chemistry 59: 4062–4076. doi: 10.1021/acs.jmedchem.5b01746.

Huang BH, Laban M, Leung CH-W, Lee L, Lee CK, Salto-Tellez M, Raju GC, Hooi SC (2005) Inhibition of histone deacetylase 2 increases apoptosis and p21Cip1/WAF1 expression, independent of histone deacetylase 1. Cell Death and Differentiation 12: 395–404. doi: 10.1038/sj.cdd.4401567.

Hubbert C, Guardiola A, Shao R, Kawaguchi Y, Ito A, Nixon A, Yoshida M, Wang X-F, Yao T-P (2002) HDAC6 is a microtubule-associated deacetylase. Nature 417: 455–458. doi: 10.1038/417455a.

Hutt DM, Herman D, Rodrigues AP, Noel S, Pilewski JM, Matteson J, Hoch B, Kellner W, Kelly JW, Schmidt A et al. (2010) Reduced histone deacetylase 7 activity restores function to misfolded CFTR in cystic fibrosis. Nature Chemical Biology 6:25-33

Hwang JJ, Kim YS, Kim T, Kim MJ, Jeong IG, Lee JH, Choi J, Jang S, Ro S, Kim CS (2012) A novel histone deacetylase inhibitor, CG200745, potentiates anticancer effect of docetaxel in prostate cancer via decreasing Mcl-1 and Bcl- XL. Investigational New Drugs 30: 1434–1442. doi: 10.1007/s10637-011-9718-1.

Ichikawa M, Williams R, Wang L, Vogl T, Srikrishna G (2011) S100A8/A9 activate key genes and pathways in colon tumor progression. Molecular cancer research 9: 133–48. doi: 10.1158/1541-7786.MCR-10-0394.

Jackson AL, Loeb LA (1998) The mutation rate and cancer. Genetics 148: 1483–1490. doi: 10.1073/pnas.93.25.14800.

Jain AN (2003) Surflex: Fully automatic flexible molecular docking using a molecular similarity-based search engine. Journal of Medicinal Chemistry 46: 499–511. doi: 10.1021/jm020406h.

Jankowsky R, Mais A, Henning SW, Hauns B, and Hentsch B, (2010) Clinical phase II development of resminostat, a novel HDAC inhibitor. European Journal of Cancer, Supplement 8: 172. doi: 10.1016/S1359-6349(10)72247-3

Jeon HS, Choi YY, Fukuoka J, Fujii M, Lyakh LA, Song SH, Travis WD, Park JY, Jen J (2013) High expression of SNIP1 correlates with poor prognosis in Non-small cell lung cancer and SNIP1 interferes with the recruitment of HDAC1 to RB in vitro. Lung Cancer 82: 24–30. doi: 10.1016/j.lungcan.2013.07.015.

Jiang F, Kim SH (1991) "Soft docking": Matching of molecular surface cubes. Journal of Molecular Biology 219: 79–102. doi: 10.1016/0022-2836(91)90859-5.

Jin JX, Li S, Hong Y, Jin L, Zhu HY, Guo Q, Gao QS, Yan CG, Kang JD, Yin XJ (2014) CUDC-101, a histone deacetylase inhibitor, improves the in vitro and in vivo developmental competence of somatic cell nuclear transfer pig embryos. Theriogenology 81: 572–578. doi: 10.1016/j.theriogenology.2013.11.011.

Johnstone RW (2002) Histone-deacetylase inhibitors: novel drugs for the treatment of cancer. Nature Reviews Drug Discovery, 1: 287–299. doi:10.1038/nrd772.

Jones G, Willett P, Glen RC, Leach AR, Taylor R (1997) Development and validation of a genetic algorithm for flexible docking. Journal of molecular biology 267: 727–48. doi: 10.1006/jmbi.1996.0897.

Jorgensen WL, Maxwell DS, Tiradorives J (1996). Development and testing of the OPLS all atom force field on conformational energetics and properties of organic liquids. Journal of American Chemical Society 118: 11225–11236. doi: 10.1021/ja9621760.

Jorgensen WL, Tirado-Rives J (1988) The OPLS Potential Functions for Proteins. Energy Minimizations for Crystals of Cyclic Peptides and Crambin. Journal of the American Chemical Society 110: 1657–1666. doi: 10.1021/ja00214a001.

Jung M (2001) Inhibitors of histone deacetylase as new anticancer agents. Current Medicinal Chemistry 8: 1505–1511.

Kadota M, Sato M, Duncan B, Ooshima A, Yang HH, Diaz-Meyer N, Gere S, Kageyama SI, Fukuoka J, Nagata T (2009) Identification of novel gene amplifications in breast cancer and coexistence of gene amplification with an activating mutation of PIK3CA. Cancer Research 69: 7357–7365. doi: 10.1158/0008-5472.CAN-09-0064.

Kalin JH, Wu M, Gomez AV, Song Y, Das J, Hayward D, Adejola N, Wu M, Panova I, Chung HJ (2018) Targeting the CoREST complex with dual histone deacetylase and demethylase inhibitors. Nature Communications 9: 53. doi:10.1038/s41467-017-02242-4.

Kalyaanamoorthy S, Chen YPP (2012) Exploring inhibitor release pathways in histone deacetylases using random acceleration molecular dynamics simulations. Journal of Chemical Information and Modeling 52: 589–603. doi: 10.1021/ci200584f.

Kao HY, Lee CH, Komarov A, Han CC, Evans RM (2002) Isolation and characterization of mammalian HDAC10 a novel histone deacetylase. The Journal of biological chemistry 277:187–193.

Kaserer T, Beck KR, Akram M, Odermatt A, Schuster D (2015) Pharmacophore Models and Pharmacophore-Based Virtual Screening: Concepts and Applications Exemplified on Hydroxysteroid Dehydrogenases. Molecules 20: 22799–22832.

Kato Y, Salumbides BC, Wang X-F, Qian DZ, Williams S, Wei Y, Sanni TB, Atadja P, Pili R (2007). Antitumor effect of the histone deacetylase inhibitor LAQ824 in combination with 13-cis-retinoic acid in human malignant melanoma. Molecular cancer therapeutics 6: 70–81. doi: 10.1158/1535-7163.MCT-06-0125.

Kausar S, Asif M, Bibi N, Rashid S (2013) Comparative Molecular Docking Analysis of Cytoplasmic Dynein Light Chain DYNLL1 with Pilin to Explore the Molecular Mechanism of Pathogenesis Caused by Pseudomonas aeruginosa PAO. PLoS ONE 8: e76730. doi: 10.1371/journal.pone.0076730.

Kawaguchi Y, Kovacs JJ, McLaurin A, Vance JM, Ito A, Yao TP (2003) The deacetylase HDAC6 regulates aggresome formation and cell viability in response to misfolded protein stress. Cell 115: 727–738. doi: 10.1016/S0092-8674(03)00939-5.

Kawai H, Li H, Avraham S, Jiang S, Avraham HK (2003) Overexpression of histone deacetylase HDAC1 modulates breast cancer progression by negative regulation of estrogen receptor alpha. International journal of cancer. Journal international du cancer 107: 353–358. doi: 10.1002/ijc.11403.

Khedkar SA, Malde AK, Coutinho EC, Srivastava S (2007) Pharmacophore Modeling in Drug Discovery and Development: An Overview. Medicinal Chemistry 3: 187-97. doi: 10.2174/157340607780059521.

Kelly WK, O'Connor OA, Krug LM, Chiao JH, Heaney M, Curley T, MacGregore-Cortelli B, Tong W, Secrist JP, Schwartz L et al. (2005) Phase I study of an oral histone deacetylase inhibitor, suberoylanilide hydroxamic acid, in patients with advanced cancer. Journal of Clinical Oncology 23: 3923–3931. doi: 10.1200/JCO.2005.14.167.

Kelly WK, Richon VM, O'Connor O, Curley T, MacGregor-Curtelli B, Tong W, Klang M, Schwartz L, Richardson S, Rosa E et al. (2003) Phase I clinical trial of histone deacetylase inhibitor: suberoylanilide hydroxamic acid administered intravenously. Clinical Cancer Research 9: 3578–3588.

Khandelwal A, Balaz S (2007) Improved estimation of ligand-macromolecule binding affinities by linear response approach using a combination of multi-mode MD simulation and QM/MM methods. Journal of Computer-Aided Molecular Design 21: 131–137. doi: 10.1007/s10822-007-9104-4.

Khorasanizadeh S (2004) The Nucleosome: From Genomic Organization to Genomic Regulation. Cell 116: 259–272. doi: 10.1016/S0092-8674(04)00044-3.

Kim HC, Choi KC, Choi HK, Kang HB, Kim MJ, Lee YH, Lee OH, Lee J, Kim YJ, Jun W (2010) HDAC3 selectively represses CREB3-mediated transcription and migration of metastatic breast cancer cells. Cellular and Molecular Life Sciences 67: 3499–3510. doi: 10.1007/s00018-010-0388-5.

Kim HJ, Bae SC (2011) Histone deacetylase inhibitors: molecular mechanisms of action and clinical trials as anti-cancer drugs. American Journal of translational Research 3: 166–179.

Kim HJ, Choo H, Cho YS, No KT, Pae AN (2008) Novel GSK-3β inhibitors from sequential virtual screening. Bioorganic and Medicinal Chemistry 16: 636–643. doi: 10.1016/j.bmc.2007.10.047.

Kim HS, Chang YG, Bae HJ, Eun JW, Shen Q, Park SJ, Shin WC, Lee EK, Park S, Ahn YM (2014) Oncogenic potential of CK2?? and its regulatory role in EGF-induced HDAC2 expression in human liver cancer. FEBS Journal 281: 851–861. doi: 10.1111/febs.12652.

Kim, JK, Noh JH, Eun JW, Jung KH, Bae HJ, Shen Q, Kim MG, Chang YG, Kim S-J, Park WS (2013) Targeted Inactivation of HDAC2 Restores p16INK4a Activity and Exerts

Antitumor Effects on Human Gastric Cancer. Molecular Cancer Research 11: 62–73. doi: 10.1158/1541-7786.MCR-12-0332.

Kitchen DB, Decornez H, Furr JR, Bajorath J (2004) Docking and scoring in virtual screening for drug discovery: methods and applications. Nature Review in Drug Discovery 3: 935–949. doi: 10.1038/nrd1549.

Knudson AG (1971) Mutation and cancer: statistical study of retinoblastoma. Proceedings of the National Academy of Sciences of the United States of America 68: 820–3. doi: 10.1073/pnas.68.4.820.

Kollman PA (1994) Theory of macromolecule-ligand interactions. Current Opinion in Structural Biology 4: 240–245. doi: 10.1016/S0959-440X(94)90315-8.

Kotian S, Liyanarachchi S, Zelent A, Parvin JD (2011) Histone deacetylases 9 and 10 are required for homologous recombination. The Journal of biological chemistry 286: 7722–7726.

Kouzarides T (2007) Chromatin Modifications and Their Function. Cell 128: 693–705. doi: 10.1016/j.cell.2007.02.005.

Kovacs JJ, Murphy PJM, Gaillard S, Zhao X, Wu JT, Nicchitta CV, Yoshida M, Toft DO, Pratt WB, Yao TP (2005) HDAC6 regulates Hsp90 acetylation and chaperone-dependent activation of glucocorticoid receptor. Molecular Cell 18: 601–607. doi: 10.1016/j.molcel.2005.04.021.

Krejsa CM, Horvath D, Rogalski SL, Penzotti JE, Mao B, Barbosa F, Migeon JC (2003) Predicting ADME properties and side effects: the BioPrint approach. Current opinion in drug discovery & development 6: 470–480.

Kuntz ID, Blaney JM, Oatley SJ, Langridge R, Ferrin TE (1982) A geometric approach to macromolecule-ligand interactions. Journal of Molecular Biology 161:. 269–288. doi: 10.1016/0022-2836(82)90153-X.

Kwon S, Zhang Y, Matthias P (2007) The deacetylase HDAC6 is a novel critical component of stress granules involved in the stress response. Genes and Development 21: 3381–3394. doi: 10.1101/gad.461107.

Lagorce D, Maupetit J, Baell J, Sperandio O, Tufféry P, Miteva MA, Galons H, Villoutreix BO (2011) The FAF-Drugs2 server: A multistep engine to prepare electronic chemical compound collections. Bioinformatics 27: 2018–2020. doi: 10.1093/bioinformatics/btr333.

Lagorce D, Sperandio O, Galons H, Miteva MA, Villoutreix BO (2008) FAF-Drugs2: Free ADME/tox filtering tool to assist drug discovery and chemical biology projects. BMC Bioinformatics 9: 396. doi: 10.1186/1471-2105-9-396.

Lai C-J, Bao R, Tao X, Wang J, Atoyan R, Qu H, Wang D-G, Yin L, Samson M, Forrester J et al. (2010) CUDC-101, a multitargeted inhibitor of histone deacetylase, epidermal

growth factor receptor, and human epidermal growth factor receptor 2, exerts potent anticancer activity.Cancer research 70: 3647–3656. doi: 10.1158/0008-5472.CAN-09-3360.

Langer T, Hoffmann RD (2006) Pharmacophore modelling: applications in drug discovery Journal. Expert Opinion on Drug Discovery 1: 261-267 https://doi.org/10.1517/17460441.1.3.261

Langer T, Hoffmann RD (2001) Virtual screening: an effective tool for lead structure discovery?. Current pharmaceutical design 7: 509–527. doi: 10.2174/1381612013397861.

Laubach JP, Moreau P, San-Miguel JF, Richardson PG (2015) Panobinostat for the Treatment of Multiple Myeloma. Clinical cancer research : an official journal of the American Association for Cancer Research 21: 4767–4774. doi: 10.1158/1078-0432.CCR-15-0530.

Lauffer BEL, Mintzer R, Fong R, Mukund S, Tam C, Zilberleyb I, Flicke B, Ritscher A, Fedorowicz G, Vallero R (2013) Histone deacetylase (HDAC) inhibitor kinetic rate constants correlate with cellular histone acetylation but not transcription and cell viability. Journal of Biological Chemistry 288: 26926–26943. doi: 10.1074/jbc.M113.490706.

Leach AR, Kuntz ID (1992) Conformational-Analysis of Flexible Ligands in Macromolecular Receptor-Sites. Journal of Computational Chemistry 13: 730–748.

Lechnert T, Carrozzat MJ, Yut Y, Grantt PA, Eberhartert A, Vanniert D, Broscht G, Stillmant DJ, Shorei D, Workmant JL (2000) Sds3 (Suppressor of Defective Silencing 3) Is an Integral Component of the Yeast Sin3·Rpd3 Histone Deacetylase Complex and Is Required for Histone Deacetylase Activity. The Journal of Biological Chemistry 275: 40961-40966. doi: 10.1074/jbc.M005730200

Lee GY, Kenny PA, Lee EH, Bissell MJ (2007) Three-dimensional culture models of normal and malignant breast epithelial cells. Nature methods 4: 359–65. doi: 10.1038/nmeth1015.

Lee H-Z, Kwitkowski VE, Del Valle PL, Ricci MS, Saber H, Habtemariam BA, Bullock J, Bloomquist E, Li Shen Y, Chen X-H (2015) FDA Approval: Belinostat for the Treatment of Patients with Relapsed or Refractory Peripheral T-cell Lymphoma. Clinical cancer research : an official journal of the American Association for Cancer Research 21: 2666–70. doi: 10.1158/1078-0432.CCR-14-3119.

Lee J, Cheng X, Swails JM, Yeom MS, Eastman PK, Lemkul JA, Wei S, Buckner J, Jeong JC, Qi Y (2016) CHARMM-GUI Input Generator for NAMD, GROMACS, AMBER, OpenMM, and CHARMM/OpenMM Simulations Using the CHARMM36 Additive Force Field. Journal of Chemical Theory and Computation 12: 405–413. doi: 10.1021/acs.jctc.5b00935.

Lee SY, Huang Z, Kang TH, Soong RS, Knoff J, Axenfeld E, Wang C, Alvarez RD, Chen CS, Hung CF et al. (2013) Histone deacetylase inhibitor AR-42 enhances E7-specific CD8+ T cell-mediated antitumor immunity induced by therapeutic HPV DNA vaccination. Journal of Molecular Medicine 91: 1221–1231. doi: 10.1007/s00109-013-1054-9.

Lee YS, Lim KH, Guo X, Kawaguchi Y, Gao Y, Barrientos T, Ordentlich P, Wang XF, Counter CM, Yao TP (2008) The cytoplasmic deacetylase HDAC6 is required for efficient oncogenic tumorigenesis. Cancer Research 68: 7561–7569. doi: 10.1158/0008-5472.CAN-08-0188.

Lehmann M, Hoffmann MJ, Koch A, Ulrich SM, Schulz WA, Niegisch G (2014) Histone deacetylase 8 is deregulated in urothelial cancer but not a target for efficient treatment. Journal of Experimental & Clinical Cancer Research 33: 59. doi: 10.1186/s13046-014-0059-8.

Lei T, Li Y, Song Y, Li D, Sun H, Hou T (2016). ADMET evaluation in drug discovery: 15. Accurate prediction of rat oral acute toxicity using relevance vector machine and consensus modeling. Journal of Cheminformatics 8: 6. doi: 10.1186/s13321-016-0117-7.

Li DR, Zhang H, Peek E, Wang S, Du L, Li G, Chin AI (2015) Synergy of Histone-Deacetylase Inhibitor AR-42 with Cisplatin in Bladder Cancer. Journal of Urology 194: 547–555. doi: 10.1016/j.juro.2015.02.2918.

Li L, Chen R, Weng Z (2003) RDOCK: Refinement of Rigid-body Protein Docking Predictions', Proteins: Structure, Function and Genetics 53: 693–707. doi: 10.1002/prot.10460.

Li Q, Bender A, Pei J, Lai L (2007) A large descriptor set and a probabilistic kernel-based classifier significantly improve drug-likeness classification. Journal of Chemical Information and Modeling 47: 1776–1786. doi: 10.1021/ci700107y.

Li Y, Peng L, Seto E (2015) Histone Deacetylase 10 Regulates the Cell Cycle G2/M Phase Transition via a Novel Let-7-HMGA2-Cyclin A2 Pathway. Molecular and cellular biology 35: 3547–3565.

Li Y, Zhao K,Yao C, Kahwash S,Tang Y, Zhang G, Patterson K, Wang Q-E, Zhao W (2016). Genes Cancer 7: 292–300. doi: 10.18632/genesandcancer.117.

Lin TY, Fenger J, Murahari S, Bear MD, Kulp SK, Wang D, Chen CS, Kisseberth WC, London CA (2010) AR-42, a novel HDAC inhibitor, exhibits biologic activity against malignant mast cell lines via down-regulation of constitutively activated Kit. Blood 115: 4217–4225. doi: 10.1182/blood-2009-07-231985.

Lipinski CA (2004) Lead- and drug-like compounds: The rule-of-five revolution. Drug Discovery Today: Technologies 1: 337–341. doi: 10.1016/j.ddtec.2004.11.007.

Lodrini M, Oehme I, Schroeder C, Milde T, Schier MC, Kopp-Schneider A, Schulte JH, Fischer M, De Preter K, Pattyn F (2013) MYCN and HDAC2 cooperate to repress miR-183 signaling in neuroblastoma. Nucleic Acids Research 41: 6018–6033. doi: 10.1093/nar/gkt346.

Lombardi PM, Angell HD, Whittington DA, Flynn EF, Rajashankar KR, Christianson DW (2011) Structure of prokaryotic polyamine deacetylase reveals evolutionary functional relationships with eukaryotic histone deacetylases. Biochemistry 50: 1808–1817. doi: 10.1021/bi101859k.

Lombardi PM, Cole KE, Dowling DP, Christianson DW (2011) Structure, mechanism, and inhibition of histone deacetylases and related metalloenzymes. Current Opinion in Structural Biology 21: 735–743. doi: S0959-440X(11)00137-0 [pii]\r10.1016/j.sbi.2011.08.004.

López-Vallejo F, Caulfield T, Martínez-Mayorga K, Giulianotti MA, Nefzi A, Houghten RA, Medina-Franco JL (2011) Integrating virtual screening and combinatorial chemistry for accelerated drug discovery. Combinatorial chemistry & high throughput screening 14: 475–87. doi: http://dx.doi.org/10.2174/138620711795767866.

Lopez G, Bill KLJ, Bid HK, Braggio D, Constantino D, Prudner B, Zewdu A, Batte K, Lev D, Pollock RE (2015) HDAC8, A potential therapeutic target for the treatment of malignant peripheral nerve sheath tumors (MPNST). PLoS ONE 10: e0133302 doi: 10.1371/journal.pone.0133302.

Lucas DM, Alinari L, West DA, Davis ME, Edwards RB, Johnson AJ, Blum KA., Hofmeister CC, Freitas MA, Parthun MR et al. (2010) The novel deacetylase inhibitor AR-42 demonstrates preclinical activity in B-Cell malignancies In Vitro and In Vivo. PLoS ONE 5: e10941. doi: 10.1371/journal.pone.0010941.

Luo G, Lu F, Qiao L, Chen X, Li G, Zhang Y (2016) Discovery of Potential Inhibitors of Aldosterone Synthase from Chinese Herbs Using Pharmacophore Modeling, Molecular Docking, and Molecular Dynamics Simulation Studies. BioMed Research International Article ID 4182595, 8 pages. doi: 10.1155/2016/4182595.

Luo J, Su F, Chen D, Shiloh A, Gu W (2000) Deacetylation of p53 modulates its effect on cell growth and apoptosis. Nature 408: 377–381. doi: 10.1038/35042612.

Ma Y, Ai G, Zhang C, Zhao M, Dong X, Han Z, Wang Z, Zhang M, Liu Y, Gao W et al. (2017) Novel linear peptides with high affinity to $\alpha v \beta 3$ integrin for precise tumor identification. Theranostics 7: 1511–1523. doi: 10.7150/thno.18401.

Mack GS (2010) To selectivity and beyond. Nature Biotechnology 28: 1259–1266. doi: 10.1038/nbt1210-1259.

MacKerell AD, Bashford D, Bellott M, Dunbrack RL, Evanseck JD, Field MJ, Fischer S, Gao J, Guo H, Ha S (1998). All-Atom Empirical Potential for Molecular Modeling and

Dynamics Studies of Proteins. The Journal of Physical Chemistry 102: 3586–3616. doi: 10.1021/jp973084f.

Madden JC (2010). 10: In Silico Approaches for Predicting ADME Properties. In Vitro.19: 283–304. doi: 10.1007/978-1-4020-9783-6.

Mai A, Massa S, Lavu S, Pezzi R, Simeoni S, Ragno R, Mariotti FR, Chiani F, Camilloni G, Sinclair DA (2005) Design, synthesis, and biological evaluation of sirtinol analogues as class III histone/protein deacetylase (sirtuin) inhibitors. Journal of Medicinal Chemistry 48: 7789–7795. doi: 10.1021/jm050100l.

Maitland G, Rigby M, Smith EB, Wakeham WA (1987) Intermolecular Forces: Their Origin and Determination. The International Series of Monographs on Chemistry 3: 616. doi: 10.1063/1.2915587.

Malde AK, Zuo L, Breeze M, Stroet M, Poger D, Nair PC, Oostenbrink C, Mark AE (2011) An Automated force field Topology Builder (ATB) and repository: Version 1.0. Journal of Chemical Theory and Computation 7: 4026–4037. doi: 10.1021/ct200196m.

Mamane Y, Petroulakis E, LeBacquer O, Sonenberg N (2006) mTOR, translation initiation and cancer. Oncogene 25: 6416–6422. doi: 10.1038/sj.onc.1209888.

Mandal S, Moudgil M, Mandal SK (2009) Rational drug design. European journal of pharmacology 625: 90–100. doi: 10.1016/j.ejphar.2009.06.065.

Mandl-Weber S, Meinel FG, Jankowsky R, Oduncu F, Schmidmaier R, Baumann P (2010) The novel inhibitor of histone deacetylase resminostat (RAS2410) inhibits proliferation and induces apoptosis in multiple myeloma (MM) cells. British Journal of Haematology 149: 518–528. doi: 10.1111/j.1365-2141.2010.08124.x.

Mann BS, Johnson JR, Cohen MH, Justice R, Pazdur R (2007) FDA approval summary: vorinostat for treatment of advanced primary cutaneous T-cell lymphoma. Oncologist 12: 1247–1252. doi: 12/10/1247 [pii]\r10.1634/theoncologist.12-10-1247.

Maragakis P, Lindorff-Larsen K, Eastwood MP, Dror RO, Klepeis JL, Arkin IT, Jensen M, Xu H, Trbovic N, Friesner RA (2008) Microsecond molecular dynamics simulation shows effect of slow loop dynamics on backbone amide order parameters of proteins. Journal of Physical Chemistry B 112: 6155–6158. doi: 10.1021/jp077018h.

Marks PA (2010) Histone deacetylase inhibitors: a chemical genetics approach to understanding cellular functions. Biochimica et Biophysica Acta 1799: 717-725.

Martinez-Pastor B, Mostoslavsky R (2012) Sirtuins, metabolism, and cancer. Frontiers in Pharmacology 3: 2. doi: 10.3389/fphar.2012.00022.

Matsuyama A, Shimazu T, Sumida Y, Saito A, Yoshimatsu Y, Seigneurin-Berny D, Osada H, Komatsu Y, Nishino N, Khochbin S (2002) In vivo destabilization of dynamic

microtubules by HDAC6-mediated deacetylation. EMBO Journal 21: 6820–6831. doi: 10.1093/emboj/cdf682.

McGann MR, Almond HR, Nicholls A, Grant JA, Brown FK (2003) Gaussian docking functions. Biopolymers 68: 76–90. doi: 10.1002/bip.10207.

McGuinness D, McGuinness DH, McCaul JA, Shiels PG (2011) Sirtuins, Bioageing, and Cancer. Journal of Aging Research Article ID 235754, 11 pages. doi: 10.4061/2011/235754.

McMartin C, Bohacek RS (1997) QXP: powerful, rapid computer algorithms for structure-based drug design. Journal of computer-aided molecular design 11, 333–344. doi: 10.1023/a:1007907728892.

Meinke PT, Liberator P (2001) Histone deacetylase: a target for antiproliferative and antiprotozoal agents. Current medicinal chemistry 8: 211–235.

Meng X-Y, Zhang H-X, Mezei M, Cui M (2011) Molecular docking: a powerful approach for structure-based drug discovery. Current computer-aided drug design 7: 146–57. doi: 10.2174/157340911795677602.

Micelli C, Rastelli G (2015) Histone deacetylases: Structural determinants of inhibitor selectivity. Drug Discovery Today 20: 718–735. doi: 10.1016/j.drudis.2015.01.007.

Millard CJ, Watson PJ, Celardo I, Gordiyenko Y, Cowley SM, Robinson CV, Fairall L, Schwabe JW (2013). Class I HDACs share a common mechanism of regulation by inositol phosphates. Molecular Cell 57–67. doi: 10.1016/j.molcel.2013.05.020.

Miller MD, Kearsley SK, Underwood DJ, Sheridan RP (1994). FLOG: A system to select "quasi-flexible" ligands complementary to a receptor of known three-dimensional structure. Journal of Computer-Aided Molecular Design 8: 153–174. doi: 10.1007/BF00119865.

Mims A, Walker AR, Huang X, Sun J, Wang H, Santhanam R, Dorrance AM, Walker C, Hoellerbauer P, Tarighat SS (2013) Increased anti-leukemic activity of decitabine via AR-42-induced up-regulation of miR-29b: a novel epigenetic-targeting approach in acute myeloid leukemia. Leukemia 27: 871–8. doi: 10.1038/leu.2012.342.

Miyake K, Yoshizumi T, Imura S, Sugimoto K, Batmunkh E, Kanemura H, Morine Y, Shimada M (2008) Expression of Hypoxia-Inducible Factor-1α, Histone Deacetylase 1, and Metastasis-Associated Protein 1 in Pancreatic Carcinoma. Pancreas 36: e1–e9. doi: 10.1097/MPA.0b013e31815f2c2a.

Miyake Y, Keusch JJ, Wang L, Saito M, Hess D, Wang X, Melancon BJ, Helquist P, Gut H, Matthias P (2016) Structural insights into HDAC6 tubulin deacetylation and its selective inhibition. Nature Chemical Biology 12: 748–754. doi: 10.1038/nchembio.2140.

Moitessier N, Englebienne P, Lee D, Lawandi J, Corbeil CR (2008) Towards the development of universal, fast and highly accurate docking/scoring methods: a long way to go. British Journal of Pharmacology 153: S7–S26. doi: 10.1038/sj.bjp.0707515.

Monneret C (2007) Histone deacetylase inhibitors for epigenetic therapy of cancer. Anticancer Drugs 18: 363- 370. doi: 10.1097/CAD.0b013e328012a5db.

Montagut C, Dalmases A, Bellosillo B, Crespo M, Pairet S, Iglesias M, Salido M, Gallen M, Marsters S, Tsai SP (2012) Identification of a mutation in the extracellular domain of the Epidermal Growth Factor Receptor conferring cetuximab resistance in colorectal cancer. Nature medicine 18: 221–3. doi: 10.1038/nm.2609.

Moroy G, Martiny VY, Vayer P, Villoutreix BO, Miteva MA (2012) Toward in silico structure-based ADMET prediction in drug discovery. Drug Discovery Today 17: 44–55. doi: 10.1016/j.drudis.2011.10.023.

Morris GM, Huey R, (2009) AutoDock4 and AutoDockTools4: Automated docking with selective receptor flexibility. Journal of Computational Chemistry 30: 2785–2791. doi: 10.1002/jcc.21256.AutoDock4.

Morris GM., Goodsell DS, Halliday RS, Huey R, Hart WE, Belew RK, Olson AJ (1998) Automated Docking Using a Lamarckian Genetic Algorithm and an Empirical Binding Free Energy Function. Journal of Computational Chemistry 19: 1639–1662.

Morschhauser F, Terriou L, Coiffier B, Bachy E, Varga A, Kloos I, Lelièvre H, Sarry AL, Depil S, Ribrag V (2015) Phase 1 study of the oral histone deacetylase inhibitor abexinostat in patients with Hodgkin lymphoma, non-Hodgkin lymphoma, or chronic lymphocytic leukaemia. Investigational New Drugs 33: 423–431. doi: 10.1007/s10637-015-0206-x.

Mortier J, Rakers C, Bermudez M, Murgueitio MS, Riniker S, Wolber G (2015) The impact of molecular dynamics on drug design: Applications for the characterization of ligand-macromolecule complexes. Drug Discovery Today 20: 686–702. doi: 10.1016/j.drudis.2015.01.003.

Mottamal M, Zheng S, Huang T, Wang G (2015) Histone Deacetylase Inhibitors in Clinical Studies as Templates for New Anticancer Agents. Molecules 20: 3898–3941. doi: 10.3390/molecules20033898.

Muegge I (2003) Selection criteria for drug-like compounds. Medicinal Research Reviews 23: 302–321. doi: 10.1002/med.10041.

Müller BM, Jana L, Kasajima A, Lehmann A, Prinzler J, Budczies J, Winzer K-J, Dietel M, Weichert W, Denkert C (2013) Differential expression of histone deacetylases HDAC1, 2 and 3 in human breast cancer - overexpression of HDAC2 and HDAC3 is associated with clinicopathological indicators of disease progression. BMC Cancer, 13: 215. doi: 10.1186/1471-2407-13-215.

Mwakwari SC, Guerrant W, Patil V, Khan SI, Tekwani BL, Gurard-Levin ZA, Mrksich M, Oyelere AK (2010) Non-peptide macrocyclic histone deacetylase inhibitors derived from tricyclic ketolide skeleton. Journal of Medicinal Chemistry 53: 6100–6111. doi: 10.1021/jm100507q.

Mysinger MM, Carchia M, Irwin JJ, Shoichet BK (2012) Directory of useful decoys, enhanced (DUD-E): Better ligands and decoys for better benchmarking. Journal of Medicinal Chemistry 55: 6582–6594. doi: 10.1021/jm300687e.

Nair SB, Teli MK, Pradeep H, Rajanikant GK (2012) Computational identification of novel histone deacetylase inhibitors by docking based QSAR. Computational Biology and Medicine 42: 697-705. doi: 10.1016/j.compbiomed.2012.04.001.

Narita N, Fujieda S, Kimura Y, Ito Y, Imoto Y, Ogi K, Takahashi N, Tanaka T, Tsuzuki H, Yamada T et al. (2010) Suppression of histone deacetylase 3 (HDAC3) enhances apoptosis induced by paclitaxel in human maxillary cancer cells in vitro and in vivo. Biochemical and Biophysical Research Communications 396: 310–316. doi: 10.1016/j.bbrc.2010.04.089.

Noh JH, Bae HJ, Eun JW, Shen Q, Park SJ, Kim HS, Nam B, Shin WC, Lee EK, Lee K et al. (2014) HDAC2 provides a critical support to malignant progression of hepatocellular carcinoma through feedback control of mTORC1 and AKT. Cancer Research 74: 1728–1738. doi: 10.1158/0008-5472.CAN-13-2109.

Noor Z, Afzal N, Rashid S (2015) Exploration of novel inhibitors for class I histone deacetylase isoforms by QSAR modeling and molecular dynamics simulation assays. PLoS ONE 10: e0143155. doi: 10.1371/journal.pone.0139588.

Norel R, Fischer D, Wolfson HJ, Nussinov R (1994) Molecular surface recognition by a computer vision-based technique. Protein Engineering, Design and Selection 7: 39–46. doi: 10.1093/protein/7.1.39.

Norinder U, Bergström CAS (2006) Prediction of ADMET properties. ChemMedChem 1: 920–937. doi: 10.1002/cmdc.200600155.

Noureen N, Kalsoom S, Rashid H (2010) Ligand based pharmacophore modelling of anticancer histone deacetylase inhibitors. African Journal of Biotechnology 9: 3923–3931. doi: 10.5897/AJB09.1985.

Novak K (2004) Epigenetics Changes in Cancer Cells. Medscape General Medicine 6: 17.

Oh ET, Park MT, Choi BH, Ro S, Choi EK, Jeong SY, Park HJ (2012) Novel histone deacetylase inhibitor CG200745 induces clonogenic cell death by modulating acetylation of p53 in cancer cells. Investigational New Drugs 30: 435–442. doi: 10.1007/s10637-010-9568-2.

Oehme I, Linke JP, Bock BC, Milde T, Lodrini M, Hartenstein B, Wiegand I, Eckert C, Roth W, Kool M et al. (2013) Histone deacetylase 10 promotes autophagy-mediated cell

survival. Proceedings of the National Academy of Sciences of the United States of America 110: E2592–2601.

Olsen CA, Montero A, Leman LJ, Ghadiri MR (2012) Macrocyclic peptoid-peptide hybrids as inhibitors of class I histone deacetylases. ACS Medicinal Chemistry Letters 3: 749–753. doi: 10.1021/ml300162r.

Oostenbrink C, Villa A, Mark AE, Van Gunsteren WF (2004) A biomolecular force field based on the free enthalpy of hydration and solvation: The GROMOS force-field parameter sets 53A5 and 53A6. Journal of Computational Chemistry 25: 1656–1676. doi: 10.1002/jcc.20090.

Oshiro CM, Kuntz ID, Dixon JS (1995) Flexible ligand docking using a genetic algorithm. Journal of Computer-Aided Molecular Design 9: 113–130. doi: 10.1007/BF00124402.

Ossenkoppele G, Lowenberg B, Zachee P, Vey N, Breems D, Van De Loosdrecht AA, Debnam P, Needham L, Bawden L, Hooftman L, (2010) CHR-2845, a monocyte/macrophage targeted histone deacetylase inhibitor in a first in man clinical trial in subjects with advanced haematological malignancies. Blood 116:3279.

Owens J, Lipinski CA (2003) Chris Lipinski discusses life and chemistry after the Rule of Five. Drug Discovery Today 8: 12–16. doi: 10.1016/S1359-6446(02)02556-4.

Oyelere AK, Chen PC, Guerrant W, Mwakwari SC, Hood R, Zhang Y, Fan Y (2009) Non-peptide macrocyclic histone deacetylase inhibitors. Journal of Medicinal Chemistry 52: 456–468. doi: 10.1021/jm801128g.

Pampaloni F, Reynaud EG, Stelzer EHK (2007) The third dimension bridges the gap between cell culture and live tissue. Nature reviews. Molecular cell biology 8: 839–845. doi: 10.1038/nrm2236.

Parab S, Shetty O, Gaonkar R, Balasinor N, Khole V, Parte P (2015) HDAC6 deacetylates alpha tubulin in sperm and modulates sperm motility in Holtzman rat. Cell and Tissue Research 359: 665–678. doi: 10.1007/s00441-014-2039-x.

Pagadala NS, Syed K, Tuszynski J (2017) Software for molecular docking: a review. Biophysical Reviews. 9: 91-102. doi: 10.1007/s12551-016-0247-1.

Parasuraman S (2011) Toxicological screening. Journal of Pharmacology and Pharmacotherapeutics 2: 74. doi: 10.4103/0976-500X.81895.

Peng L,Seto E (2011) Deacetylation of nonhistone proteins by HDACs and the implications in cancer. Handbook of Experimental Pharmacology 206: 39–56. doi: 10.1007/978-3-642-21631-2_3.

Perola E, Walters WP, Charifson PS (2004) A detailed comparison of current docking and scoring methods on systems of pharmaceutical relevance. Proteins: Structure, Function and Genetics 56: 235–249. doi: 10.1002/prot.20088.

Pevsner J (2015) Bioinformatics and functional genomics. Third Edition, John Wiley and Son, Limited, West Sussex, United kingdom.

Phillips JC, Braun R, Wang W, Gumbart J, Tajkhorshid E, Villa E, Chipot C, Skeel RD, Kalé, L. and Schulten, K. (2005). Scalable molecular dynamics with NAMD. Journal of Computational Chemistry 26: 1781–1802. doi: 10.1002/jcc.20289.

Plumb JA, Finn PW, Williams RJ, Bandara MJ, Romero MR, Watkins CJ, La Thangue NB, Brown R (2003) Pharmacodynamic response and inhibition of growth of human tumor xenografts by the novel histone deacetylase inhibitor PXD101. Molecular Cancer Therapy 2: 721–728.

Prakash S, Foster BJ, Meyer M, Wozniak A, Heilbrun LK, Flaherty L, Zalupski M, Radulovic L, Valdivieso M, LoRusso PM (2001). Chronic oral administration of CI-994: a phase 1 study. Investigational new drugs 19: 1–11. doi: 10.1023/A:1006489328324.

Press B, Di Grandi D (2008) Permeability for intestinal absorption: Caco-2 assay and related issues. Current drug metabolism 9: 893–900. doi: 10.2174/138920008786485119.

Press OU (2013) Design: A Very Short Introduction. Journal of Chemical Information and Modeling 53: 1689–1699. doi: 10.1017/CBO9781107415324.004.

Porter NJ, Wagner FF, Christianson DW (2018) Entropy as a Driver of Selectivity for Inhibitor Binding to Histone Deacetylase 6. Biochemistry. doi: 10.1021/acs.biochem.8b00367.

Qian X, LaRochelle WJ, Ara G, Wu F, Petersen KD, Thougaard A, Sehested M, Lichenstein HS, Jeffers M (2006) Activity of PXD101, a histone deacetylase inhibitor, in preclinical ovarian cancer studies. Molecular cancer therapeutics 5: 2086–2095. doi: 10.1158/1535-7163.MCT-06-0111.

Rajak H, Kumar P, Parmar P, Thakur BS, Veerasamy R, Sharma PC, Sharma AK, Gupta AK, Dangi JS (2012) Appraisal of GABA and PABA as linker: design and synthesis of novel benzamide based histone deacetylase inhibitors. European Journal of Medicinal Chemistry (2012) 53:390-397.

Rajak H, Singh A, Dewangan PK, Patel V, Jain DK, Tiwari SK, Veerasamy R, Sharma PC (2013) Peptide Based Macrocycles: Selective Histone Deacetylase Inhibitors with Antiproliferative Activity. Current Medicinal Chemistry 20: 1887–1903. doi: 10.2174/0929867311320140006.

Rajendran P, Delage B, Dashwood WM, Yu T-W, Wuth B, Williams DE, Ho E, Dashwood RH (2011) Histone deacetylase turnover and recovery in sulforaphane-treated colon cancer cells: competing actions of 14-3-3 and Pin1 in HDAC3/SMRT corepressor complex dissociation/reassembly.Molecular Cancer 10: 68. doi: 10.1186/1476-4598-10-68.

Ranaldi G, Consalvo R, Sambuy Y, Scarino ML (2003) Permeability characteristics of parental and clonal human intestinal Caco-2 cell lines differentiated in serum-supplemented and

serum-free media. Toxicology in Vitro 17: 761–767. doi: 10.1016/S0887-2333(03)00095-X.

Rarey M, Kramer B, Lengauer T, Klebe G (1996) A fast flexible docking method using an incremental construction algorithm. Journal of molecular biology 261: 470–89. doi: 10.1006/jmbi.1996.0477.

Ravitz O, Zsoldos Z, Simon A (2011) Improving molecular docking through eHiTS' tunable scoring function. Journal of Computer-Aided Molecular Design 25: 1033–1051. doi: 10.1007/s10822-011-9482-5.

Rayan A, Marcus D, Goldblum A (2010) Predicting oral drug-likeness by iterative stochastic elimination. Journal of Chemical Information and Modeling 50: 437–445. doi: 10.1021/ci9004354.

Razak AR, Hotte SJ, Siu LL, Chen EX, Hirte HW, Powers J, Walsh W, Stayner LA, Laughlin A, Novotny-Diermayr V (2011) Phase I clinical, pharmacokinetic and pharmacodynamic study of SB939, an oral histone deacetylase (HDAC) inhibitor, in patients with advanced solid tumours', British Journal of Cancer 104: 756–762. doi: 10.1038/bjc.2011.13.

Remiszewski SW (2003) The discovery of NVP-LAQ824: from concept to clinic. Current medicinal chemistry 10: 2393–402. doi: 10.2174/0929867033456675.

Richards DA, Boehm KA, Waterhouse DM, Wagener DJ, Krishnamurthi SS, Rosemurgy A, Grove W, Macdonald K, Gulyas S, Clark M et al. (2006) Gemcitabine plus CI-994 offers no advantage over gemcitabine alone in the treatment of patients with advanced pancreatic cancer: results of a phase II randomized, double-blind, placebo-controlled, multicenter study. Annals of Oncology 17: 1096–1102. doi: 10.1093/annonc/mdl081.

Richmond TJ, Davey CA (2003) The structure of DNA in the nucleosome core. Nature 423: 145–50. doi: 10.1038/nature01595.

Richon VM, Sandhoff TW, Rifkind RA, Marks PA. (2000) Histone deacetylase inhibitor selectively induces p21WAF1 expression and gene-associated histone acetylation. Proceeding of the National Academy of Science of the United State of America 97(18), pp. 10014–10019. doi: 10.1073/pnas.180316197.

Risch A, Plass C (2008) Lung cancer epigenetics and genetics. International Journal of Cancer 123: 1–7. doi: 10.1002/ijc.23605.

Rodríguez-Paredes M, Esteller M (2011) Cancer epigenetics reaches mainstream oncology Nature Medicine 17: 330–339. doi: 10.1038/nm.2305.

Ropero S, Ballestar E, Alaminos M, Arango D, Schwartz S, Esteller M (2008) Transforming pathways unleashed by a HDAC2 mutation in human cancer. Oncogene: 27: 4008–4012. doi: 10.1038/onc.2008.31.

Rosenberg JE, Hoffman-Censits J, Powles T, van der Heijden MS, Balar AV, Necchi A, Dawson N, O'Donnell PH, Balmanoukian A, Loriot Y et al. (2016) Atezolizumab in patients with locally advanced and metastatic urothelial carcinoma who have progressed following treatment with platinum-based chemotherapy: a single-arm, multicentre, phase 2 trial. Lancet 387 :1909-20. doi: 10.1016/S0140-6736(16)00561-4.

Roskelley CD, Desprez PY, Bissell MJ (1994) Extracellular matrix-dependent tissue-specific gene expression in mammary epithelial cells requires both physical and biochemical signal transduction. Proceedings of the National Academy of Sciences of the United States of America 91: 12378–82. doi: 10.1073/pnas.91.26.12378.

Roth M, Chen WY (2014) Sorting out functions of sirtuins in cancer. Oncogene 33: 1609–1620. doi: 10.1038/onc.2013.120.

Roth SY, Denu JM, Allis D (2001) Histone Acetyltransferases. Annual. Review of Biochemistry 70: 81–120. doi: 10.1146/annurev.biochem.70.1.81.

de Ruijter AJM, van Gennip AH, Caron HN, Kemp S, van Kuilenburg ABP (2003) Histone deacetylases (HDACs): characterization of the classical HDAC family. The Biochemical journal 370: 737–49. doi: 10.1042/BJ20021321.

Ruiz-Carmona S, Alvarez-Garcia D, Foloppe N, Garmendia-Doval AB, Juhos S, Schmidtke P, Barril X, Hubbard RE, Morley SD (2014) rDock: A Fast, Versatile and Open Source Program for Docking Ligands to Proteins and Nucleic Acids. PLoS Computational Biology 10: e1003571. doi: 10.1371/journal.pcbi.1003571.

Saji S, Kawakami M, Hayashi S, Yoshida N, Hirose M, Horiguchi SI, Itoh A, Funata N, Schreiber SL, Yoshida M, Toi M (2005) Significance of HDAC6 regulation via estrogen signaling for cell motility and prognosis in estrogen receptor-positive breast cancer. Oncogene 24: 4531–4539. doi: DOI 10.1038/sj.onc.1208646.

Sakkiah S, Senese S, Yang Q, Lee KW, Torres JZ (2014) Dynamic and multi-pharmacophore modeling for designing Polo-box Domain inhibitors. PLoS ONE 9: e101405. doi: 10.1371/journal.pone.0101405.

Sakuma T, Uzawa K, Onda T, Shiiba M, Yokoe H, Shibahara T, Tanzawa H (2006) Aberrant expression of histone deacetylase 6 in oral squamous cell carcinoma. International Journal of Oncology 29: 117–124. doi: 10.3892/ijo.29.1.117.

Sali A, Blundell TL (1993) Comparative protein modelling by satisfaction of spatial restraints. Journal of Molecular Biology 234: 779–815. https://doi.org/10.1006/jmbi.1993.1626.

Salvador MA, Wicinski J, Cabaud O, Toiron Y, Finetti P, Josselin E, Lelièvre H, Kraus-Berthier L, Depil S, Bertucci F et al. (2013) The histone deacetylase inhibitor abexinostat induces Cancer stem cells differentiation in breast Cancer with low Xist expression. Clinical Cancer Research 19: 6520–6531. doi: 10.1158/1078-0432.CCR-13-0877.

Sander T, Liljefors T, Balle T (2008) Prediction of the receptor conformation for iGluR2 agonist binding: QM/MM docking to an extensive conformational ensemble generated using normal mode analysis. Journal of Molecular Graphics and Modelling, 26: 1259–1268. doi: 10.1016/j.jmgm.2007.11.006.

Saunders LR, Verdin E (2007) Sirtuins: critical regulators at the crossroads between cancer and aging. Oncogene 26: 5489–5504. doi: 10.1038/sj.onc.1210616.

Schapira M, Abagyan R, Totrov MJ (2003) Nuclear hormone receptor targeted virtual screening. Journal of Medicinal Chemistry 46: 3045-59.

Schnecke V, Kuhn LA (2000) Virtual screening with solvation and ligand-induced complementarity. Perspectives in Drug Discovery and Design, pp. 20: 171–190. doi: 10.1023/A:1008737207775.

Schneider G, Neidhart W, Giller T, Schmid G, (1999) "Scaffold-Hopping" by topological pharmacophore search: A contribution to virtual screening. Angewandte Chemie - International Edition 38: 2894–2896.

Schölz C, Weinert BT, Wagner SA, Beli P, Miyake Y, Qi J, Jensen LJ, Streicher W, McCarthy AR, Westwood NJ et al. (2015) Acetylation site specificities of lysine deacetylase inhibitors in human cells. Nature Biotechnology 33: 415–423. doi: 10.1038/nbt.3130.

Schuetz A, Min J, Allali-Hassani A, Schapira M, Shuen M, Loppnau P, Mazitschek R, Kwiatkowski NP, Lewis TA, Maglathin RL (2008) Human HDAC7 harbors a class IIa histone deacetylase-specific zinc binding motif and cryptic deacetylase activity. Journal of Biological Chemistry 283: 11355–11363. doi: 10.1074/jbc.M707362200.

Schuffenhauer A (2012) Computational methods for scaffold hopping. Wiley Interdisciplinary Reviews: Computational Molecular Science 2: 842–867. doi: 10.1002/wcms.1106.

Schüler S, Fritsche P, Diersch S, Arlt A, Schmid RM, Saur D, Schneider G (2010) HDAC2 attenuates TRAIL-induced apoptosis of pancreatic cancer cells. Molecular cancer 9: 80. doi: 10.1186/1476-4598-9-80.

Seigneurin-Berny D, Verdel A, Curtet S, Lemercier C, Garin J, Rousseaux S, Khochbin S (2001) Identification of components of the murine histone deacetylase 6 complex: link between acetylation and ubiquitination signaling pathways. Molecular and cellular biology 21: 8035–44. doi: 10.1128/MCB.21.23.8035-8044.2001.

Selvam C, Jachak SM, Thilagavathi R, Chakraborti AK (2005) Design, synthesis, biological evaluation and molecular docking of curcumin analogues as antioxidant, cyclooxygenase inhibitory and anti-inflammatory agents. Bioorganic and Medicinal Chemistry Letters 15: 1793–1797. doi: 10.1016/j.bmcl.2005.02.039.

Senese S, Zaragoza K, Minardi S, Muradore I, Ronzoni S, Passafaro A, Bernard L, Draetta GF, Alcalay M, Seiser C et al. (2007) Role for histone deacetylase 1 in human tumor cell

proliferation. Molecular Cell Biology 27: 4784–4795. doi: MCB.00494-07 [pii]\r10.1128/MCB.00494-07.

Shao Y, Gao Z, Marks PA, Jiang X (2004) Apoptotic and autophagic cell death induced by histone deacetylase inhibitors. Proceedings of the National Academy of Sciences of the United States of America 101: 18030–18035. doi: 10.1073/pnas.0408345102.

Shapiro GI. and et al. (2015). A phase I, dose-escalation, safety, pharmacokinetic, pharmacodynamic study of thioureidobutyronitrile, a novel p53 targeted therapy, in patients with advanced solid tumors. Journal of Clinical Oncology 33:15_supplementary TPS2613-TPS2613.

Sharma S, Kelly TK, Jones PA (2009) Epigenetics in cancer. Carcinogenesis 31: 27–36. doi: 10.1093/carcin/bgp220.

Shen J, Cheng F, Xu Y, Li W, Tang Y (2010). Estimation of ADME properties with substructure pattern recognition. Journal of Chemical Information and Modeling 50: 1034–1041. doi: 10.1021/ci100104j.

Sherman W, Day T, Jacobson MP, Friesner RA, Farid R (2006) Novel Procedure for Moldeing Ligand/Receptor Induced Fit Effects. Journal of Medicinal Chemistry 49: 534–553. doi: 10.1021/jm050540c.

Shimizu T, LoRusso PM, Papadopoulos KP, Patnaik A, Beeram M, Smith LS, Rasco DW, Mays TA, Chambers G, Ma A (2014) Phase I first-in-human study of CUDC-101, a multitargeted inhibitor of HDACs, EGFR, and HER2 in patients with advanced solid tumors. Clinical Cancer Research 20: 5032–5040. doi: 10.1158/1078-0432.CCR-14-0570.

Shin H.K., Kang Y.M., No K.T. (2016) Predicting ADME Properties of Chemicals. In: Leszczynski J. (eds) Handbook of Computational Chemistry. Springer, Dordrecht.

Sholler GS, Currier EA, Dutta A, Slavik MA, Illenye SA, Mendonca MCF, Dragon J, Roberts SS, Bond JP (2013) PCI-24781 (abexinostat), a novel histone deacetylase inhibitor, induces reactive oxygen species-dependent apoptosis and is synergistic with bortezomib in neuroblastoma. Journal of Cancer Therapeutics and Research 2: 21. doi: 10.7243/2049-7962-2-21.

Shultz M, Fan J, Chen C, Cho YS, Davis N, Bickford S, Buteau K, Cao X, Holmqvist M, Hsu M (2011) The design, synthesis and structure-activity relationships of novel isoindoline-based histone deacetylase inhibitors. Bioorganic & medicinal chemistry letters 21: 4909–12. doi: 10.1016/j.bmcl.2011.06.015.

Singh BN, Zhang G, Hwa YL, Li J, Dowdy SC, Jiang S-W (2010) Nonhistone protein acetylation as cancer therapy targets. Expert review of anticancer therapy 10: 935–954. doi: 10.1586/era.10.62.

Sippl MJ (1993) Recognition of errors in three-dimensional structures of proteins. Proteins, 17: 355-362. doi: 10.1002/prot.340170404.

Sippl MJ (1995) Knowledge-based potentials for proteins. Current Opininion in Structural Biology: 5:229-235.

Somoza JR, Skene RJ, Katz BA, Mol C, Ho JD, Jennings AJ, Luong C, Arvai A, Buggy JJ, Chi E et al. (2004) Structural snapshots of human HDAC8 provide insights into the class I histone deacetylases. Structure 12: 1325–1334. doi: 10.1016/j.str.2004.04.012.

Song C, Zhu S, Wu C, Kang J (2013) Histone deacetylase (HDAC) 10 suppresses cervical cancer metastasis through inhibition of matrix metalloproteinase (MMP) 2 and 9 expression. The Journal of biological chemistry 288: 28021–28033.

Soragni E, Xu C, Cooper A, Plasterer HL, Rusche JR, Gottesfeld JM (2011) Evaluation of histone deacetylase inhibitors as therapeutics for neurodegenerative diseases. Methods in Molecular Biology 793: 495–508. doi: 10.1007/978-1-61779-328-8_32.

Spurling CC, Godman CA, Noonan EJ, Rasmussen TP, Rosenberg DW, Giardina C (2008) HDAC3 overexpression and colon cancer cell proliferation and differentiation. Molecular Carcinogenesis 47: 137–147. doi: 10.1002/mc.20373.

Stilgenbauer S, Eichhorst B, Schetelig J, Coutre S, Seymour JF, Munir T, Puvvada SD, Wendtner CM, Roberts AW et al. (2016) Venetoclax in relapsed or refractory chronic lymphocytic leukaemia with 17p deletion: a multicentre, open-label, phase 2 study. The Lancet Oncology 17: 768-778. doi: 10.1016/S1470-2045(16)30019-5.

Stojanovic N, Hassan Z, Wirth M, Wenzel P, Beyer M, Schäfer C, Brand P, Kroemer A, Stauber RH, Schmid RM et al. (2017) HDAC1 and HDAC2 integrate the expression of p53 mutants in pancreatic cancer. Oncogene 36: 1804–1815. doi: 10.1038/onc.2016.344.

Strausberg RL, Feingold EA, Grouse LH, Derge JG, Klausner RD, Collins FS, Wagner L, Shenmen CM, Schuler GD, Altschul SF, et al. (2002). Mammalian Gene Collection Program Team. Generation and initial analysis of more than 15,000 full-length human and mouse cDNA sequences. Proceedings of the National Academy of Science United State of America 99: 16899-903.

Subramanian J, Sharma S, B-Rao C (2006) A novel computational analysis of ligand-induced conformational changes in the ATP binding sites of cyclin dependent kinases. Journal of Medicinal Chemistry 49: 5434–5441. doi: 10.1021/jm060172s.

Suzuki K, Okuno Y, Kawashima N, Muramatsu H, Okuno T, Wang X, Kataoka S, Sekiya Y, Hamada M, Murakami N et al. (2016) MEF2D-BCL9 fusion gene is associated with high-risk acute B-cell precursor lymphoblastic leukemia in adolescents. Journal of Clinical Oncology 34: 3451–3459. doi: 10.1200/JCO.2016.66.5547.

Suzuki T, Miyata N (2005) Non-hydroxamate Histone Deacetylase Inhibitors. Current Medicinal Chemistry 12: 2867–2880. doi: 10.2174/092986705774454706.

Taha TY, Aboukhatwa SM, Knopp RC, Ikegaki N, Abdelkarim H, Neerasa J, Lu Y, Neelarapu R, Hanigan TW, Thatcher GRJ et al. (2017) Design, Synthesis, and Biological Evaluation of Tetrahydroisoquinoline-Based Histone Deacetylase 8 Selective Inhibitors. ACS Medicinal Chemistry Letters 8: 824–829.

Takeda H, Wei Z, Koso H, Rust AG, Yew CCK, Mann MB, Ward JM, Adams DJ, Copeland NG, Jenkins NA (2015) Transposon mutagenesis identifies genes and evolutionary forces driving gastrointestinal tract tumor progression. Nature Genetics 47: 142–150. doi: 10.1038/ng.3175.

Tamborero D, Gonzalez-Perez A, Perez-Llamas C, Deu-Pons J, Kandoth C, Reimand J, Lawrence MS, Getz G, Bader GD, Ding L et al. (2013) Comprehensive identification of mutational cancer driver genes across 12 tumor types. Scientific Report 3: 2650. doi: 10.1038/srep02650.

Tambunan USF, Bakri R, Prasetia T, Parikesit AA, Kerami D (2013) Molecular dynamics simulation of complex Histones Deacetylase (HDAC) Class II Homo Sapiens with suberoylanilide hydroxamic acid (SAHA) and its derivatives as inhibitors of cervical cancer. Bioinformation 9: 696–700. doi: 10.6026/97320630009696.

Tan J, Cang S, Ma Y, Petrillo RL, Liu D (2010) Novel histone deacetylase inhibitors in clinical trials as anti-cancer agents. Journal of hematology & oncology 3: 5. doi: 10.1186/1756-8722-3-5.

Tang J, Cho NW, Cui G, Manion EM, Shanbhag NM, Botuyan MV, Mer G, Greenberg RA. (2013) Acetylation limits 53BP1 association with damaged chromatin to promote homologous recombination. Nature Structural & Molecular Biology 20: 317–325. doi: 10.1038/nsmb.2499.

Tao L, Zhang P, Qin C, Chen SY, Zhang C, Chen Z, Zhu F, Yang SY, Wei YQ, Chen YZ. (2015) Recent progresses in the exploration of machine learning methods as in-silico ADME prediction tools. Advanced Drug Delivery Reviews 86: 83–100. doi: 10.1016/j.addr.2015.03.014.

Tap WD, Jones RL, Van Tine BA, Chmielowski B, Elias AD, Adkins D, Agulnik M, Cooney MM, Livingston MB, Pennock G, Hameed MR (2016) Olaratumab and doxorubicin versus doxorubicin alone for treatment of soft-tissue sarcoma: an open-label phase 1b and randomised phase 2 trial. Lancet 388: 488-97. doi: 10.1016/S0140-6736(16)30587-6

Tapadar S, Fathi S, Raji I, Omesiete W, Kornacki JR, Mwakwari SC, Miyata M, Mitsutake K, Li JD, Mrksich M et al. (2015) A structure-activity relationship of non-peptide macrocyclic histone deacetylase inhibitors and their anti-proliferative and anti-inflammatory activities. Bioorganic and Medicinal Chemistry 23: 7543–7564. doi: 10.1016/j.bmc.2015.10.045.

Taylor JS, Burnett RM (2000) DARWIN: A program for docking flexible molecules. Proteins: Structure, Function and Genetics 41: 173–191.

Terranova-Barberio M, Roca MS, Zotti AI, Leone A, Bruzzese F, Vitagliano C, Scogliamiglio G, Russo D, D'Angelo G, Franco R (2016) Valproic acid potentiates the anticancer activity of capecitabine in vitro and in vivo in breast cancer models via induction of thymidine phosphorylase expression. Oncotarget 7: 7715–7731. doi: 10.18632/oncotarget.6802.

Tewari AK, Srivastava P, Singh VP, Singh A, Goel RK, Mohan CG (2010) Novel anti-inflammatory agents based on pyrazole based dimeric compounds; design, synthesis, docking and in vivo activity. Chemical & pharmaceutical bulletin 58: 634–8. doi: JST.JSTAGE/cpb/58.634 [pii].

Thangapandian S, John S, Lee KW (2012) Molecular dynamics simulation study explaining inhibitor selectivity in different class of histone deacetylases. Journal of biomolecular structure & dynamics 29: 677–698. doi: 10.1080/07391102.2012.10507409.

The HP, González-Álvarez I, Bermejo M, Sanjuan VM, Centelles I, Garrigues TM, Cabrera-Pérez MÁ (2011) In silico prediction of caco-2 cell permeability by a classification QSAR approach. Molecular Informatics 30: 376–385. doi: 10.1002/minf.201000118.

Thurn KT, Thomas S, Moore A, Munster PN (2011) Rational therapeutic combinations with histone deacetylase inhibitors for the treatment of cancer. Future Oncology 7: 263–283. doi: 10.2217/fon.11.2.

Tseng YC, Kulp SK, Lai IL, Hsu EC, He WA, Frankhouser DE, Yan PS, Mo X, Bloomston M, Lesinski GB et al. (2015) Preclinical Investigation of the Novel Histone Deacetylase Inhibitor AR-42 in the Treatment of Cancer-Induced Cachexia. Journal of the National Cancer Institute, 107: djv274. doi: 10.1093/jnci/djv274.

Tong JJ, Liu J, Bertos NR, Yang XJ (2002) Identification of HDAC10 a novel class II human histone deacetylase containing a leucine-rich domain. Nucleic acids research 30:1114–1123.

Tsunoyama K, Amini A, Sternberg MJE, Muggleton SH (2008) Scaffold Hopping in Drug Discovery Using Inductive Logic Programming. Journal of Chemical Information and Modeling 48: 949–957. doi: 10.1021/ci700418f.

Uba AI, Yelekçi K (2017a) Identification of potential isoform-selective histone deacetylase inhibitors for cancer therapy: a combined approach of structure-based virtual screening, ADMET prediction and molecular dynamics simulation assay. Journal of Biomolecular Structure and Dynamics. 1–15. doi: 10.1080/07391102.2017.1384402.

Uba AI, Kemal Yelekci (2017b). Exploration of the binding pocket of histone deacetylases: the design of potent and isoform-selective inhibitors. Turkish Journal of Biology, 41(6): 901-918. doi: 10.3906/biy-1701-26.

Uba AI, Yelekçi K (2018) Carboxylic acid derivatives display potential selectivity for human histone deacetylase 6: Structure-based virtual screening, molecular docking and dynamics simulation studies. Computational Biology and Chemistry 75: 131-142. doi: 10.1016/j.compbiolchem.2018.05.004

Urwyler S (2011) Allosteric modulation of family C G-protein-coupled receptors: from molecular insights to therapeutic perspectives. Pharmacological Reviews 63: 59–126. doi: pr.109.002501 [pii]\r10.1124/pr.109.002501.

Vainio MJ, Kogej T, Raubacher F, Sadowski J (2013) Scaffold hopping by fragment replacement. Journal of Chemical Information and Modeling 53: 1825–1835. doi: 10.1021/ci4001019.

Vannini A, Volpari C, Filocamo G, Casavola EC, Brunetti M, Renzoni D, Chakravarty P, Paolini C, De Francesco R, Gallinari P et al. (2004) Crystal structure of a eukaryotic zinc-dependent histone deacetylase, human HDAC8, complexed with a hydroxamic acid inhibitor. Proceedings of the National Academy of Sciences of the United States of America 101: 15064–9. doi: 10.1073/pnas.0404603101.

Vannini A, Volpari C, Gallinari P, Jones P, Mattu M, Francesco RD, Steinkühler C, Marco S, Di Carfí A, De Francesco R et al. (2007) Substrate Binding to Histone Deacetylases as Revealed by Crystal Structure of HDAC8-Substrate Complex - Supplementary Information. EMBO reports 8: 879–84. doi: 10.1038/sj.embor.7401047.

Vanommeslaeghe K, MacKerell AD (2012) Automation of the CHARMM general force field (CGenFF) I: Bond perception and atom typing. Journal of Chemical Information and Modeling, 52: 3144–3154. doi: 10.1021/ci300363c.

Vanommeslaeghe K, Raman EP, MacKerell AD (2012) Automation of the CHARMM General Force Field (CGenFF) II: Assignment of Bonded Parameters and Partial Atomic Charges. Journal of Chemical Information and Modeling 52: 3155–3168. doi: 10.1021/ci3003649.

Venkatachalam CM, Jiang X, Oldfield T, Waldman M (2003) LigandFit: A novel method for the shape-directed rapid docking of ligands to protein active sites. Journal of Molecular Graphics and Modelling 21: 289–307. doi: 10.1016/S1093-3263(02)00164-X.

Verdel A, Curtet S, Brocard MP, Rousseaux S, Lemercier C, Yoshida M, Khochbin S (2000) Active maintenance of mHDA2/mHDAC6 histone-deacetylase in the cytoplasm. Current Biology 10: 747–749. doi: 10.1016/S0960-9822(00)00542-X.

Verdel A, Khochbin S (1999) Identification of a new family of higher eukaryotic histone deacetylases: Coordinate expression of differentiation-dependent chromatin modifiers. Journal of Biological Chemistry 274: 2440–2445. doi: 10.1074/jbc.274.4.2440.

Verdonk ML, Cole JC, Hartshorn MJ, Murray CW, Taylor RD (2003) Improved protein-ligand docking using GOLD. Proteins: Structure, Function and Genetics 52: 609–623. doi: 10.1002/prot.10465.

Vigushin DM, Coombes RC (2004) Targeted histone deacetylase inhibition for cancer therapy. Current Cancer Drug Targets 4: 205–218. doi: 10.2174/1568009043481560.

Vlachakis D, Tsagrasoulis D, Megalooikonomou V, Kossida S (2013) Introducing Drugster: A comprehensive and fully integrated drug design, lead and structure optimization toolkit', Bioinformatics 29: 126–128. doi: 10.1093/bioinformatics/bts637.

Vogl DT, Raje N, Jagannath S, Richardson P, Hari P, Orlowski R, Supko JG, Tamang D, Yang M, Jones SS (2017) Ricolinostat, the first selective histone deacetylase 6 inhibitor, in combination with bortezomib and dexamethasone for relapsed or refractory multiple myeloma. Clinical Cancer Research 23: 3307–3315. doi: 10.1158/1078-0432.CCR-16-2526.

Vuorinen A, Schuster D (2015) Methods for generating and applying pharmacophore models as virtual screening filters and for bioactivity profiling. Methods 71: 113-134

Wagner JM, Hackanson B, Lübbert M, Jung M (2010) Histone deacetylase (HDAC) inhibitors in recent clinical trials for cancer therapy. Clinical Epigenetics 1: 117-136. doi: 10.1007/s13148-010-0012-4.

Wagner FF, Olson DE, Gale JP, Kaya T, Weïwer M, Aidoud N, Thomas M, Davoine EL, Lemercier BC, Zhang YL et al. (2013) Potent and selective inhibition of histone deacetylase 6 (HDAC6) does not require a surface-binding motif. Journal of Medicinal Chemistry 56: 1772–1776. doi: 10.1021/jm301355j.

Walters WP, Stahl MT, Murcko MA (1998). Virtual screening—an overview. Drug Discovery Today 3: 160–178. doi: 10.1016/S1359-6446(97)01163-X.

Walters W, Stahl M, Murcko M (1998) Virtual Screening – an overview. Drug Discovery Today 3: 160–178. doi: 10.1016/s1359-6446(97)01163-x.

Wang H, Yu N, Chen D, Lee KC, Lye PL, Chang JW, Deng W, Ng MC, Lu T, Khoo ML et al. (2011) Discovery of (2E)-3-{2-butyl-1-[2-(diethylamino)ethyl]-1H-benzimidazol-5-yl}-N-hydroxyacrylamide (SB939), an orally active histone deacetylase inhibitor with a superior preclinical profile. Journal of Medicinal Chemistry 54: 4694-720. doi: 10.1021/jm2003552

Wang J, Pursell NW, Samson MES, Atoyan R, Ma AW, Selmi A, Xu W, Cai X, Voi M, Savagner P et al. (2013) Potential advantages of CUDC-101, a multitargeted HDAC, EGFR, and HER2 inhibitor, in treating drug resistance and preventing cancer cell migration and invasion. Molecular cancer therapeutics 12: 925–36. doi: 10.1158/1535-7163.MCT-12-1045.

Wang J, Wolf RM, Caldwell JW, Kollman PA, Case DA (2004) Development and testing of a general Amber force field. Journal of Computational Chemistry 25: 1157–1174. doi: 10.1002/jcc.20035.

Wang Z, Hop CE, Leung KH, Pang J (2000). Determination of in vitro permeability of drug candidates through a caco-2 cell monolayer by liquid chromatography/tandem mass spectrometry. Journal of mass spectrometry 35: 71–76.

Wang ZT, Chen ZJ, Jiang GM, Wu YM, Liu T, Yi YM, Zeng J, Du J, Wang HS (2016) Histone deacetylase inhibitors suppress mutant p53 transcription via HDAC8/YY1 signals in triple negative breast cancer cells. *Cellular Signalling* 28: 506–515. doi: 10.1016/j.cellsig.2016.02.006.

van de Waterbeemd H, Gifford E (2003) ADMET in silico modelling: towards prediction paradise? Nature Reviews Drug Discovery 2: 192–204. doi: 10.1038/nrd1032.

Watson, PJ, Fairall L, Schwabe JWR (2012) Nuclear hormone receptor co-repressors: structure and function. Molecular and Cellular Endocrinology 348: 440–449.

Watson PJ, Fairall L, Santos GM, Schwabe JWR (2012) Structure of HDAC3 bound to co-repressor and inositol tetraphosphate. Nature 481: 335–40. doi: 10.1038/nature10728.

Watson PJ, Millard CJ, Riley AM, Robertson NS, Wright LC, Godage HY, Cowley SM, Jamieson AG, Potter BV, Schwabe JW (2016) Insights into the activation mechanism of class I HDAC complexes by inositol phosphates. Nature Communication 2016 7:11262. doi: 10.1038/ncomms11262.

Webb B, Sali A (2016) Comparative Protein Structure Modeling Using MODELLER. Current Protocol in Bioinformatics 54: 5.6.1-5.6.37. https://doi.org/10.1002/cpbi.3

Weichert W, Röske A, Gekeler V, Beckers T, Stephan C, Jung K, Fritzsche FR, Niesporek S, Denkert C, Dietel M, Kristiansen G (2008) Histone deacetylases 1, 2 and 3 are highly expressed in prostate cancer and HDAC2 expression is associated with shorter PSA relapse time after radical prostatectomy. British journal of cancer 98: 604–10. doi: 10.1038/sj.bjc.6604199.

Welch W, Ruppert J, Jain AN (1996) Hammerhead: fast, fully automated docking of flexible ligands to protein binding sites. Chemistry & Biology 3: 449–462. doi: 10.1016/S1074-5521(96)90093-9.

Wermuth CG, Ganellin CR, Lindberg P, Mitscher LA (1998). Glossary of terms used in medicinal chemistry (IUPAC Recommendations 1997) Annual Reports in Medicinal Chemistry 33: 385-395.

Whitehead L, Dobler MR, Radetich B, Zhu Y, Atadja PW, Claiborne T, Grob JE, McRiner A, Pancost MR, Patnaik A et al. (2011) Human HDAC isoform selectivity achieved via exploitation of the acetate release channel with structurally unique small molecule

inhibitors. Bioorganic and Medicinal Chemistry 19: 4626–4634. doi: 10.1016/j.bmc.2011.06.030.

Wiech NL, Fisher JF, Helquist P, Wiest O (2009) Inhibition of histone deacetylases: a pharmacological approach to the treatment of non-cancer disorders. Current Topics in Medicinal Chemistry 9: 257-271. doi: 10.2174/156802609788085241.

Wiederstein M, Sippl MJ (2007) ProSA-web: interactive web service for the recognition of errors in three-dimensional structures of proteins.

Wilson AJ, Byun DS, Popova N, Murray LB, L'Italien K, Sowa Y, Arango D, Velcich A, Augenlicht LH, Mariadason JM (2006) Histone deacetylase 3 (HDAC3) and other class I HDACs regulate colon cell maturation and p21 expression and are deregulated in human colon cancer. Journal of Biological Chemistry 281: 13548–13558. doi: 10.1074/jbc.M510023200.

Wilson AJ, Chueh AC, Tögel L, Corner GA, Ahmed N, Goel S, Byun DS, Nasser S, Houston MA, Jhawer M (2010) Apoptotic sensitivity of colon cancer cells to histone deacetylase inhibitors is mediated by an Sp1/Sp3-activated transcriptional program involving immediate-early gene induction. Cancer Research 70: 609–620. doi: 10.1158/0008-5472.CAN-09-2327.

Wilson GL, Lill MA (2011) Integrating structure-based and ligand-based approaches for computational drug design. Future Medicinal Chemistry 3: 735–750. doi: 10.4155/fmc.11.18.

Witt O, Deubzer HE, Milde T, Oehme I (2009) HDAC family: What are the cancer relevant targets? Cancer Letters 8–21. doi: 10.1016/j.canlet.2008.08.016.

Wooster R, Bignell G, Lancaster J, Swift S, Seal S, Mangion J, Collins N, Gregory S, Gumbs C, Micklem G (1995). Identification of the breast cancer susceptibility gene BRCA2. Nature 378: 789–92. doi: 10.1038/378789a0.

Xie HJ, Noh JH, Kim JK, Jung KH, Eun JW, Bae HJ, Kim MG, Chang YG, Lee JY, Park H (2012) HDAC1 inactivation induces mitotic defect and caspase-independent autophagic cell death in liver cancer. PLoS ONE 7: doi: 10.1371/journal.pone.0034265.

Xing M (2005) BRAF mutation in thyroid cancer. Endocrine-Related Cancer 12: 245–262. doi: 10.1677/erc.1.0978.

Xu W, Xu B, Yao Y, Yu X, Shen J (2015) The novel HDAC inhibitor AR-42-induced anti-colon cancer cell activity is associated with ceramide production. Biochemical and Biophysical Research Communications 463: 545–550. doi: 10.1016/j.bbrc.2015.05.078.

Xue Y, Wong J, Moreno GT, Young MK, Côté J, Wang W (1998) NURD, a novel complex with both ATP-dependent chromatin-remodeling and histone deacetylase activities. Molecular Cell 2: 851-61.

Yamashita F, Hashida M (2004) In silico approaches for predicting ADME properties of drugs', Drug metabolism and pharmacokinetics 19: 327–338. doi: JST.JSTAGE/dmpk/19.327 [pii].

Yang S-Y (2010) Pharmacophore modeling and applications in drug discovery: challenges and recent advances. Drug Discovery Today 15: 444-450.

Yang XJ, Seto E (2008) Lysine Acetylation: Codified Crosstalk with Other Posttranslational Modifications. Molecular Cell 449–461. doi: 10.1016/j.molcel.2008.07.002.

Yang Y, Huang Y, Wang Z, Wang H, Duan B, Ye D, Wang C, Jing R, Leng Y, Xi J et al. (2016) HDAC10 promotes lung cancer proliferation via AKT phosphorylation. Oncotarget 7: 59388–59401.

Yao Y, Liao C, Li Z, Wang Z, Sun Q, Liu C, Yang Y, Tu Z, Jiang S (2014) Design, synthesis, and biological evaluation of 1, 3-disubstituted-pyrazole derivatives as new class I and IIb histone deacetylase inhibitors. European journal of medicinal chemistry 86: 639–652. doi: 10.1016/j.ejmech.2014.09.024.

Yee AJ, Voorhees PM, Bensinger W, Berdeja JG, Supko JG, Richardson PG, Tamang D, Jones SS, Patrick G, Wheeler C, Raje N (2014) Ricolinostat (ACY-1215), a Selective HDAC6 Inhibitor, in Combination with Lenalidomide and Dexamethasone: Results of a Phase 1b Trial in Relapsed and Relapsed Refractory Multiple Myeloma. Blood 124: 4772.

Yee S (1997) In vitro permeability across Caco-2 cells (colonic) can predict in vivo (small intestinal) absorption in man - Fact or myth. Pharmaceutical Research 14: 763–766. doi: 10.1023/A:1012102522787.

Yilmaz S, Altinkanat-Gelmez G, Bolelli K, Guneser-Merdan D, Over-Hasdemir MU, Yildiz I, Aki-Yalcin E, Yalcin I (2014) Pharmacophore generation of 2-substituted benzothiazoles as AdeABC efflux pump inhibitors in A. baumannii. SAR and QSAR in Environmental Research 25: 551–563. doi: 10.1080/1062936X.2014.919357.

Yokota J (2000) Tumor progression and metastasis. Carcinogenesis 21: 497–503. doi: 10.1093/carcin/21.3.497.

You A, Tong JK, Grozinger CM, Schreiber SL (2001) CoREST is an integral component of the CoREST-human histone deacetylase complex. Proceedings of the National Academy of Sciences of the United States of America 98: 1454–1458.

Younes A, Bociek RG, Kuruvilla J, Laneuville P, Fung HC, Drouin M, Patterson T, Besterman J, Martell RE (2010) Mocetinostat (MGCD0103), an isotype-selective histone deacetylase (HDAC) inhibitor, produces clinical responses in relapsed/refractory hodgkin lymphoma (HL): Update from a phase II clinical study. Blood 116:1763.

Yu L, Liu F, Chen Y, You Q (2009) Pharmacophore identification of hydroxamate HDAC 1 inhibitors. Chinese Journal of Chemistry 27: 557–564. doi: 10.1002/cjoc.200990091.

Zabkiewicz J, Gilmour M, Hills R, Vyas P, Bone E, Davidson A, Burnett A, Knapper S (2016) The targeted histone deacetylase inhibitor tefinostat (CHR-2845) shows selective in vitro efficacy in monocytoid-lineage leukaemias. Oncotarget 7: 16650–62. doi: 10.18632/oncotarget.7692.

Zhang J, Zhong Q (2014) Histone deacetylase inhibitors and cell death. Cellular and molecular life sciences 71: 3885–3901. doi: 10.1007/s00018-014-1656-6.

Zhang K, Dent SYR (2005) Histone modifying enzymes and cancer: Going beyond histones. Journal of Cellular Biochemistry 96: 1137–1148. doi: 10.1002/jcb.20615.

Zhang S, Huang W, Li X, Yang Z, Feng B (2015) Synthesis, biological evaluation and computer aided drug designing of new derivatives of hyperactive suberoylanilide hydroxamic acid histone deacetylase inhibitors. Chemical Biology & Drug Design 86: 795-804. doi: 10.1111/cbdd.12554.

Zhang S, Suvannasankha A, Crean CD, White VL, Chen C-S, Farag SS (2011) The novel histone deacetylase inhibitor, AR-42, inhibits gp130/Stat3 pathway and induces apoptosis and cell cycle arrest in multiple myeloma cells. International journal of cancer. Journal international du cancer 129: 204–13. doi: 10.1002/ijc.25660.

Zhang X, Zhao X, Fiskus W, Lin J, Lwin T, Rao R, Zhang Y, Chan JC, Fu K, Marquez VE et al. (2012) Coordinated Silencing of MYC-Mediated miR-29 by HDAC3 and EZH2 as a Therapeutic Target of Histone Modification in Aggressive B-Cell Lymphomas. Cancer Cell 22: 506–523. doi: 10.1016/j.ccr.2012.09.003.

Zhang Y, Gilquin B, Khochbin S, Matthias P (2006) Two catalytic domains are required for protein deacetylation. Journal of Biological Chemistry 281: 2401–2404. doi: 10.1074/jbc.C500241200.

Zhang Y, Li N, Caron C, Matthias G, Hess D, Khochbin S, Matthias P (2003) HDAC-6 interacts with and deacetylates tubulin and microtubules in vivo. EMBO Journal 22: 1168–1179. doi: 10.1093/emboj/cdg115.

Zhang Z, Yamashita H, Toyama T, Sugiura H, Omoto Y, Ando Y, Mita K, Hamaguchi M, Hayashi SI, Iwase H (2004) HDAC6 expression is correlated with better survival in breast cancer. Clinical Cancer Research 10: 6962–6968. doi: 10.1158/1078-0432.CCR-04-0455.

Zhao G, Wang G, Bai H, Li T, Gong F, Yang H, Wen J, Wang W (2017) Targeted inhibition of HDAC8 increases the doxorubicin sensitivity of neuroblastoma cells via up regulation of miR-137. European Journal of Pharmacology 802: 20–26. doi: 10.1016/j.ejphar.2017.02.035.

Zhao H, Caflisch A (2013) Discovery of ZAP70 inhibitors by high-throughput docking into a conformation of its kinase domain generated by molecular dynamics. Bioorganic and Medicinal Chemistry Letter. 2013 Oct 15; 23(20):5721-6.

Zhao H, Caflisch A (2015) Molecular dynamics in drug design. European journal of medicinal chemistry 91: 4–14. doi: 10.1016/j.ejmech.2014.08.004.

Zhijun H, Shusheng W, Han M, Jianping L, Li-sen Q, Dechun L (2016) Preclinical characterization of 4SC-202, a novel class I HDAC inhibitor, against colorectal cancer cells. Tumor Biology 37: 10257–10267. doi: 10.1007/s13277-016-4868-6.

Zhu P, Martin E, Mengwasser J, Schlag P, Janssen KP, Göttlicher M (2004) Induction of HDAC2 expression upon loss of APC in colorectal tumorigenesis. Cancer Cell 5: 455–463. doi: 10.1016/S1535-6108(04)00114-X.

Zimmermann S, Kiefer F, Prudenziati M, Spiller C, Hansen J, Floss T, Wurst W, Minucci S, Göttlicher M (2007) Reduced body size and decreased intestinal tumor rates in HDAC2-mutant mice. Cancer Research 67: 9047–9054. doi: 10.1158/0008-5472.CAN-07-0312.

Zoete V, Daina A, Bovigny C, Michielin O (2016) SwissSimilarity: A Web Tool for Low to Ultra High Throughput Ligand-Based Virtual Screening. Journal of Chemical Information and Modeling 56: 1399-1404.

Zou H, Wu Y, Navre M, Sang BC (2006) Characterization of the two catalytic domains in histone deacetylase 6. Biochemical and Biophysical Research Communications 341: 45–50. doi: 10.1016/j.bbrc.2005.12.144.

Zsoldos Z, Reid D, Simon A, Sadjad BS, Johnson AP (2006) eHiTS: an innovative approach to the docking and scoring function problems. Current protein & peptide science 7: 421–435. doi: 10.2174/138920306778559412.

Zsoldos Z, Reid D, Simon A, Sadjad SB, Johnson AP (2007) eHiTS: A new fast, exhaustive flexible ligand docking system. Journal of Molecular Graphics and Modelling 26: 198–212. doi: 10.1016/j.jmgm.2006.06.002.

CURRICULUM VITAE

Personal Information

Name Surname   : ABDULLAHI IBRAHIM UBA
Place and Date of Birth   : Kurnar Madatai Kano, Nigeria, 1st April 1987

Education

Undergraduate Education   : Bayero University Kano (September 2007-March 2011)
Graduate Education   : Fatih University Istanbul (September 2012-January 2014)
Foreign Language Skills   : Hausa (Native) English (Official), Turkish (Basic)

Work Experience

Name of Employer and Dates of Employment: Bayero University Kano, March 2015-Date

Contact:

Telephone   : +905397743581; +2348161712612
E-mail Address   : aiuba.cbr@buk.edu.ng; abdullahi.iu2@gmail.com

Publications

1. **Abdullahi Ibrahim Uba**, Kemal Yelekçi (2018). In search for potential selective inhibitors of human histone deacetylase 6 via pharmacophore-based virtual screening. *Journal of Molecular Modelling* (Under consideration)

2. **Abdullahi Ibrahim Uba,** Kemal Yelekçi (2018). Carboxylic acid derivatives display potential selectivity for human histone deacetylase 6: structure-based virtual screening, molecular docking and dynamics simulation studies. In press *Computational Biology and Chemistry*, 75: 131-142. doi: 10.1016/j.compbiolchem.2018.05.004 @ Elsevier publishing company

3. **Abdullahi Ibrahim Uba**, Kemal Yelekci (2017). Identification of potential isoform-selective histone deacetylase inhibitors for cancer therapy: a combined

approach of structure-based virtual screening, ADMET prediction and molecular dynamics simulation assay. *Journal of Biomolecular Structure and Dynamics*, 1-16. Epub ahead of print, 23rd October 17, 2017.
doi: 10.1080/07391102.2017.1384402. @ Tailor & Francis, Informa Group plc.

4. **Abdullahi Ibrahim Uba**, Kemal Yelekci (2017). Exploration of the binding pocket of histone deacetylases: the design of potent and isoform-selective inhibitors. *Turkish Journal of Biology,* 41(6): 901-918.
DOI: 10.3906/biy-1701-26 @ TUBITAK

5. **Abdullahi I. Uba**[*], Haşim O. Tabakoğlu, Umar A. Abdullahi, Musbahu M. Sani (2017). Closure of skin incision by dual wavelength laser application. *Journal of cosmetic and laser theraphy*, 19 (2): 109-113. doi: http://dx.doi.org/10.1080/14764172.2016.1248442 @ Tailor & Francis, Informa Group plc.

6. Abdulazeez M, Aminu H, Ndanusa S, **Uba A** (2016). Isolation and Characterization of a New Angiotensin-converting Enzyme Inhibitory Peptide from Heterobronchus bidorsalis. *Journal of Biologically Active Products from Nature,* 6 (3): 237-249. doi: 10.1080/22311866.2016.1232625@ Tailor & Francis, Informa Group plc.

7. Tabakoglu HO, Sani MM, **Uba AI**, Abdullahi UA (2016). Assessment of circular wound healing in rats after exposure to 808-nm laser pulses during specific healing phases. *Lasers in Surgery and Medicine,* 48:409–415. doi: 10.1002/lsm.22462. @ Wiley Periodicals, Inc.

8. **Uba AI**[*], Dilcan G, Usman SS (2016). Progress in HIV-1 Prevention, Control and Treatment: Genetic Manipulation or Pharmacological Blockade of Chemokine Receptor 5? *Journal of Advances in Biology & Biotechnology,* 7 (1): 1-9. doi: 10.9734/JABB/2016/2676 @ Science Domain International

9. Alhassan DA, **Uba AI***, Muhammad AU, Muhammad YY. (2016). Phytochemical Screening and Antimicrobial Activity of Crude Stem Bark Extracts of *Anogeissus leiocarpus.* European Journal of Medicinal Plant, 11(2): 1-7, Article no.EJMP.22443. doi: 10.9734/EJMP/2016/22443 @ Science Domain International

10. **Uba AI**[*], Usman SS, Musbahu MS, Abdullahi UA, Mustafa GM, et al. (2015) Genetic Redundancy and Chemokines: CCR5 Δ32 HIV Resistance Allele. *Tropical Medicine and Surgery,* 3 (3): 191. doi:10.4172/2329-9088.1000191. @ OMICS publishing group

11. **Uba AI**[*], Abdulazeez MA, Usman SS, Tabakoglu HO, Abubakar H. (2015). Phage Display Technology as a Strong Alternatıve to Hybridoma Technology for Monoclonal Antıbody Productıon. *International Journal of Science and Technology*, 4 (3): 125-131

12. Umar AA, Muhammad MS, **Uba AI**, Hasim OT, Senel M. (2015). Analysis of pulsed mode laser skin soldering: gelatin and chitosan as solder materials mixed with indocyanine green as chromophore. *International journal for research & development in technology,* 4(2): 46-53

13. SS Usman, **AI Uba**, I Yunusa, Y Sadiq, U Huzaifa. (2015). S-nitrosylation in Sporadic Parkinson's Disease and Cancer (Brain and Thyroid) Prevention. *Annals of Experimental Biology,* 3(1):13-19

14. **Uba AI**[*], Banagana K,Usman MT, Alhassan DA, Uba MI. (2015). Effect of Kola Nut Consumptıon on Hematologıcal Parameters. *International Journal of Scientific Research in Knowledge*, 3(5): 139-144. doi: http://dx.doi.org/10.12983/ijsrk-2015-p0139-0144

15. **Uba AI**[*], Abdullahi IL, Abdullahi SA, Adamu H. (2015). The status of lipid profile in stress-related pre-insomnia. *European Journal of Biomedical and Pharmaceutical Sciences,* 2 (1): 89-98.

16. **Uba AI**[*], Abubakar H, Atiku M.K, Wudil A.M. Proposed genetic approach to protecting infants to be breastfed by HIV positive mothers against HIV infection (2014). *International Journal of Infectious and Tropical Diseases*, 1(2):73-76. doi: http://dx.doi.org/10.14194/ijitd.1.2.4

17. SS Usman, I Yunusa, **AI Uba**, I. M Ahmad (2014). α-Synuclein, Synphilin and E3 Ubiquitin-Ligase (SIAH and Parkin): The Key to Understanding Parkinson's Disease *Annals of Experimental Biology,* 2(4):28-32.

18. Atiku M.K and **Uba A.I**[*] (2014). Relationship between stress levels and the status of serum antioxidantvitamins. *International Journal of Medicine and Biomedical Research*, 3(2):132-136. doi:http://dx.doi.org/10.14194/ijmbr.3.2.9

19. **AI Uba**[*], MK Atiku, AM Wudil, MS Aminu. (2014). Serum lipid profile status in examination stress condition *European Journal of Biomedical and Pharmaceutical Sciences*, 1 (2) 551-557

Conference/Workshop Participation

26th International Medical Sciences Student Congress (IMSSC), **Istanbul University Faculty of Medicine (4th-6th May, 2018).**

Invited Trainer to European Cooperation in Science and Technology COST Action CM1406: Training School on Computer Aided Drug Discovery at **Kadir Has University, Istanbul, Turkey (22nd-24th March, 2018)**

European Cooperation in Science and Technology (COST) Action CM1406: Epigenetic Chemical Biology ECI Workshop and Core Group Meeting, **Institut Pasteur, Paris, France (15th February, 2018).**

5th Multithematic Biomedical Congress (IMBMC), **European University, Cyprus** (**2nd-4th November, 2017**) (Abstract published).

5th International Bahçeşehir University (BAU) Drug Design Congress: Recent Developments in Structure- and Ligand-based Drug Design Methodologies, **Istanbul (19th -21st October, 2017).**

ISER-9th International conference on Recent Advances in Medical Sciences, **Istanbul (10 October 10, 2015).**

Awards/Grants/Fellowship

European Cooperation in Science and Technology (COST) Action CM1406: Epigenetic Chemical Biology ECI Workshop Sponsorship Award (15 February, 2018).

cientific and Technological Research Council of Turkey (TUBITAK) Research Assistant Fellowship (Grant no: 215S009) (March 2017-June, 2018).

Bayero University "Needs Assessment Grant" for PhD fellowship (February, 2015-January, 2018).
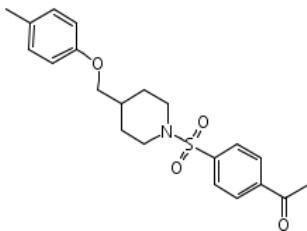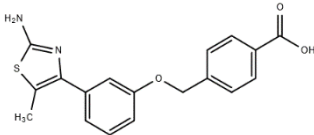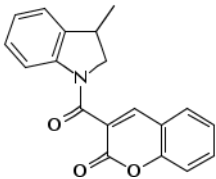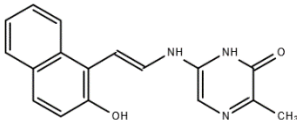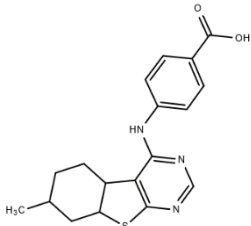
Kano State Government Overseas Postgraduate Studies Scholarship (September, 2012).

APPENDIX A

Appendix A 1. Structures, estimated binding energy (ΔG) and inhibition constant (Ki) of the isoform-selective/selective inhibitors of class I HDACs identified through structure-based virtual screening.

Table A. 1. HDAC1-Selective Inhibitors.

S/N	Otava Code	Structure	ΔG (Kcal/mol)	Ki (nM)
1	3368838		-11.14	6.77
2	P1167483		-10.44	22.38
3	4562316		-10.1	39.56
4	P0105480004		-9.95	51.25
5	P7012340203		-9.66	83.35
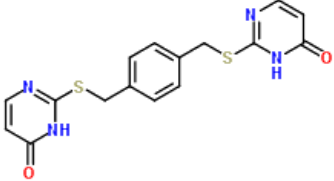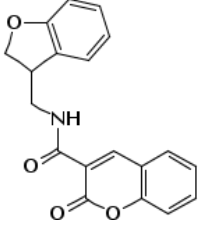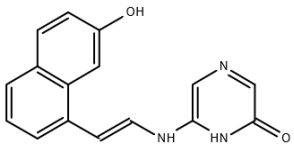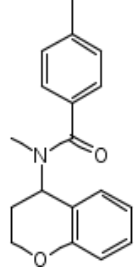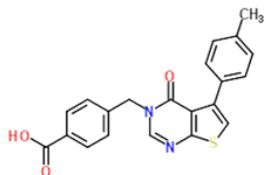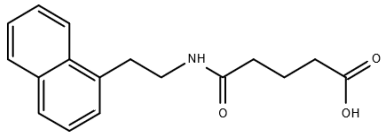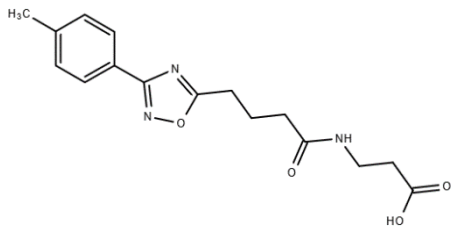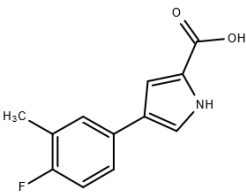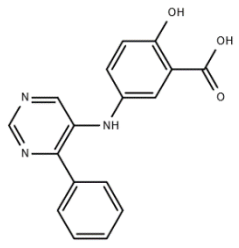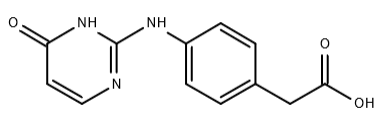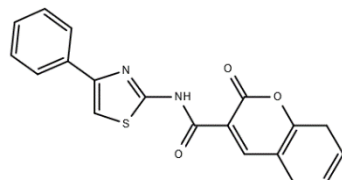
6	P7016000027		-9.62	89.3
7	4562295		-9.54	101.04
8	P0217690002		-9.3	151.28
9	4562397		-9.17	188.38
10	P7013831126		-9.06	258.38

Table A. 2. HDAC2-Selective Inhibitors.

S/N	Otava Code	Structure	ΔG (Kcal/mol)	Ki (nM)
11	P7020400743		-12.63	0.55
12	P2194599		-11.83	2.15
13	P1146482		-11.48	3.88
14	P7020090764		-10.68	14.86
15	P7020350445		-10.6	16.97
16	125320080		-10.46	21.5
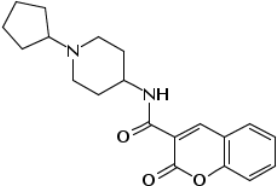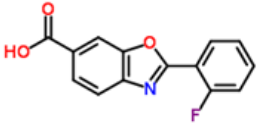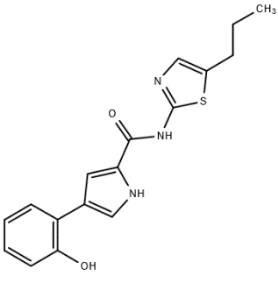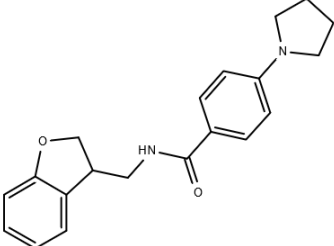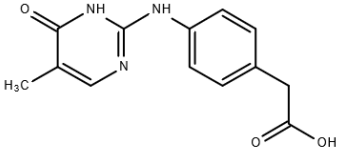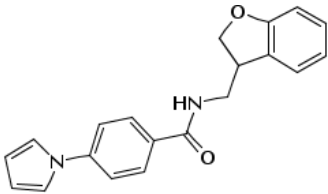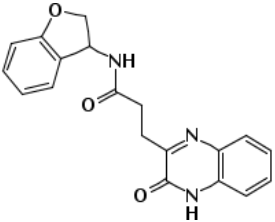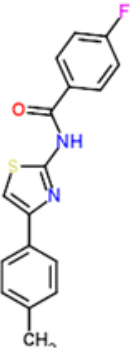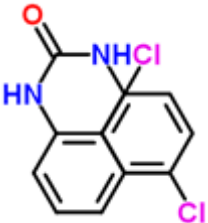
17	4562375		-10.22	32.41
18	P1357221		-10.11	38.69
19	P1688898		-9.93	52.49
20	4562294		-9.69	78.59

Table A. 3. HDAC3-Selective Inhibitors.

S/N	Otava Code	Structure	ΔG (Kcal/mol)	Ki (nM)
21	P7020350446		-10.24	31.05
22	4562273		-9.75	71.39
23	4562274		-9.46	116.1
24	7.21E+09		-8.98	261.17
25	115030968		-8.79	361.08

26	P7016361082		-8.68	435.89
27	105850571		-8.65	459.18
28	127441798		-8.63	469.99
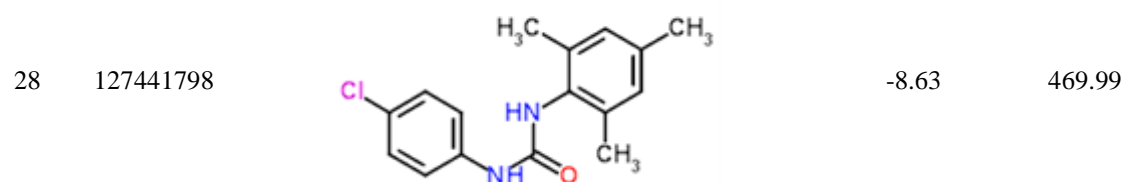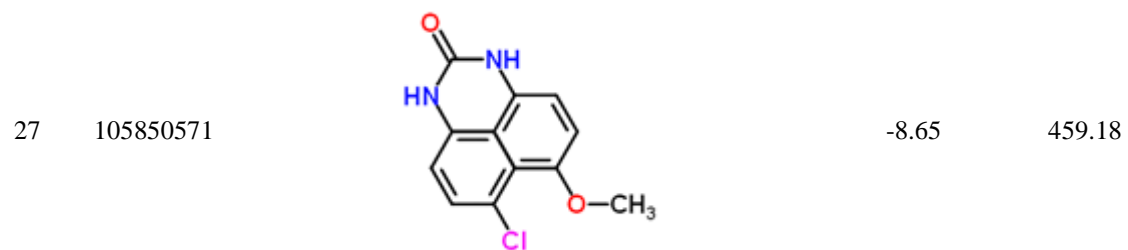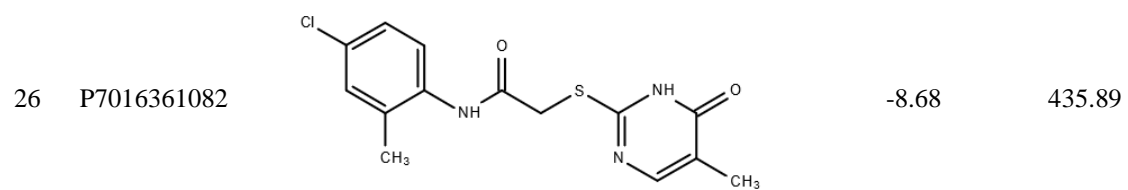
Table A. 4. HDAC6-selective Inhibitors.
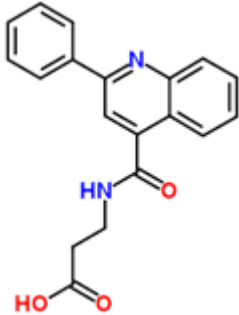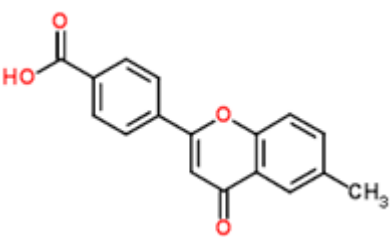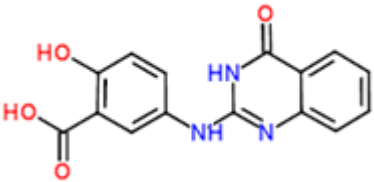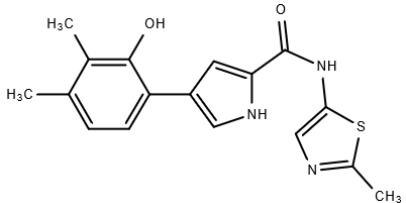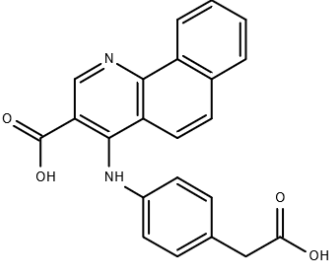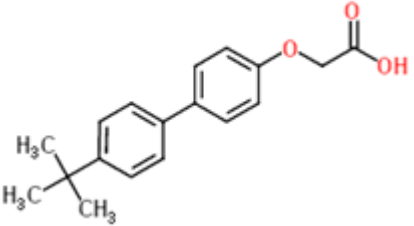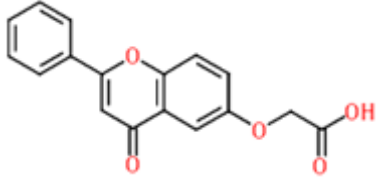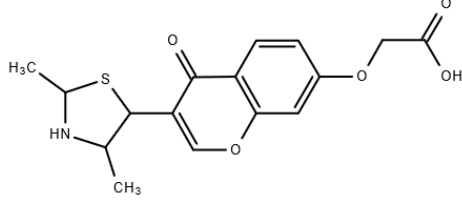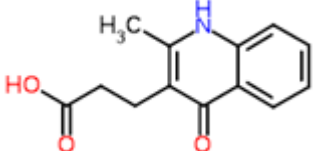
S/N	Otava Code	Structure	ΔG (Kcal/mol)	Ki (nM)
29	P2194879		-11.44	4.12
30	P7715560117		-10.1	39.34
31	P3823745		-9.32	148.29
32	P7119982880		-9.01	225.87

Table A. 5. HDAC8-Selective Inhibitors.

S/N	Otava Code	Structure	ΔG (Kcal/mol)	Ki (nM)
33	P7019081225		-13.63	0.1
34	P1364003		-12.28	1.00
35	P7017470060		-12.2	1.15
36	P0127442890		-11.94	1.78
37	P7020420366		-11.54	3.5
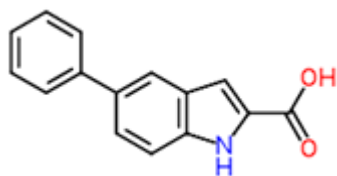
38	P1365606		-10.83	11.62
39	P0108480094		-10.81	12.00
40	P7114490082		-9.68	79.58
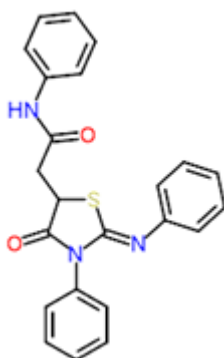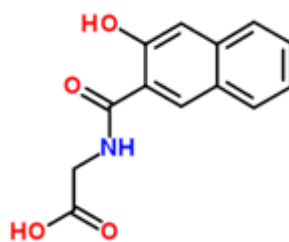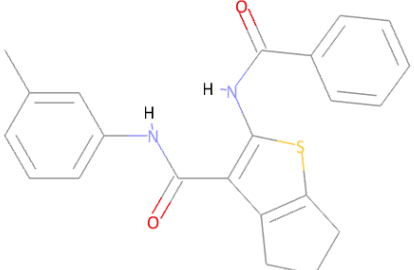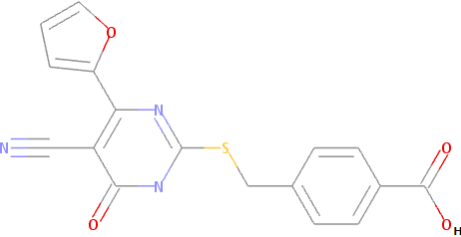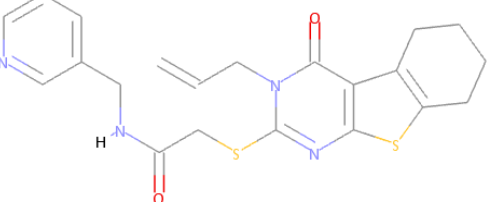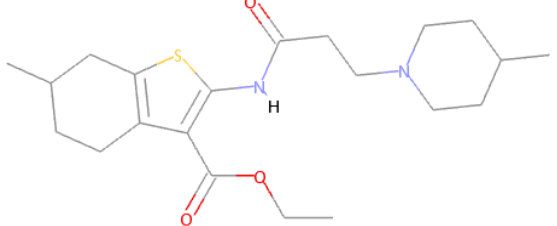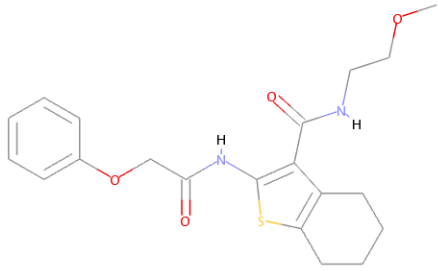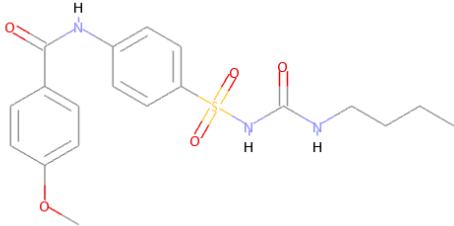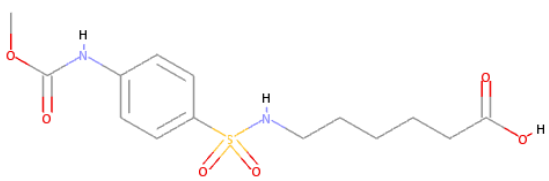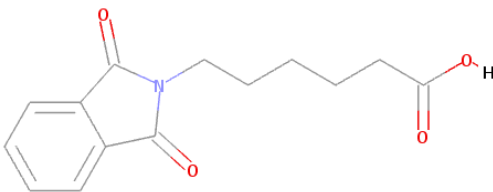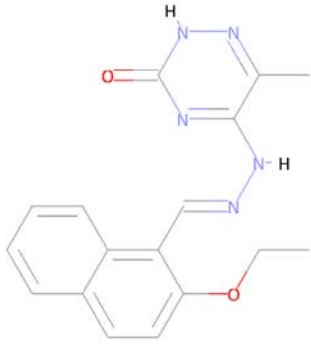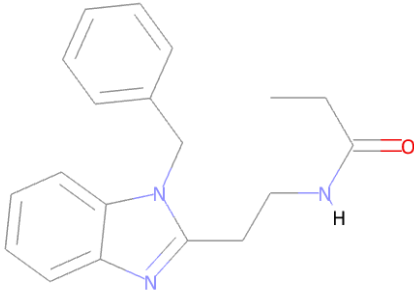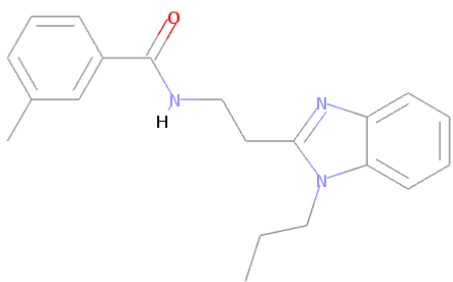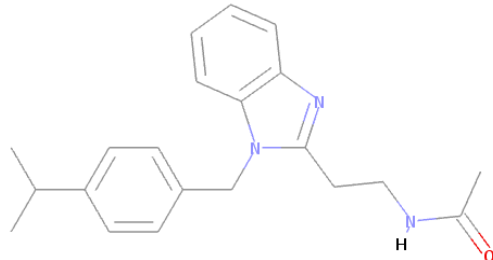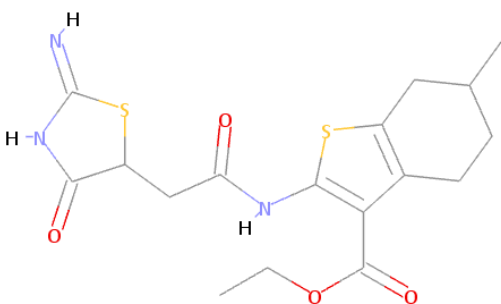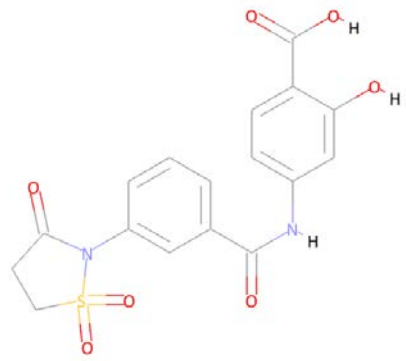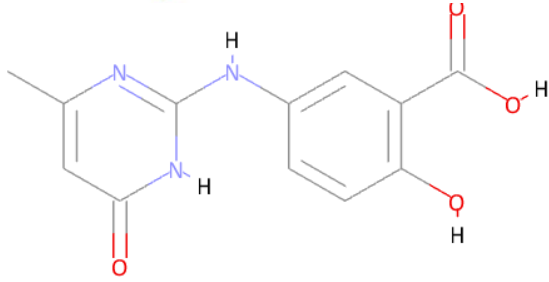
APPENDIX B

Appendix B. 1 Identification of Lead Compounds for the Design of HDAC6-Selective Inhibitors

Table B. 1. Nonselective HDAC inhibitors from identified via structure-based virtual screening. These compounds showed reasonable binding orientation in HDAC6 active site.

Otava Code	Structure	ΔG (kcal/mol)	
		HDAC6	HDAC7
P7112880082		-10.29	-10.32
P7020580660		-10.22	-10.35
P7110390012		-10.38	-10.33
P7211790586		-11.09	-10.75

P7412660574		-10.63	-10.94
P7717640005		-10.38	-10.53
P0113630043		-10.24	-10.92
P0123400435		-10.74	-10.25
P7714230380		-10.01	-10.22
P7217980127		-10.05	-10.11

P7119500989	-11.25	-10.92
P7119730586	-10.05	-10.03
P7114880011	-10.2	-10.43
P1444899	-11.61	-10.91
P3823736	-10.35	-10.56
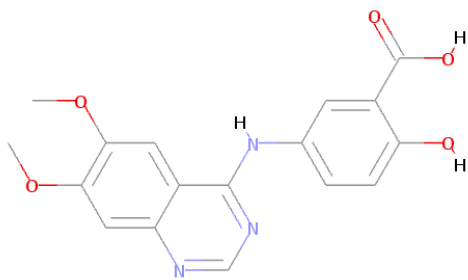
| P7020420008 | | -10.05 | -10.26 |

Table B. 2. Calculated pKa values of the neighboring residues in the catalytic channels of HDAC6 and HDAC7.

HDAC6		HDAC7	
Residue	**Calculated pKa**	**Residue**	**Calculated pKa**
A:ASP486	3.563	A:ASP525	3.707
A:ASP497	2.811	A:ASP537	2.303
A:ASP567	3.123	A:ASP600	3.29
A:ASP615	3.449	A:ASP624	4.296
A:ASP647	7.597	A:ASP626	2.819
A:ASP649	2	A:ASP647	3.748
A:ASP662	2.841	A:ASP672	2.999
A:ASP663	3.973	A:ASP705	2
A:ASP675	2.721	A:ASP707	2
A:ASP684	3.697	A:ASP721	3.339
A:ASP712	3.541	A:ASP733	2.963
A:ASP714	4.026	A:ASP734	3.415
A:ASP742	6.797	A:ASP745	2.922
A:ASP747	3.171	A:ASP766	3.325
A:ASP801	3.13	A:ASP771	4.57
A:GLU543	4.102	A:GLU543	2.509
A:GLU552	4.658	A:GLU557	3.954
A:GLU558	3.912	A:GLU565	4.761
A:GLU562	4.536	A:GLU575	3.821
A:GLU591	3.74	A:GLU576	4.55
A:GLU597	4.614	A:GLU583	4.174
A:GLU613	4.418	A:GLU631	4.137
A:GLU661	4.607	A:GLU656	4.583
A:GLU685	2.768	A:GLU746	5.536
A:GLU729	5.165	A:GLU753	4.482
A:GLU733	4.274	A:GLU773	5.674
A:GLU757	4.274	A:GLU788	5.044
A:GLU779	6.502	A:GLU804	4.03
A:GLU789	3.997	A:GLU840	5.329
A:GLU822	4.416	A:GLU853	4.767
A:TYR668	12.2	A:TYR524	12.2
A:TYR674	12.2	A:TYR589	12.2
A:TYR715	12.2	A:TYR719	12.2
A:TYR728	12.2	A:TYR726	12.2
A:TYR759	12.2	A:TYR774	12.2
A:TYR782	12.2	A:TYR813	12.2

A:TYR830	10.184	A:TYR822	11.246
A:CYS512	10.514	A:CYS533	6.124
A:CYS523	12.2	A:CYS535	6.361
A:CYS539	12.2	A:CYS564	12.2
A:CYS572	11.761	A:CYS566	11.582
A:CYS578	12.2	A:CYS618	3.316
A:CYS587	12.2	A:CYS680	12.2
A:CYS618	12.2	A:CYS689	12.2
A:CYS621	12.2	A:CYS819	12.2
A:CYS752	12.2	A:CYS849	12.2
A:CYS794	12.2	A:CYS855	12.2
A:HIS499	6.549	A:HIS531	6.619
A:HIS500	5.504	A:HIS541	2
A:HIS540	7.955	A:HIS544	5.161
A:HIS547	7.767	A:HIS581	5.97
A:HIS560	6.82	A:HIS585	7.506
A:HIS610	10.994	A:HIS633	6.08
A:HIS611	6.488	A:HIS669	8.724
A:HIS632	8.373	A:HIS670	2.114
A:HIS639	6.807	A:HIS673	6.179
A:HIS651	7.141	A:HIS709	2
A:HIS652	7.544	A:HIS710	3.685
A:HIS658	9.827	A:HIS730	7.98
A:HIS672	10.781	A:HIS732	6.324
A:HIS676	7.047	A:HIS806	6.807
A:HIS720	6.623	A:HIS814	7.53
A:HIS761	7.441	A:HIS843	5.872
A:HIS764	6.941	A:HIS891	7.71
A:LYS553	10.667	A:LYS571	9.745
A:LYS555	10.685	A:LYS603	11.087
A:ARG549	12.2	A:ARG540	12.2
A:ARG557	12.2	A:ARG547	12.2
A:ARG561	12.2	A:ARG554	12.2
A:ARG588	12.2	A:ARG558	12.2
A:ARG606	12.2	A:ARG561	12.2
A:ARG631	12.2	A:ARG568	12.2
A:ARG642	12.2	A:ARG570	12.2
A:ARG673	12.2	A:ARG584	12.2
A:ARG693	12.2	A:ARG639	12.2
A:ARG709	12.2	A:ARG665	12.2
A:ARG721	12.2	A:ARG690	12.2
A:ARG745	12.2	A:ARG731	12.2

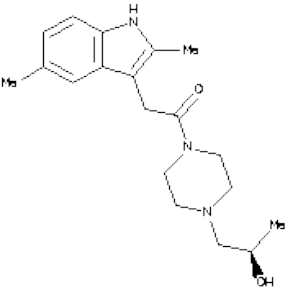|			
A:ARG773	12.2	A:ARG779	12.2
A:ARG796	12.2	A:ARG787	12.2
A:ARG810	12.2	A:ARG863	12.2
A:ARG828	12.2	A:ARG882	12.2
A:ARG829	12.2	A:ARG889	12.2
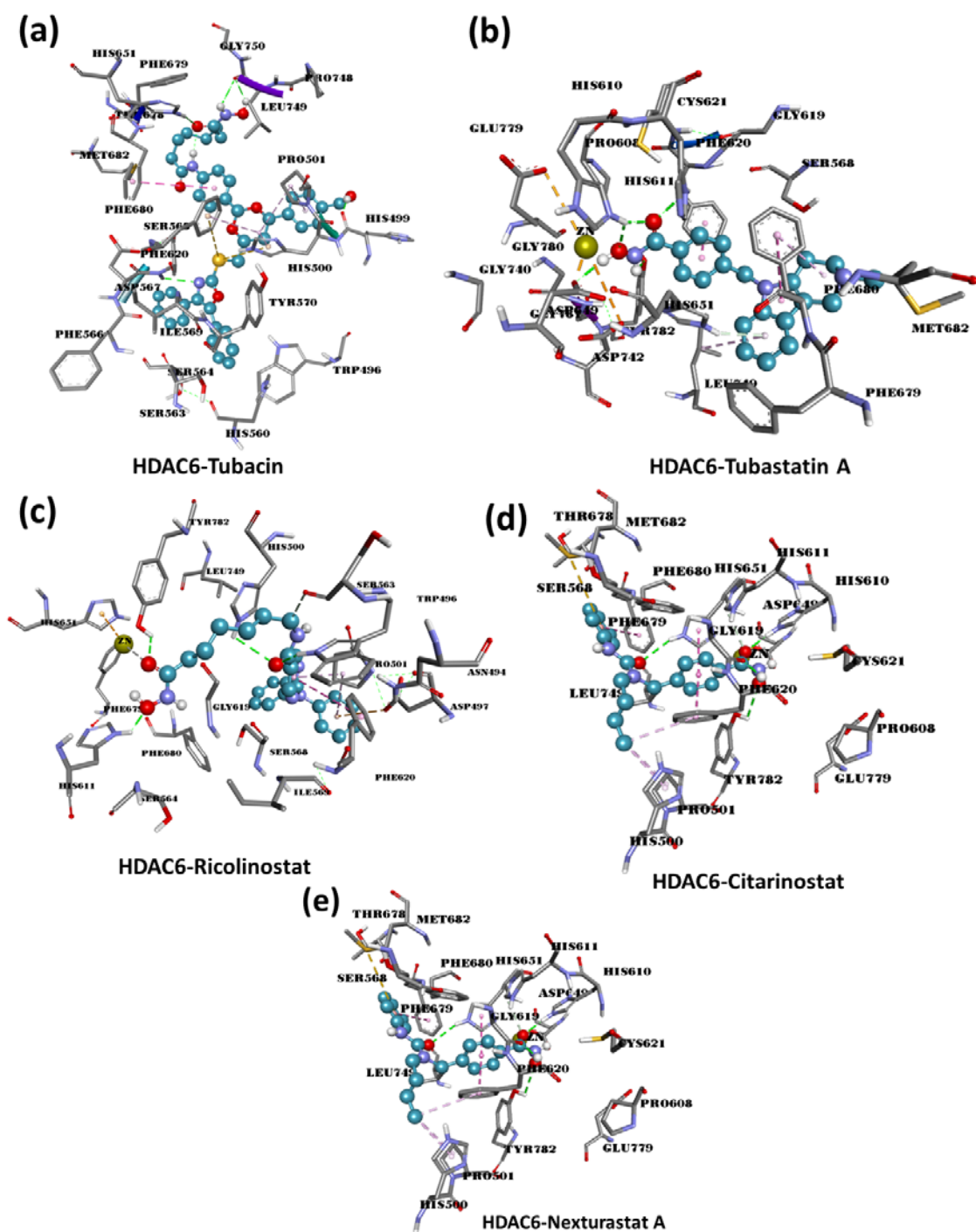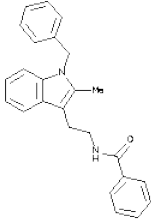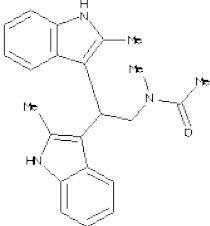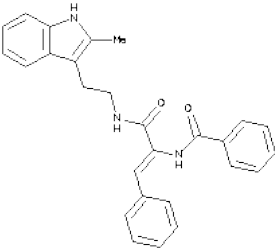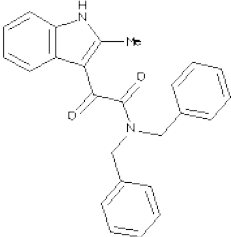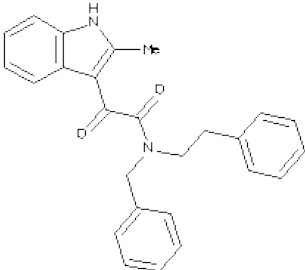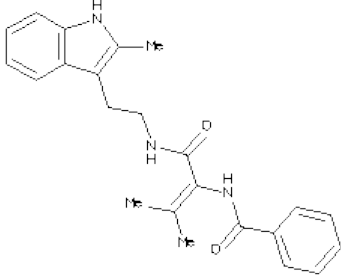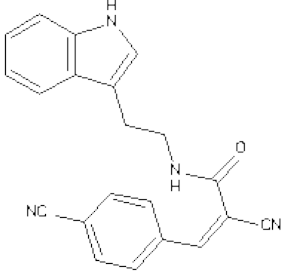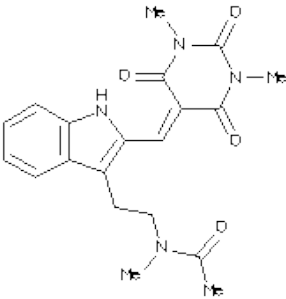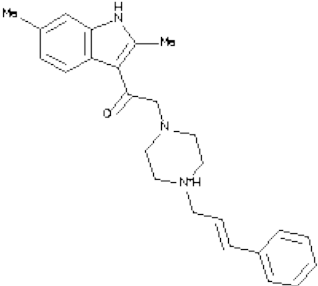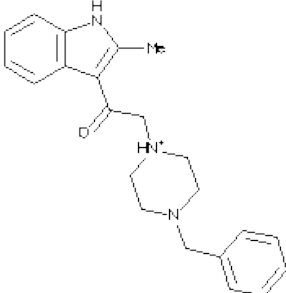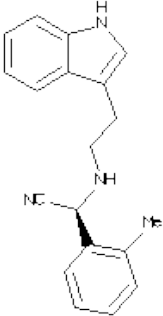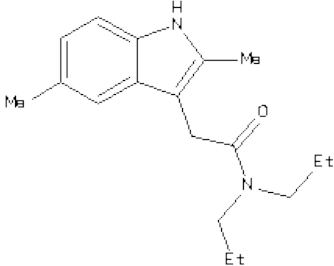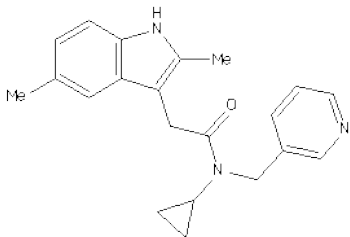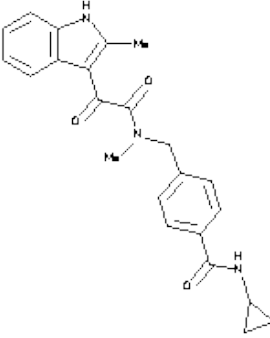
Figure B. 1. Binding modes of the known HDAC6-selective inhibitors. They all bound HDAC6 with their cap-linker-chelator pharmacophore feature, except for Tubacin, whose bulky cap made steric clashes at the entrance, and thereby changing the set of interactions deep inside the channel.
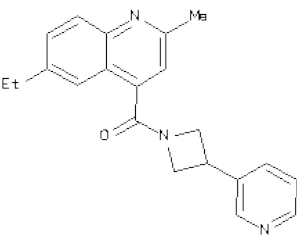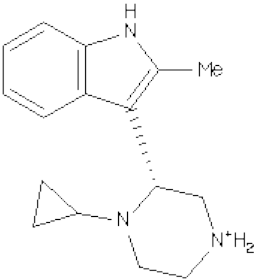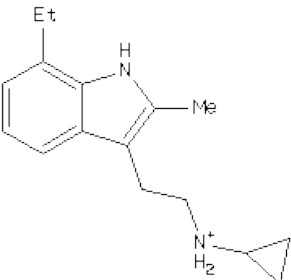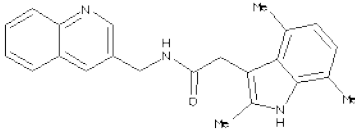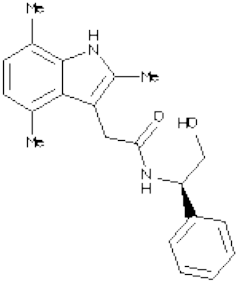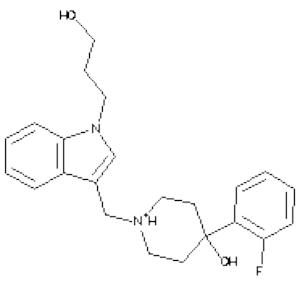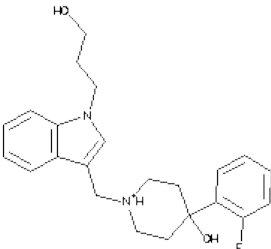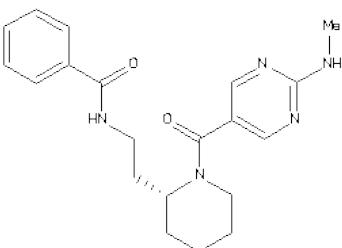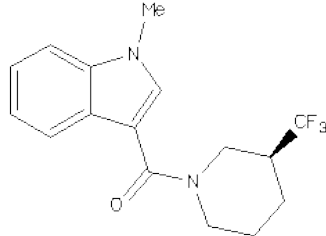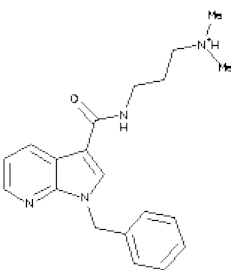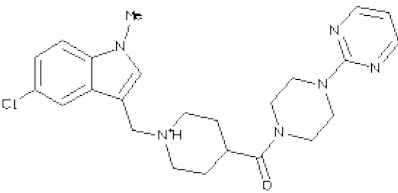
Table C. 1.Binding energy (ΔG) and inhibition constant (Ki) (against HDACs 6 and 10) of drug-like compounds retrieved from ZINC database by ligand-based virtual screening
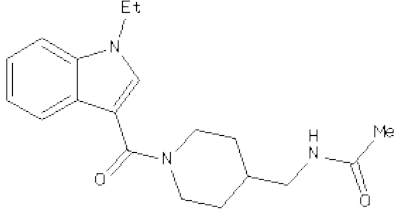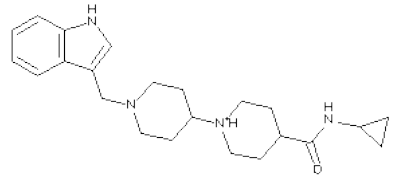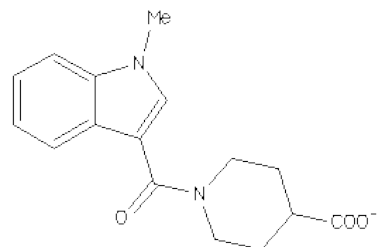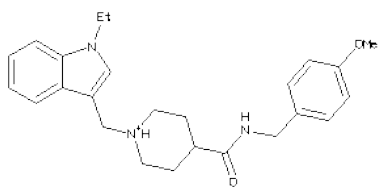
compound	structure	HDAC6		HDAC10	
		ΔG (kcal/mol)	Ki (nM)	ΔG (kcal/mol)	Ki (nM)
ZINC860648		-7.75	2100	7.75	2100
ZINC1719423		-7.63	2530	-6.97	7820
ZINC3619218		-7.84	1790	-8.13	1100
ZINC4163417		-7.44	3530	-7.16	5610
ZINC4163419		-7.18	5500	-7.42	3630

ZINC4593737	-6.81	10210	-8.43	658.53
ZINC4851153	-6.03	37790	-7.98	1430
ZINC5428788	-7.20	5290	-7.32	4300
ZINC19372554	-8.53	558.82	-11.01	8.5
ZINC19899798	-7.56	2900	-10.12	37.91

208

ZINC19987434	-7.17	5570	-8.24	905.34
ZINC24536692	-6.68	12690	-5.98	41060
ZINC24770883	-7.66	2420	-6.49	17610
ZINC30895181	-7.49	3240	-7.51	31400
ZINC71871194	-7.78	1990	-7.75	2090

ZINC72148254		-9.00	252.65	-7.35	4100
ZINC76301072		-6.57	15340	-7.91	1590
ZINC82608551		-7.64	2500	-7.32	4310
ZINC91603338		-6.80	10330	-7.86	1730
ZINC91820315		-6.08	35030	-6.60	14430
ZINC12240515		-7.37	3990	-7.96	3430

ZINC12118287		-7.33	4200	-8.37	731.32
ZINC19749069		-7.91	1600	-9.68	466.49
ZINC40472959		-6.00	4015	-5.56	83960
ZINC72323260		-7.02	7180	-7.61	2630
ZINC35562277		-8.19	993.25	-10.05	43.04

ZINC48357626		-7.97	1430	-7.4	3770
ZINC15069992		-8.11	1140	-9.42	123.48
ZINC37433253		-11.96	1.71	-8.85	55890
ZINC64669819		-8.25	890.14	-9.3	152.61